UNIVERSITÄT
BERN

Some sources of hydroclimate and renewable energy variability in tropical South America

Inaugural dissertation
of the Faculty of Science
University of Bern

Presented by

Nicolás Duque Gardeazábal

Supervisor of the doctoral thesis:
Prof. Dr. Stefan Brönnimann
Oeschger Centre for Climate Change Research
Institute of Geography
Faculty of Science of the University of Bern

UNIVERSITÄT
BERN

Some sources of hydroclimate and renewable energy variability in tropical South America

Inaugural dissertation
of the Faculty of Science

University of Bern

Presented by

Nicolás Duque Gardeazábal

Supervisor of the doctoral thesis:
Prof. Dr. Stefan Brönnimann
Oeschger Centre for Climate Change Research
Institute of Geography
Faculty of Science of the University of Bern

Accepted by the Faculty of Science

Bern, November 24th, 2025

The Dean:
Prof. Dr. Jean-Louis Reymond

Supervisor
Prof. Dr. Stefan Brönnimann
Oeschger Centre for Climate Change Research
Institute of Geography
Faculty of Science of the University of Bern

Co-supervisor
Prof. Dr. Olivia Romppainen-Martius
Oeschger Centre for Climate Change Research
Institute of Geography
Faculty of Science of the University of Bern

Advisor
Dr. Andrew R. Friedman
Institute of Geography
Faculty of Science of the University of Bern

External examiner
Prof. Dr. Francina Dominguez
Department of Climate, Meteorology and Atmospheric Sciences
School of Earth, Society and Environment of the University of Illinois Urbana-Champaign

"*Papá sabe bien,*
perdi una batalla ...
Tarda en llegar, pero al final,
al final, hay recompensas"

Gustavo Cerati

"*Somewhere, something incredible is waiting to be discovered.*"

Carl Sagan

Some sources of hydroclimate and renewable energy variability in tropical South America

Abstract

Tropical South America (SAm) has significant physical and biological resources. SAm's hydroclimate variability influences its ecosystems, hydropower, and food and water security, yet the mechanisms controlling these variations are not completely understood. This thesis investigates how a chain of physical processes, induced by ocean–atmospheric modes, modulate SAm's hydroclimatic variability and the potential solar and wind energy. It also explores how external aerosol forcing influences the mechanisms and afterwards SAm's rainfall.

Chapter 2 examines how Atlantic modes of variability influence SAm's Evapotranspiration, a key variable for the carbon cycle. Using reanalysis and satellite data, our study identifies how the Atlantic Meridional Mode (AMM) and the Atlantic Niño (Atl3) affect the regional atmospheric circulation and other variables in the chain. Results show that the impacts of the modes are seasonally and geographically different. The AMM-related anomalies of soil moisture, radiation and evapotranspiration migrate from eastern South America during austral autumn toward western Orinoco by austral spring. These impacts are caused by meridional wind anomalies. The Atl3 exerts more localised impacts in the Guianas and eastern Orinoco through changes in pressure and trade winds. The Atlantic modes alter the water and energy cycles in different regions compared to El Niño–Southern Oscillation (ENSO).

Chapter 3 focuses on the implications of the altered chain for solar and wind energy production. Considering climate variability into energy planning and storage strategies is relevant to achieve the energy transition to a decarbonised world. We use composites and partial correlations to investigate how ENSO, AMM, and Atl3 influence wind and solar capacity factors across three energy hubs: the North Caribbean, Eastern Brazil, and the Andes (Peru/Bolivia). ENSO-induced sea level pressure anomalies, which modify winds, moisture divergence and radiation, while Atlantic variability generates cross-equatorial wind and cloud anomalies that impact the energy hubs. Our study also investigates the complementarity between the two renewable sources. It found limited complementarity between wind and solar energy at interannual scales.

Chapter 4 addresses long-term hydroclimatic variability by comparing the impacts of anthropogenic and volcanic aerosols on the chain of processes and on SAm's rainfall. Using historical reanalyses, observations, and a paleo-reanalysis, the study shows that anthropogenic aerosols progressively reduced the interhemispheric temperature gradient, displacing the Hadley circulation southward and also rainfall. In contrast, volcanic aerosols are primarily associated with an overall reduction in rainfall, with some eruptions linked to meridional displacements of precipitation.

Our results can lead to better predictions of droughts, floods, and renewable energy variability. They can help build or strengthen early-warning systems and support adaptation strategies in a region highly vulnerable to extreme weather events.

Contents

Abstract **vii**

List of Figures **xi**

List of Tables **xiii**

List of Abbreviations **xv**

1 Introduction **1**
1.1 Tropical South America, its natural resources and their sustainable use 1
1.2 Sources of climate variability and their influence in tropical South America . . . 2
1.3 Chain of physical processes - mechanisms . . . 4
1.3.1 Processes modulating South America's evapotranspiration . . . 4
1.3.2 Processes modulating South America's potential wind and solar energy . . . 5
1.3.3 Aerosols influencing the ocean-atmospheric modes, global circulation and precipitation in South America . . . 5
1.4 Objective, questions, and outline of this thesis . . . 5
References . . . 6

2 An Atlantic influence on evapotranspiration in the Orinoco and Amazon basins **11**
2.1 Introduction . . . 13
2.2 Data . . . 14
2.2.1 Reanalysis . . . 15
2.2.2 Satellite . . . 16
2.3 Methods . . . 16
2.3.1 Determining the location and annual cycle of local ET controllers 17
2.3.2 Composites . . . 17
2.3.3 Conjoint effect with ENSO . . . 18
2.4 Results . . . 18
2.4.1 Key local evapotranspiration controllers . . . 18
2.4.2 Chain of physical processes between the Atlantic modes and continental evapotranspiration . . . 19
2.4.3 Atlantic modes connection with ENSO and impacts on evapotranspiration . . . 25
2.5 Discussion . . . 26
2.6 Conclusions . . . 29
Appendix . . . 32
References . . . 38

3 Solar and wind energy variability in tropical South America: seasonal ocean-atmospheric modulators **47**
3.1 Introduction . . . 50
3.2 Data . . . 51
3.2.1 Datasets . . . 51
3.2.2 Wind capacity factor . . . 52
3.2.3 Solar capacity factor . . . 53
3.3 Methods . . . 53
3.3.1 Modes of variability . . . 54
3.3.2 Identifying the physical mechanisms of the teleconnection . . . 54
3.3.3 Complementarity of wind and solar energy . . . 55
3.4 Results . . . 55
3.4.1 Identifying renewable energy hubs and their seasonal variability . . . 55
3.4.2 Ocean-atmospheric oscillations associated with the variability of the energy hubs . . . 57
3.4.3 Physical mechanisms associated with the energy variability . . . 59
3.4.4 Complementarity between solar and wind resources . . . 63
3.5 Discussion . . . 66
3.6 Conclusions . . . 68
Appendix . . . 71
References . . . 80

4 Possible effects of anthropogenic and volcanic aerosols on the ITCZ and tropical rainfall, over South America **87**
4.1 Introduction . . . 89
4.2 Results and discussion . . . 90
4.2.1 Impacts on the hydroclimate of tropical South America . . . 90
4.2.2 Aerosol concentrations . . . 91
4.2.3 Interhemispheric temperature gradient (IHTG) and shifts in regional atmospheric circulation . . . 94
4.2.4 Effects on regional moisture transport (VIMF) . . . 95
4.3 Conclusions . . . 99
4.4 Methods . . . 100
4.4.1 Data . . . 100
4.4.2 Atmospheric moisture and energy fluxes . . . 102
4.4.3 Anomalies and composites for volcanic eruptions . . . 103
4.4.4 Atmospheric indices . . . 103
4.4.5 Trends in the tropospheric aerosols . . . 103
Appendix . . . 106
References . . . 110

5 Conclusions and Outlook **117**
5.1 Conclusions . . . 117
5.2 Outlook . . . 119
References . . . 120

Acknowledgements **125**

List of Figures

1.1 Schematic figure of the chain of physical processes that impact ecology and socio-economic variables 4

2.1 Evapotranspiration regimes - Regression of ERA5 ET onto Soil Moisture and Net Radiation 19
2.2 Chain of events for AMM in MAM - Composites of the Atlantic Meridional Mode for March to May 21
2.3 Chain of events for Atl3 in JJA - Composites of the Atlantic Meridional Mode for March to May 23
2.4 Seasonal migration of the impacts of the Atlantic Meridional Mode. Anomalies of ET in the AMM phases for seasons MAM, JJA and SON . 24
2.5 Conjoint effects of the Atlantic modes and ENSO on evapotranspiration 26
2.6 Time series of the conjoint effects of the Atlantic modes and ENSO . . 27
2.7 Summary figure of the chain of processes linking the ocean-atmospheric modes with the evapotranspiration 30
2.8 Figure S1. Changes in regional atmospheric circulation - Composites Sea Level Pressure and low level winds for both Atlantic modes 32
2.9 Figure S2. ESA CCI Soil Moisture anomalies for both Atlantic modes . 33
2.10 Figure S3. GLEAM ET anomalies for both Atlantic modes 34
2.11 Figure S4 – Chain between the AMM in JJA and the evaporation in South America 35
2.12 Figure S5 – Chain between the AMM in SON and the evaporation in South America 36
2.13 Figure S6 – Time series of boxed regions in JJA and SON for the AMM 37
2.14 Figure S7 – Asymmetry in the VIMF, Soil Moisture and Evaporation . . 37
2.15 Figure S8 – Sea Surface Temperature Anomalies Principal Components Loadings and time series of SST indices 38

3.1 Energy hubs - Long term availability of solar and wind energy 56
3.2 Energy hubs - Interannual variability of solar and wind energy 57
3.3 Correlation of Energy hubs with selected Ocean-atmospheric modes of variability 58
3.4 Influence of ENSO on the Wind CF 60
3.5 Influence of the AMM on the Wind CF 61
3.6 Influence of ENSO on the Solar CF 62
3.7 Influence of the AMM on the Wind CF 63
3.8 Complementarity between Wind and Solar energy under the influence of ENSO 65
3.9 Complementarity between Wind and Solar energy under the influence of the AMM 66

3.10 Figure S1 – Sea Surface Temperature Anomalies Principal Components Loadings and time series of SST indices 71
3.11 Figure S2. Maps of correlation between the Wind Capacity Factor (CF) and the three ocean-atmospheric indices (ELI, AMM and Atl3) 72
3.12 Figure S3. Maps of correlation between the Solar Capacity Factor (CF) and the three ocean-atmospheric indices (ELI, AMM and Atl3) 73
3.13 Figure S4 – Wind CF composites for ENSO in seasons MAM and JJA . 74
3.14 Figure S5 – Wind CF composites for AMM in seasons SON and DJF . . 75
3.15 Figure S6 – Wind CF composites for Atl3 76
3.16 Figure S7 – Solar CF composites for ENSO in seasons MAM and JJA . 77
3.17 Figure S8 – Solar CF composites for AMM in seasons SON and DJF . . 78
3.18 Figure S9 – Solar CF composites for Atl3 79

4.1 Boreal summer changes in the hydroclimate of tropical South America 92
4.2 Latitudinal distribution of aerosols in the boreal summer - JJA 94
4.3 Interhemispheric temperature gradient and shifts in regional strong ascent for the boreal summer - JJA 96
4.4 Changes in regional moisture transport, convergence and rainfall. . . . 98
4.5 Figure S1 – Other hydroclimate anomalies in tropical South America . 106
4.6 Figure S2 – Meridional total energy transport in the 20th and 21st century 107
4.7 Figure S3 – Global position of the strong ascent of moist air 108
4.8 Figure S4 – Changes in Sea Level Pressure and low level winds 109
4.9 Figure S5 – Early 19th century anomalies of the temperature contrast between the land and the ocean in the tropics 110

List of Tables

2.1 Overview of the datasets used for studying the evapotranspiration in South America 15

3.1 Datasets used for studying the solar and wind energy in South America 52
3.2 Classification of solar and wind energy hubs by geographic proximity. 56
3.3 Multi-annual mean renewable energy capacity factor availability and its changes 64
3.4 Table S1. Quantitative complementarity with Spearman correlation . . 80

List of Abbreviations

AMM	**A**tlantic **M**eridional **M**ode
AMO	**A**tlantic **M**ultidecadal **O**scillation
Atl3	**Atl**antic equatorial El Niño mode - region **3**
CESM-LME	**C**ommunity **E**arth **S**ystem **M**odel - **L**arge **M**illennium **E**nsemble
CERA-20C	**C**ouple **E**CMWF **R**etrospective **A**nalysis of the **20**th **C**entury
CF	**C**apacity **F**actor
CHIRPS	**C**limate **H**azards **I**nfra**R**ed **P**recipitation with **S**tations
CMIP	**C**oupled **M**odel **I**ntercomparisson **P**roject
DJF	**D**ecember-**J**anuary-**F**ebruary
D(0)JF(+1)	**D**ecember-**J**anuary-**F**ebruary for ENSO transition to next year
ECMWF	**E**uropean **C**enter for**M**edium range **W**eather **F**orecast
ELI	**E**l Niño **L**ongitude **I**ndex
ENSO	**E**l **N**iño - **S**outhern **O**scillation
EB	**E**astern **B**razil
ERSST	**E**xtended **R**econstructed **S**ea **S**urface **T**emperature
ERA5	**E**CMWF **R**etrospective **A**nalysis 5th generation
ET	**E**vapo**T**ranspiration
FAO	**F**ood and **A**griculture **O**rganisation
GHG	**G**reen**H**ouse **G**ases
GLEAM	**G**lobal **L**and **E**vaporation **A**msterdam **M**odel
GPCC	**G**lobal **P**recipitation **C**limatology **C**enter
HadSST	**Had**ley **S**ea **Surface** **T**emperature
IHTG	**I**nter**H**emispheric **T**emperature **G**radient
IPO	**I**nterdecadal **P**acific **O**scillation
ITCZ	**I**nter**T**ropical **C**onvergence **Z**one
JJA	**J**une-**J**uly-**A**ugust
LIA	**L**ittle **I**ce **A**ge
MAM	**M**arch-**A**pril-**M**ay
MDiv	vertically Integrated **M**oisture **Div**ergence
ModE-Sim	**M**odern **E**ra -**Sim**ulations
ModE-RA	**M**odern **E**ra -**R**e**A**nalysis
MSWEP	**M**ulti-**S**ource **W**eighted-**E**nsemble **P**recipitation
ONI	**O**ceanic **N**iño **I**ndex
Ppt	**P**recipitation
Rn	**n**et **R**adiation
SAm	**S**outh **Am**erica
SDGs	**S**ustainable **D**evelopment **G**oals
SM	**S**oil **M**oisture
SLP	**S**ea **L**evel **P**ressure
SST	**S**ea **Surface** **T**emperature
SSTA	**S**ea **Surface** **T**emperature **A**nomaly

SON	**S**eptember-**O**ctober-**N**ovember
TNA	**T**ropical **N**orth **A**tlantic
TSA	**T**ropical **S**outh **A**tlantic
UN	**U**nited **N**ations
VIMF	**V**ertically **I**ntegrated **M**oisture **F**lux (water vapour transport)
VITEF	**V**ertically **I**ntegrated **T**otal **E**nergy **F**lux
WPB	**W**estern **P**erú/**B**olivia
20CR	**20**th **C**entury **R**eanalysis

Introduction

1.1 Tropical South America, its natural resources and their sustainable use

South America (SAm) has significant physical, social and biological resources, all under pressure from global trade and influenced by climate. The Orinoco, the Amazon basin, together with the Andes mountain range, hold several biodiversity hotspots, the largest rainforest (an essential carbon sink), and the most voluminous river in the world (hydropower is the primary renewable energy source). Moreover, new breadbasket regions have recently consolidated across SAm since many people make their livelihoods through export-oriented production of soybean, rice, avocados, coffee and cacao (FAO, 2025; Zeigler & Truitt Nakata, 2014). All these environmental and socio-economic systems are impacted by the hydroclimate variability of tropical SAm, which consists of features at intra- and inter-annual scales.

The annual hydroclimatic cycle of SAm is associated with the Intertropical Convergence Zone (ITCZ), which also exhibits interannual and decadal variability (Arias et al., 2021; Garreaud et al., 2009). The ITCZ migrates following the solar annual cycle, placing itself in the tropical south from December to January (DJF, the initial letters of the months), and in the tropical north from June to August (JJA), with some regional exceptions (e.g. northeastern Brazil). The moisture feeding the ITCZ mainly originates from neighbouring oceans and is transported by the tropical easterly winds and westerlies close to northwestern SAm (Poveda et al., 2014). The ITCZ determine the timing of the rainy and dry seasons, the annual cycle of evapotranspiration, and thus shapes the dynamics of ecosystems, agriculture and energy supply. Hence, the Amazon forest dynamics are associated with the ITCZ annual cycle, dynamics that provide a cooling effect which influences climate globally (making it a climate tipping point, Armstrong McKay et al., 2022). Approximately 357 million people live near the ITCZ in SAm, underscoring the relevance of understanding its variability for water, food and energy security.

Seasonal climate variability phenomena modulate weather across SAm for weeks and months, influencing extreme hydrometeorological events. South Americans are vulnerable to these events that might disrupt their first socio-economic sector activities, energy production and demand, and their public health (Castellanos et al., 2023). Climate variability might severely affect SAm's breadbasket regions and threaten sustainable agriculture as it influences deforestation dynamics through modulating dry and flammable conditions (Feron et al., 2024; Vogel et al., 2019). Weather also constrains SAm's plant and crop phenology, thereby affecting crop yields and

food security (Ummenhofer & Meehl, 2017), while also affecting the Amazon's carbon cycle through impacts on primary productivity (Zhao & Running, 2010). Extreme events such as flash floods pose recurrent risks to South American lives, livelihoods, and infrastructure (Merz et al., 2021). Prolonged and strong rainy seasons (recurrent weather) saturate soil moisture earlier than usual, increasing the probability of slow-onset floods, creating similar risks (A. Mishra et al., 2022). Drought – particularly hydrological drought – is a slow-onset phenomenon which consolidates after prolonged precipitation deficiency (several months or a season); evapotranspiration variability also plays a role in its development (A. K. Mishra & Singh, 2010; Van Loon, 2015). Moreover, rainfall variability constrains SAm's hydropower production, often pressuring countries to rely on more expensive fossil fuels (Gonzalez-Salazar & Poganietz, 2021). Weather also impacts wind speed and solar radiation, the main local controllers of renewable energy production (Engeland et al., 2017). The increased solar radiation is an unexpected benefit of droughts from an energy management perspective. As solar and wind energy continue to expand within the energy matrix, accounting for climate variability becomes critical to ensure a reliable and decarbonised energy supply across SAm (Bustos et al., 2017). All the aforementioned dynamics evidence the need and relevance of studying the sources and impacts of climate variability in SAm.

Is it possible to explain some share of the South American tropical hydroclimate and its potential renewable energy variability? Which are the influencers or drivers of that variability? In this thesis, we study possible sources of climate variability and its impacts on SAm's evapotranspiration (chapter 2), solar and wind energy variability (chapter 3), and the influence that external aerosol forcing might impose on the mechanisms that modulate rainfall variability (chapter 4).

1.2 Sources of climate variability and their influence in tropical South America

South American hydroclimate variability is influenced by several factors which originate from the unequal spatial distribution of energy. In tropical regions, including tropical SAm, quasi-fluctuating ocean-atmospheric interactions are a major source of variability at seasonal to interannual scales (also called variability modes; Cai et al., 2019).

El Niño/Southern Oscillation (ENSO) is the most consequential mode worldwide, characterised by 2 to 7 year interannual cycle in tropical Pacific sea surface temperatures (SST)(Brönnimann, 2007; Timmermann et al., 2018). The warm El Niño phase creates an atmospheric bridge from the Pacific, generating atmospheric subsidence over eastern equatorial SAm that limits convection and rainfall; it also weakens westerly low-level jets, moisture transport and rainfall (Cai et al., 2020; Poveda et al., 2014). Whereas the cold La Niña phase strengthens the atmospheric circulation, moisture transport and rainfall. ENSO also generates different impacts on rainfall and temperature depending on the season analysed (Cai et al., 2020). The internal ENSO dynamics create diversity among events, diversity related to zonal shifts in the Walker circulation (Thual & Dewitte, 2023; I. N. Williams & Patricola, 2018). Other ocean-atmospheric modes in other basins have substantial covariability with ENSO, e.g. the Indian Ocean Basin mode (Andrian et al., 2024; Cai et al., 2019; Compo & Sardeshmukh, 2010).

Apart from ENSO, Atlantic ocean-atmospheric modes also modulate the hydroclimate in different regions across SAm (Arias et al., 2020; Hoyos et al., 2019). The

main Atlantic modes are the Atlantic Meridional mode (AMM) and the Atlantic equatorial El Niño mode (Atl3), both influence rainfall via altered regional atmospheric circulation (Fernandes et al., 2015; Rodrigues & McPhaden, 2014; Vallès-Casanova et al., 2020). The aforementioned modes are connected with ENSO through tropical and extratropical mechanisms, but they also have specific individual sea level pressure (SLP) dynamics and thus their own mechanisms (García-Serrano et al., 2017; Martín-Rey et al., 2014). The ocean-atmospheric modes can also have a direct influence on specific weather events; for example, El Niño provokes strong convection at the Peruvian coast, creating heavy rainfall and flash floods (Bayer et al., 2014).

Other phenomena influence the South American hydroclimate at shorter scale, such as the Madden-Julian Oscillations (MJO), Caribbean or African easterly waves, among others (P. D. Williams et al., 2017). Some of these phenomena also operate as fluctuations that have intra-annual or interannual cycles (Builes-Jaramillo et al., 2025; Kim et al., 2018). Our research focuses on the impacts of tropical seasonal to interannual ocean-atmospheric modes (hereafter also referred to as internal Earth system drivers), and thus, we exclude the aforementioned short-scale phenomena from our analyses.

All chapters in this dissertation consider the influence of either ENSO, the AMM and/or the Atl3 modes. Each chapter studies a particular impact of the modes on variables relevant to ecology or socio-economic sectors.

Other SST phenomena might exist at longer time scales, or the interannual modes might be influenced by long-scale external systems, often called forced variability. External forcings include variations in top-of-the-atmosphere solar radiation (the "solar constant"), volcanic eruptions or anthropogenic activities (e.g. greenhouse gases, aerosols or land cover changes; Brönnimann, 2015; Brönnimann et al., 2019; Paik et al., 2020). Long-term SST phenomena, such as the Atlantic Multidecadal Oscillation (AMO) and the Interdecadal Pacific Oscillation (IPO), operate on multidecadal scales within the subtropical and extratropical oceans (Henley et al., 2015; Knight et al., 2006). Recently, some share of these multidecadal variability modes was attributed to being influenced by external anthropogenic aerosols (He et al., 2023; Qin et al., 2020)(see Sect. 1.3.3); this is still debated, as these oscillations also display natural variability probably linked to tropical ocean dynamics (Henley et al., 2015). Previous studies have also researched how anthropogenic forcing – greenhouse gases and aerosols – modulate the mechanisms driving the hydroclimate of SAm (Hua et al., 2019); however, other knowledge gaps must be addressed regarding the role of volcanic aerosols. Moreover, the influence of these long-term SST phenomena is associated with variations in the interhemispheric temperature gradient (IHTG; Friedman et al., 2020). The IHTG modulates the poleward redistribution of energy through shifts in the meridional atmospheric circulation, i.e. the Hadley cell and associated branches such as the ITCZ (Brönnimann et al., 2015; Schneider et al., 2014). Consequently, tropical precipitation variability – including SAm's rainfall – is also linked to multidecadal and forced variability phenomena.

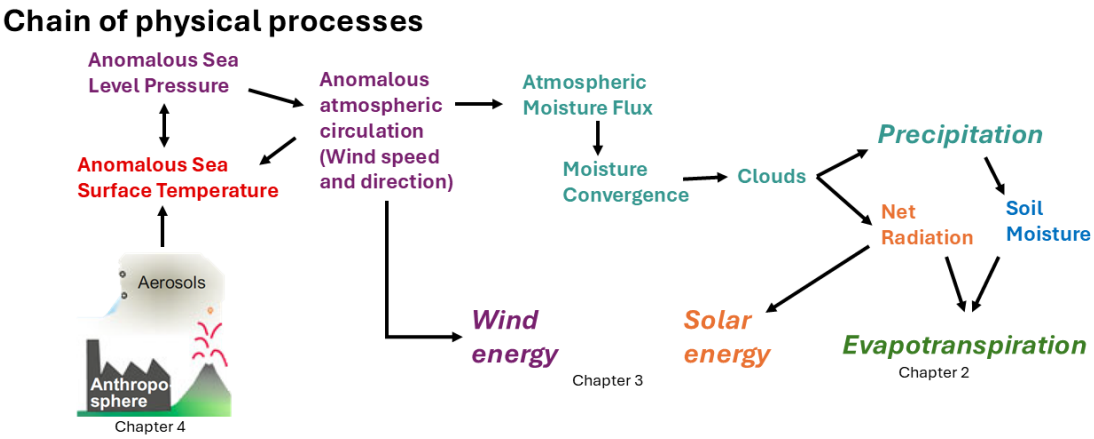

FIGURE 1.1: Schematic figure of the chain of physical processes that impact ecology and socio-economic variables. The chain starts at the coupling between SST and SLP; external forcing elements, such as aerosols, modulate the chain by influencing the radiation balance and surface temperature.

1.3 Chain of physical processes - mechanisms

The ocean-atmospheric modes are expected to enforce variability through a chain of progressive physical processes (Fig. 1.1), often referred to as a mechanism (Brönnimann, 2015). The chain begins with coupled SST and SLP anomalies, involving exchange of heat and moisture, convection, Gill-type responses, the wind-evaporation-SST feedback, and Ekman pumping (Gill, 1980; Mahajan et al., 2009; Priyanka et al., 2025). These coupled processes consolidate at seasonal scale since large-scale SST patterns change slowly due to the ocean's thermal inertia (Wang et al., 2013). The SLP anomalies modify regional atmospheric circulation – i.e. anomalies of wind direction and speed – triggering subsequent processes along the chain. Altered winds modify the atmospheric moisture transport (VIMF), which then modulates the variability of regional moisture flux divergence (MDiv). The latter influences the local weather and is associated with other important variables for ecology and socio-economic dynamics (e.g. precipitation, radiation, temperature, among others).

How do the changes in the chain impact evapotranspiration (a variable connected to ecology, agriculture and heat)? How do they impact solar and wind energy? How might an external factor, such as aerosol forcing, influence the mechanisms modulating the precipitation? In the following, we detail the steps down the chain that impact the hydroclimatology and have other socio-economic impacts.

1.3.1 Processes modulating South America's evapotranspiration

After the ocean-atmospheric modes seasonally change the VIMF, MDiv, clouds, rainfall and radiation (local weather), the chain continues with land-surface processes. Precipitation then affects soil moisture, and afterwards, the soil moisture and the net radiation locally control evapotranspiration (Fig. 1.1). This is described in chapter 2, where our results show how the chain is also mediated by the climatological cycle of the evapotranspiration regime (i.e. water- or energy-limited). The chapter focuses on the seasonal to interannual effects of the AMM and Atl3 modes and how they have conjoint impacts with ENSO on the evapotranspiration across South America. It also discusses plant physiological processes, partially considered in the used

datasets, as well as other phenomena such as moisture recycling and the influence of the AMO in the AMM as an Earth system driver of the chain.

1.3.2 Processes modulating South America's potential wind and solar energy

Likewise, after the modes influence wind speed and local weather, the chain continues with the impacts on wind and solar energy production (Fig. 1.1). Chapter 3 examines the seasonal to interannual variability of both energy sources, focusing on their links with ENSO and the AMM. The chapter also analyses the complementarity between both sources of energy, for long-term planning, and under the influence of the interannual modes for energy management. Complementarity with hydropower is briefly discussed. Furthermore, the chapter discusses how the understanding of these mechanisms can enhance energy forecasts, and also how the multidecadal modes or phenomena at shorter time scales might also have impacts on renewable energy production.

1.3.3 Aerosols influencing the ocean-atmospheric modes, global circulation and precipitation in South America

The SST-related onset of the chain might also be forced by external factors – such as aerosols – through altered surface radiation and temperature. Aerosols perturb the energy cycle mainly through absorption and scattering of solar radiation (Li et al., 2022), which then reduces the energy reaching the surface, energy uptake, and thus the surface cools. These changes affect SSTs and SLP, which is the initial coupled element of the chain (the coupled ocean-atmospheric modes; Fig. 1.1), and subsequently alter the mechanisms affecting the regional and global atmospheric circulation (i.e. the Hadley cell). Hence, we study the effects of aerosols on the chain of processes around SAm, looking at features of the ITCZ and the impacts on tropical precipitation (chapter 4). We investigate the changes in VIMF, MDiv and precipitation during two periods with high concentrations of aerosols in the troposphere and stratosphere at the interannual and decadal scales. The chosen periods represent notable examples of stratospheric injections of volcanic aerosols and decadal anthropogenic-related trends in tropospheric aerosols.

All chapters in our thesis consider the described chain of processes to understand how SAm is affected. They look at how changes in individual chain components are associated with specific impacts on the hydroclimatology, the renewable energy (as a socio-economic impact), or the modulation of the chain by an external forcing. For example, they all include how the altered VIMF influences weather and thus how the modes are associated with impacts. The conceptual framework of the chain is both a research outcome and a unifying structure across chapters, visually representing the underlying physical mechanisms involved in the teleconnections.

1.4 Objective, questions, and outline of this thesis

The objective of this thesis is to identify the physical mechanisms that are associated with some climate variability in tropical SAm, and some external forcing modulating those mechanisms. We focus on the seasonal to interannual scale and on variables associated with ecological and socio-economic impacts. With this objective, we intend to answer specific questions related to the topics mentioned in sections 1.3.1, 1.3.2 and 1.3.3, and to partially answer the following broad question.

Which phenomena and which related mechanisms explain some share of the seasonal to interannual hydroclimate variability in tropical South America and its potential solar and wind energy variability?

In chapter 2, we intend to tackle the following specific questions related to the evapotranspiration variability:

- Where and in which season is the evapotranspiration dominated by a water- or energy-limited regime?
- How do the Atlantic modes drive anomalous atmospheric circulation and influence the variability in local atmospheric conditions, and how do they then affect the local controllers and thus affect evapotranspiration?
- Where do the dynamics and, thus, the impacts of the Atlantic modes overlap with those of ENSO in time and space?

In chapter 3, we address the following specific questions associated with the solar and wind energy variability in tropical SAm:

- Which ocean-atmospheric modes are associated with the inter-annual variability of solar and wind energy at collocated high energy availability regions (energy hubs)?
- Which mechanisms influence the weather over the energy hubs and thus modulate the renewable energy production?
- In which seasons do both sources of renewables complement each other under the influence of the ocean-atmospheric modes?

In chapter 4, we explore the following questions associated with the forced interannual to decadal variability of precipitation in tropical SAm:

- In which regions did precipitation change in the early 19th and late 20th centuries, associated with the high aerosol concentration?
- When did global changes in aerosol optical depth and surface temperature manifest in the regional ocean-atmospheric modes?
- How did the altered elements of the chain modify the regional circulation, and affected the subsequent elements of the chain around SAm (e.g. the VIMF and the MDiv) and the precipitation?

After this introduction, the thesis is structured into the aforementioned three main chapters. We restate the conclusions of the chapters and present further research questions based on our conclusions in chapter 5.

References

Andrian, L. G., Osman, M., & Vera, C. S. (2024). The role of the Indian Ocean Dipole in modulating the austral spring ENSO teleconnection to the Southern Hemisphere. *Weather and Climate Dynamics*, *5*(4), 1505–1522. https://doi.org/10.5194/wcd-5-1505-2024

Arias, P. A., Garreaud, R., Poveda, G., Espinoza, J. C., Molina-Carpio, J., Masiokas, M., Viale, M., Scaff, L., & van Oevelen, P. J. (2021). Hydroclimate of the Andes Part II: Hydroclimate Variability and Sub-Continental Patterns. *Frontiers in Earth Science*, *8*(February), 1–25. https://doi.org/10.3389/feart.2020.505467

Arias, P. A., Martínez, J. A., Mejía, J. D., Pazos, M. J., Espinoza, J. C., & Wongchuig-Correa, S. (2020). Changes in Normalized Difference Vegetation Index in the Orinoco and Amazon River Basins: Links to Tropical Atlantic Surface Temperatures. *Journal of Climate*, *33*(19), 8537–8559. https://doi.org/10.1175/JCLI-D-19-0696.1

Armstrong McKay, D. I., Staal, A., Abrams, J. F., Winkelmann, R., Sakschewski, B., Loriani, S., Fetzer, I., Cornell, S. E., Rockström, J., & Lenton, T. M. (2022). Exceeding 1.5°C global warming could trigger multiple climate tipping points. *Science*, *377*(6611). https://doi.org/10.1126/science.abn7950

Bayer, A. M., Danysh, H. E., Garvich, M., Gonzálvez, G., Checkley, W., Álvarez, M., & Gilman, R. H. (2014). An unforgettable event: a qualitative study of the 1997–98 El Niño in northern Peru. *Disasters*, *38*(2), 351–374. https://doi.org/10.1111/disa.12046

Brönnimann, S. (2007). Impact of El Niño–Southern Oscillation on European climate. *Reviews of Geophysics*, *45*(3). https://doi.org/10.1029/2006RG000199

Brönnimann, S. (2015). *Climatic Changes Since 1700* (Vol. 55). Springer International Publishing. https://doi.org/10.1007/978-3-319-19042-6

Brönnimann, S., Fischer, A. M., Rozanov, E., Poli, P., Compo, G. P., & Sardeshmukh, P. D. (2015). Southward shift of the northern tropical belt from 1945 to 1980. *Nature Geoscience*, *8*(12), 969–974. https://doi.org/10.1038/ngeo2568

Brönnimann, S., Franke, J., Nussbaumer, S. U., Zumbühl, H. J., Steiner, D., Trachsel, M., Hegerl, G. C., Schurer, A., Worni, M., Malik, A., Flückiger, J., & Raible, C. C. (2019). Last phase of the Little Ice Age forced by volcanic eruptions. *Nature Geoscience*, *12*(8), 650–656. https://doi.org/10.1038/s41561-019-0402-y

Builes-Jaramillo, A., Yepes, J., Salas, H. D., Bedoya-Soto, J. M., Rivera, P., Valencia, J., & Carmona, A. M. (2025). Intraseasonal Oscillations and Hydroclimate of Northern South America, Central America and Mexico. *International Journal of Climatology*, 1–17. https://doi.org/10.1002/joc.8848

Bustos, C., Watts, D., & Ayala, M. (2017). Financial risk reduction in photovoltaic projects through ocean-atmospheric oscillations modeling. *Renewable and Sustainable Energy Reviews*, *74*(March), 548–568. https://doi.org/10.1016/j.rser.2016.11.034

Cai, W., McPhaden, M. J., Grimm, A. M., Rodrigues, R. R., Taschetto, A. S., Garreaud, R. D., Dewitte, B., Poveda, G., Ham, Y. G., Santoso, A., Ng, B., Anderson, W., Wang, G., Geng, T., Jo, H. S., Marengo, J. A., Alves, L. M., Osman, M., Li, S., … Vera, C. (2020). Climate impacts of the El Niño–Southern Oscillation on South America. *Nature Reviews Earth and Environment*, *1*(4), 215–231. https://doi.org/10.1038/s43017-020-0040-3

Cai, W., Wu, L., Lengaigne, M., Li, T., McGregor, S., Kug, J. S., Yu, J. Y., Stuecker, M. F., Santoso, A., Li, X., Ham, Y. G., Chikamoto, Y., Ng, B., McPhaden, M. J., Du, Y., Dommenget, D., Jia, F., Kajtar, J. B., Keenlyside, N., … Chang, P. (2019). Pantropical climate interactions. *Science*, *363*(6430). https://doi.org/10.1126/science.aav4236

Castellanos, E., Lemos, M., Astigarraga, L., Chacón, N., Cuvi, N., Huggel, C., Miranda, L., Moncassim Vale, M., Ometto, J., Peri, P., Postigo, J., Ramajo, L., Roco, L., & Rusticucci, M. (2023, June). Central and South America. In *Climate*

change 2022 – impacts, adaptation and vulnerability (pp. 1689–1816). Cambridge University Press. https://doi.org/10.1017/9781009325844.014

Compo, G. P., & Sardeshmukh, P. D. (2010). Removing ENSO-related variations from the climate record. *Journal of Climate*, *23*(8), 1957–1978. https://doi.org/10.1175/2009JCLI2735.1

Engeland, K., Borga, M., Creutin, J. D., François, B., Ramos, M. H., & Vidal, J. P. (2017). Space-time variability of climate variables and intermittent renewable electricity production – A review. *Renewable and Sustainable Energy Reviews*, *79*(May 2016), 600–617. https://doi.org/10.1016/j.rser.2017.05.046

FAO. (2025). Food and Agriculture Organization of the United Nations statistical database. https://www.fao.org/faostat/en/%7B%5C#%7Dhome

Fernandes, K., Giannini, A., Verchot, L., Baethgen, W., & Pinedo-Vasquez, M. (2015). Decadal covariability of Atlantic SSTs and western Amazon dry-season hydroclimate in observations and CMIP5 simulations. *Geophysical Research Letters*, *42*(16), 6793–6801. https://doi.org/10.1002/2015GL063911

Feron, S., Cordero, R. R., Damiani, A., MacDonell, S., Pizarro, J., Goubanova, K., Valenzuela, R., Wang, C., Rester, L., & Beaulieu, A. (2024). South America is becoming warmer, drier, and more flammable. *Communications Earth and Environment*, *5*(1), 1–10. https://doi.org/10.1038/s43247-024-01654-7

Friedman, A. R., Hegerl, G. C., Schurer, A. P., Lee, S. Y., Kong, W., Cheng, W., & Chiang, J. C. (2020). Forced and unforced decadal behavior of the interhemispheric SST contrast during the instrumental period (1881–2012): Contextualizing the late 1960s–early 1970s shift. *Journal of Climate*, *33*(9), 3487–3509. https://doi.org/10.1175/JCLI-D-19-0102.1

García-Serrano, J., Cassou, C., Douville, H., Giannini, A., & Doblas-Reyes, F. J. (2017). Revisiting the ENSO teleconnection to the tropical North Atlantic. *Journal of Climate*, *30*(17), 6945–6957. https://doi.org/10.1175/JCLI-D-16-0641.1

Garreaud, R. D., Vuille, M., Compagnucci, R., & Marengo, J. (2009). Present-day South American climate. *Palaeogeography, Palaeoclimatology, Palaeoecology*, *281*(3-4), 180–195. https://doi.org/10.1016/j.palaeo.2007.10.032

Gill, A. E. (1980). Some simple solutions for heat-induced tropical circulation. *Quarterly Journal of the Royal Meteorological Society*, *106*(449), 447–462. https://doi.org/10.1002/qj.49710644905

Gonzalez-Salazar, M., & Poganietz, W. R. (2021). Evaluating the complementarity of solar, wind and hydropower to mitigate the impact of El Niño Southern Oscillation in Latin America. *Renewable Energy*, *174*, 453–467. https://doi.org/10.1016/j.renene.2021.04.048

He, C., Clement, A. C., Kramer, S. M., Cane, M. A., Klavans, J. M., Fenske, T. M., & Murphy, L. N. (2023). Tropical Atlantic multidecadal variability is dominated by external forcing. *Nature*, *622*(October). https://doi.org/10.1038/s41586-023-06489-4

Henley, B. J., Gergis, J., Karoly, D. J., Power, S., Kennedy, J., & Folland, C. K. (2015). A Tripole Index for the Interdecadal Pacific Oscillation. *Climate Dynamics*, *45*(11-12), 3077–3090. https://doi.org/10.1007/s00382-015-2525-1

Hoyos, I., Cañón-Barriga, J., Arenas-Suárez, T., Dominguez, F., & Rodríguez, B. A. (2019). Variability of regional atmospheric moisture over Northern South America: patterns and underlying phenomena. *Climate Dynamics*, *52*(1-2), 893–911. https://doi.org/10.1007/s00382-018-4172-9

Hua, W., Dai, A., Zhou, L., Qin, M., & Chen, H. (2019). An Externally Forced Decadal Rainfall Seesaw Pattern Over the Sahel and Southeast Amazon. *Geophysical Research Letters*, *46*(2), 923–932. https://doi.org/10.1029/2018GL081406

Kim, H., Vitart, F., & Waliser, D. E. (2018). Prediction of the Madden-Julian oscillation: A review. *Journal of Climate*, *31*(23), 9425–9443. https://doi.org/10.1175/JCLI-D-18-0210.1

Knight, J. R., Folland, C. K., & Scaife, A. A. (2006). Climate impacts of the Atlantic multidecadal oscillation. *Geophysical Research Letters*, *33*(17), 2–5. https://doi.org/10.1029/2006GL026242

Li, J., Carlson, B. E., Yung, Y. L., Lv, D., Hansen, J., Penner, J. E., Liao, H., Ramaswamy, V., Kahn, R. A., Zhang, P., Dubovik, O., Ding, A., Lacis, A. A., Zhang, L., & Dong, Y. (2022). Scattering and absorbing aerosols in the climate system. *Nature Reviews Earth & Environment*, *3*(6), 363–379. https://doi.org/10.1038/s43017-022-00296-7

Mahajan, S., Saravanan, R., & Chang, P. (2009). The role of the wind-evaporation-sea surface temperature (WES) feedback in air-sea coupled tropical variability. *Atmospheric Research*, *94*(1), 19–36. https://doi.org/10.1016/j.atmosres.2008.09.017

Martín-Rey, M., Rodríguez-Fonseca, B., Polo, I., & Kucharski, F. (2014). On the Atlantic–Pacific Niños connection: a multidecadal modulated mode. *Climate Dynamics*, *43*(11), 3163–3178. https://doi.org/10.1007/s00382-014-2305-3

Merz, B., Blöschl, G., Vorogushyn, S., Dottori, F., Aerts, J. C., Bates, P., Bertola, M., Kemter, M., Kreibich, H., Lall, U., & Macdonald, E. (2021). Causes, impacts and patterns of disastrous river floods. *Nature Reviews Earth and Environment*, *2*(9), 592–609. https://doi.org/10.1038/s43017-021-00195-3

Mishra, A., Mukherjee, S., Merz, B., Singh, V. P., Wright, D. B., Villarini, G., Paul, S., Kumar, D. N., Khedun, C. P., Niyogi, D., Schumann, G., & Stedinger, J. R. (2022). An Overview of Flood Concepts, Challenges, and Future Directions. *Journal of Hydrologic Engineering*, *27*(6), 1–30. https://doi.org/10.1061/(ASCE)HE.1943-5584.0002164

Mishra, A. K., & Singh, V. P. (2010). A review of drought concepts. *Journal of Hydrology*, *391*(1-2), 202–216. https://doi.org/10.1016/j.jhydrol.2010.07.012

Paik, S., Min, S. K., Iles, C. E., Fischer, E. M., & Schurer, A. P. (2020). Volcanic-induced global monsoon drying modulated by diverse El Ninõ responses. *Science Advances*, *6*(21), 1–8. https://doi.org/10.1126/sciadv.aba1212

Poveda, G., Jaramillo, L., & Vallejo, L. F. (2014). Seasonal precipitation patterns along pathways of South American low-level jets and aerial rivers. *Water Resources Research*, *50*(1), 98–118. https://doi.org/10.1002/2013WR014087

Priyanka, K., Sarangi, R. K. K., Jeyapragash, D., & Saravanakumar, A. (2025). Ekman pumping dynamics and atmospheric aerosol concentration enhancing nitrogen and carbon uptake in the Arabian Sea during winter. *Ocean Dynamics*, *75*(4), 33. https://doi.org/10.1007/s10236-025-01678-3

Qin, M., Dai, A., & Hua, W. (2020). Aerosol-forced multidecadal variations across all ocean basins in models and observations since 1920. *Science Advances*, *6*(29), 1–8. https://doi.org/10.1126/sciadv.abb0425

Rodrigues, R. R., & McPhaden, M. J. (2014). Why did the 2011-2012 La Niña cause a severe drought in the Brazilian Northeast? *Geophysical Research Letters*, *41*(3), 1012–1018. https://doi.org/10.1002/2013GL058703

Schneider, T., Bischoff, T., & Haug, G. H. (2014). Migrations and dynamics of the intertropical convergence zone. *Nature*, *513*(7516), 45–53. https://doi.org/10.1038/nature13636

Thual, S., & Dewitte, B. (2023). ENSO complexity controlled by zonal shifts in the Walker circulation. *Nature Geoscience*, *16*(April). https://doi.org/10.1038/s41561-023-01154-x

Timmermann, A., An, S. I., Kug, J. S., Jin, F. F., Cai, W., Capotondi, A., Cobb, K., Lengaigne, M., McPhaden, M. J., Stuecker, M. F., Stein, K., Wittenberg, A. T., Yun, K. S., Bayr, T., Chen, H. C., Chikamoto, Y., Dewitte, B., Dommenget, D., Grothe, P., … Zhang, X. (2018). El Niño–Southern Oscillation complexity. *Nature*, *559*(7715), 535–545. https://doi.org/10.1038/s41586-018-0252-6

Ummenhofer, C. C., & Meehl, G. A. (2017). Extreme weather and climate events with ecological relevance: a review. *Philosophical Transactions of the Royal Society B: Biological Sciences*, *372*(1723), 20160135. https://doi.org/10.1098/rstb.2016.0135

Vallès-Casanova, I., Lee, S.-K., Foltz, G. R., & Pelegrí, J. L. (2020). On the Spatiotemporal Diversity of Atlantic Niño and Associated Rainfall Variability Over West Africa and South America. *Geophysical Research Letters*, *47*(8), 1–10. https://doi.org/10.1029/2020GL087108

Van Loon, A. F. (2015). Hydrological drought explained. *WIREs Water*, *2*(4), 359–392. https://doi.org/10.1002/wat2.1085

Vogel, E., Donat, M. G., Alexander, L. V., Meinshausen, M., Ray, D. K., Karoly, D., Meinshausen, N., & Frieler, K. (2019). The effects of climate extremes on global agricultural yields. *Environmental Research Letters*, *14*(5). https://doi.org/10.1088/1748-9326/ab154b

Wang, C., Xie, S.-P., & Carton, J. A. (2013, March). A Global Survey of Ocean-Atmosphere Interaction and Climate Variability. https://doi.org/10.1029/147GM01

Williams, I. N., & Patricola, C. M. (2018). Diversity of ENSO Events Unified by Convective Threshold Sea Surface Temperature: A Nonlinear ENSO Index. *Geophysical Research Letters*, *45*(17), 9236–9244. https://doi.org/10.1029/2018GL079203

Williams, P. D., Alexander, M. J., Barnes, E. A., Butler, A. H., Davies, H. C., Garfinkel, C. I., Kushnir, Y., Lane, T. P., Lundquist, J. K., Martius, O., Maue, R. N., Peltier, W. R., Sato, K., Scaife, A. A., & Zhang, C. (2017). A Census of Atmospheric Variability From Seconds to Decades. *Geophysical Research Letters*, *44*(21), 11, 201–11, 211. https://doi.org/10.1002/2017GL075483

Zeigler, M., & Truitt Nakata, G. (2014, April). *The Next Global Breadbasket: How Latin America Can Feed the World: A Call to Action for Addressing Challenges & Developing Solutions*. Inter-American Development Bank. https://doi.org/10.18235/0012835

Zhao, M., & Running, S. W. (2010). Drought-Induced Reduction in Global Terrestrial Net Primary Production from 2000 Through 2009. *Science*, *329*(5994), 940–943. https://doi.org/10.1126/science.1192666

Chapter 2

An Atlantic influence on evapotranspiration in the Orinoco and Amazon basins

Nicolás Duque-Gardeazabal[1,2], Andrew R.Friedman[1,2,3], Stefan Brönnimann[1,2]

1. Oeschger Centre for Climate Change Research, University of Bern, Bern, Switzerland.
2. Institute of Geography, University of Bern, Bern, Switzerland.
3. now at Laboratoire de Météorologie Dynamique / Institute Pierre-Simon Laplace, Paris, France

Article:

Duque-Gardeazabal, N., Friedman, A. R., and Brönnimann, S. (2025). An Atlantic influence on evapotranspiration in the Orinoco and Amazon basins. *Hydrology and Earth System Sciences*, 29(14), 3277–3295.https://doi.org/10.5194/hess-29-3277-2025

Abstract

Tropical South America's hydroclimate is influenced by ocean-atmospheric variability modes (drivers of climate variability). It is still not known which physical mechanisms teleconnect the Atlantic modes of variability with South America's soil moisture, net radiation and terrestrial evaporation (evapotranspiration). Understanding these mechanisms is essential to predict the response of ecosystems. This study uses composites of reanalysis and satellite data to identify the processes linking land-surface anomalies and ocean-atmospheric modes. It estimates the control soil moisture and net radiation impose on evapotranspiration (categorised as water- or energy-limited regimes). It shows that these two local controllers of evapotranspiration are influenced by the position of the Intertropical Convergence Zone (ITCZ). However, the evapotranspiration anomalies are driven by the phase of each climate mode which alter water and radiation availability. The Atlantic Meridional Mode (AMM) generates cross-equatorial wind anomalies that affect moisture convergence, which in turn modify the cloud cover, precipitation, soil moisture, radiation availability and hence evapotranspiration. The anomalies have important geographical differences depending on the season analysed; they migrate from the east in Austral autumn towards the central Amazon and western Orinoco in Austral spring. The Atlantic Niño Equatorial mode (Atl3) affects evapotranspiration in the Guianas and eastern Orinoco by means of pressure and trade wind variability, which in turn affect local hydrometeorological conditions and evapotranspiration. Both Atlantic modes mainly impact regions different from those impacted by El Niño/Southern Oscillation (ENSO), although northeast Brazil and the Guianas might experience overlapping effects. Therefore, these ocean-atmospheric modes impact the water, energy and carbon cycles; they might influence regional climate extremes (e.g. droughts and floods), and are critical for achieving sustainable development goals (SDGs).

2.1 Introduction

The hydroclimate of tropical South America is strongly influenced by ocean-atmospheric variability modes (climate drivers), for instance, El Niño/Southern Oscillation (ENSO) (Cai et al., 2020; Garreaud et al., 2009; Grimm & Zilli, 2009). Other sources of seasonal variability stem from other ocean basins (e.g. the Atlantic, Indian Ocean, etc), and at other temporal scales from Madden-Julian Oscillation or local features like topography or land-atmosphere interactions (Cai et al., 2019; Pabón & Dorado, 2008). The modes cause impacts through atmospheric circulation anomalies and hence drive local atmospheric conditions; the latter enforces hydrological variability, which is evidenced by anomalies of precipitation, soil moisture (SM), surface temperature, evapotranspiration and streamflow. The atmospheric anomalies might also influence extreme events (e.g. droughts and floods)(Merz et al., 2021; Mishra & Singh, 2010), and their consideration in long-term planning is critical for achieving sustainable development.

Among the hydrological fluxes, terrestrial evaporation is key for water, energy and carbon cycles (Wang & Dickinson, 2012). This flux mainly consists of evaporation from soil, interception and plant transpiration (hereafter all jointly referred as evapotranspiration - ET). Limitations in ET influence growth processes and hence carbon uptake, previous studies have linked net primary or biome production variability to SM-atmosphere feedbacks and climate/earth system drivers, e.g. through climate-driven droughts (Humphrey et al., 2021; Nemani et al., 2003; Zhao & Running, 2010). There is evidence that individual extreme weather events can coerce plant phenology, for instance on flowering, leaf senescence and plant growth (Ummenhofer & Meehl, 2017). Therefore, to predict ecosystem activity, it is essential to identify the mechanisms of internal climate variability drivers that enforce a response in ET. Moreover, estimating the response of ET to climate variability drivers is also necessary to unravel the effects of climate change on hydrology (IPCC, 2021), and to estimate irrigation requirements (Kaune et al., 2019).

In the following, we consider oceanic variability modes in the Pacific and Atlantic as drivers of the climate variability in the Amazon and Orinoco basins (Lübbecke et al., 2018). Some studies statistically looked at the Pacific and Atlantic joint effects on precipitation (Gu & Adler, 2009; Ronchail et al., 2002). Others studied the interannual changes in moisture transport dynamics – imposed by oceanic climatic drivers – and their associated rainfall anomalies over South America (Hoyos et al., 2019; Ruiz-Vásquez et al., 2024). Atlantic trade winds strength and the precipitation anomalies are related to ocean variability modes such as: the Tropical North Atlantic mode (TNA)(Arias et al., 2015, 2020; Enfield, 1996), the Atlantic Meridional Mode (AMM) (Chiang et al., 2002; Drumond et al., 2014; Fernandes et al., 2015; Paccini et al., 2021; Rodrigues & McPhaden, 2014) and the Atlantic Niño Equatorial mode (Atl3) (Ruiz-Barradas et al., 2000; Torralba et al., 2015; Vallès-Casanova et al., 2020). The Atlantic modes tend to be active and peak between the Austral autumn and spring – MAM, JJA and SON (the initial letters of the months) – contrary to ENSO which peaks at the end of the year (SON and D(0)JF(+1)). These Atlantic modes might have contributed to northeast Brazil droughts and the Magdalena River floods in 2011-2012, as well as the Amazon droughts in 2005 and 2010 (Lopes et al., 2016; Marengo & Espinoza, 2016). Although the Atlantic modes are associated with ENSO through atmospheric bridges or extratropical pathways (Casselman et al., 2023; Compo & Sardeshmukh, 2010; García-Serrano et al., 2017; Martín-Rey et al., 2014), each of them has specific regional impacts on sea-level pressure (SLP) and hence on atmospheric circulation.

However, the variability of evapotranspiration has received less attention than

precipitation. Previous research has established SM and Net Radiation (Rn) as the primary local controllers of ET (Hirschi et al., 2014; Seneviratne et al., 2010); consequently, ET is classified into two regimes: water- or energy-limited. The annual cycle and the location of the regimes are not known in South America and are important for understanding ET variability. Some studies have statistically investigated the teleconnections of ENSO (Le & Bae, 2020; Miralles et al., 2014; Moura et al., 2019) or other climate drivers with the ET around the world (Martens et al., 2018), but the physical causes for these connections are not known. Specifically, it is not known how the interannual changes in moisture transport impact net radiation. In our paper, we focus on the Atlantic modes, which have received less attention in the literature. Moisture recycling is another factor that can impact surface radiation, but previous studies have focused on its impact on regional and distant precipitation rather than radiation (Staal et al., 2018; van der Ent & Savenije, 2011; Wang-Erlandsson et al., 2018; Zemp et al., 2014). Other research has looked at the influence of Amazon soil moisture memory on ET (Zanin et al., 2024) or how anomalous moisture transport from the TNA affects SM and vegetation indices (Arias et al., 2020), but other Atlantic modes have been overlooked.

Consequently, it is still not known how the variations in regional atmospheric circulation – driven by the Atlantic modes – alter local continental atmospheric conditions and afterwards affect net surface radiation and soil moisture, the two key local controllers of ET. We refer to the latter as the physical mechanisms of the teleconnection, which consist of a chain of progressive physical processes. Ecological processes respond to the variability of hydrometeorological conditions (Eagleson, 2013); by understanding the mechanisms leading to that variability, the community can increase the potential predictability of ecosystem activity. Therefore, this study aims to investigate the physical causes of the link between the AMM and Atl3 with ET in tropical South America, at seasonal scale. Other drivers (such as the Indian Ocean Dipole mode, the Atlantic Multidecadal Oscillation (AMO), etc.) are excluded from our study (see Sect. 2.3 and 2.5). Moisture recycling is only briefly discussed in Sect. 2.5. We aim to answer the following questions:

1. Where and in which season is the evapotranspiration dominated by a water- or energy-limited regime?
2. How do the Atlantic modes drive anomalous atmospheric circulation and influence the variability in local atmospheric conditions, and how do they then affect the local controllers and thus affect evapotranspiration?
3. Where do the dynamics and, thus, the impacts of the Atlantic modes overlap with those of ENSO in time and space?

2.2 Data

This study uses net radiation, soil moisture (SM) and ET, as well as atmospheric circulation variables, such as SLP, winds, moisture transport, convergence and rainfall. We use those atmospheric variables because ocean-atmospheric modes drive the regional atmospheric circulation, which afterwards influences the local ET controllers. Sea Surface Temperature Anomalies (SSTAs) are used to identify the ocean-atmospheric modes (Sect. 2.3). All datasets are downloaded at monthly time scale and used between Dec-1979 and Nov-2020 (except for satellite-based soil moisture, details in Sect. 2.2.2); they are aggregated at seasonal scale and analysed for each season individually and synchronously. The aggregation method for all variables is

TABLE 2.1: Overview of the datasets used in this study. ERA5 is described in Hersbach et al. (2020), and ERA5-Land is in Muñoz-Sabater et al. (2021) and ECMWF (2023)

	Reanalysis			Satellite		
Variable	Dataset	Spatial resolution	Temporal resolution	Dataset	Spatial resolution	Temporal resolution
Sea Level Pressure	ERA5	0.25°	Monthly	-	-	-
Winds at 850 hPa			Monthly	-	-	-
Vertically Integrated Water Vapor Flux (VIMF)			Monthly	-	-	-
Moisture Divergence (MDiv)			Monthly	-	-	-
Precipitation	-	-	-	MSWEP v2.8 (Beck et al., 2019)	0.1°	Monthly
Net Surface Thermal Radiation	ERA5-Land	0.1°	Monthly	CLARA-A3 Cloud Area Fraction (Karlsson et al., 2023)	0.25°	Monthly
Net Surface Solar Radiation			Monthly			
Soil Moisture (volumetric water content 1st soil layer)			Monthly	ESA-CCI-SM v08.1 (Gruber et al., 2019)	0.25°	Daily (Aggregated to Monthly)
Total Evaporation			Monthly	GLEAM v3.8a (Martens et al., 2017)	0.25°	Monthly
Sea Surface Temperature Anomalies	ERSST v5 (Huang et al., 2017)				2°	Monthly
	HadSST v4.0.1 (Kennedy et al., 2019)				5°	Monthly

the average of the three monthly values, except for precipitation and ET, where we use the sums (Duque-Gardeazabal, 2025).

Satellite and reanalysis data sources each have strengths and limitations. Satellite data can provide some of the needed data mainly over land but moisture transport is not available from this source. Reanalysis data are considered physically-based interpolations of observations and provide atmospheric variables that satellites do not directly acquire. Satellite-based datasets have difficulties in measuring soil moisture over densely forested canopies (Beck et al., 2021). Errors in the root zone SM compromise the estimation of plant water stress and, thus, the skill of the ET estimate. On the other hand, simulations of ET which ingest reanalysis outputs might inherit their biases (Gebrechorkos et al., 2024; Valencia et al., 2023). Although the performance of both data sources has improved in recent years (Beck et al., 2021; Xie et al., 2024), their estimates remain uncertain, and confidence in their inter-annual dynamics rests on the fact that the analysed signals are evident in independent datasets. Therefore, we look for consistency in the dynamics of both sources of information; we do not regrid and do not merge any datasets because we do not perform operations between them. We display the datasets conjointly when necessary and analyse the dynamics unfolding in both data sources (Table 2.1).

We use SSTAs from the Extended Reconstructed SST version 5 (Huang et al., 2017) – which is used as the primary dataset – and the Hadley Center Sea Ice and SST version 4.0.1 (Kennedy et al., 2019). ERSST is at 2°, and HadSST is at 5° resolution.

2.2.1 Reanalysis

The European Center for Medium-range Weather Forecast (ECMWF) ERA5 reanalysis provides information on atmospheric variables that influence the local controllers of evapotranspiration and also relate to the dynamics of the coupled ocean-atmospheric modes (Hersbach et al., 2020). Monthly time series of winds, Vertically Integrated water vapour Flux (VIMF), mean SLP and vertically integrated Moisture

flux Divergence (MDiv) are taken from it. All atmospheric variables from ERA5 have 0.25° spatial resolution.

ERA5-Land is a land-surface simulation operationally forced by ERA5, which includes detailed modules on infiltration, four-layer physically-based soil water storage, plant water uptake, phenology and transpiration, and evaporation from soil and canopy interception (ECMWF, 2023; Muñoz-Sabater et al., 2021). From it, we download or derive the net surface radiation (Rn), the volumetric soil water content in the first soil layer (hereafter soil moisture - SM) and the total evaporation (hereafter also referred to as evapotranspiration - ET). All variables from ERA5-Land have 0.1° resolution.

2.2.2 Satellite

This research uses the Multi-Source Weighted-Ensemble Precipitation v2.8 (MSWEP) (Beck et al., 2019) with a spatial resolution of 0.1°. The dataset is created with rain gauges, satellite and reanalysis data. MSWEP uses ERA5 rainfall estimates mainly in the extratropics, whereas the ingested satellite data is given stronger weight in the tropics.

In addition we use three satellite-based datasets: the European Space Agency Climate Change Initiative for Soil Moisture v08.1 (ESI-CCI-SM) (Gruber et al., 2019), total evaporation from the Global Land Evaporation Amsterdam Model v3.8a (GLEAM) (Martens et al., 2017), and the EUMETSAT CLARA-A3 cloud area fraction as a proxy for net radiation (Karlsson et al., 2023), all of them at 0.25° resolution. ESA-CCI-SM was downloaded at daily resolution and transformed to monthly values by averaging the days within each month as long as the month had at least four values; the remaining spatial gaps were not filled and were excluded from calculations. GLEAM uses a three-layer conceptual root zone soil module from which vegetation can access water (which considers ESA-CCI-SM assimilation where available). It includes a module for plant stress based on SM and vegetation phenology, and it also provides evaporation from interception and bare soil. GLEAM uses ERA5 radiation as forcing.

Some eddy-covariance towers are located in the Amazon and other places in South America; their measurements are –in general– after 2000. Baker et al. (2021) managed to use records from one tower with 19 years of data (1999-2017) but highlighted teh fact that the data in the other towers were only available for a few years (mainly between 1999 and 2006). Other global products based on FLUXNET towers, such as FLUXCOM (Jung et al., 2019), also have data after 2001. The short time series constrains the possibility of registering several events to analyse the effect of the climate modes (few degrees of freedom). The performance of GLEAM and ERA5-Land ET have been evaluated against eddy-covariance towers and have found correlations of around 0.6 and 0.7 for the Evergreen Broadleaf Forest ecoregion, respectively (Muñoz-Sabater et al., 2021; Xie et al., 2024). Therefore, we choose not to analyse eddy-covariance data and assume a fair performance of the other two sources.

2.3 Methods

Climate modes and their atmospheric circulation anomalies are expected to impact evapotranspiration through a chain of progressive physical processes. The processes start with anomalies in atmospheric circulation (coupled with SSTA), and moisture

transport (VIMF). Then, the latter changes moisture flux divergence (MDiv), affecting cloud formation; which simultaneously influences precipitation and radiation availability. Precipitation then affects soil moisture, and afterwards, the two local controllers impact evapotranspiration. However, the impacts of the chain are also mediated by the climatological cycle of the ET regime (water- or energy-limited). Consequently, our research starts by determining the annual cycle of the ET regime and of the local controllers (section 2.3.1). Then, we use composites to show how the chain unfolds with its final impacts on ET (section 2.3.2). Finally, we study the joint effects of the Atlantic modes and ENSO (section 2.3.3)(Duque-Gardeazabal, 2025). Moisture recycling is discussed in section 2.5.

2.3.1 Determining the location and annual cycle of local ET controllers

This study explores the two main local controllers of ET (soil moisture and net radiation) (Seneviratne et al., 2010), to afterwards search for the ocean-atmospheric modes that drive those controllers. SM and net radiation are classified by the slope of their multi-linear regression against evapotranspiration, using their seasonally standardised anomalies. This analysis can suggest whether the ET anomalies are associated with water availability or a radiation anomaly (ET regime). The multiple linear regression is then expressed as:

$$ET_{ij} = a_{ij} * SM_{ij} + b_{ij} * Rn_{ij} + C \tag{2.1}$$

where ET is the total evaporation, SM is the volumetric soil water content in the first layer, Rn is the surface net radiation, i refers to a specific longitude and j refers to a specific latitude. a and b are then the regression slope coefficients and C the intercept.

2.3.2 Composites

This study uses composite analysis to exemplify the state of the atmosphere and the land surface during the active phase of the Atlantic modes. The composites reveal the physical processes/mechanisms that connect the variables.

Coupled ocean-atmospheric modes are identified with SSTA indices. The SSTA are first detrended to exclude the effect of climate change from the analysis using a regression with de-seasonalised CO_2 ($R^2 = 0.92$, $p < 0.001$) (Thoning et al., 1989); the CO_2 concentration is used to consider its continuous change in the 20th and 21st century and to avoid subtracting the internal variability. We performed Principal Components Analysis over the detrended Atlantic SSTA and the resulting loadings were compared with the literature review (Fernandes et al., 2015; Ruiz-Barradas et al., 2000; Vallès-Casanova et al., 2020)(supplementary Figure S8). Correlation analysis between the principal components and hydrological variables revealed which modes possibly have an impact on South America (not shown). Other climate modes, such as the Indian Ocean Dipole, the AMO, etc., unfold over basins that are not close to our study area, and hence, they do not alter tropical South America's atmospheric circulation. Consequently, we discard them from our analysis. We define the Atlantic indices based on SSTA area-average boxes similar to the principal component loadings of the Atlantic SSTs (Figure S8).

- The AMM monthly index is defined as the difference between the spatially averaged tropical north Atlantic (TNA) SSTA [70°W-15°W]x[5°N-25°N] and the tropical south Atlantic (TSA) [40°W-0°W]x[25°S-5°S]; the spatial definition of the AMM comprises the TNA.

- The Atl3 monthly index is identified as the spatial average of eastern equatorial Atlantic SSTAs [20°W-0°]x[3°S-3°N].

To define the composite time steps, the phases of each mode are established based on the indices. The positive and negative phases are identified when their indices are above or below ±1 standard deviation, respectively, and otherwise are defined as neutral phase. The latter is defined individually for each season (indices time series in Figure S8). The asymmetric impacts of the modes are assessed by adding both extreme phases (positive plus negative), allowing the recognition of the different impacts exerted by each phase. The composite's statistical significance is assessed with the two-sample Student's two-tailed T-test, testing positive or negative phase against the neutral. Regarding precipitation, half of the cell's time series have skewed distributions (Shapiro-Wilk test; not shown). Thus, the Mann-Whitney U test is used instead. We did not find a significant correlation between evapotranspiration and CO_2. Nevertheless, ET time series are detrended with a linear trend to also exclude global warming (Zhang et al., 2016), before being used in the composites.

ENSO develops in the second semester and its peak season is DJF. On the other hand, the AMM is more active from February onwards but might last until SON (Yoon & Zeng, 2010), and the Atl3 is more active in JJA (Vallès-Casanova et al., 2020). In DJF, the AMM-associated anomalies are evident over the Atlantic but its effect over the continent is diluted (not shown). Therefore, we analyse the influence of the Atlantic modes from March to September.

2.3.3 Conjoint effect with ENSO

We also perform grid-wise partial correlation analysis between the two Atlantic indices, the El Niño Longitude Index (ELI)(Williams & Patricola, 2018), and evapotranspiration. The ELI considers the type of ENSO event (east or central Pacific). The purpose of this analysis is to find those regions that are driven by an Atlantic mode but might also have impacts from another mode when it is also active (i.e. simultaneously controlling the analysis by the effect of ENSO and the other Atlantic mode).

2.4 Results

2.4.1 Key local evapotranspiration controllers

The classification of the ET regime follows the migration of the Intertropical Convergence Zone (ITCZ, located in the southern Amazon in DJF and over northern Orinoco in JJA)(Fig. 2.1). The reason is associated with the heavy rainfall of the ITCZ which saturates the soils and influences the locations of the energy-limited regime. Panels (a) to (h) in Figure 2.1 show the slope coefficients of the regressions, which are then ranked in panels (i) to (l). Values below 0 indicate that the other independent variable is the main controller of ET. In MAM (Fig. 2.1a,e,i), the north-easterly winds bring moisture from the Atlantic and produce convergence and rainfall over the Amazon in such amounts that the soil saturates (and thus is above the soil's water field capacity), giving the conditions for energy-limited ET. However, the north of the Orinoco basin still behaves like a water-limited environment. As the ITCZ moves northward in JJA (Fig. 2.1b,f,j), the rainfall recharges SM, changing Orinoco's behaviour to energy-limited regime, whereas other regions transform from energy- to water-limited regimes, such as northeast Brazil and the southern Amazon. The

core of the Amazon rainforest is energy-limited throughout the year. In SON (Fig. 2.1c,g,k), the ITCZ begins to move southward, but the energy-limited regime is concentrated in the west of the Amazon. The east and southeast basins are still in a water-limited regime. The Orinoco still behaves as energy-limited even though this is the transition season from wet to dry. In DJF (Fig. 2.1d,h,l), the ET in the southern Amazon depends on the available energy, as the ITCZ has reached its southern continental location; above-average net radiation (Rn) would produce more ET. The energy-limited regions correspond to those where SM is above the soil's field capacity (ECMWF, 2023)(not shown), and not all of the continent is primarily controlled by variations in energy supply.

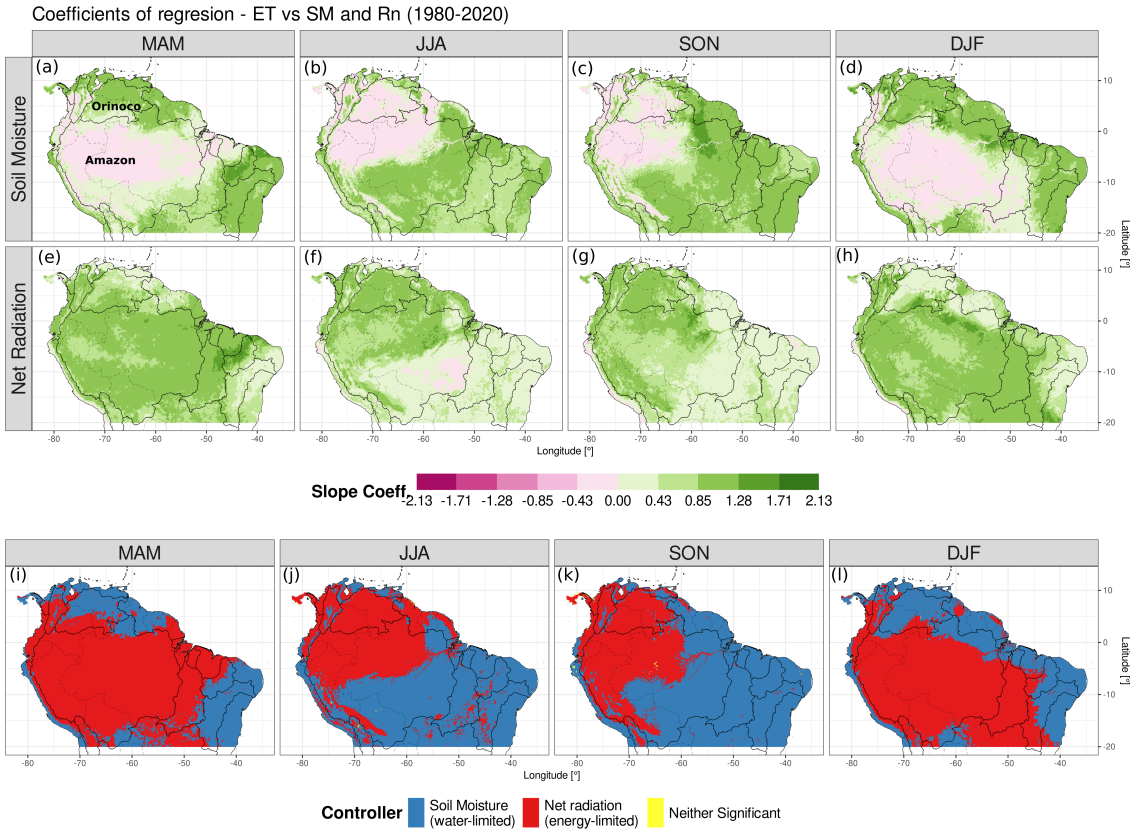

FIGURE 2.1: Classification of ERA5-Land evapotranspiration (ET) controller based on regression coefficients for each season. (a-d) multiple linear regression slope coefficient for soil moisture (SM), (e-h) slope coefficient for the net radiation (Rn) and (i-l) variable with the highest significant linear slope coefficient ($p \leq 0.05$). Panels are divided by the seasons (a,e,i) for MAM, (b,f,j) for JJA, (c,g,k) for SON and (d,h,l) for DJF. Black lines delineate the major river basins; the same boundaries are used in the following figures.

2.4.2 Chain of physical processes between the Atlantic modes and continental evapotranspiration

This section shows the composites of the variables involved in the chain (see Section 2.3). The steps in the chain repeat as long as a mode is active. However, the impacts have important geographical differences depending on the mode and the season analysed.

March - May (MAM) Austral Autumn

The Atlantic Meridional Mode (AMM) consists of a SST and SLP seesaw between the Tropical North and South Atlantic, creating cross-equatorial wind anomalies (see Figure S1 for SLP and 850 hPa winds composites). In Austral autumn, the positive phase redirects and advects moist air northward, towards the Orinoco, where it provokes positive convergence and precipitation anomalies (Fig. 2.2a). The location of the satellite precipitation and reanalysed convergence anomalies are consistent in both datasets. The positive convergence creates more clouds that then reduce net surface radiation (Fig. 2.2c). Soil moisture (SM) is impacted by the anomalous rainfall; Figure 2.2e shows that the SM anomalies in northern Orinoco are sensitive to the AMM in positive phase. ESA-CCI-SM is available for this region and shows similar dynamics (Fig. S2). The western and southern Amazon have SM anomalies lower than a 2% absolute value, as it is the rainy season and the soil is near saturation.

The evapotranspiration is impacted afterwards. The Orinoco behaves as water-limited (Fig. 2.1i) since this is the transition from dry to wet season, then the increase in rainfall and SM causes above-average ET (Fig. 2.2g). Over northeast Brazil, the positive phase produces divergence anomalies and less cloud cover (Fig. 2.2a and c). The latter increases radiation but enforces higher evapotranspiration than average due to the high SM availability above the soil's field capacity which allows the region to act as energy-limited (Fig. 2.1i and 2.2g). GLEAM independently shows similar results over northern Orinoco – more extended increase in ET – but over northeast Brazil the area with increased ET is smaller than in ERA5-Land and is surrounded by negative anomalies (Fig. S3). We will examine the box area-averaged time series in Figure 2.6.

In the negative phase, the AMM redirects the VIMF southward towards northeast Brazil (Fig. 2.2b). The anomalous winds generate greater moisture convergence, which reduces radiation and then ET over that region (Fig. 2.2b,d and h). Over the northern Orinoco, the southward moisture advection causes a reduction in rainfall and below-average SM, further limiting ET. The eastern Amazon evapotranspiration is not affected in the same way as in the positive phase (asymmetry). However, GLEAM estimates show that in northeast Brazil the impacted area is not as big as in ERA5-Land and does not show ET anomalies where the ESA-CCI-SM was unable to detect values (Fig. S2 and S3).

Comparing positive and negative phases, the mode shows asymmetric atmospheric circulation, with the negative phase being stronger in magnitude for the VIMF (Fig. S7). The latter causes a decrease in SM over the northeast Amazon that is higher than the increase in the positive phase, considering absolute values. Regarding ET, some regions are affected only in one phase of the mode, such as the eastern Amazon and its river delta.

June - August (JJA) Austral Winter

The Atlantic Niño (Atl3) is characterised by a decrease in SLP and an increase in SST over the equatorial east Atlantic that usually peaks in JJA (Fig. S1). It weakens the trade winds through the Bjerknes feedback with effects on VIMF and precipitation over the continent (Fig. 2.3a). SM and evapotranspiration are not extensively impacted by the Atl3 positive phase as changes in radiation are barely visible (Fig. 2.3c, e and g). The Atl3 impacts are not clear in other seasons (SON and DJF) when the AMM and ENSO exert a more discernible influence (not shown).

Conversely, stronger JJA trade winds increase Ekman pumping and mixing over the Atlantic and manifest as colder SST (known as Atlantic Niña – Atl3 negative

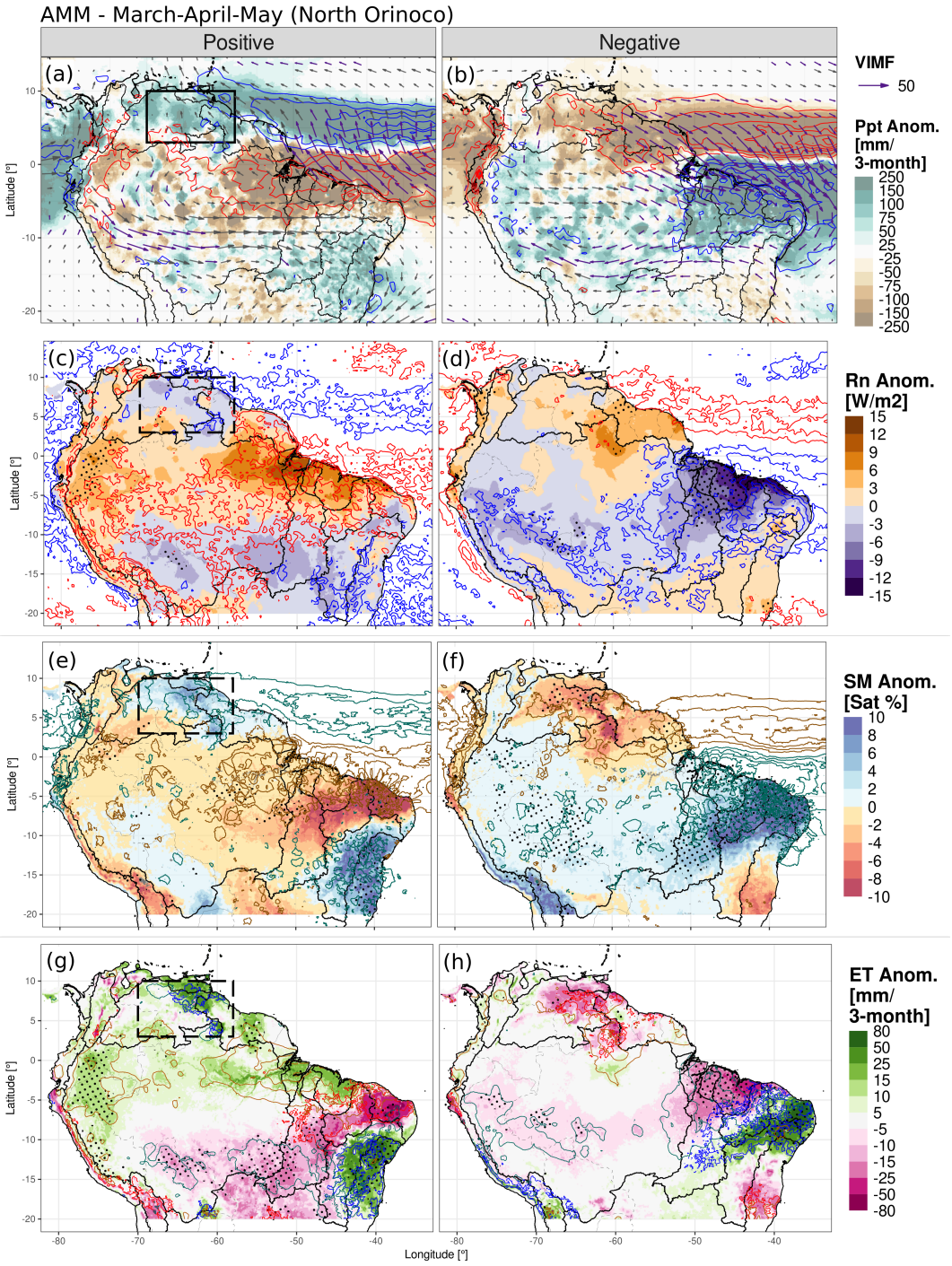

FIGURE 2.2: Anomaly composites of AMM in MAM for (a) VIMF (arrows), MDiv (contours) and MSWEP precipitation (shading) anomalies in the positive phase; positive MDiv anomalies are in red and negative in blue every 3 kg/m^2. VIMF is in kg/m/s and depicted in purple when it is statistically significant at a 90% confidence level and in grey otherwise. Right panels (b,d,f and h) are the same as left panels (a,c,e and g) but for the negative phase. (c,d) ERA5-Land surface net radiation (shading), and satellite CLARA cloud cover anomalies (contours); positive cloud cover anomalies are in blue and negative in red repeated every 4%. (continues in next page)

(continued.)(e,f) Composites of ERA5-Land soil moisture anomalies in saturation percentage (shadings), and MSWEP precipitation anomalies (contours); positive precipitation anomalies are drawn in aquamarine and negative in gold repeated every 100 mm. (g,h) Composites of ERA5-Land evapotranspiration (shading), Rn anomalies (contours, gold for positive and aquamarine for negative), and SM anomalies (contours, blue for positive and red for negative); Rn anomalies are repeated every 3 W/m^2 and SM anomalies are repeated every 5%. In every panel, black stippling depicts regions where the shaded variable is significantly different from the neutral phase at a 95% confidence level. Boxed region: Northern Orinoco, also applies for the negative phase.

phase). The strengthened easterly winds – and VIMF – create negative anomalies of convergence and precipitation in an extended region over the East of the continent (Fig. 2.3b). However, greater MDiv and radiation increase ET over the eastern Orinoco and the Guianas due to the energy-limited environment, whereas over northeast Brazil and the eastern Amazon the anomalies are negative as they behave as water-limited and the SM is also lower-than-average (Fig. 2.1j and 2.3d,f,h). ESA-CCI-SM is not available over the Guianas and partially over northeast Brazil (Fig. S2) and then GLEAM shows a similar pattern to ERA5-Land, but the signal is weaker over the eastern Orinoco, Amazon delta and northeast Brazil (Fig. S3). The negative phase is more pronounced due to stronger anomalies in all three variables (Figure S7 for asymmetric conditions). The ET between the two phases is very asymmetric as the eastern Orinoco and northeast Brazil are not affected in the positive phase, but they are in the negative (Fig. 2.3g and h, and Fig. S7).

Regarding the Atlantic Meridional Mode (AMM)(Fig. 2.4), the impacted place migrates depending on the season. In JJA, the positive phase redirects the VIMF anomalies northward (Fig. S4). This enhances convergence over the Caribbean and the divergence over the central Amazon and southern Orinoco (the latter having enhanced convergence in the previous season); hence, it reduces clouds and rainfall over the continent (Fig. S4 a and c). The SM levels guarantee an energy-limited environment in the northern Amazon (Fig. 2.1j), and the AMM-related divergence generates above-average radiation, causing higher-than-average ET in the tropical forest (Fig. 2.4c) but below-average over northeast Brazil. The places impacted migrate westward compared to the previous season - MAM (Fig. 2.4a). In the southern area, the combination of the dry season and below-average SM causes trees to take up water probably just through their deep roots, generating water stress and reduced ET (see Sect. 2.5 Discussion). However, GLEAM estimates do not show any significant anomaly in the Amazon where the availability of ESA-CCI-SM estimates are scarce (Fig. S2 and S3). Both ET datasets show similar anomalies over the continental north coast.

In the JJA negative phase, southward moisture flux brings more rainfall to the Orinoco but it is not clear over the Amazon, an asymmetric condition compared to the positive phase (Fig. S4). Then, the AMM negative phase produces positive but not significant SM and ET anomalies in the southeast (Fig. 2.4d), although ERA5 suggests enhanced convergence (Fig. S4b). An important difference when comparing JJA to MAM is the westward migration of the divergence anomalies from northeast Brazil to the central Amazon and the effects on SM and ET (Fig. 2.4a and c).

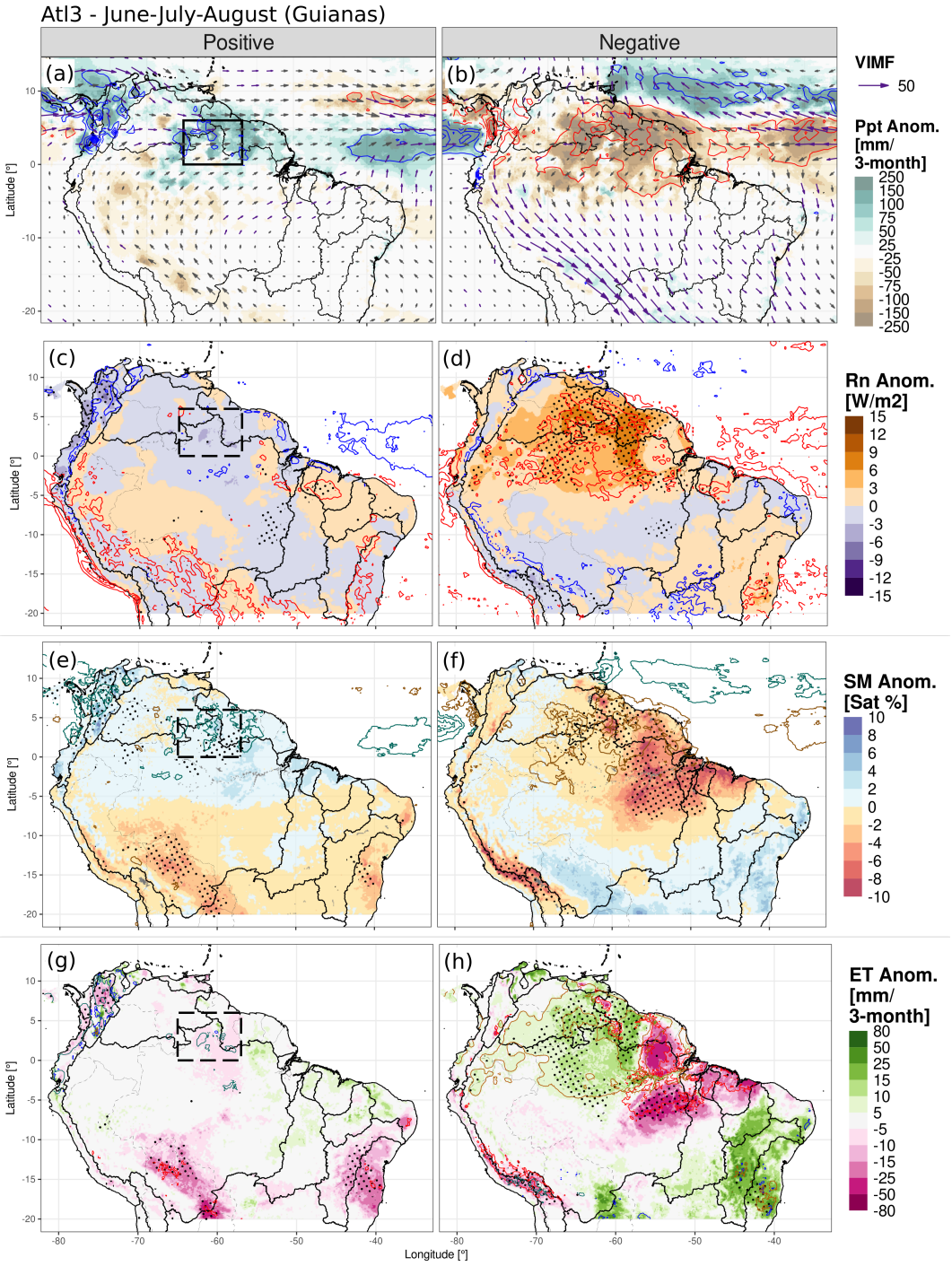

FIGURE 2.3: As in Figure 2.2 but for the Atlantic Niño Equatorial Mode (Atl3) in June to August (JJA). Boxed region: the Guianas, also applies for the negative phase.

September - November (SON) Austral Spring

For this season, the AMM-related anomalies migrate to the western Orinoco and western Amazon since the rainfall is concentrated on the Andes' eastern slope. The reduction in VIMF and convergence in the positive phase lead to high radiation anomalies that interact with the SM, causing above-average ET over the Orinoco (Fig. 2.4e and S5a,c,e). This is generated by SM remaining high in the region, creating

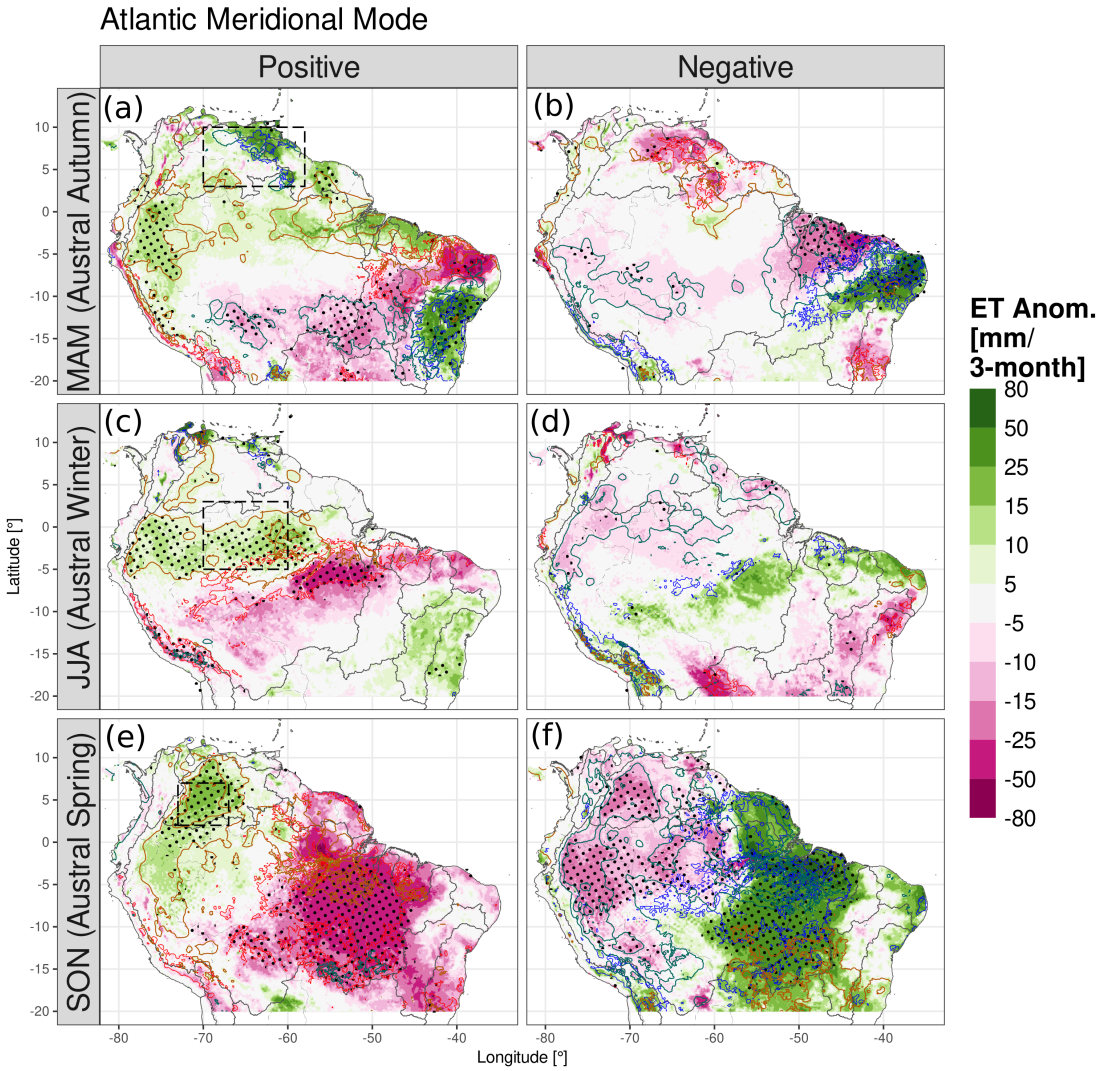

FIGURE 2.4: Anomalies of ERA5-Land ET (shadings) in the positive and negative Atlantic Meridional Mode (AMM) phases, for seasons (a,b) March-May, (c,d) June-August, (e,f) September-November. Positive phase in panels (a,c,e) and negative (b,d,f). Net surface radiation anomalies are in contours (gold for positive and aquamarine for negative), as well as soil moisture anomalies (contours, blue for positive and red for negative); radiation anomalies are repeated every 3 W/m^2 and SM anomalies are repeated every 5%. Black stippling depicts regions where the difference with the neutral phase is statistically significant at a 95% confidence level. Boxed regions: (a,b) Northern Orinoco, (c,d) Central Amazon, (e,f) Western Orinoco, also applies for the negative phase. Box-averaged time series for JJA and SON in Figure S6.

an energy-limited environment although it is not the core of the rainy season and the SM anomalies are less than 2% (Fig. 2.1k and Fig. S5e). Moreover, the positive phase causes a decline in SM and ET over the water-limited southeast due to the reduction in rainfall. There is no significant change in the central northern Amazon, just in the west or the east.

In the negative phase, the AMM brings extra moisture more strongly than the positive phase, although in both phases the southeastern Amazon is impacted (Fig.

S5a,b and S7). In the latter region, the SM shows higher-than-average values(Fig. S5e), which grant the land surface the extra moisture to increase ET in the water-limited zone (Fig. 2.4f). Over the Orinoco, the reduced radiation causes less ET, as well as over the western and northern Amazon (the latter region not affected in the positive phase, asymmetry in Fig. S7). GLEAM shows similar results except for the central Amazon, again a region where the satellite SM is not assimilated in the model (Fig. S2 and S3).

The interactions between SM availability, plant water uptake and radiation lead – in some cases – to above-average evapotranspiration during negative precipitation anomalies (reduced moisture convergence and clouds). This behaviour is present in energy-limited regimes, whereas in water-limited environments, negative moisture convergence anomalies bring less rainfall and cause below-average evapotranspiration.

2.4.3 Atlantic modes connection with ENSO and impacts on evapotranspiration

Both ENSO and the Atlantic modes are connected through tropical and extra-tropical mechanisms, but each of them has effects on South American hydroclimate. Figures 2.5 and 2.6, separate the effects of each mode in the spatial and temporal dimensions, respectively.

ENSO and AMM have impacts on ET at similar but also over different locations depending on the analysed season. Figures 2.5(a,b,e,f) show the influence of both modes on ET in northeast Brazil in MAM and in JJA, yet ENSO mainly impacts the eastern Amazon and the AMM impacts the Orinoco (see Sect. 2.5 Discussion). ENSO usually also induces droughts in the Amazon during El Niño events – mostly during its peak season DJF – and causes heavy rainfall and floods during La Niña events. Figure 2.5(c,d) show the spatial impact of the increased evapotranspiration during ENSO-driven droughts and Figure 2.6(c,d) display the impacts on rainfall and ET of specific events (e.g. 1983, 1992, 1997 and 2015). However, Figures 2.5(a,e) and 2.6(a,b) show that in the northern Orinoco the ENSO forcing might be superseded by the meridional moisture advection induced by the AMM (e.g. 1983 – El Niño year but higher rainfall and ET; 1985 and 1989 – La Niña year but drought). The correlation of the AMM with rainfall is up to 0.64, and with SM and ET are up to 0.5, all significant. Another period when the AMM superseded ENSO impacts was in 2010 during La Niña when the central Amazon experienced a prolonged drought (Fig. 2.5f and S6); the cause was the positive AMM event (see Sect. 2.5 Discussion). Note also the reduction or increment of ET when SM changes (water-limited regime). For season SON (Fig. 2.5 c and g), the AMM and ENSO tend to impact different regions: ENSO being strong over the Guianas and the AMM over the west and southeast.

The Atl3 does not seem to strongly correlate with ET over the Guianas, and the ENSO pattern for JJA is very similar to the Atl3 negative phase composites (Fig. 2.5b,h and 2.3h). This indicates some overlapping dynamics between the two modes, which are probably more associated with the atmospheric dynamics of El Niño phase that has simultaneously unfolded with the Atl3 negative phase (Fig. 2.6c and d and Fig. S8). We discuss the latter in Section 2.5. Figure 2.6c and d show the droughts over the northeast Amazon and Guianas during Atl3 negative events with the corresponding increase in ET, which are also expected effects of El Niño phase. The correlation of the Atl3 with the area-average ERA5-Land ET is -0.46 but 0.14 with GLEAM; the index correlates well with SM and also with rainfall. However, only some Atl3 positive events significantly reduced radiation and ET in the

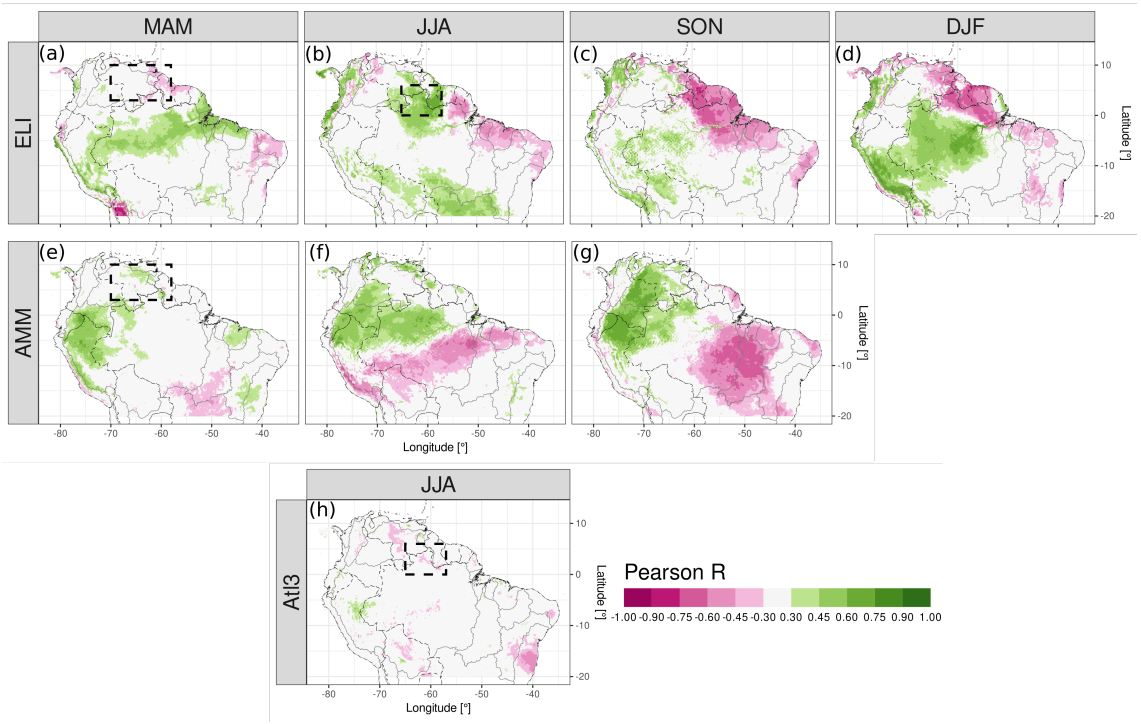

FIGURE 2.5: Partial correlation of ET from ERA5-Land with the main tropical ocean modes in the Atlantic and Pacific. Panels a-d are the correlations with ELI for each season, controlled by the two Atlantic indices, e-g are the correlations with the AMM except for DJF, which is controlled by ELI and Atl3, and panel h is the correlation with the Atl3 controlling by ELI and the AMM. Just 95% confidence level values are shown in colours. Boxed regions: Northern Orinoco and Guianas, same as in Fig.2.2 and 2.3.

region (e.g. 1988, 1999 and 2008); other events kept ET close to the average (1987, 1998 and 2016).

2.5 Discussion

Much of the research has focused on precipitation variability rather than on evapotranspiration (Arias et al., 2021; Espinoza et al., 2011; Marengo & Espinoza, 2016; Poveda et al., 2006). Regarding ET, Martens et al. (2018) used machine learning to globally estimate the impacts of the AMM – and other modes – finding the increased evapotranspiration over northeast Brazil in MAM and some cells in the central Amazon in JJA. However, our research focused on the modes that alter the atmospheric circulation close to the continent and constitute the physical mechanism causing the teleconnection. Other investigations focused specifically on ENSO's impact on Amazon evapotranspiration and SM (Moura et al., 2019; Poveda et al., 2001). Specifically, Moura et al. (2019) showed the anomalies of evapotranspiration for both the southern Amazon's rainy – DJF – and dry seasons during ENSO events, finding the increase in the ET also shown in our correlation analysis in DJF. Our research focuses on the interaction between the atmosphere and the land surface, finding that the impacts migrate from the eastern Amazon to the western Orinoco and that important asymmetries exist between phases. Hasler and Avissar (2007) found an increase

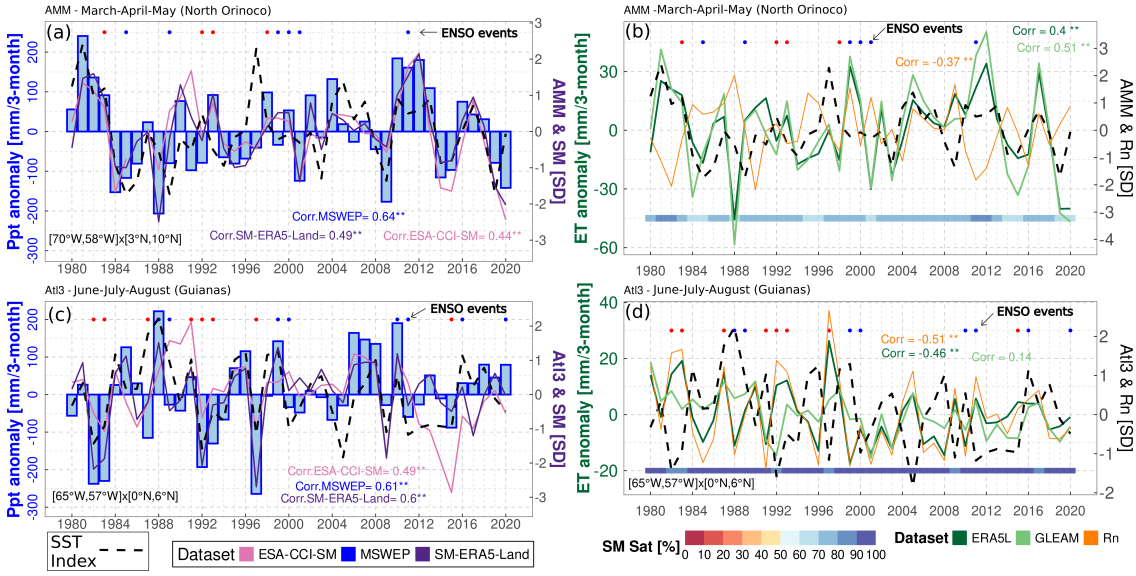

FIGURE 2.6: (a,c) Area-average precipitation (bars) and SM standardised anomalies time series (lines) for the same boxes in Figure 2.2 and 2.3, respectively; the Atlantic index time series is in black dashed lines in standard deviation (right axis), and top points show ENSO active periods (positive phase in red and negative in blue). (b,d) Area-average evapotranspiration time series (greens), ERA5-Land net surface radiation (orange), standardised Atlantic index (black dashed) and ERA5-Land absolute SM in saturation percentage at the bottom of the panel with coloured rectangles. For the same boxes of panels (a) and (b). For all panels, Pearson correlations are calculated between the variable – either precipitation, SM, Rn or ET – with the respective Atlantic index, 95% confidence level is indicated with **. Boxed regions: Northern Orinoco (a and b); Northeast Amazon and Guianas (c and d).

in ET in the equatorial Amazon during the dry season related to radiation anomalies, as found in our ERA5-Land composites. The retained SM above critical values (soil's field capacity), up to the next season, might cause positive evapotranspiration anomalies during below-average precipitation and above-average radiation periods (Zanin et al., 2024); this is evident in our results in the transition from the wet to the dry season.

Differences between GLEAM and ERA5-Land stem from their formulation structures and assimilated data, which are then propagated to the composite analysis. In forested areas, roots deeper than 1.5 m allow the water uptake from deep layers as a survival mechanism (Jarvis, 1976; O'Connor et al., 2019; Roberts et al., 2005), the main local controller of ET is most likely the incoming radiation but trees might still feel water stress (Lian et al., 2024). The latter is partially considered in ERA5-Land as the depth of the last layer is deeper than 1.5 m and plants withdraw soil moisture root percentage-wise (ECMWF, 2023), whereas in GLEAM the depth of the three soil layers is not specified and plants withdraw water from the wettest layers (Martens et al., 2017). D'Acunha et al. (2024) found low ET rates in cropland and pasture sites inside the southeast Amazon rainforest compared to natural land use; the structure of both datasets in our study considers the grasslands and the other land covers, with some limitations. The influence of wind speed on evapotranspiration is not considered in GLEAM v3.8, and the soil module and plant physiology are more accurate

in ERA5-Land. The impediment of assimilating SM due to the scarcity of ESA-CCI-SM data in dense forest areas might compromise the uncertainty in GLEAM estimates (Baker et al., 2021), e.g. over the northern Amazon and Delta, and over the Guianas (Fig. 2.4d,e and 2.5d,e). Some studies have compared both datasets against eddy-covariance towers and water-balance approaches and concluded that ERA5-Land estimates are more realistic than GLEAM (Muñoz-Sabater et al., 2021; Xie et al., 2024). The bias in ERA5's rainfall might be diverted towards the streamflow (Towner et al., 2021), rather than generating a bias on the SM and the ET. These limitations are probably the main cause of the differences between the composites using each dataset.

The variability of ET has implications for moisture-recycling, mainly for south-eastern South America as pointed out by Drumond et al. (2014). Although moisture recycling inside the Amazon comprises between 25% and 35% of rainfall, Dominguez et al. (2022) discovered that it is a short-lifetime phenomenon strongly linked to the diurnal cycle of advected moisture and convection; recycled moisture precipitates quickly. Staal et al. (2018) measured the distance of transpired water before precipitating again over land, finding that for the particles transpired in the Amazon, the distance is below or around 500 km (which is short compared to the size of the Amazon basin). Our results show the places that affect the sources of that moisture recycling due to the seasonal aggregated increments or reductions in ET. Makarieva et al. (2023) determined the influence of ET on moisture convergence, which might potentially influence radiation. It remains to be clarified to what extent moisture-recycling influences radiation availability and soil moisture at other locations in South America; this is out of the scope of our research.

The AMM and the Atl3 are influenced by and also have feedback with ENSO (Cai et al., 2019; García-Serrano et al., 2017; Martín-Rey et al., 2014). Our results show that each mode impacts different regions, except for northeast Brazil and northern Amazon where they overlap through El Niño enforcing convection inhibition and the AMM producing meridional anomalous moisture advection (for instance, in 2010)(Arias et al., 2020; Chiang et al., 2002); these mechanisms then modify convergence, rainfall, radiation availability and thus evapotranspiration. The AMM negative phase has been less recurrent in SON in the last decades associated with a positive phase of the Atlantic Multidecadal Oscillation (AMO)(general interhemispheric temperature gradient) (Brönnimann et al., 2015; Friedman et al., 2020). The latter is apparently related to the reduced aerosol forcing over the northern hemisphere and its associated radiation scattering (He et al., 2023; Hua et al., 2019). The Atl3 negative phase has co-occurred with the ENSO positive phase (El Niño)(Münnich & Neelin, 2005), whose impacts are evident in our composites and partial-correlation analysis. ENSO causes downward atmospheric movement over the east of the Amazon that hampers convection and precipitation (Cai et al., 2020); simultaneously, the strengthened easterlies – typical of the negative Atl3 – add to the moisture divergence over the Guianas, undermining precipitation. However, the relationship between ENSO and the Atl3 is inconsistent (Chang et al., 2006; Lübbecke & McPhaden, 2012). The interactions between climate modes have implications for their continental impacts (i.e. over the hydrological cycle).

Several ocean-atmospheric drivers have been identified as influences on the hydrometeorology of South America. Rodrigues and McPhaden (2014) analysed the AMM effects on precipitation in northeast Brazil and the Amazon, while others focused on the decadal variations in precipitation and streamflow or the low atmospheric dynamics (Fernandes et al., 2015; Lopes et al., 2016; Olmo et al., 2022). Our research shows that the chain of events starts with the SSTA and SLP and transfers to

VIMF, MDiv and precipitation, whose anomalies are linked to the variability in ET. However, we also show that the AMM also affects the Orinoco basin in MAM, JJA and might even extend into SON (Yoon & Zeng, 2010), over not just the Amazon and precipitation but also over the SM and the evapotranspiration. There is agreement in the comparison of the location of reanalysed convergence and satellite precipitation; the rainfall anomalies influence the peak river flow, and our results agree with the location of peak river flow reduction during TNA anomalies reported by Towner et al. (2021) – decrease in central Amazon in the positive phase. Regarding the Atl3, most of the studies have focused on its statistical relationship with continental precipitation anomalies (Gu & Adler, 2009; Torralba et al., 2015), and the atmospheric dynamics of its development (Vallès-Casanova et al., 2020).

Although coupled ocean-atmospheric modes are important drivers at seasonal time scale as shown here, other sources of variability at other scales – such as those mentioned in Sect. 2.1 (Introduction) – influence precipitation and might also influence ET (Mariotti et al., 2018). They might affect the transition and migration of the anomalies from one season to the following one. Phenomena with longer frequencies, such as the AMO, have also been discussed here, but the impacts of all those sources on ET deserve further research.

Our results are underpinned by the consistency between independent observations of land-surface and atmospheric variables whose robustness comes from physically-based interpolations (reanalysis) or satellite-based observations. Limitations arise from the dataset's uncertainty and satellite retrievals; deforestation dynamics are also not included in the datasets. Nevertheless, the general circulation is still well represented due to the assimilation of atmospheric pressure, and models and measurements are as accurate as possible. Both sources of information show similar impacts but with local differences mostly in densely forested areas where physically based models like ERA5-Land might be more reliable. Longer time series of eddy-covariance towers could help the community confirm the dynamics discovered in our study. All in all, the datasets are accurate enough to analyse interannual variability.

2.6 Conclusions

This research advances the current understanding of the physical mechanisms that cause the interannual climate and land-surface variability in Tropical South America, focusing on soil moisture (SM), net radiation (Rn) and evapotranspiration (ET). It elucidates the influence of the Atlantic SST modes on upwind conditions that impact the Orinoco basin and not just northeast Brazil or the Amazon. Atlantic ocean-atmospheric interactions drive moisture convergence anomalies, which in turn modify water and radiation availability, which then control the SM, the net radiation and the ET anomalies. However, the chain of processes is modulated by the annual cycle of the evapotranspiration regimen which is not completely energy-limited throughout the tropical region and throughout the annual cycle. A summarising depiction of the processes can be seen in Figure 2.7.

The Atlantic Niño Equatorial mode (Atl3) weakens the trade winds in JJA, producing convergence over the Guianas and eastern Orinoco. However, its effect on the SM, radiation and ET is not strong. The negative phase – in conjunction with ENSO warm phase – strengthens the trade winds and produces divergence over an extended region which significantly changes the SM, Rn and ET.

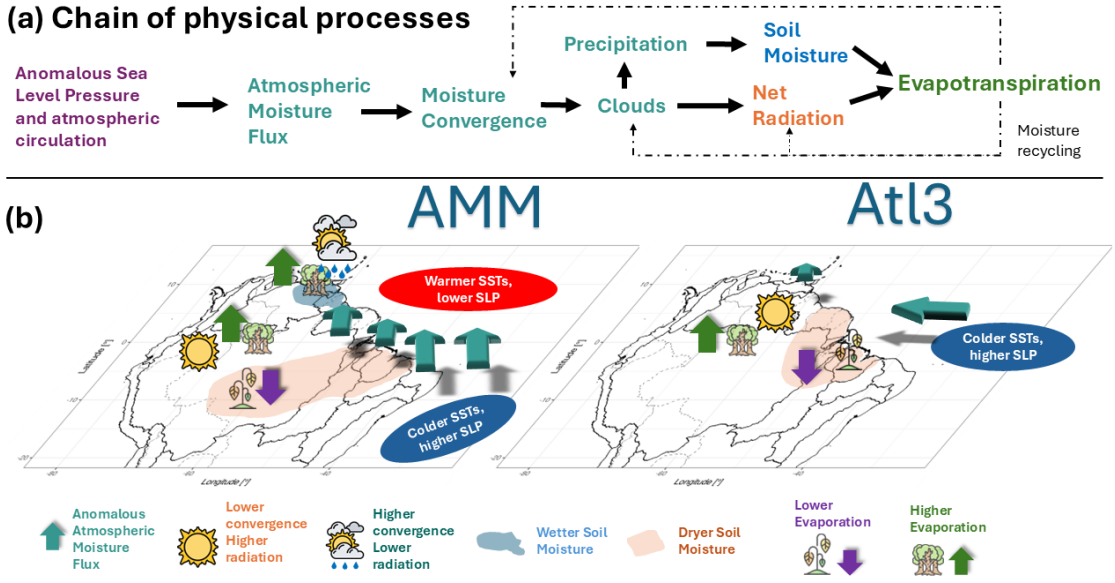

FIGURE 2.7: Schematic figure of the (a) variables involved in the chain of physical processes in the teleconnection between a climate mode and the evapotranspiration. (b) Geographical location of the processes involved in the connection between the continental evapotranspiration and the Atlantic Meridional Mode (AMM), and the Atlantic Niño Equatorial mode (Atl3).

The Atlantic Meridional Mode (AMM) creates cross-equatorial SLP anomalies that deflect climatological winds over not just the ocean but also over the continent. It sends moisture northward in the positive phase, on occasions increasing and on others reducing convergence, precipitation and radiation depending on the location and season, hence causing the land-surface anomalies (SM and ET). The negative phase causes the opposite effect but with strong asymmetries. In MAM, the moisture is redirected towards the Orinoco from northeast Brazil, whereas in JJA and SON it is taken from southern Orinoco and northern Amazon (or brought to the same regions in the other phase with important differences in zonal direction). The changes in moisture transport depend on the annual wind pattern, producing opposite effects when comparing MAM and JJA over the Orinoco. AMM and ENSO conjointly affect the breadbasket region of northeast Brazil and the central Amazon but the AMM affects more the western Amazon and Orinoco.

The regions impacted in each phase might be different. Analysing just one phase might cause misleading estimations of SM, Rn and ET.

Evapotranspiration is influenced in its regime by not only the ITCZ position but also by the phase of the ocean-atmospheric mode. This is related to the fact that SM is not resilient to the activation of the modes unless it is the rainy season and the soil is saturated regardless of the phase (thus the SM is above the soil's water field capacity, the threshold for energy-limited ET). For instance, evapotranspiration anomalies in the transition season from wet-to-dry are energy-limited, but the sign of the anomaly depends on the phase of the mode which alters radiation and then ET. In the transition season from dry to wet, the ET regime is most likely water-limited, and the ET anomaly is influenced by the variability of SM, which depends on the phase of the climate driver through precipitation. The SM saturation percentage closely varies with the ITCZ position.

The phenomena analysed have implications for the relationship between SM and

heat extremes, gross primary production, irrigation requirements, and the carbon and energy cycles and can potentially be used to predict the response of ecosystem activity. The chain is mainly – but not exclusively – applicable to other tropical regions worldwide.

Code availability

We coded scripts in R (https://www.R-project.org/) to perform the analysis of the datasets (Duque-Gardeazabal, 2025). They can be consulted at: https://github.com/nduqueg/ET_var_SAme or https://doi.org/10.5281/zenodo.15389246.

Data Availability

Extended Reconstructed SST version 5 (Huang et al., 2017) is available at: https://www.ncei.noaa.gov/pub/data/cmb/ersst/v5/netcdf/. Hadley Center Sea Ice and SST version 4.0.1 (Kennedy et al., 2019) is available at: https://www.metoffice.gov.uk/hadobs/hadsst4/data/download.html. Mauna Loa CO2 concentrations are available at https://gml.noaa.gov/ccgg/trends/data.html. ECMWF ERA5 reanalysis (Hersbach et al., 2020) and the ERA5-Land reanalysis (Muñoz-Sabater et al., 2021) data are available from Copernicus Climate Data Store web portal https://cds.climate.copernicus.eu. MSWEP (Beck et al., 2019) is available at: http://www.gloh2o.org/mswep/. ESA CCI SM (Gruber et al., 2019) is available at: https://catalogue.ceda.ac.uk/uuid/ff890589c21f4033803aa550f52c980c. GLEAM (Martens et al., 2017) is available at: https://www.gleam.eu/. EUMETSAT CLARA-A3 (Karlsson et al., 2023) is available at: https://wui.cmsaf.eu/safira/action/viewProduktDetails?fid=40&eid=22277_22492. HydroSHEDS basins are available at: https://www.hydrosheds.org/products/hydrobasins (Lehner & Grill, 2013).

Author Contributions

Conceptualization: N.D-G and S.B.; Data Curation: N.D-G, A.R.F.; Formal Analysis: N.D-G; Funding Acquisition: N.D-G, S.B.; Investigation:N.D-G, A.R.F, S.B.; Methodology: N.D-G, A.R.F., S.B.; Project Administration: N.D-G., S.B.; Resources: S.B.; Software: N.D-G; Supervision: S.B.; Validation: N.D-G, A.R.F., S.B.; Visualisation: N.D-G; Writing - original draft: N.D-G; Writing - review and editing: N.D-G, A.R.F., S.B.

Acknowledgements

We thank the anonymous reviewers and the editor for the constructive comments that helped improve the manuscript. N.D-G. was supported by the Federal Commission for Scholarships for Foreign Students through the Swiss Government Excellence Scholarship (ESKAS No. 2022.0563) for the academic year(s) 2022-2024. A.R.F. was funded by the European Union's Horizon 2020 research and innovation program under the Marie Skłodowska-Curie grant No. 894064 (AQUATIC). S.B. acknowledges funding by the Swiss National Science Foundation (10001375). We are grateful with the institutions that gather and freely disseminate the data used in this research, and to Noemi Imfeld, Sonia Dupuis and Adrian Huerta for recommending datasets or coding functions. N.D-G thanks Helena Gardeazabal, Joaquin Duque and friends for the emotional support throughout this research.

Appendix

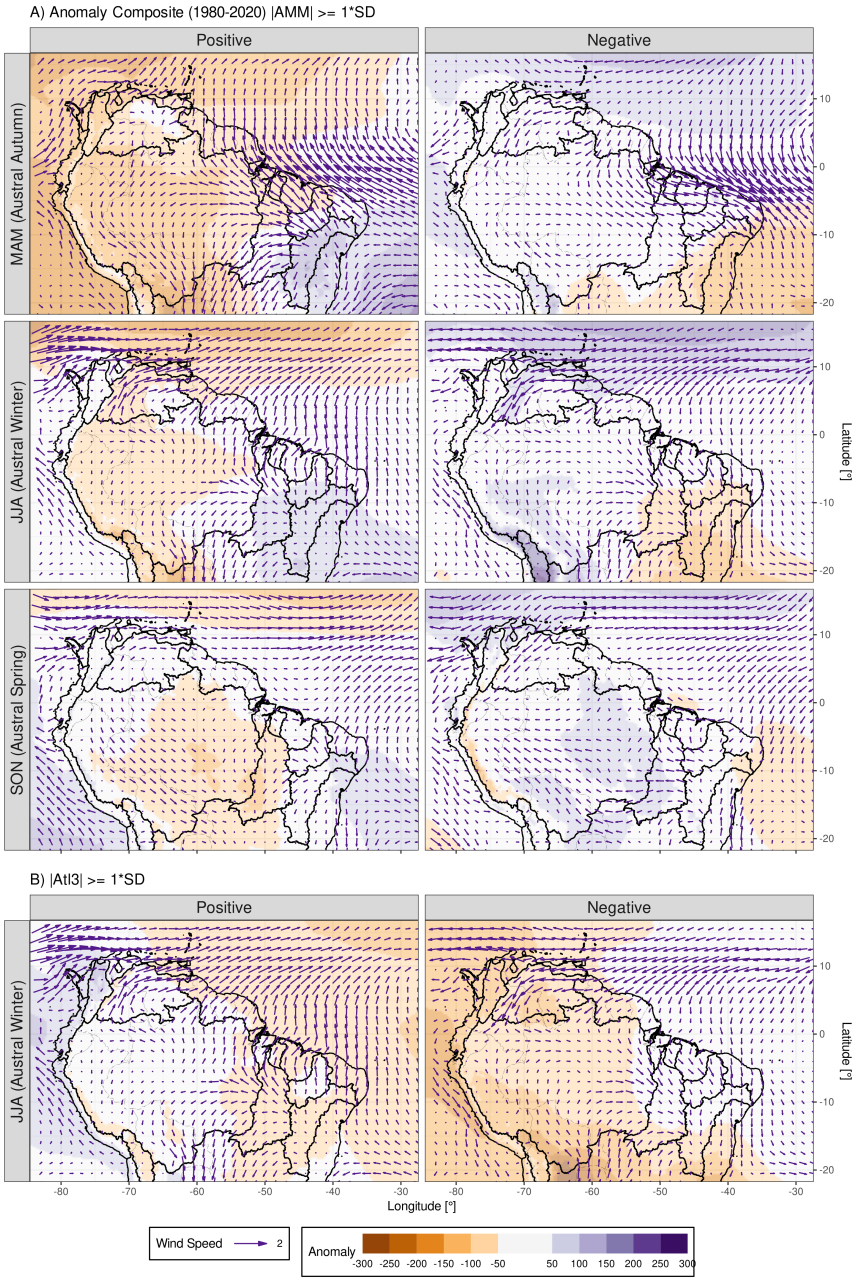

Figure S1. Composites of ERA5 Sea Level Pressure (shading) and 850 hPa wind anomalies (arrows) in the positive and negative phase for the peak season of A) AMM except for austral summer and B) Atl3.

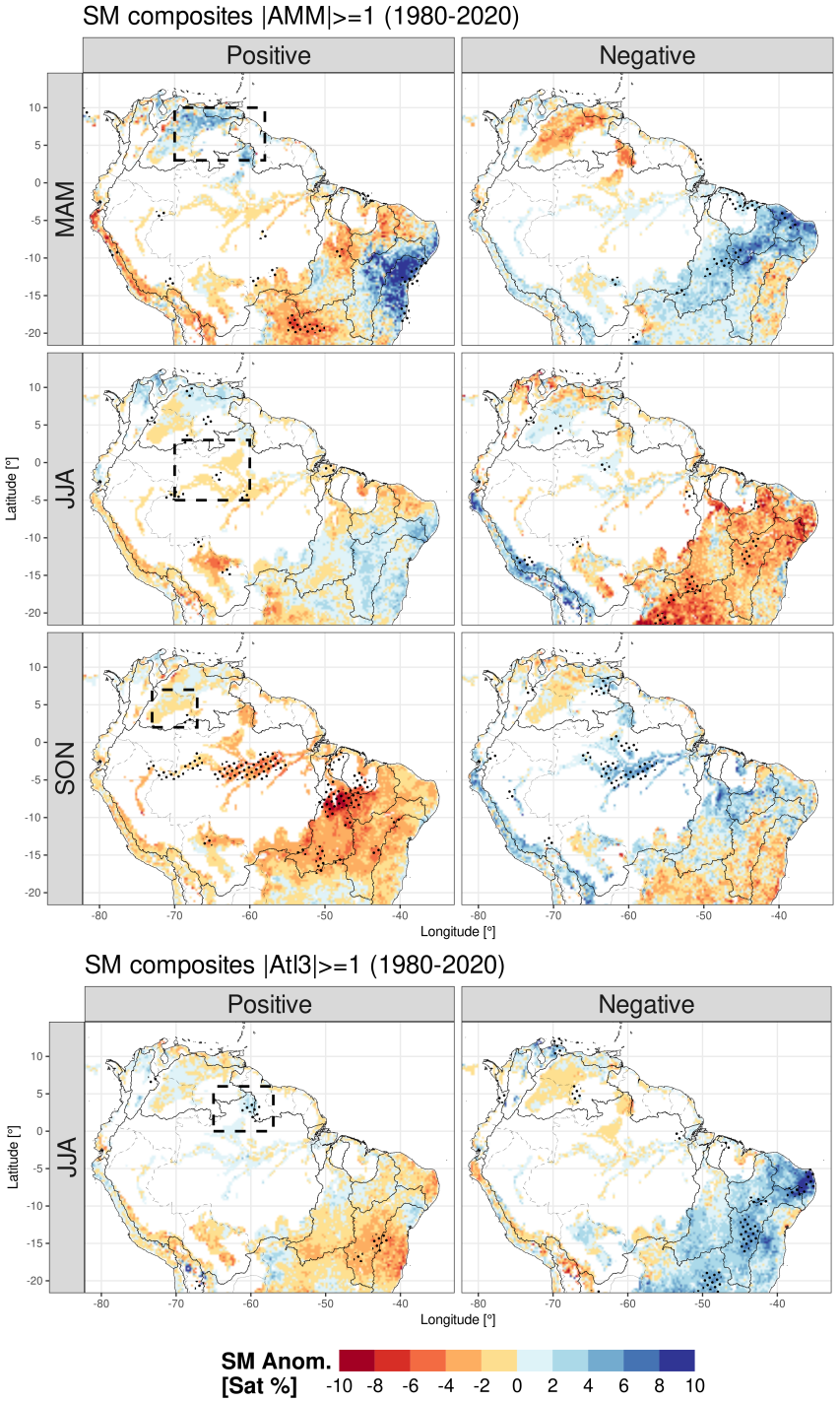

Figure S2. ESA CCI SM saturation anomaly composites. Anomalies are drawn with contours at every 5% with positive in purple and negative in gold. Black dots hatching shows the regions where the difference between the anomalies of each phase with respect to the neutral phase are statistically significant at 95% confidence level.

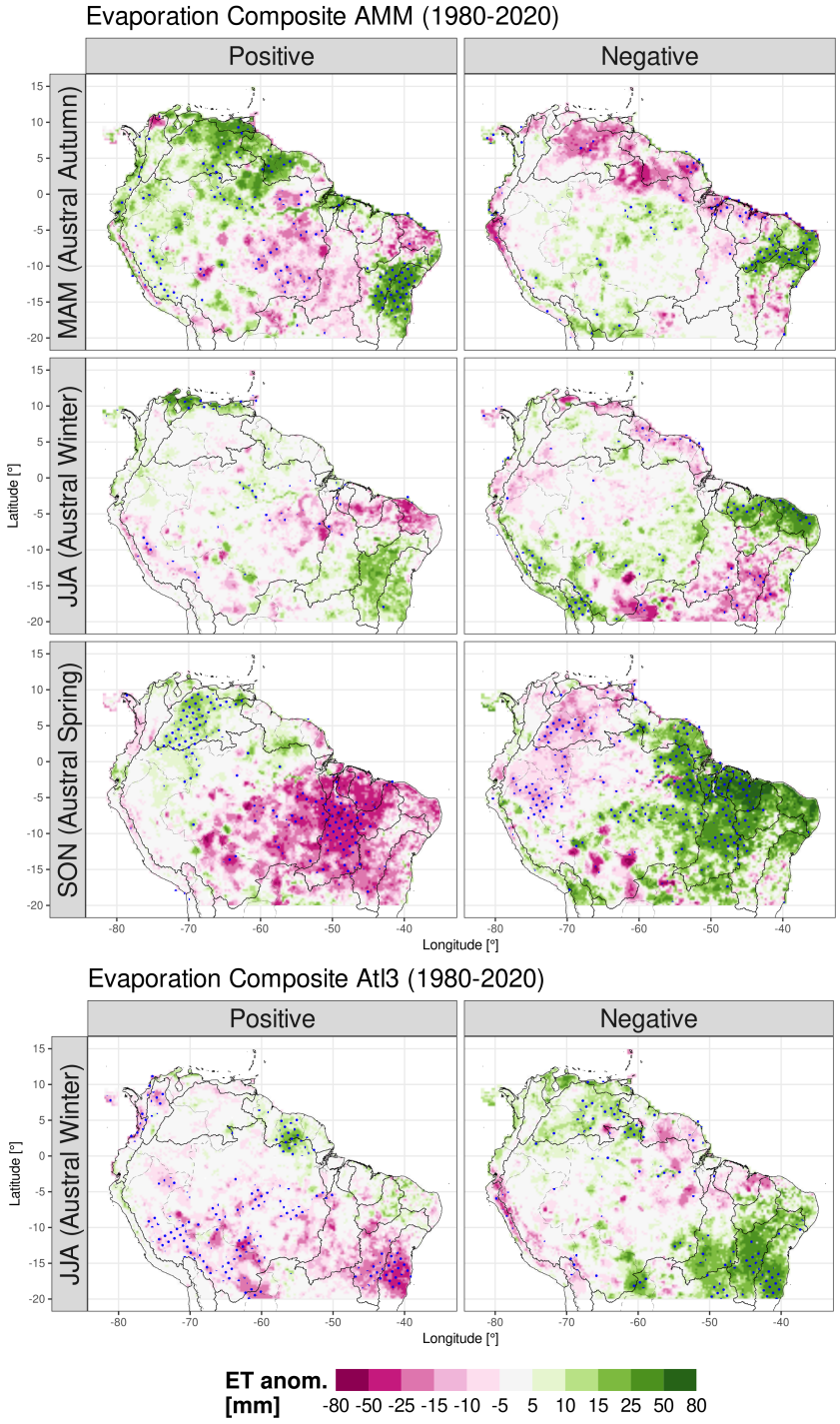

Figure S3. GLEAM anomaly composites. Blue dots hatching shows the regions where the difference between the anomalies of each phase with respect to the neutral phase are statistically significant at 95% confidence level.

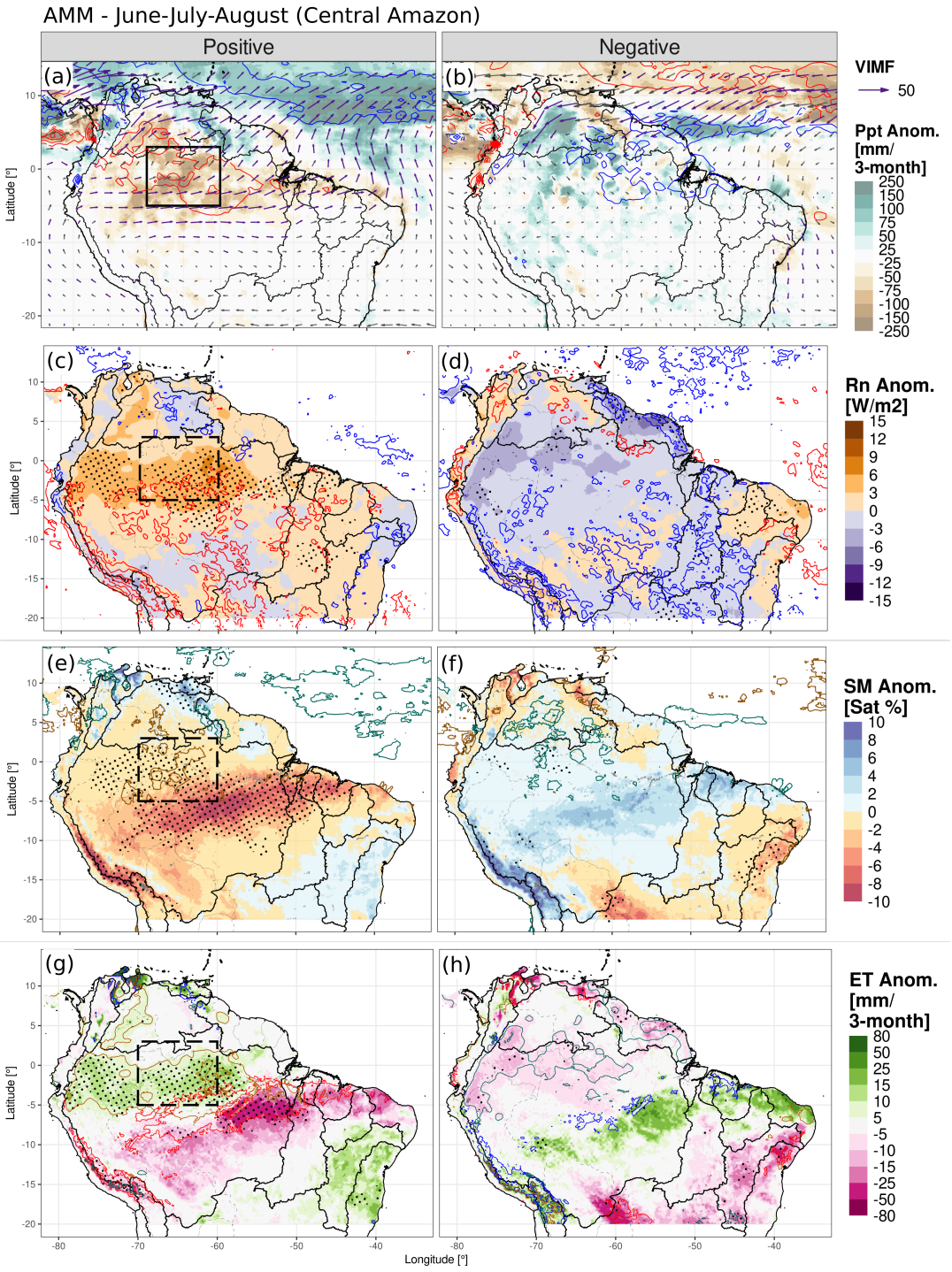

Figure S4. As in Figure 2 but for the Atlantic Meridional Mode (AMM) in June to August (JJA). Boxed region: Central Amazon.

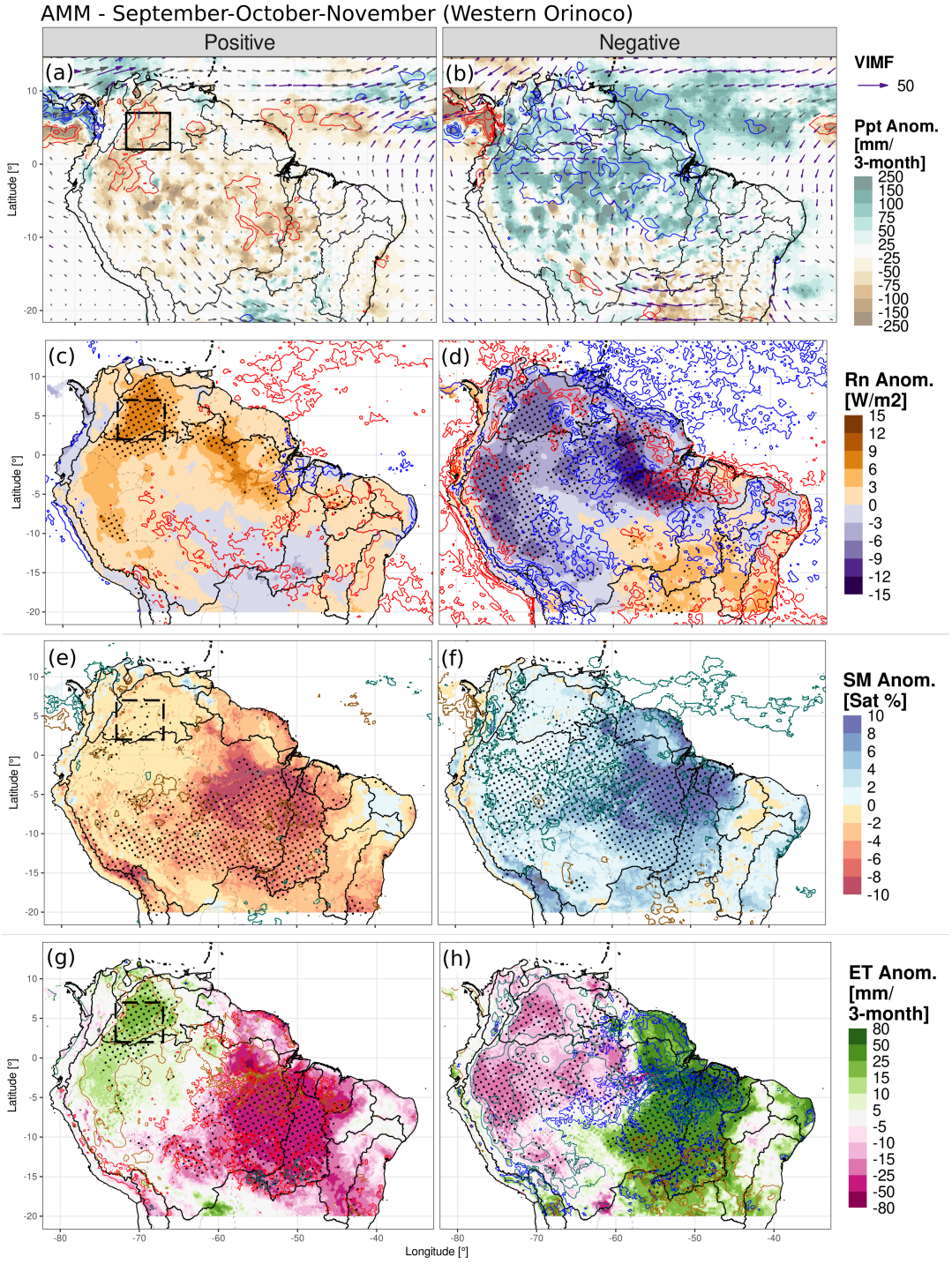

Figure S5. As in Figure 2 but for the Atlantic Meridional Mode (AMM) in September to November (SON). Boxed region: Western Orinoco.

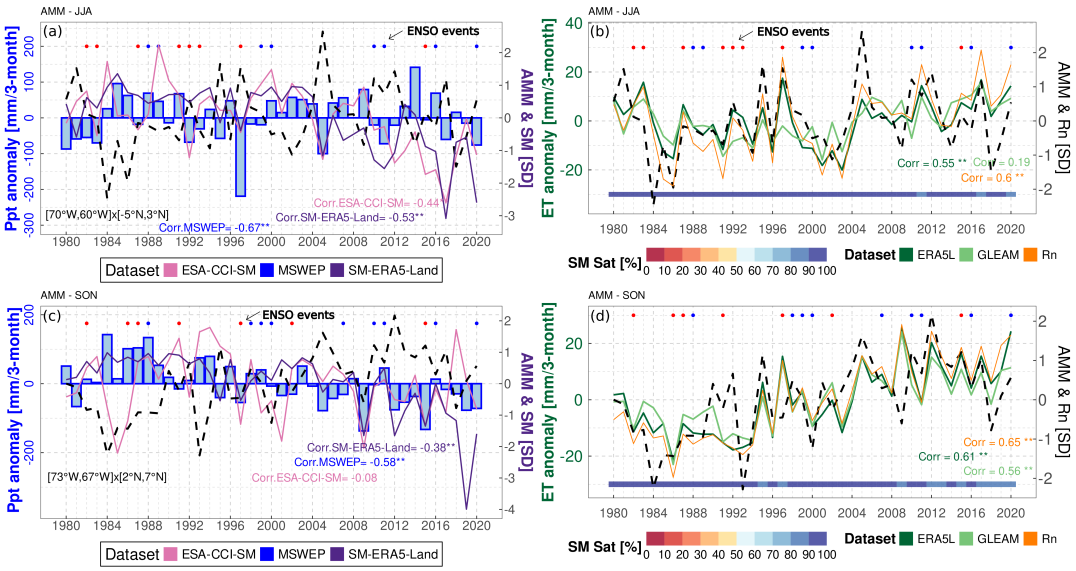

Figure S6. As in Figure 6 but for the Central Amazon in JJA (a,b) and Western Orinoco in SON (c,d).

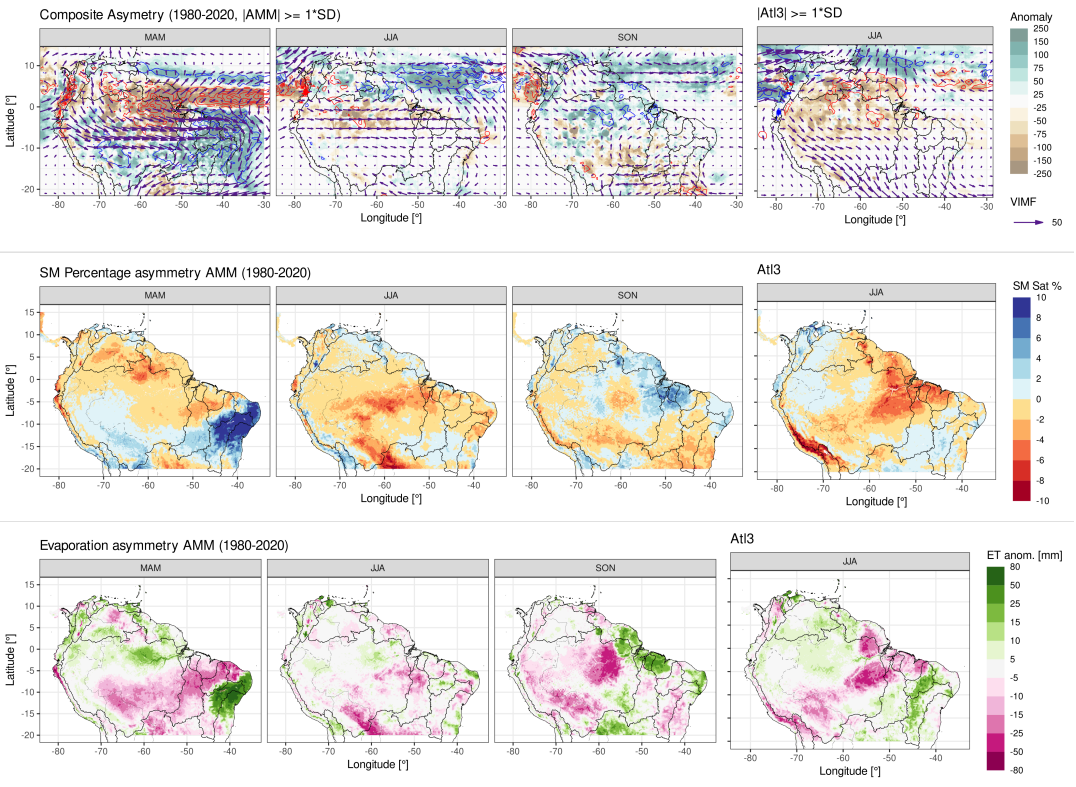

Figure S7. ERA5 and ERA5-Land Composites, positive plus negative phase (asymmetry) of – top panels – VIMF, MDiv and Ppt for the peak season of A) AMM except for austral summer and B) Atl3. Asymmetry of SM anomalies – middle panels – for A) AMM except for austral summer and B) Atl3. Asymmetry of evaporation anomalies – lower panels – for A) AMM except for austral summer and B) Atl3.

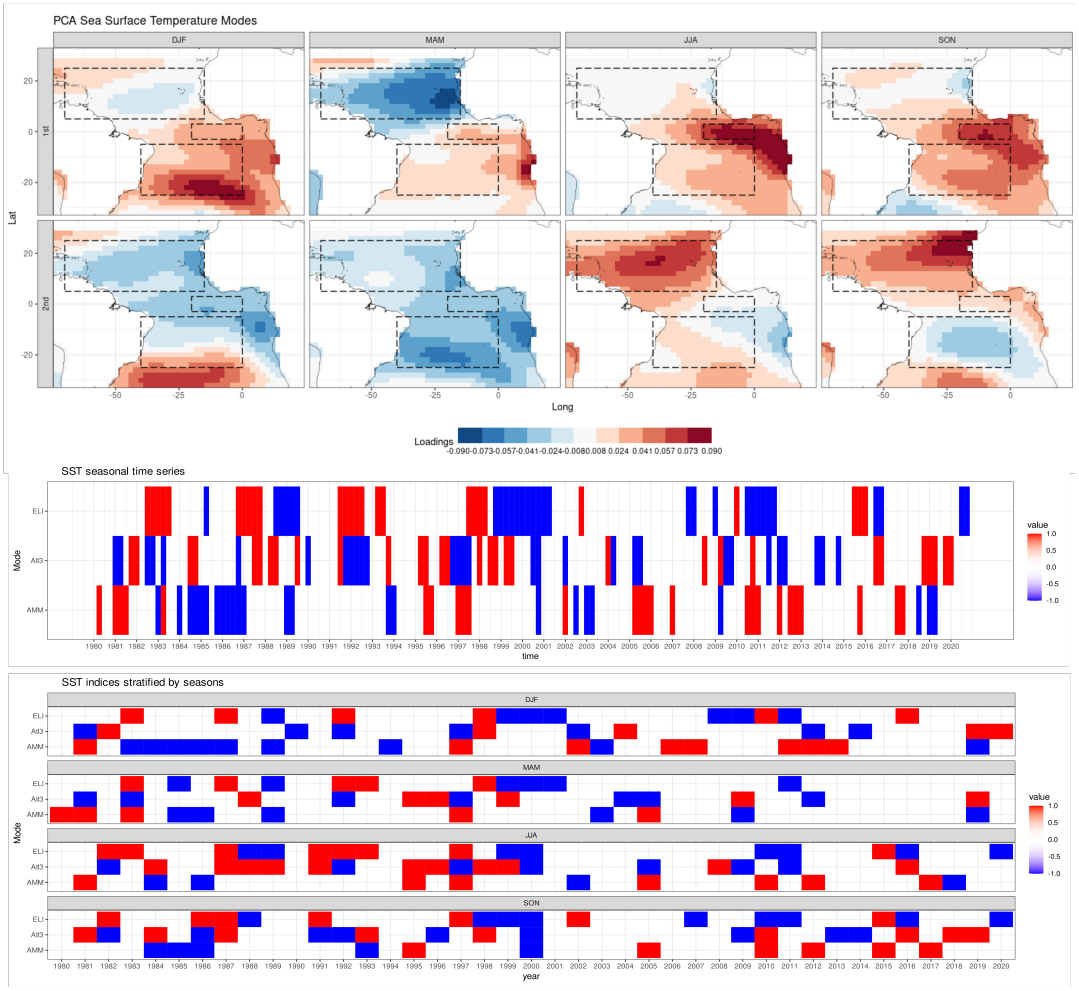

Figure S8. (Top panels) Loadings of the 1st and 2nd Principal components of the Tropical Atlantic SSTs in ERSSTv5. (Middle panel) Seasonal time series of the three SST indices described in the methods section. The Atlantic El Niño (AEN)(Atl3), the Atlantic Meridional Mode (AMM) and the El Niño Longitude Index (ELI) in ERSSTv5. (Lower panels) Seasonal SST indices time series but stratified by season.

References

Arias, P. A., Garreaud, R., Poveda, G., Espinoza, J. C., Molina-Carpio, J., Masiokas, M., Viale, M., Scaff, L., & van Oevelen, P. J. (2021). Hydroclimate of the Andes Part II: Hydroclimate Variability and Sub-Continental Patterns. *Frontiers in Earth Science*, *8*(February), 1–25. https://doi.org/10.3389/feart.2020.505467

Arias, P. A., Martínez, J. A., Mejía, J. D., Pazos, M. J., Espinoza, J. C., & Wongchuig-Correa, S. (2020). Changes in Normalized Difference Vegetation Index in the Orinoco and Amazon River Basins: Links to Tropical Atlantic Surface Temperatures. *Journal of Climate*, *33*(19), 8537–8559. https://doi.org/10.1175/JCLI-D-19-0696.1

Arias, P. A., Martínez, J. A., & Vieira, S. C. (2015). Moisture sources to the 2010–2012 anomalous wet season in northern South America. *Climate Dynamics*, *45*(9-10), 2861–2884. https://doi.org/10.1007/s00382-015-2511-7

Baker, J. C., Garcia-Carreras, L., Gloor, M., Marsham, J. H., Buermann, W., Da Rocha, H. R., Nobre, A. D., De Carioca Araujo, A., & Spracklen, D. V. (2021). Evapotranspiration in the Amazon: Spatial patterns, seasonality, and recent trends in observations, reanalysis, and climate models. *Hydrology and Earth System Sciences*, *25*(4), 2279–2300. https://doi.org/10.5194/hess-25-2279-2021

Beck, H. E., Pan, M., Miralles, D. G., Reichle, R. H., Dorigo, W. A., Hahn, S., Sheffield, J., Karthikeyan, L., Balsamo, G., Parinussa, R. M., van Dijk, A. I. J. M., Du, J., Kimball, J. S., Vergopolan, N., & Wood, E. F. (2021). Evaluation of 18 satellite- and model-based soil moisture products using in situ measurements from 826 sensors. *Hydrology and Earth System Sciences*, *25*(1), 17–40. https://doi.org/10.5194/hess-25-17-2021

Beck, H. E., Wood, E. F., Pan, M., Fisher, C. K., Miralles, D. G., van Dijk, A. I. J. M., McVicar, T. R., & Adler, R. F. (2019). MSWEP V2 Global 3-Hourly 0.1° Precipitation: Methodology and Quantitative Assessment. *Bulletin of the American Meteorological Society*, *100*(3), 473–500. https://doi.org/10.1175/BAMS-D-17-0138.1

Brönnimann, S., Fischer, A. M., Rozanov, E., Poli, P., Compo, G. P., & Sardeshmukh, P. D. (2015). Southward shift of the northern tropical belt from 1945 to 1980. *Nature Geoscience*, *8*(12), 969–974. https://doi.org/10.1038/ngeo2568

Cai, W., McPhaden, M. J., Grimm, A. M., Rodrigues, R. R., Taschetto, A. S., Garreaud, R. D., Dewitte, B., Poveda, G., Ham, Y. G., Santoso, A., Ng, B., Anderson, W., Wang, G., Geng, T., Jo, H. S., Marengo, J. A., Alves, L. M., Osman, M., Li, S., … Vera, C. (2020). Climate impacts of the El Niño–Southern Oscillation on South America. *Nature Reviews Earth and Environment*, *1*(4), 215–231. https://doi.org/10.1038/s43017-020-0040-3

Cai, W., Wu, L., Lengaigne, M., Li, T., McGregor, S., Kug, J. S., Yu, J. Y., Stuecker, M. F., Santoso, A., Li, X., Ham, Y. G., Chikamoto, Y., Ng, B., McPhaden, M. J., Du, Y., Dommenget, D., Jia, F., Kajtar, J. B., Keenlyside, N., … Chang, P. (2019). Pantropical climate interactions. *Science*, *363*(6430). https://doi.org/10.1126/science.aav4236

Casselman, J. W., Lübbecke, J. F., Bayr, T., Huo, W., Wahl, S., & Domeisen, D. I. V. (2023). The teleconnection of extreme El Niño–Southern Oscillation (ENSO) events to the tropical North Atlantic in coupled climate models. *Weather and Climate Dynamics*, *4*(2), 471–487. https://doi.org/10.5194/wcd-4-471-2023

Chang, P., Fang, Y., Saravanan, R., Ji, L., & Seidel, H. (2006). The cause of the fragile relationship between the Pacific El Nĩo and the Atlantic Nĩo. *Nature*, *443*(7109), 324–328. https://doi.org/10.1038/nature05053

Chiang, J. C., Kushnir, Y., & Giannini, A. (2002). Deconstructing Atlantic Intertropical Convergence Zone variability: Influence of the local cross-equatorial sea surface temperature gradient and remote forcing from the Eastern Equatorial Pacific. *Journal of Geophysical Research Atmospheres*, *107*(1-2). https://doi.org/10.1029/2000jd000307

Compo, G. P., & Sardeshmukh, P. D. (2010). Removing ENSO-related variations from the climate record. *Journal of Climate*, *23*(8), 1957–1978. https://doi.org/10.1175/2009JCLI2735.1

D'Acunha, B., Dalmagro, H., Zanella de Arruda, P., Biudes, M., Lathuillière, M., Uribe, M., Couto, E., Brando, P., Vourlitis, G., & Johnson, M. (2024). Changes in evapotranspiration, transpiration and evaporation across natural and managed landscapes in the Amazon, Cerrado and Pantanal biomes. *Agricultural and Forest Meteorology*, *346*, 109875. https://doi.org/10.1016/j.agrformet.2023.109875

Dominguez, F., Eiras-Barca, J., Yang, Z., Bock, D., Nieto, R., & Gimeno, L. (2022). Amazonian Moisture Recycling Revisited Using WRF With Water Vapor Tracers. *Journal of Geophysical Research: Atmospheres*, *127*(4). https://doi.org/10.1029/2021JD035259

Drumond, A., Marengo, J., Ambrizzi, T., Nieto, R., Moreira, L., & Gimeno, L. (2014). The role of the Amazon Basin moisture in the atmospheric branch of the hydrological cycle: A Lagrangian analysis. *Hydrology and Earth System Sciences*, *18*(7), 2577–2598. https://doi.org/10.5194/hess-18-2577-2014

Duque-Gardeazabal. (2025). An Atlantic influence on evaporation in the Orinoco and Amazon basins - codes. https://doi.org/10.5281/zenodo.15389246

Eagleson, P. S. (2013). *Ecohydrology: Darwinian expression of vegetation form and function* (Vol. 53). https://doi.org/10.1017/CBO9781107415324.004

ECMWF. (2023). IFS Documentation CY48R1 - Part IV: Physical Processes. In *Ifs documentation cy48r1*. https://doi.org/10.21957/02054f0fbf

Enfield, D. B. (1996). Relationships of inter-American rainfall to tropical Atlantic and Pacific SST variability. *Geophysical Research Letters*, *23*(23), 3305–3308. https://doi.org/10.1029/96GL03231

Espinoza, J. C., Ronchail, J., Guyot, J. L., Junquas, C., Vauchel, P., Lavado, W., Drapeau, G., & Pombosa, R. (2011). Climate variability and extreme drought in the upper Solimões River (western Amazon Basin): Understanding the exceptional 2010 drought. *Geophysical Research Letters*, *38*(13), n/a–n/a. https://doi.org/10.1029/2011GL047862

Fernandes, K., Giannini, A., Verchot, L., Baethgen, W., & Pinedo-Vasquez, M. (2015). Decadal covariability of Atlantic SSTs and western Amazon dry-season hydroclimate in observations and CMIP5 simulations. *Geophysical Research Letters*, *42*(16), 6793–6801. https://doi.org/10.1002/2015GL063911

Friedman, A. R., Hegerl, G. C., Schurer, A. P., Lee, S. Y., Kong, W., Cheng, W., & Chiang, J. C. (2020). Forced and unforced decadal behavior of the interhemispheric SST contrast during the instrumental period (1881–2012): Contextualizing the late 1960s–early 1970s shift. *Journal of Climate*, *33*(9), 3487–3509. https://doi.org/10.1175/JCLI-D-19-0102.1

García-Serrano, J., Cassou, C., Douville, H., Giannini, A., & Doblas-Reyes, F. J. (2017). Revisiting the ENSO teleconnection to the tropical North Atlantic. *Journal of Climate*, *30*(17), 6945–6957. https://doi.org/10.1175/JCLI-D-16-0641.1

Garreaud, R. D., Vuille, M., Compagnucci, R., & Marengo, J. (2009). Present-day South American climate. *Palaeogeography, Palaeoclimatology, Palaeoecology*, *281*(3-4), 180–195. https://doi.org/10.1016/j.palaeo.2007.10.032

Gebrechorkos, S. H., Leyland, J., Dadson, S. J., Cohen, S., Slater, L., Wortmann, M., Ashworth, P. J., Bennett, G. L., Boothroyd, R., Cloke, H., Delorme, P., Griffith, H., Hardy, R., Hawker, L., McLelland, S., Neal, J., Nicholas, A., Tatem, A. J., Vahidi, E., … Darby, S. E. (2024). Global-scale evaluation of precipitation datasets for hydrological modelling. *Hydrology and Earth System Sciences*, *28*(14), 3099–3118. https://doi.org/10.5194/hess-28-3099-2024

Grimm, A. M., & Zilli, M. T. (2009). Interannual variability and seasonal evolution of summer monsoon rainfall in South America. *Journal of Climate*, *22*(9), 2257–2275. https://doi.org/10.1175/2008JCLI2345.1

Gruber, A., Scanlon, T., van der Schalie, R., Wagner, W., & Dorigo, W. (2019). Evolution of the ESA CCI Soil Moisture climate data records and their underlying merging methodology. *Earth System Science Data*, *11*(2), 717–739. https://doi.org/10.5194/essd-11-717-2019

Gu, G., & Adler, R. F. (2009). Interannual variability of boreal summer rainfall in the equatorial Atlantic. *International Journal of Climatology*, *29*(2), 175–184. https://doi.org/10.1002/joc.1724

Hasler, N., & Avissar, R. (2007). What Controls Evapotranspiration in the Amazon Basin? *Journal of Hydrometeorology*, *8*(3), 380–395. https://doi.org/10.1175/JHM587.1

He, C., Clement, A. C., Kramer, S. M., Cane, M. A., Klavans, J. M., Fenske, T. M., & Murphy, L. N. (2023). Tropical Atlantic multidecadal variability is dominated by external forcing. *Nature*, *622*(October). https://doi.org/10.1038/s41586-023-06489-4

Hersbach, H., Bell, B., Berrisford, P., Hirahara, S., Horányi, A., Muñoz-Sabater, J., Nicolas, J., Peubey, C., Radu, R., Schepers, D., Simmons, A., Soci, C., Abdalla, S., Abellan, X., Balsamo, G., Bechtold, P., Biavati, G., Bidlot, J., Bonavita, M., … Thépaut, J. N. (2020). The ERA5 global reanalysis. *Quarterly Journal of the Royal Meteorological Society*, *146*(730), 1999–2049. https://doi.org/10.1002/qj.3803

Hirschi, M., Mueller, B., Dorigo, W., & Seneviratne, S. I. (2014). Using remotely sensed soil moisture for land-atmosphere coupling diagnostics: The role of surface vs. root-zone soil moisture variability. *Remote Sensing of Environment*, *154*, 246–252. https://doi.org/10.1016/j.rse.2014.08.030

Hoyos, I., Cañón-Barriga, J., Arenas-Suárez, T., Dominguez, F., & Rodríguez, B. A. (2019). Variability of regional atmospheric moisture over Northern South America: patterns and underlying phenomena. *Climate Dynamics*, *52*(1-2), 893–911. https://doi.org/10.1007/s00382-018-4172-9

Hua, W., Dai, A., Zhou, L., Qin, M., & Chen, H. (2019). An Externally Forced Decadal Rainfall Seesaw Pattern Over the Sahel and Southeast Amazon. *Geophysical Research Letters*, *46*(2), 923–932. https://doi.org/10.1029/2018GL081406

Huang, B., Thorne, P. W., Banzon, V. F., Boyer, T., Chepurin, G., Lawrimore, J. H., Menne, M. J., Smith, T. M., Vose, R. S., & Zhang, H. M. (2017). Extended reconstructed Sea surface temperature, Version 5 (ERSSTv5): Upgrades, validations, and intercomparisons. *Journal of Climate*, *30*(20), 8179–8205. https://doi.org/10.1175/JCLI-D-16-0836.1

Humphrey, V., Berg, A., Ciais, P., Gentine, P., Jung, M., Reichstein, M., Seneviratne, S. I., & Frankenberg, C. (2021). Soil moisture–atmosphere feedback dominates land carbon uptake variability. *Nature*, *592*(7852), 65–69. https://doi.org/10.1038/s41586-021-03325-5

IPCC. (2021, July). *Climate Change 2021: The Physical Science Basis*. Cambridge University Press. https://doi.org/10.1017/9781009157896

Jarvis, P. (1976). The interpretation of the variations in leaf water potential and stomatal conductance found in canopies in the field. *Philosophical Transactions of the Royal Society of London. B, Biological Sciences*, *273*(927), 593–610. https://doi.org/10.1098/rstb.1976.0035

Jung, M., Koirala, S., Weber, U., Ichii, K., Gans, F., Camps-Valls, G., Papale, D., Schwalm, C., Tramontana, G., & Reichstein, M. (2019). The FLUXCOM ensemble of global land-atmosphere energy fluxes. *Scientific Data*, *6*(1), 74. https://doi.org/10.1038/s41597-019-0076-8

Karlsson, K.-G., Riihelä, A., Trentmann, J., Stengel, M., Solodovnik, I., Meirink, J. F., Devasthale, A., Jääskeläinen, E., Kallio-Myers, V., Eliasson, S., Benas, N., Johansson, E., Stein, D., Finkensieper, S., Håkansson, N., Akkermans, T., Clerbaux, N., Selbach, N., Marc, S., & Hollmann, R. (2023). CLARA-A3: CM SAF

cLoud, Albedo and surface RAdiation dataset from AVHRR data - Edition 3. https://doi.org/10.5676/EUM_SAF_CM/CLARA_AVHRR/V003

Kaune, A., Werner, M., López López, P., Rodríguez, E., Karimi, P., & De Fraiture, C. (2019). Can global precipitation datasets benefit the estimation of the area to be cropped in irrigated agriculture? *Hydrology and Earth System Sciences*, *23*(5), 2351–2368. https://doi.org/10.5194/hess-23-2351-2019

Kennedy, J. J., Rayner, N. A., Atkinson, C. P., & Killick, R. E. (2019). An Ensemble Data Set of Sea Surface Temperature Change From 1850: The Met Office Hadley Centre HadSST.4.0.0.0 Data Set. *Journal of Geophysical Research: Atmospheres*, *124*(14), 7719–7763. https://doi.org/10.1029/2018JD029867

Le, T., & Bae, D.-H. (2020). Response of global evaporation to major climate modes in historical and future Coupled Model Intercomparison Project Phase 5 simulations. *Hydrology and Earth System Sciences*, *24*(3), 1131–1143. https://doi.org/10.5194/hess-24-1131-2020

Lehner, B., & Grill, G. (2013). Global river hydrography and network routing: baseline data and new approaches to study the world's large river systems. *Hydrological Processes*, *27*(15), 2171–2186. https://doi.org/10.1002/hyp.9740

Lian, X., Morfopoulos, C., & Gentine, P. (2024). Water deficit and storm disturbances co-regulate Amazon rainforest seasonality. *Science Advances*, *10*(36). https://doi.org/10.1126/sciadv.adk5861

Lopes, A. V., Chiang, J. C. H., Thompson, S. A., & Dracup, J. A. (2016). Trend and uncertainty in spatial-temporal patterns of hydrological droughts in the Amazon basin. *Geophysical Research Letters*, *43*(7), 3307–3316. https://doi.org/10.1002/2016GL067738

Lübbecke, J. F., & McPhaden, M. J. (2012). On the Inconsistent Relationship between Pacific and Atlantic Niños. *Journal of Climate*, *25*(12), 4294–4303. https://doi.org/10.1175/JCLI-D-11-00553.1

Lübbecke, J. F., Rodríguez-Fonseca, B., Richter, I., Martín-Rey, M., Losada, T., Polo, I., & Keenlyside, N. S. (2018). Equatorial Atlantic variability—Modes, mechanisms, and global teleconnections. *Wiley Interdisciplinary Reviews: Climate Change*, *9*(4), 1–18. https://doi.org/10.1002/wcc.527

Makarieva, A. M., Nefiodov, A. V., Nobre, A. D., Baudena, M., Bardi, U., Sheil, D., Saleska, S. R., Molina, R. D., & Rammig, A. (2023). The role of ecosystem transpiration in creating alternate moisture regimes by influencing atmospheric moisture convergence. *Global Change Biology*, *29*(9), 2536–2556. https://doi.org/10.1111/gcb.16644

Marengo, J. A., & Espinoza, J. C. (2016). Extreme seasonal droughts and floods in Amazonia: Causes, trends and impacts. *International Journal of Climatology*, *36*(3), 1033–1050. https://doi.org/10.1002/joc.4420

Mariotti, A., Ruti, P. M., & Rixen, M. (2018). Progress in subseasonal to seasonal prediction through a joint weather and climate community effort. *npj Climate and Atmospheric Science*, *1*(1), 2–5. https://doi.org/10.1038/s41612-018-0014-z

Martens, B., Miralles, D. G., Lievens, H., Van Der Schalie, R., De Jeu, R. A., Fernández-Prieto, D., Beck, H. E., Dorigo, W. A., & Verhoest, N. E. (2017). GLEAM v3: Satellite-based land evaporation and root-zone soil moisture. *Geoscientific Model Development*, *10*(5), 1903–1925. https://doi.org/10.5194/gmd-10-1903-2017

Martens, B., Waegeman, W., Dorigo, W. A., Verhoest, N. E. C., & Miralles, D. G. (2018). Terrestrial evaporation response to modes of climate variability. *npj*

Climate and Atmospheric Science, *1*(1), 43. https://doi.org/10.1038/s41612-018-0053-5

Martín-Rey, M., Rodríguez-Fonseca, B., Polo, I., & Kucharski, F. (2014). On the Atlantic–Pacific Niños connection: a multidecadal modulated mode. *Climate Dynamics*, *43*(11), 3163–3178. https://doi.org/10.1007/s00382-014-2305-3

Merz, B., Blöschl, G., Vorogushyn, S., Dottori, F., Aerts, J. C., Bates, P., Bertola, M., Kemter, M., Kreibich, H., Lall, U., & Macdonald, E. (2021). Causes, impacts and patterns of disastrous river floods. *Nature Reviews Earth and Environment*, *2*(9), 592–609. https://doi.org/10.1038/s43017-021-00195-3

Miralles, D. G., Van Den Berg, M. J., Gash, J. H., Parinussa, R. M., De Jeu, R. A., Beck, H. E., Holmes, T. R., Jiménez, C., Verhoest, N. E., Dorigo, W. A., Teuling, A. J., & Johannes Dolman, A. (2014). El Niño-La Niña cycle and recent trends in continental evaporation. *Nature Climate Change*, *4*(2), 122–126. https://doi.org/10.1038/nclimate2068

Mishra, A. K., & Singh, V. P. (2010). A review of drought concepts. *Journal of Hydrology*, *391*(1-2), 202–216. https://doi.org/10.1016/j.jhydrol.2010.07.012

Moura, M. M., dos Santos, A. R., Pezzopane, J. E. M., Alexandre, R. S., da Silva, S. F., Pimentel, S. M., de Andrade, M. S. S., Silva, F. G. R., Branco, E. R. F., Moreira, T. R., da Silva, R. G., & de Carvalho, J. R. (2019). Relation of El Niño and La Niña phenomena to precipitation, evapotranspiration and temperature in the Amazon basin. *Science of the Total Environment*, *651*, 1639–1651. https://doi.org/10.1016/j.scitotenv.2018.09.242

Münnich, M., & Neelin, J. D. (2005). Seasonal influence of ENSO on the Atlantic ITCZ and equatorial South America. *Geophysical Research Letters*, *32*(21). https://doi.org/10.1029/2005GL023900

Muñoz-Sabater, J., Dutra, E., Agustí-Panareda, A., Albergel, C., Arduini, G., Balsamo, G., Boussetta, S., Choulga, M., Harrigan, S., Hersbach, H., Martens, B., Miralles, D. G., Piles, M., Rodríguez-Fernández, N. J., Zsoter, E., Buontempo, C., & Thépaut, J. N. (2021). ERA5-Land: A state-of-the-art global reanalysis dataset for land applications. *Earth System Science Data*, *13*(9), 4349–4383. https://doi.org/10.5194/essd-13-4349-2021

Nemani, R. R., Keeling, C. D., Hashimoto, H., Jolly, W. M., Piper, S. C., Tucker, C. J., Myneni, R. B., & Running, S. W. (2003). Climate-Driven Increases in Global Terrestrial Net Primary Production from 1982 to 1999. *Science*, *300*(5625), 1560–1563. https://doi.org/10.1126/science.1082750

O'Connor, J., Santos, M. J., Rebel, K. T., & Dekker, S. C. (2019). The influence of water table depth on evapotranspiration in the Amazon arc of deforestation. *Hydrology and Earth System Sciences*, *23*(9), 3917–3931. https://doi.org/10.5194/hess-23-3917-2019

Olmo, M. E., Espinoza, J. C., Bettolli, M. L., Sierra, J. P., Junquas, C., Arias, P. A., Moron, V., & Balmaceda-Huarte, R. (2022). Circulation Patterns and Associated Rainfall Over South Tropical South America: GCMs Evaluation During the Dry-To-Wet Transition Season. *Journal of Geophysical Research: Atmospheres*, *127*(12). https://doi.org/10.1029/2022JD036468

Pabón, J., & Dorado, J. (2008). INTRASEASONAL VARIABILITY OF RAINFALL OVER NORTHERN SOUTH AMERICA AND CARIBBEAN REGION. *Earth Sciences Research Journal*, *12*(2), 194–212.

Paccini, L., Hohenegger, C., & Stevens, B. (2021). Explicit versus Parameterized Convection in Response to the Atlantic Meridional Mode. *Journal of Climate*, *34*(9), 3343–3354. https://doi.org/10.1175/JCLI-D-20-0224.1

Poveda, G., Jaramillo, A., Gil, M. M., Quiceno, N., & Mantilla, R. I. (2001). Seasonally in ENSO-related precipitation, river discharges, soil moisture, and vegetation index in Colombia. *Water Resources Research*, *37*(8), 2169–2178. https://doi.org/10.1029/2000WR900395

Poveda, G., Waylen, P. R., & Pulwarty, R. S. (2006). Annual and inter-annual variability of the present climate in northern South America and southern Mesoamerica. *Palaeogeography, Palaeoclimatology, Palaeoecology*, *234*(1), 3–27. https://doi.org/10.1016/j.palaeo.2005.10.031

Roberts, J. M., Gash, J. H. C., Tani, M., & Bruijnzeel, L. A. (2005, January). Controls on evaporation in lowland tropical rainforest. In *Forests, water and people in the humid tropics* (pp. 287–313). Cambridge University Press. https://doi.org/10.1017/CBO9780511535666.019

Rodrigues, R. R., & McPhaden, M. J. (2014). Why did the 2011-2012 La Niña cause a severe drought in the Brazilian Northeast? *Geophysical Research Letters*, *41*(3), 1012–1018. https://doi.org/10.1002/2013GL058703

Ronchail, J., Cochonneau, G., Molinier, M., Guyot, J. L., De Miranda Chaves, A. G., Guimarães, V., & De Oliveira, E. (2002). Interannual rainfall variability in the Amazon basin and sea-surface temperatures in the equatorial Pacific and the tropical Atlantic Oceans. *International Journal of Climatology*, *22*(13), 1663–1686. https://doi.org/10.1002/joc.815

Ruiz-Barradas, A., Carton, J. A., & Nigam, S. (2000). Structure of Interannual-to-Decadal climate variability in the tropical Atlantic sector. *Journal of Climate*, *13*(18), 3285–3297. https://doi.org/10.1175/1520-0442(2000)013<3285:SOITDC>2.0.CO;2

Ruiz-Vásquez, M., Arias, P. A., & Martínez, J. A. (2024). Enso influence on water vapor transport and thermodynamics over Northwestern South America. *Theoretical and Applied Climatology*, *155*(5), 3771–3789. https://doi.org/10.1007/s00704-024-04848-3

Seneviratne, S. I., Corti, T., Davin, E. L., Hirschi, M., Jaeger, E. B., Lehner, I., Orlowsky, B., & Teuling, A. J. (2010). Investigating soil moisture-climate interactions in a changing climate: A review. *Earth-Science Reviews*, *99*(3-4), 125–161. https://doi.org/10.1016/j.earscirev.2010.02.004

Staal, A., Tuinenburg, O. A., Bosmans, J. H. C., Holmgren, M., van Nes, E. H., Scheffer, M., Zemp, D. C., & Dekker, S. C. (2018). Forest-rainfall cascades buffer against drought across the Amazon. *Nature Climate Change*, *8*(6), 539–543. https://doi.org/10.1038/s41558-018-0177-y

Thoning, K. W., Tans, P. P., & Komhyr, W. D. (1989). Atmospheric carbon dioxide at Mauna Loa Observatory: 2. Analysis of the NOAA GMCC data, 1974-1985. *Journal of Geophysical Research: Atmospheres*, *94*(D6), 8549–8565. https://doi.org/10.1029/JD094iD06p08549

Torralba, V., Rodríguez-Fonseca, B., Mohino, E., & Losada, T. (2015). The non-stationary influence of the Atlantic and Pacific niños on north Eastern South American rainfall. *Frontiers in Earth Science*, *3*(September), 1–10. https://doi.org/10.3389/feart.2015.00055

Towner, J., Ficchí, A., Cloke, H. L., Bazo, J., Coughlan de Perez, E., & Stephens, E. M. (2021). Influence of ENSO and tropical Atlantic climate variability on flood characteristics in the Amazon basin. *Hydrology and Earth System Sciences*, *25*(7), 3875–3895. https://doi.org/10.5194/hess-25-3875-2021

Ummenhofer, C. C., & Meehl, G. A. (2017). Extreme weather and climate events with ecological relevance: a review. *Philosophical Transactions of the Royal Society B:*

Biological Sciences, *372*(1723), 20160135. https://doi.org/10.1098/rstb.2016.0135

Valencia, S., Marín, D. E., Gómez, D., Hoyos, N., Salazar, J. F., & Villegas, J. C. (2023). Spatio-temporal assessment of Gridded precipitation products across topographic and climatic gradients in Colombia. *Atmospheric Research*, *285*, 106643. https://doi.org/10.1016/j.atmosres.2023.106643

Vallès-Casanova, I., Lee, S.-K., Foltz, G. R., & Pelegrí, J. L. (2020). On the Spatiotemporal Diversity of Atlantic Niño and Associated Rainfall Variability Over West Africa and South America. *Geophysical Research Letters*, *47*(8), 1–10. https://doi.org/10.1029/2020GL087108

van der Ent, R. J., & Savenije, H. H. G. (2011). Length and time scales of atmospheric moisture recycling. *Atmospheric Chemistry and Physics*, *11*(5), 1853–1863. https://doi.org/10.5194/acp-11-1853-2011

Wang, K., & Dickinson, R. E. (2012). A review of global terrestrial evapotranspiration: Observation, modeling, climatology, and climatic variability. *Reviews of Geophysics*, *50*(2), 1–54. https://doi.org/10.1029/2011RG000373

Wang-Erlandsson, L., Fetzer, I., Keys, P. W., van der Ent, R. J., Savenije, H. H. G., & Gordon, L. J. (2018). Remote land use impacts on river flows through atmospheric teleconnections. *Hydrology and Earth System Sciences*, *22*(8), 4311–4328. https://doi.org/10.5194/hess-22-4311-2018

Williams, I. N., & Patricola, C. M. (2018). Diversity of ENSO Events Unified by Convective Threshold Sea Surface Temperature: A Nonlinear ENSO Index. *Geophysical Research Letters*, *45*(17), 9236–9244. https://doi.org/10.1029/2018GL079203

Xie, Z., Yao, Y., Tang, Q., Liu, M., Fisher, J. B., Chen, J., Zhang, X., Jia, K., Li, Y., Shang, K., Jiang, B., Yang, J., Yu, R., Zhang, X., Guo, X., Liu, L., Ning, J., Fan, J., & Zhang, L. (2024). Evaluation of seven satellite-based and two reanalysis global terrestrial evapotranspiration products. *Journal of Hydrology*, *630*, 130649. https://doi.org/10.1016/j.jhydrol.2024.130649

Yoon, J. H., & Zeng, N. (2010). An Atlantic influence on Amazon rainfall. *Climate Dynamics*, *34*(2), 249–264. https://doi.org/10.1007/s00382-009-0551-6

Zanin, P. R., Pareja-Quispe, D., & Espinoza, J.-c. (2024). Evapotranspiration in the Amazon Basin: Couplings, hydrological memory and water feedback. *Agricultural and Forest Meteorology*, *352*(April), 110040. https://doi.org/10.1016/j.agrformet.2024.110040

Zemp, D. C., Schleussner, C.-F., Barbosa, H. M. J., van der Ent, R. J., Donges, J. F., Heinke, J., Sampaio, G., & Rammig, A. (2014). On the importance of cascading moisture recycling in South America. *Atmospheric Chemistry and Physics*, *14*(23), 13337–13359. https://doi.org/10.5194/acp-14-13337-2014

Zhang, Y., Peña-Arancibia, J. L., McVicar, T. R., Chiew, F. H., Vaze, J., Liu, C., Lu, X., Zheng, H., Wang, Y., Liu, Y. Y., Miralles, D. G., & Pan, M. (2016). Multi-decadal trends in global terrestrial evapotranspiration and its components. *Scientific Reports*, *6*(August 2015), 1–12. https://doi.org/10.1038/srep19124

Zhao, M., & Running, S. W. (2010). Drought-Induced Reduction in Global Terrestrial Net Primary Production from 2000 Through 2009. *Science*, *329*(5994), 940–943. https://doi.org/10.1126/science.1192666

Chapter 3

Solar and wind energy variability in tropical South America: seasonal ocean-atmospheric modulators

Nicolás Duque-Gardeazabal[1,2], Stefan Brönnimann[1,2], Andrew R.Friedman[1,2,3], Edgar Dolores-Tesillos[1,2], Olivia Martius[1,2]

1. Oeschger Centre for Climate Change Research, University of Bern, Bern, Switzerland.
2. Institute of Geography, University of Bern, Bern, Switzerland.
3. now at Laboratoire de Météorologie Dynamique / Institute Pierre-Simon Laplace, Paris, France

Article submitted to *Meteorological Applications*:
Duque-Gardeazabal, N., Brönnimann, S., Friedman, A. R., Dolores-Tesillos and Martius, O. (Reviewed). Solar and wind energy variability in tropical South America: seasonal ocean-atmospheric modulators.

Abstract

Interannual climate variability strongly influences renewable energy availability, making it a critical factor for achieving UN Sustainable Development Goals (SDGs). However, our knowledge about the potential solar and wind energy production in tropical South America and its relation to ocean-atmospheric modes of variability is limited; modes such as El Niño/Southern Oscillation (ENSO), the Atlantic Meridional Mode (AMM), among others.

Therefore, we investigate the influence of ENSO and modes in the Atlantic Ocean on solar and wind energy. We apply partial correlations and composite analyses to reanalysis and satellite data to identify the processes connecting large-scale ocean-atmospheric variability to seasonal anomalies in renewable power generation. Our study identifies three energy hubs as regions with high climatological mean energy availability: the north Caribbean (NC), eastern Brazil (EB), and western Perú/Bolivia (WPB).

ENSO influences the sea level pressure (SLP) gradients, generating wind anomalies that directly affect the wind capacity factor (CF). ENSO also affects the solar CF through reduced atmospheric moisture transport and convergence, which results in fewer clouds leading to higher-than-average surface radiation, or by atmospheric subsidence. ENSO impacts the NC and EB hubs, with weaker effects in the WPB hub.

The AMM is associated with cross-equatorial wind anomalies that modulate wind CF, as well as moisture convergence and cloud cover, thereby influencing solar CF. Wind CF in the NC and EB hubs are inversely modulated; the NC experiences weaker winds and reduced radiation in the positive phase, while northeastern Brazil shows stronger winds and increased radiation. The Atlantic equatorial El Niño mode (Atl3) exerts minor effects, with anomalies confined to the equatorial Atlantic.

Overall, we find limited complementarity between solar and wind energy at interannual time-scale. Our results provide insights for forecasting energy production and managing energy storage for periods of low renewable energy availability.

Graphical Abstract

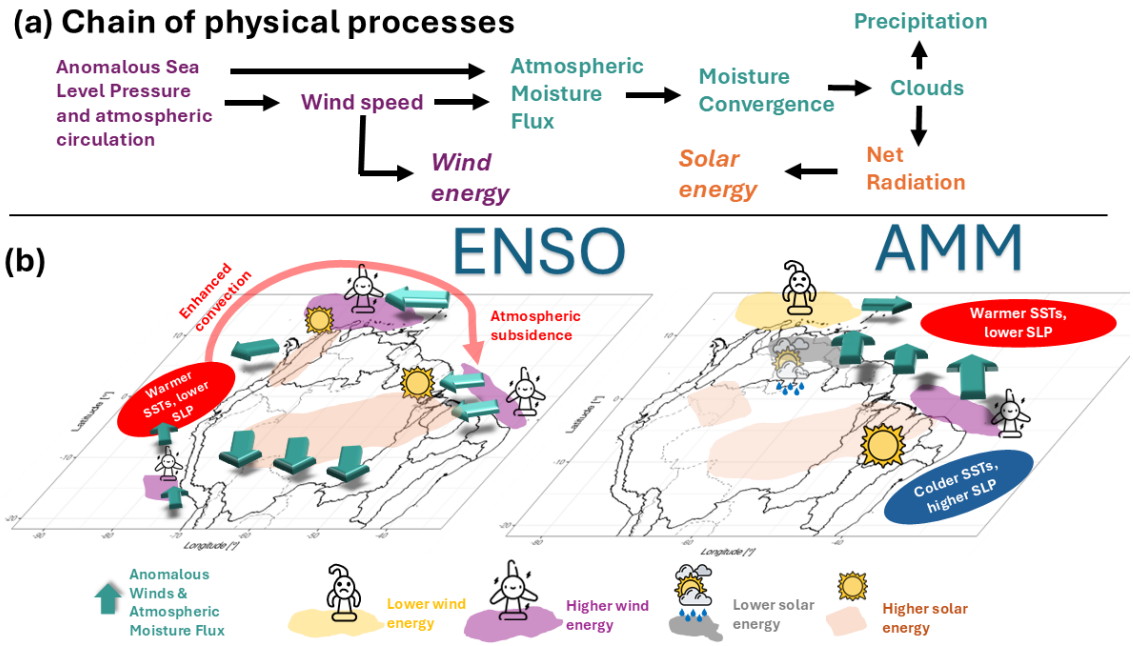

Climate variability affects renewable energy production and thus considering it in planning is essential for achieving sustainable development. We present how climate (ocean-atmospheric) variability modes modulate wind and solar radiation variability, thereby influencing renewable power generation in tropical South America. El Niño/Southern Oscillation simultaneously enhances both energy sources in the El Niño phase, while La Niña suppresses them. The Atlantic Meridional Mode creates a sea level pressure seesaw that modulates renewable generation along the eastern and northern coast of South America. Solar and wind power rarely complement each other, but they can serve as valuable complements to hydropower, which is expanding in the Amazon and has several environmental impacts.

3.1 Introduction

Climate variability significantly affects livelihoods by influencing renewable energy generation (Bustos et al., 2017; Engeland et al., 2017). Renewable energy sources are key to achieving the UN Sustainable Development Goals, specifically through building a reliable and decarbonised energy grid (UN, 2015). Both solar and wind energy production are strongly dependent on local weather conditions. Then, considering intra- and interannual atmospheric variability is crucial for renewable energy planning and management (Boretti & Castelletto, 2020).

South America has one of the world's highest shares of renewable energy (Kieffer & López-Peña, 2016). Hydropower dominates, but reliance on carbon- and gas-based facilities increases during droughts (Arango & Larsen, 2010). Solar and wind energy sources are expanding (Eelsalu et al., 2024; Gil Ruiz et al., 2021; Vargas Gil et al., 2020), highlighting the need to understand their climate sensitivities.

Coupled ocean-atmospheric variability modes strongly influence the atmospheric circulation and local weather conditions in the tropics and South America, particularly at seasonal time scale (Cai et al., 2019). El Niño/Southern Oscillation (ENSO) is the most influential mode of climate variability worldwide (Timmermann et al., 2018). It strongly modulates tropical atmospheric circulation, thereby modifying near-surface wind speeds, atmospheric convergence, and short-wave radiation (Cai et al., 2020). Then, it affects renewable energy production across South America (Bianchi et al., 2022; Perini de Souza et al., 2022).

Atlantic variability modes also modulate atmospheric circulation and conditions over South America, thereby affecting renewable energy production. Moreover, they affect the hydrological cycle through changes in atmospheric water vapour circulation and convergence (Duque-Gardeazabal et al., 2025; Lopes et al., 2016; Towner et al., 2021). The Atlantic Meridional Mode (AMM) modulates the strength of the Atlantic trade winds and subtropical cloud cover (Chiang & Sobel, 2002; Drumond et al., 2014). The Atlantic El Niño equatorial mode (Atl3) is the leading mode in the tropical Atlantic and is also associated with winds and rainfall variability (Ruiz-Barradas et al., 2000; Vallès-Casanova et al., 2020). ENSO is connected to the development of other ocean-atmospheric modes – both in the Atlantic and Indian oceans – through extratropical circulation changes and tropical atmospheric bridges (Andrian et al., 2024; Cai et al., 2019; Compo & Sardeshmukh, 2010; García-Serrano et al., 2017; Martín-Rey et al., 2014). Nevertheless, the Atlantic modes are characterised by their own changes in sea surface temperature (SST) and sea level pressure (SLP), which generate distinct regional atmospheric circulation patterns (Lübbecke et al., 2018).

Other sources of variability operate at shorter or longer timescales, and thus, might modulate solar and wind energy production. These can be the Madden-Julian Oscillations (Pabón & Dorado, 2008) and multi-decadal modes associated with aerosol forcing such as the Atlantic Multidecadal Oscillation (AMO)(He et al., 2023) or Interdecadal Pacific Oscillation (IPO)(Henley et al., 2015).

However, there has not been an assessment of how ENSO and the major tropical Atlantic modes jointly influence the potential solar and wind energy in tropical South America. Bianchi et al. (2022)) found that ENSO, the Antarctic Oscillation and the AMO drive wind and solar energy in southern South America by changing the Atlantic circulation patterns and the moisture transport. Renewable energy sources might complement each other during energy droughts (Otero et al., 2022). Gonzalez-Salazar and Poganietz (2021) found that wind and solar energy can complement hydropower deficits during warm ENSO events using the existing generation capacity

in South America. However, no studies have assessed wind-solar complementarity under Atlantic variability modes.

Therefore, our study aims to elucidate the correlations between ENSO, Atl3 and AMM ocean-atmospheric modes, and the seasonal interannual variability of potential wind and solar energy, as well as to identify the underlying physical mechanisms. Understanding these physical mechanisms can improve sub-seasonal to seasonal forecasts. Energy companies prioritise stable production to ensure a stable and reliable energy supply (Boretti & Castelletto, 2020); hence, forecasts can guide mitigation strategies, including supply and storage management. We focus on ENSO, the AMM and the Atl3 because these are the dominant interannual modes of the neighbouring tropical Atlantic and Pacific basins, which most strongly modify the regional atmospheric circulation (see section 3 methods for identification of the specific modes). We exclude the Indian Ocean modes, Madden-Julian Oscillations, and multidecadal phenomena such as the AMO and IPO (see section 5 Discussion).

Finally, we assess the wind-solar complementarity in tropical South America under each ocean-atmospheric mode (ENSO, AMM and Atl3). We exclude hydropower energy since it is strongly shaped by site-specific topographic features of the dams and reservoirs.

3.2 Data

3.2.1 Datasets

Meteorological reanalyses are widely used to estimate wind and solar energy production (Bloomfield et al., 2020; Cannon et al., 2015). Our study mainly relies on the ERA5 dataset, the latest ECMWF reanalysis (Hersbach et al., 2020). It provides interpolated data to a grid resolution of 0.25° and 37 pressure levels. Moreover, the hourly temporal resolution enables analysis of the diurnal cycle of wind speed, cloud cover and radiation.

Our study uses wind speed at 100 m and surface short-wave downward radiation to determine wind and solar energy capacity factors (sect. 3.2.2 and 3.2.3). Moreover, we use atmospheric circulation variables because they are related to the mechanism linking the ocean-atmospheric modes with local continental weather (Table 3.1). All datasets are restricted to December-1979 and November-2020 since they cover different periods. They were seasonally aggregated and analysed for each season individually (i.e. four values per year from DJF 1980 to SON 2020, later used in the analysis - Sect. 3.3 methods). The aggregation method is by seasonal average, except for precipitation, when we use the sum. As in other studies, we assume that meteorological conditions at the location of energy installations are adequately represented by ERA5 grid box values.

Focusing on wind resources, Gualtieri (2022) evaluated ERA5 and other reanalyses and concluded that ERA5 is reliable in offshore and in flat onshore areas. Gil Ruiz et al. (2021) reported close agreement between wind energy production estimated with ERA5 and observations over northern South America, using the intensity-duration-frequency distributions for the estimation.

Solar radiation estimated by reanalysis generally shows a positive bias of ERA5 compared to observations (Kies et al., 2021; Wilczak et al., 2024), pecially tropical regions and South America. Nevertheless, temporal correlations are mostly above 0.9, with minima near 0.8 (Ramirez Camargo & Schmidt, 2020); ERA5 underestimate short-wave radiation in clear-sky conditions (Sianturi et al., 2020).

TABLE 3.1: Datasets and variables used to study the wind and solar energy

Source	Variable	Temporal resolution	Spatial resolution
ERA5 – Reanalysis (Hersbach et al., 2020)	Wind speed at 100 m Sea Level Pressure (SLP) Vertically integrated water vapour flux (VIMF) Vertically integrated moisture divergence (MDiv) Surface short-wave downward radiation 2 m temperature	Hourly	0.25°
MSWEP (Beck et al., 2019) Gauge, satellite and reanalysis	Precipitation	Monthly	0.1°
EUMETSAT-CLARA A3 (Karlsson et al., 2023) Satellite	Cloud cover fraction	Monthly	0.25°
ERSSTv5 (Huang et al., 2019) Gauge (ships, buoys, and floats)	Sea Surface Temperature	Monthly	2°

Sea Surface Temperature Anomalies (SSTAs) are used to identify the key ocean-atmospheric modes (Sect. 3.3.1). We use SSTAs from the Extended Reconstructed SST version 5 (Huang et al., 2017).

Cloud cover is expected to influence the surface downward shortwave radiation. We use vertically integrated water vapour flux components (also known as vertically integrated moisture flux, VIMF) and the vertically integrated moisture divergence (MDiv) from ERA5, the latter related to cloud cover. We also used the satellite-based EUMETSAT CLARA-A3 cloud cover area fraction (Karlsson et al., 2023) to verify the dynamics in several sources of information. Precipitation data comes from the Multi-Source Weighted-Ensemble Precipitation v2.8 (MSWEP)(Beck et al., 2019); this dataset integrates rain gauges, satellite and reanalysis data.

3.2.2 Wind capacity factor

The wind capacity factor (CF) represents the ratio between actual and maximum possible energy production of a wind turbine that operates at rated power (Bloomfield et al., 2022). We estimate the wind CF at 100 m – the typical height of wind turbines – because it provides a dimensionless energy variable comparable to other energy sources, such as solar. Other wind energy variables, such as the wind power

density (WPD), are more suitable for comparing different locations without assuming specific turbines (Antonini et al., 2024), but comparing WPD with solar energy requires assuming transformation coefficients (WPD was also calculated but is not shown). The wind CF is calculated from ERA5 wind fields using the power curve from the assumed Vestas V117 – 3.45 turbine (used in similar regional studies; Gil Ruiz et al. (2021) and Wind-turbine-models (2025)), dividing the power output by its rated power of 3450 kW. Our method excludes the wake effects induced by surrounding turbines and grid-induced curtailment since detailed information on current and planned energy facilities is not consistently available region-wide (Dolores-Tesillos et al., 2025). Given our aim is to estimate the interannual variability and its associated modulators, we interpret the estimated wind CF as potential wind energy.

As the wind CF depends on the cube of the wind speed, calculating it at different time scales yields different distributions. Therefore, we use hourly fields from ERA5 – the finest publicly available resolution – and afterwards aggregate the hourly CF to seasonal means for the posterior analysis. SLP is expected to influence wind components; hence, we use SLP from ERA5 to study the modulation mechanisms of the ocean-atmospheric modes (Table 3.1).

3.2.3 Solar capacity factor

Photovoltaic modules (PV) have a wide range of different panels whose efficiency is affected by temperature and surface solar radiation (Evans & Florschuetz, 1977). We analyse the solar capacity factor (CF), which enables site comparison without specifying the type of solar panel or the characteristics of current and future energy facilities. Bett and Thornton (2016) presented an empirical relationship for calculating the solar CF that estimates the cell efficiency from the downward surface solar radiation, the module temperature and the irradiance at standard test conditions (Gstc = 1000 W/m^2)(see appendix of Bett and Thornton (2016)). The module temperature considers 2 m air temperature and the surface downward short-wave radiation to establish the working efficiency of the panel. The higher the ambient and module temperature, the lower the panel efficiency.

Our study then uses hourly fields of solar radiation and air temperature from ERA5. The potential solar CF is then filtered to only daytime and aggregated to seasonal averages, the latter consistent with the wind CF methodology.

3.3 Methods

We first map the multiannual availability of solar and wind energy to identify regions of high potential for renewable energy production, hereafter referred to as "energy hubs". Second, we identify the seasonal ocean-atmospheric variability modes that are statistically associated with the wind and solar capacity factors (Sect. 3.3.1), and analyse the underlying physical mechanisms behind these associations using composite analysis (Sect. 3.3.2). Third, we assess the complementarity between both sources of energy (Sect. 3.3.3).

Results are presented in Section 4, where we first identify the energy hubs (Sect. 3.4.1), then detail the influence the ocean-atmospheric modes on these regions (Sect. 3.4.2 and 3.4.3) and finally assess how the modes modulate energy complementarity (Sect. 3.4.4). We conclude with a discussion of the broader implications of these relationships.

3.3.1 Modes of variability

Our study identifies coupled ocean-atmospheric modes with SSTA indices. SSTA are detrended with a regression with de-seasonalised CO_2 concentrations ($R^2 = 0.92$, $p < 0.001$) (Thoning et al., 1989) to focus on interannual variability and exclude the effect of global warming. Principal component analysis is applied to detrended SSTs in the Atlantic and Pacific oceans to extract dominant ocean-atmospheric modes. Other ocean basins that are not close to the study area were excluded because their teleconnections are closely related to those exerted by ENSO (Cai et al., 2019)(see correlations analysis below). PCA loadings are used to define spatial boxes, from which box-averaged climatic indices are built (boxes boundaries were consistent with the literature review (K. Fernandes et al., 2015; Vallès-Casanova et al., 2020). Hence, our study defines the Atlantic indices as:

- The AMM monthly index is defined as the difference between the spatially averaged northern tropical Atlantic SSTA [70°W-15°W, 5°N-25°N] and southern tropical Atlantic SSTA [40°W-0°W, 25°S-5°S].
- The Atl3 monthly index is identified as the spatial average of eastern equatorial Atlantic SSTA [20°W-0°, 3°S-3°N].

To analyse ENSO, we calculate the El Niño Longitude Index (ELI) because it considers the diversity of east- and central-Pacific ENSO events (Williams & Patricola, 2018). This index represents the decomposition of tropical Pacific variability better than fixed box-average indices, which is important for the variability of tropical convection. High ELI values correspond to warm central/eastern Pacific SSTAs (El Niño), while low values indicate cold anomalies (La Niña). Time series of the indices and PCA loadings are shown in Figure S1.

To map the impacts of the modes, we compute partial correlation between the three indices (ELI, AMM, Atl3) and the wind and solar CF, at each grid point. Removing the simultaneous confounding effects from other modes (Y and Z) indicates the relation of a mode X with the analysed variable. We also show the results for the energy hubs. Partial correlations with other indices different from the ELI, AMM and the Atl3 were performed but are not shown, since their teleconnections are closely related to ENSO (Cai et al., 2019).

3.3.2 Identifying the physical mechanisms of the teleconnection

We establish the physical processes of the connection through anomaly composite analysis (mean of anomaly fields at specific times; (Arias et al., 2020; Vallès-Casanova et al., 2020)). The composites are defined based on the seasonally averaged values of the SST indices (indices time series in Figure S1); when values exceed ±1 standard deviation from the mean – for the given season distribution, e.g. boreal summer – the mode is considered to be in its positive or negative phase, respectively. For the ELI, the threshold is set to ±0.75 standard deviations to align with the Oceanic El Niño Index events.

Composites are built with the variables influencing wind speed and radiation (i.e. SLP, winds, VIMF, MDiv, and cloud cover). Composites are always compared to the neutral phase (defined when indices' values are within the previous thresholds). The composites' statistical significance is estimated with a two-sample Student's T-test.

El Niño – ENSO positive warm phase – develops in the boreal summer (JJA, June to August, by the initial letters of the months), grows from September to November

(SON) and peaks in boreal winter D(0)JF(+1)(Timmermann et al., 2018). Conversely, the Atl3 mode peaks in JJA, and the AMM can be active year-round but it is strongest in boreal spring (MAM)(Ruiz-Barradas et al., 2000; Vallès-Casanova et al., 2020). Accordingly, we focus the ENSO analysis on SON and DJF, and the Atlantic modes on MAM and JJA.

3.3.3 Complementarity of wind and solar energy

We assess the complementarity of both energy sources by comparing their standardised anomalies under the influence of each mode. This is at the time steps of the previous composite analysis. The energy hubs are collocated regions with high multiannual potential CF, identified in our first analysis (Sect. 3.4.1). Complementarity is assessed between hubs paired geographically (shortest centroids distance between solar hub and wind hub), to reflect realistic integration potential within regional grids. Complementarity between distant hubs is not considered practical or even possible.

Two scales of complementarity are evaluated. First, a multi-annual mean complementarity seeks to assess differences in the climatological seasonal cycles of the solar and wind CF. Second, an interannual complementarity is based on the variability modes exert over the renewable energy. It compares composites across energy sources, phases of the modes (negative, neutral and positive) and for each season and hub individually. We also quantify complementarity with Spearman correlation, since it handles skewed distributions (e.g. wind CF) and extreme events better than Pearson correlation.

3.4 Results

3.4.1 Identifying renewable energy hubs and their seasonal variability

We identify three key regions based on the 1980-2020 mean seasonal wind CF (Fig. 3.1a-d), and also three with high solar CF (Fig. 3.1e-h). We then group them into three paired energy hubs (Table 3.2), since all have another region with high potential from the opposite sources close to them.

Wind hubs are located in coastal/oceanic areas. Two hubs have a CF value exceeding 0.6 in at least two seasons (North Caribbean and Southwestern Perú)(Fig. 3.1a-d). The Caribbean coast shows nearly year-round high wind resource, which attenuates in SON when the Intertropical Convergence Zone (ITCZ) moves northward. The northeastern Brazilian coast has a long strip that exceeds 0.6 in JJA and SON but is weaker in other seasons (Fig. 3.1c and d). Low wind CF values over the ocean also move with the annual solar cycle and the ITCZ.

The solar CF exhibit a significant annual cycle (Fig. 3.1e-h) also linked to the annual migration of the ITCZ. Three high solar CF regions are located in the north, east and west of tropical South America, close to wind hubs (Fig. 3.1a-d). For eastern Brazil and the Bolivian Altiplano in the southwest, the solar CF exceeds 0.4 in at least three seasons, while the Orinoco savannas in the northern hub the CF is higher than 0.35 in DJF, but drop to 0.2 in JJA. The Bolivian altiplano in the Western hub shows substantial seasonal cycle, with values higher than 0.5 in SON and lower than 0.35 in JJA. Table 3.2presents the identified high potential renewable energy regions (energy hubs, Fig. 3.1).

Energy companies seek low variability to ensure a stable and predictable energy supply (Boretti & Castelletto, 2020). We estimate the CF variability with the

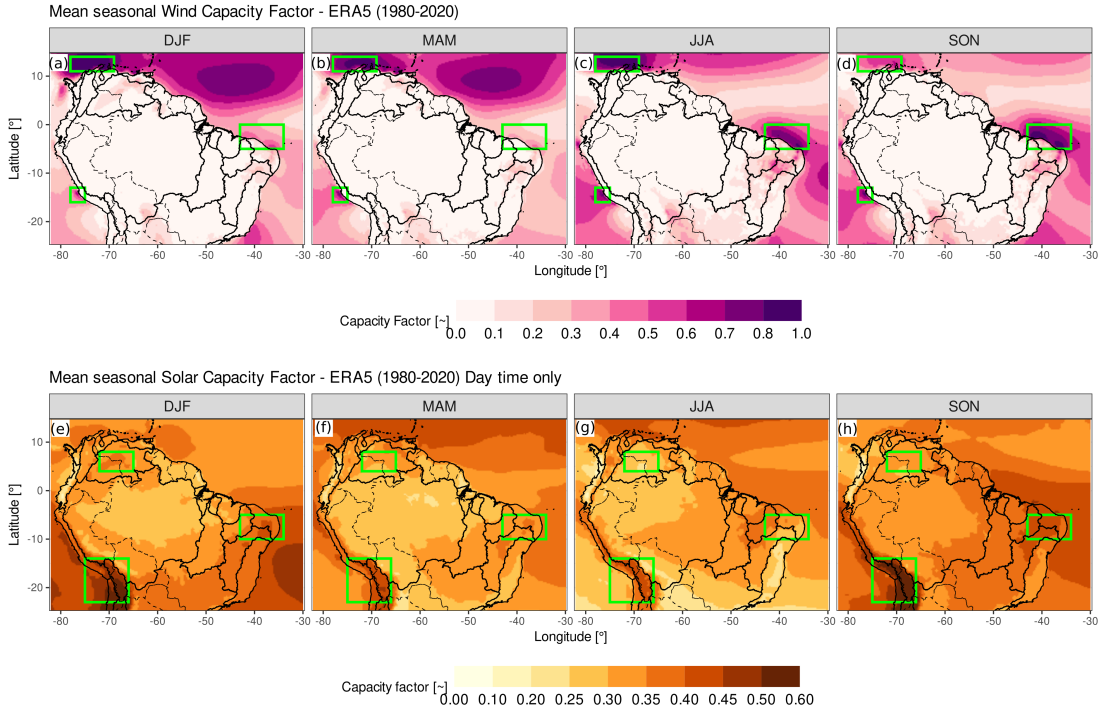

FIGURE 3.1: (a-d) (a-d) Multi-annual mean seasonal wind CF at 100 m above ground. (e-h) multi-annual mean seasonal daytime solar CF. Green rectangles highlight the regions with the highest potential wind and solar CF considering all seasons (energy hubs). Black continuous lines are river basins; dashed lines are country borders. Titles of panels refer to the first letters of the months in each season, i.e., December to February for panels (a) and (e).

TABLE 3.2: Classification of solar and wind energy hubs by geographic proximity

Energy hub	Wind	Solar
#1 Northern Caribbean hub	Caribbean coast	Orinoco's savannas
#2 Eastern Brazil hub	Northeast Brazil coast	East Brazil
#3 Western Perú/Bolivia hub	Southwestern Peruvian coast	Bolivian altiplano

.

coefficient of variation (ratio of the standard deviation and mean, $CV = \sigma/\mu$) and afterwards we look for phenomena modulating that variability which could aid in its prediction (see Sect. 3.4.2 and 3.4.3).

Wind CF seasonal interannual variability is generally below 25% over the oceans but higher over the continent (Fig. 3.2a-d), due to surface friction of wind with topography, which imposes shear stress and turbulence, in turn reducing momentum and wind speed. Conversely, the northern Caribbean and the Peruvian hubs remain relatively stable with a CV bigger than 15% in only one of the seasons (SON and DJF, respectively). Northeastern Brazil hub reaches ca. 25% in MAM when the ITCZ variability strongly affects the wind speeds..

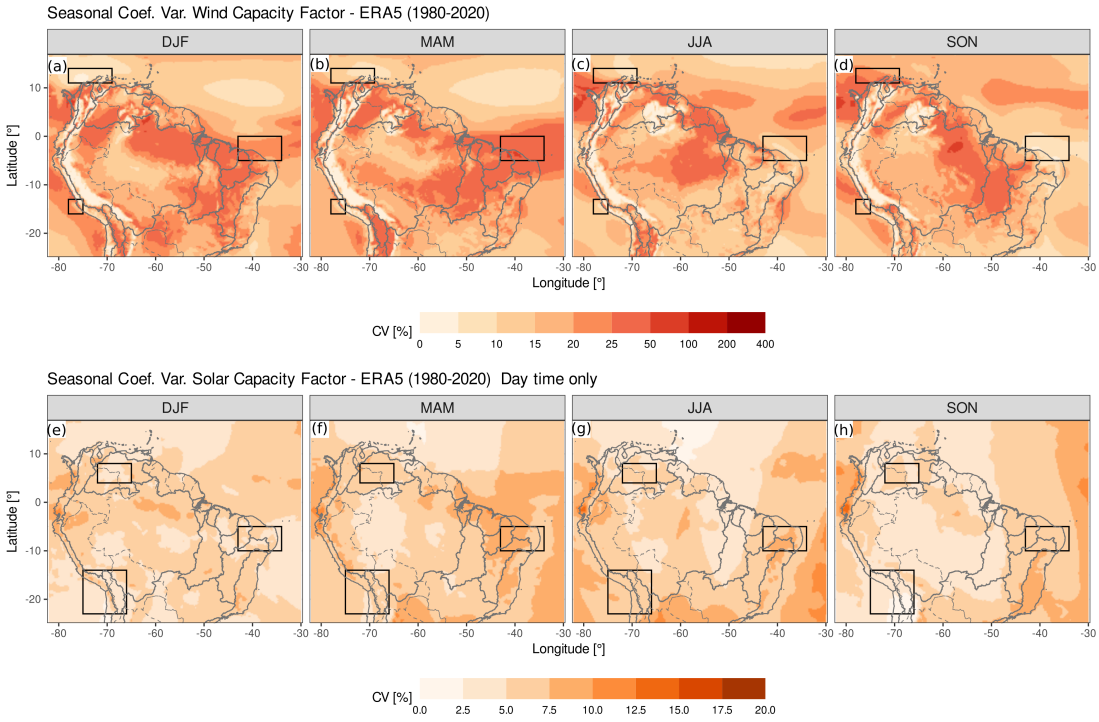

FIGURE 3.2: Coefficient of variation (CV) for (a-d) wind CF for each season and (e-h) daytime-only solar CF for each season. Black rectangles are the same energy hubs as in 3.1.

The solar CF reflects the cloud-radiances assimilated data from polar orbiting satellites (Fig. 3.2e-h), where some swaths have a slightly higher variability, e.g over the Caribbean and northeast Brazil in JJA (Fig. 3.2g). However, almost everywhere the CV is below 10% and just over northeast Brazil and the northwestern coast reaches a higher variability; none of the solar hubs reach a coefficient of variation higher than 10%. The CV is below 7% in all seasons over the western Bolivian solar hub due to the high-altitude topography and low atmospheric moisture which give this hub a special geographical advantage for solar energy. Solar CF variability is, in general, lower than wind CF variability.

3.4.2 Ocean-atmospheric oscillations associated with the variability of the energy hubs

Ocean-atmospheric modes influence wind speed across most of the study domain and, therefore also the wind CF in the identified energy hubs (Fig. 3.3). he magnitude of the correlations changes geographically and seasonally (Fig. S2 for correlation maps, see Sect. 3.5 Discussion).

The wind CF is positively correlated with ENSO over the northern hub during its growing phase (from June to its peak in DJF, Fig. 3.3c and d) and with the eastern wind hub in MAM and JJA. The western hub is affected by ENSO in DJF (Fig. 3.3i). The AMM is associated with a seesaw effect over the north coastline and eastern Brazil hub (negative correlation for the northern and positive for the eastern hub, Fig. 3.3c, d, g and h). This effect is observed year-round but is strongest between March and November. The western hub correlates with the AMM, but because this mode is associated with the Atlantic basin thermodynamics, these relationships might be spurious (physical mechanisms in section 3.4.3). In contrast, the Atl3 shows

limited influence on the wind CF (Fig. S2). Its main signal occurs in MAM over the tropical western Atlantic, a region also affected by ENSO and the AMM but with opposite sign. Significant correlations between the Atl3 and the northern hub might also be spurious (see Sect. 3.5 Discussion).

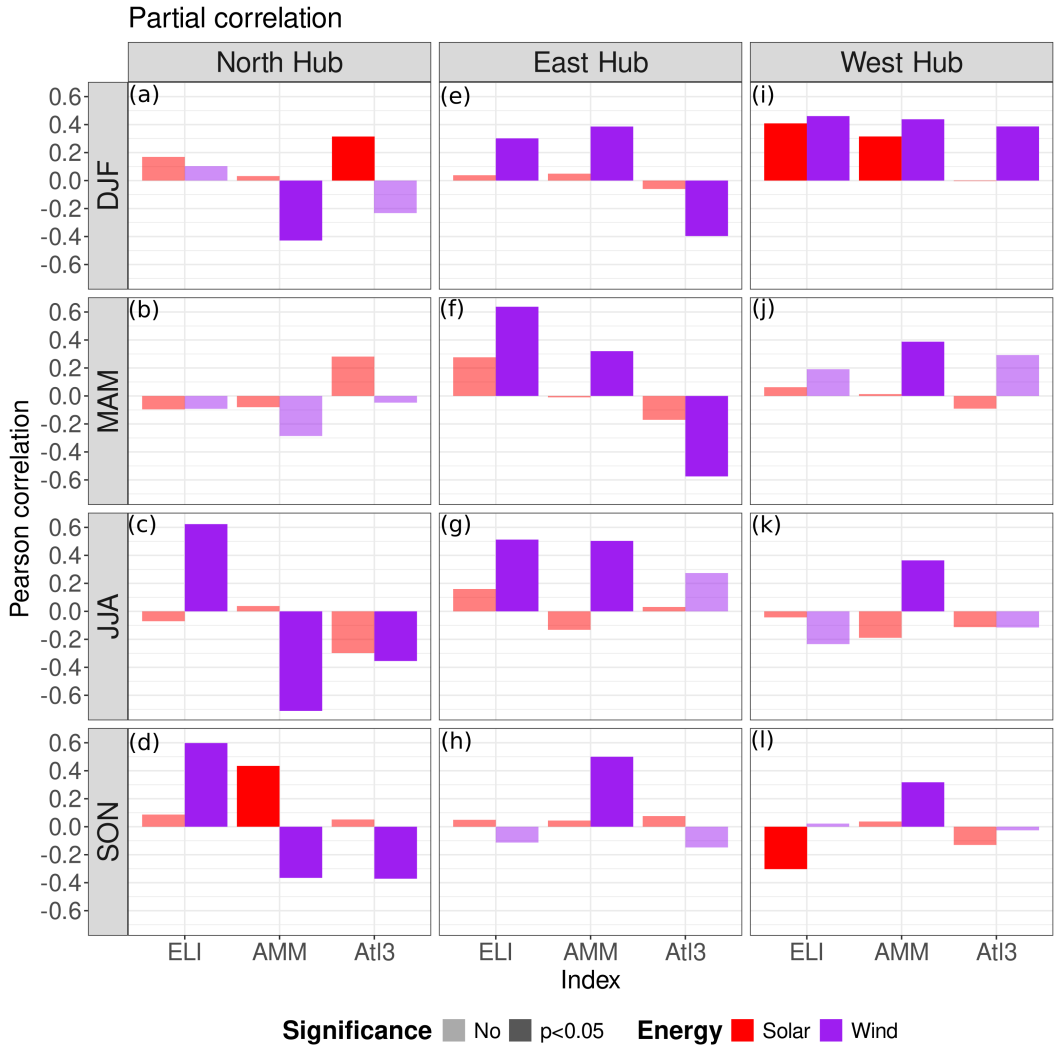

FIGURE 3.3: Pearson partial correlations between the ocean-atmospheric modes of variability and the solar and wind CF, classified by season and by energy hub. Panels (a-d) show correlations for the northern hub, (e-h) for the eastern, and (i-l) for the southern hub. Panels (a, e, and i) are for season DJF and so on for the other seasons.

The influence of ocean-atmospheric modes on the solar CF is more localised over land and also weaker over the energy hubs (Fig. 3.3 and S3). ENSO affects eastern and northwestern South America (Fig. 3.3a,f,i), with the largest affected area during DJF (Fig. S3), consistent with the well-documented influence over the continent and the Amazon basin. The AMM also produces a seesaw effect – same as with the wind CF – between the eastern equatorial continent and the Caribbean coast; the impacts change depending on the season (Fig. 3.3a-d). In MAM, the AMM modulates radiation over eastern Amazonia, migrating to the central Amazon in JJA (Fig. S3). In SON, it modulates radiation over the Orinoco savannas and western Amazon, affecting the northern solar hub (Fig. 3.3d and S3). ENSO is the only mode that

affects the Bolivian solar hub, particularly in DJF and SON (Fig. 3.3i and l). The correlation between the solar western hub and the AMM might be spurious. The Atl3 influences radiation over the equatorial Atlantic and with impacts concentrated over eastern South America (Fig. S3).

The correlations of the Atl3 with the wind and solar CF are less widespread than those from ENSO and the AMM. It rarely influences any of the energy hubs (Figures S2 and S3).

3.4.3 Physical mechanisms associated with the energy variability

Figure 3.4 shows the wind CF anomaly composites associated with ENSO phases. Wind vectors represent anomalies relative to the multi-annual mean; vectors pointing opposite to the mean wind direction indicate a reduction in absolute wind speed and thus in wind CF.

During El Niño, anomalously warm SSTs and low SLP develop over the central and eastern equatorial Pacific (JJA to DJF). The reduced SLP strengthens the easterly trade winds from the Caribbean to the South Pacific in SON and DJF (Fig. 3.4a and c), boosting the wind CF over the northern wind hub and the southwestern Perú. Composites for MAM and JJA are shown in Fig. S4; JJA shows patterns similar to SON while the northward anomalies in MAM resemble the positive phase of the AMM (Fig. 3.5a; see sect. 3.5 discussion). El Niño also promotes anomalous descending motion over the western equatorial Atlantic – especially in DJF – through an atmospheric bridge (Cai et al., 2020). This strongly increases SLP over the Atlantic and accelerates the easterly trade winds (Fig. 3.4c), rising wind CF at the eastern hub. During La Niña, the stronger SLP and winds over the eastern Pacific in SON weaken the Caribbean trade winds (Fig. 3.4b), decreasing wind CF in the northern hub. In DJF, La Niña increases convergence and rainfall over the Amazon and northeastern Brazil, accompanied by a slight SLP decrease over the continent (Fig. 3.4d), reducing wind CF speed in the western equatorial Atlantic.

The AMM is associated with opposing SST and SLP anomalies between the tropical North and South Atlantic (Chiang & Sobel, 2002). It generates cross-equatorial wind anomalies, most active between February and August, that accelerate or decelerate wind speeds (Fig. 3.5). In its positive phase, negative SLP anomalies in the northern Atlantic and positive anomalies in the southern Atlantic are associated with northward wind anomalies. This enhances wind CF over northeast Brazil (Fig. 3.5a and c),while the weakened northeasterly trade winds result in reduced wind CF over the northern Caribbean hub. The negative phase causes the opposite and redirects wind southward (Fig. 3.5b and d),with stronger influences in JJA, whereas the positive phase dominates in MAM. There are some differences in other seasons such as a clear influence in SON in the northern hub but not in the east hub (Fig. S5). AMM-related changes in wind CF over southwestern Peru are likely driven by other processes, as this mode is not linked to significant eastern Pacific SLP anomalies (see Sect. 3.5 discussion). Overall, the AMM inversely modulates wind CF between the Caribbean and northeast Brazil hubs.

The Atl3, in its positive phase, features warm SSTs and low SLP in the eastern equatorial Atlantic (Fig. S6, JJA), weakening trade winds, depicted as westerly wind anomalies. These anomalies exert minimal influence on wind CF, since circulation changes remain largely confined to the eastern equatorial Atlantic. Stronger easterlies in the Atl3 negative phase are associated with El Niño (see Sect. 3.5 Discussion). Atl3 effects on wind CF over the energy hubs or the continent remain modest.

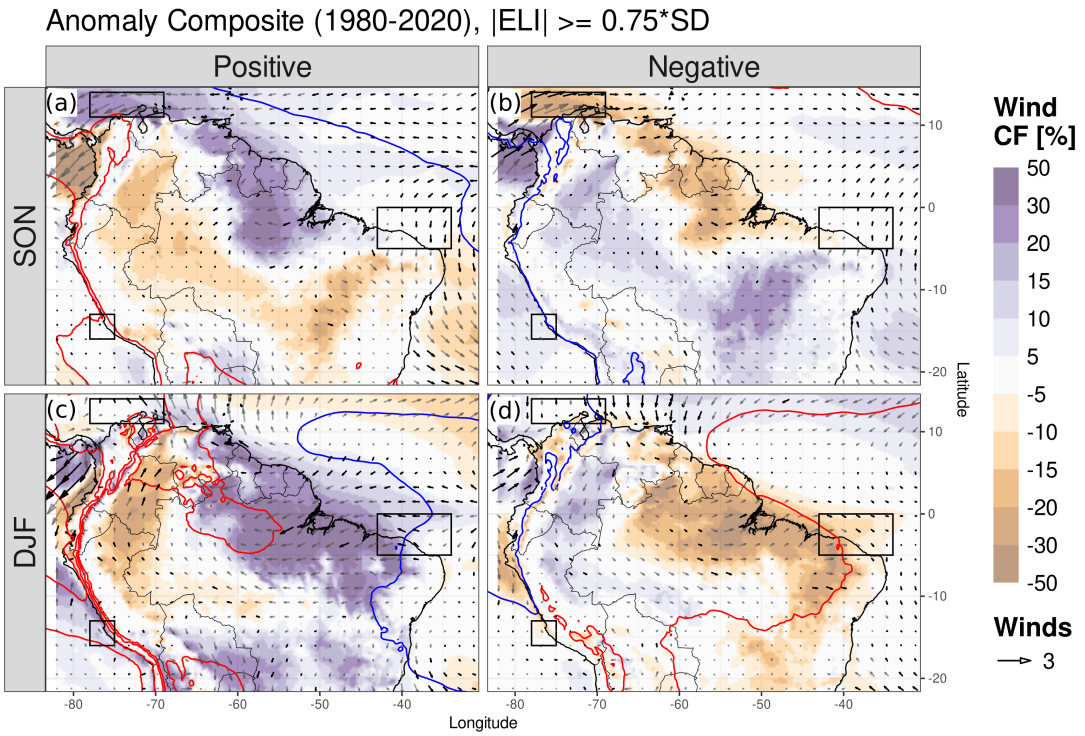

FIGURE 3.4: Anomaly composite – during both phases of ENSO – of wind CF (shadings), sea level pressure (SLP, contours every 100 Pa, negative in red, positive in blue), and 100 m wind (arrows). Wind anomalies are depicted in black where the difference from the neutral phase is statistically significant at 95% confidence level, and in grey otherwise. Panels (a,c) correspond to the positive and (b,d) for the negative. Panels (a,b) show SON and (c,d) DJF. Wind hubs are outlined with black boxes, as in Figure 3.1a-d.

Notably, in boreal spring (MAM), the AMM and Atl3 generate similar but opposite-signed atmospheric circulation anomalies (see the positive phase of the AMM and the negative phase of the Atl3, Fig. 3.5a and Fig. S6, respectively). This is associated with the connection between the two modes (see Sect. 3.5 Discussion).

Regarding the solar CF, El Niño is associated with suppressed convection over eastern South America via atmospheric subsidence, which reduces cloud cover and increases surface solar radiation (Fig. 3.6). In northwestern South America, weaker low-level winds decrease moisture advection and convergence (Fig. 3.6a and c),further reducing clouds and increasing solar CF (Fig. 3.6e and g). However, the northern solar hub shows modest CF changes. An exception unfolds over the Orinoco lowlands in MAM, when increased moisture advection and convergence generate more clouds, reducing the solar CF (Fig. S7); this is related to Caribbean SLP dynamics (Fig. S4). Increased solar CF over the western Bolivian hub in the DJF-positive phase might be associated with the stronger northerly winds along the Andes, advecting moisture southward to Argentina (Fig. 3.6c and g); moisture that does not climb the Andes eastern slope, resulting in reduced cloud cover over the hub. Conversely, La Niña phase intensifies Amazonian and northwestern convergence and cloudiness, reducing the solar CF but only notably in the northern hub (bigger than 2%, Fig. 3.6h). Moreover, there are asymmetric responses between phases, e.g. the eastern hub is just affected in El Niño phase in DJF (Fig. 3.6g). Cloud cover anomalies – and hence in solar energy – seasonally change location with the position of the ITCZ.

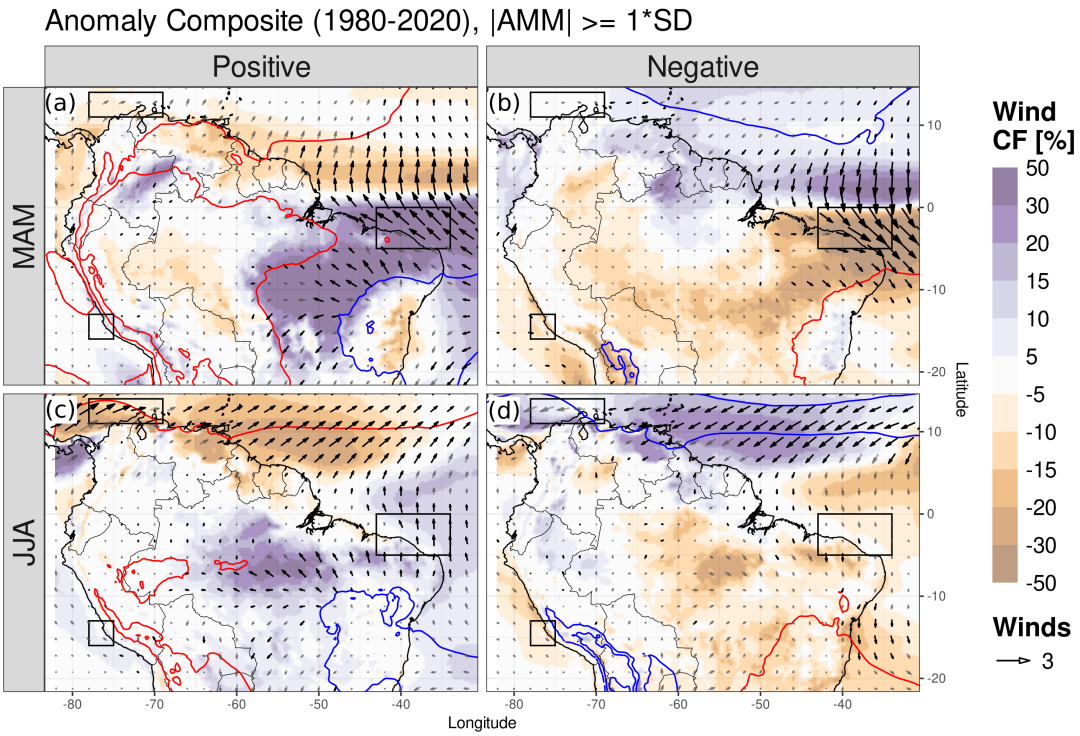

FIGURE 3.5: As in Figure 3.4, but for the positive and negative phases of the AMM. Contours of SLP are at 75 Pa intervals.

Agreement across gauge-satellite precipitation, satellite cloud cover, and reanalysed moisture convergence supports the robustness of these mechanisms.

The AMM influences solar radiation through meridional moisture advection, anomalous moisture convergence and clouds, thereby affecting the solar CF (Fig. 3.7). For MAM positive phase, northward advection enhances convergence, cloud cover and are associated with less radiation over northern South America, diminishing the solar CF in the northern hub (Fig. 3.7a,e). Simultaneously, displaced moisture generates divergence near the equatorial east, reduces clouds, and increases radiation, though this does not extend into the eastern hub (Fig. 3.7a,e). This mechanism differs from that exerted by ENSO – downward atmospheric movement. Conversely, in the negative phase, southward moisture advection from the Atlantic is associated with increased moisture convergence and cloud cover, which affects the eastern solar hub (Fig. 3.7b and f). These effects are asymmetric across phases. Moreover, in JJA, the anomalies in convergence move towards the northern Amazon, but solar hubs are not significantly affected (Fig. 3.7c, d, g and h). However, in SON, Caribbean moisture advection modulates solar CF in the Orinoco hub (Fig. S8). The western Bolivian hub is apparently unaffected by the AMM, likely due to its distance from the Atlantic atmospheric circulation changes. Across seasons, AMM-related solar CF anomalies migrate westward, from eastern Brazil in DJF and MAM, to the central Amazon in JJA, and toward the Andes in SON (Fig. 3.7 and S8).

Regarding the Atl3 (Fig. S9), it only exerts weak influence on the solar CF in JJA when reduced SLP over the equatorial east Atlantic increases moisture convergence and clouds over the eastern South America. Conversely, the JJA negative phase is associated with reduced cloud cover and increased solar CF due to strengthened easterly winds, often coinciding with Pacific El Niño conditions (see Sect. 3.5).

In both ENSO and AMM cases, solar CF anomalies are consistent with satellite

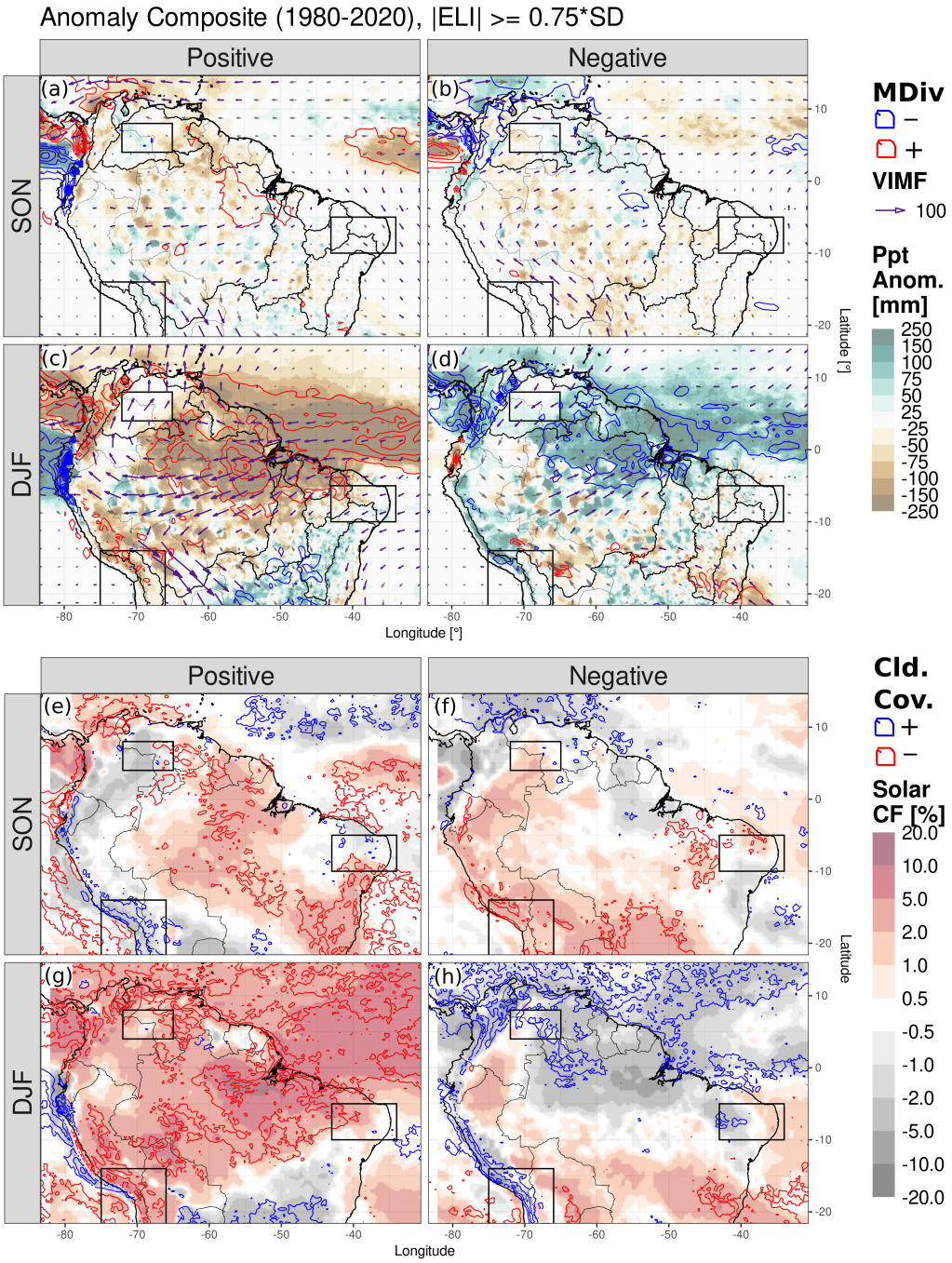

FIGURE 3.6: (a to d) Anomaly composite – in the two phases of ENSO – of vertically integrated water vapour flux components (VIMF; arrows depicted in aquamarine where the difference with the neutral phase is statistically significant at 90% confidence level, and in grey otherwise), moisture divergence anomalies (MDiv; contours at 3 kg/m^2 intervals; positive in red, negative in blue) and MSWEP precipitation (shading). (e to h) Solar capacity factor (CF, shading) and satellite cloud cover fraction (contours at 4% intervals; negative in red, positive in blue). Panels (a,c,e,g) correspond to El Niño phase and (b,d,f,h) to La Niña phase. Panels (a,b,e,f) show SON and (c,d,g,h) show DJF. Solar energy hubs are outlined with black boxes, as in Figures 3.1e-h

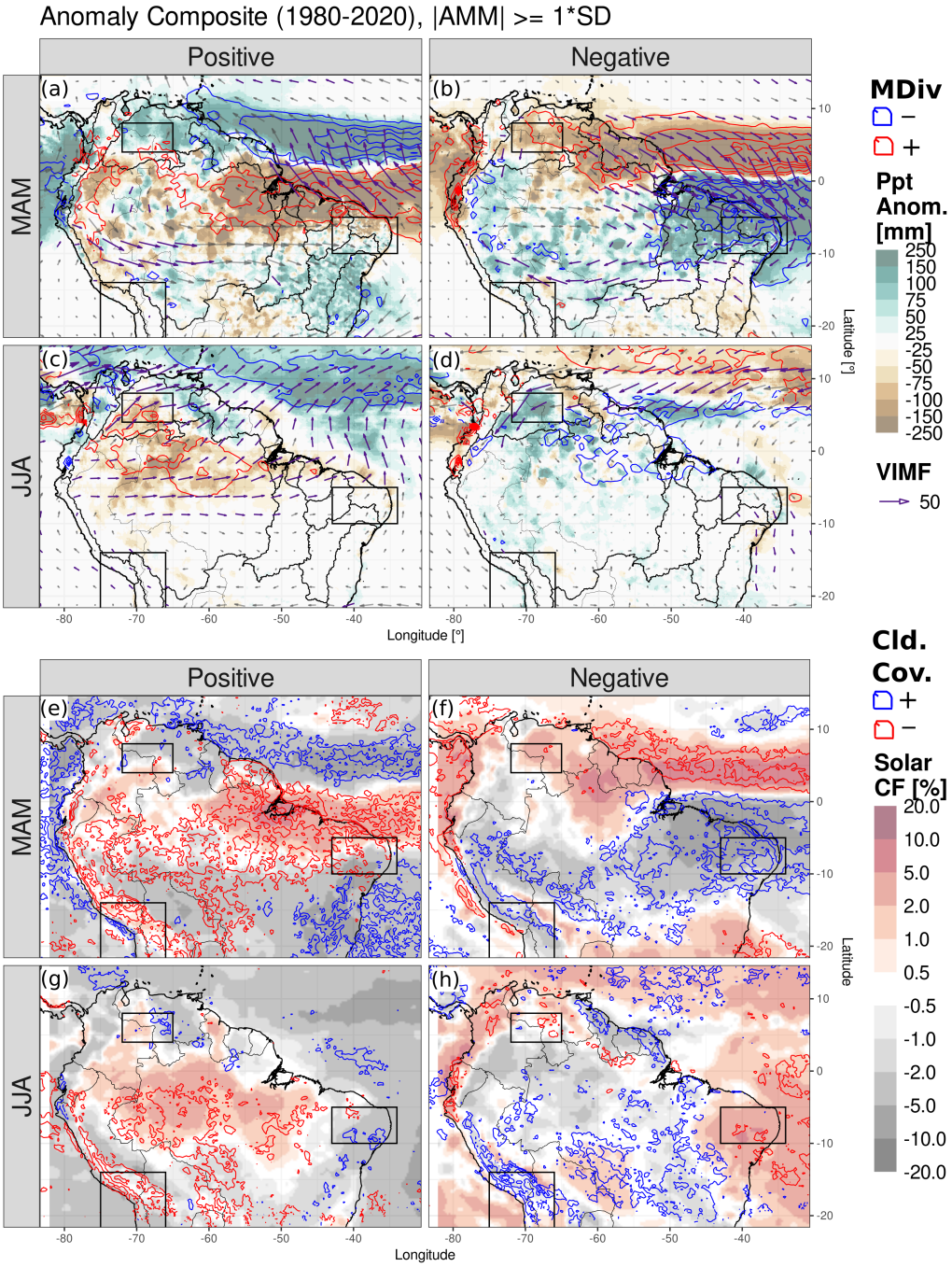

FIGURE 3.7: As in Figure 3.6, but for the positive and negative phases of the AMM in MAM (a,b,e,f) and JJA (c,d,g,h)

cloud cover changes (Fig. 3.6 and 3.7), reinforcing the physical basis of these relationships.

3.4.4 Complementarity between solar and wind resources

Planning the construction and the grid interconnection of power plants depends on both multi-annual availability and the annual cycle of solar or wind resources (Fig. 3.1). Table 3.3 shows that each hub experiences at least one season when both wind and solar CF fall below the multi-annual mean. For instance, in SON the northern

hub wind CF is 0.22 below average, while the solar CF is slightly above average (+0.01). In MAM, both the eastern and western hubs experience simultaneous reductions in both energy sources, hampering complementarity. Conversely, each hub also has at least one season when one energy source increases while the other one decreases (i.e. they partially complement each other); these are JJA for the north hub, DJF for the east and west hubs.

TABLE 3.3: Multi-annual mean renewable energy capacity factors. Values represent area-average over the energy hubs defined in Figure 3.1 and Table 3.2. Values in parentheses show the seasonal difference from the annual long-term mean, and in brackets give the relative percentage with respect to that mean. Values in **bold** indicate seasons when both sources decreases, while *italics* highlight seasons when one source substantially increases as the other decreases (complementarity).

		Hub					
Season	**Energy**	**#1 Northern**		**#2 Eastern**		**#3 Western**	
DJF	Wind	0.78	(0.11) [17%]	0.30	*(-0.11) [-26%]*	0.29	*(-0.10) [-25%]*
	Solar	0.34	(0.03) [10%]	0.39	*(0.02) [5%]*	0.45	*(0.05) [11%]*
MAM	Wind	0.70	(0.04) [6%]	0.20	**(-0.21) [-50%]**	0.38	**(-0.01) [-2%]**
	Solar	0.31	(0.00) [0%]	0.34	**(-0.03) [-7%]**	0.37	**(-0.03) [-8%]**
JJA	Wind	0.74	*(0.07) [11%]*	0.52	*(0.11) [28%]*	0.46	*(0.06) [16%]*
	Solar	0.27	*(-0.04) [-12%]*	0.32	*(-0.04) [-12%]*	0.34	*(-0.07) [-17%]*
SON	Wind	0.44	**(-0.22) [-34%]**	0.61	(0.20) [48%]	0.43	(0.04) [11%]
	Solar	0.32	**(0.01) [2%]**	0.42	(0.05) [13%]	0.46	(0.06) [14%]
Annual	Wind	0.67		0.41		0.39	
	Solar	0.31		0.37		0.41	

Considering the ocean-atmospheric variability modes is essential for anticipating seasonal energy availability and operations. ENSO does not considerably enhance or reduce complementarity; its effects depend on hub location and season (Fig. 3.8). In the northern hub, ENSO phases influence energy towards the same anomaly sign in DJF and MAM, with a clear decrease in MAM during the positive phase (Fig. 3.8a,d). Whereas in JJA and SON, solar and wind anomalies diverge, providing some seasonal complementarity (Fig. 3.8g,j). In the eastern energy hub (Fig. 3.8b,e,h,k), complementarity is virtually non-existent independent of the analysed ENSO phase because both energy sources move in the same direction. Fortunately, El Niño generates positive anomalies, which could offset the hydropower deficits that Brazil typically experiences during these events (Gonzalez-Salazar & Poganietz, 2021). The western hub shows a similar pattern: little to no complementarity in most seasons and ENSO phases (Fig. 3.8c,f,i,l). Sub-distribution variability is large, as reflected in wide error bars.

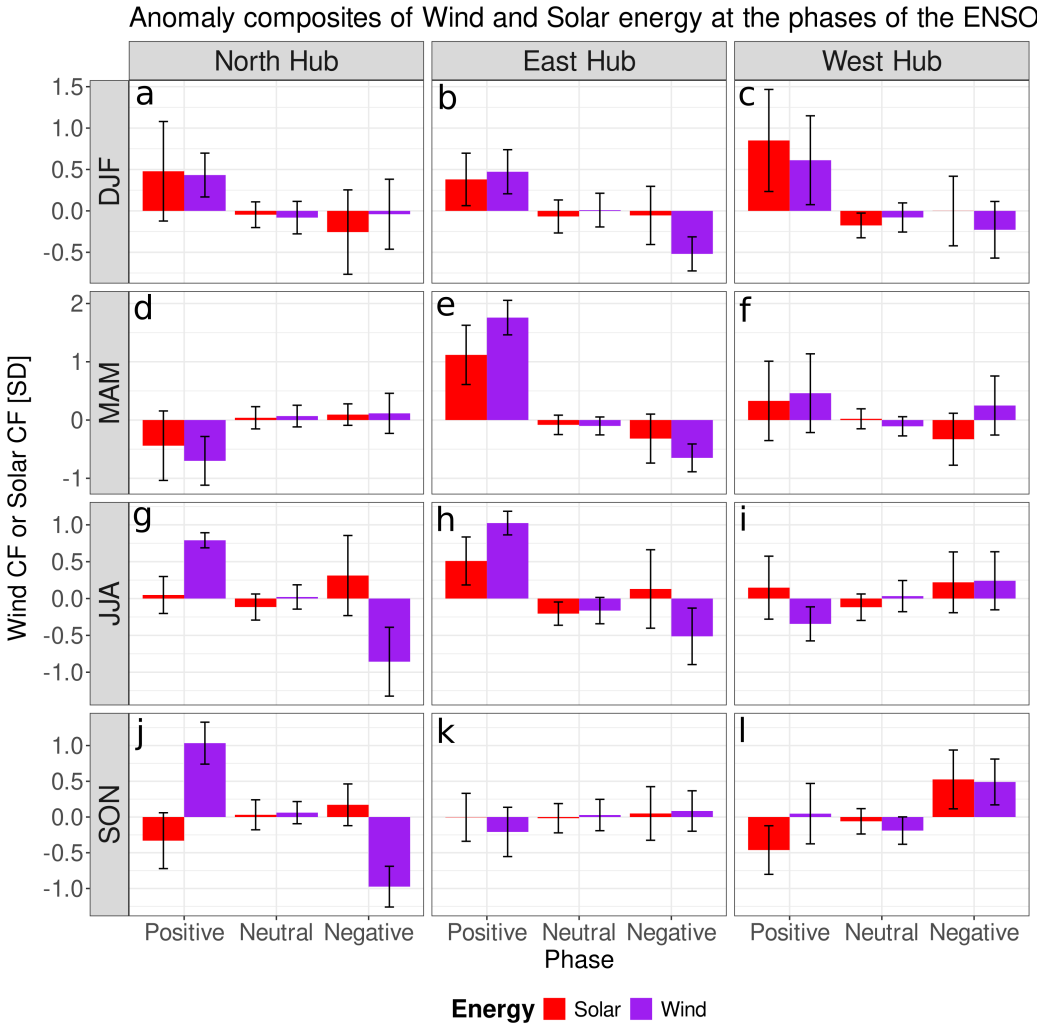

FIGURE 3.8: Average wind and solar CF anomaly composites for the three phases of ENSO (positive, neutral and negative), grouped by season and by energy hub. All anomalies are expressed in standard deviations. Panels (a,d,g,j) depict the northern hub, (b,e,h,k) the eastern hub and (c,f,i,l) the western hub. Panels (a,b and c) correspond to DJF, and so on for the other seasons. Whiskers indicate the standard error of the composites.

The AMM is also associated with non-complementary anomalies in many seasons and phases. However, the AMM generates more opportunities for complementarity than ENSO (Fig. 3.9). For the northern hub, opposite-sign anomalies emerge during DJF negative phase and in SON (Fig. 3.9a,j). In MAM, complementarity is weak to non-existent, with high variability (Fig. 3.9d). In JJA, AMM affects wind CF but not solar CF, limiting complementarity (Fig. 3.9g, ITCZ over northern South America in JJA). In the eastern hub, complementarity arises in JJA and SON positive phases (Fig. 3.9h,k), while in DJF and MAM, both sources respond similarly (Fig. 3.9b,e). In the western hub, the AMM positive phases produce complementary anomalies in JJA and SON, but the other seasons and phases do not (Fig. 3.9i,l). As with ENSO, variability across composites is large, and asymmetries between AMM phases are common (i.e. one phase reports complementarity, but in the other phase, both energy sources do not complement each other, see Fig. 3.9b,e).

Overall, the atmospheric teleconnections between the Atl3 and renewable energy

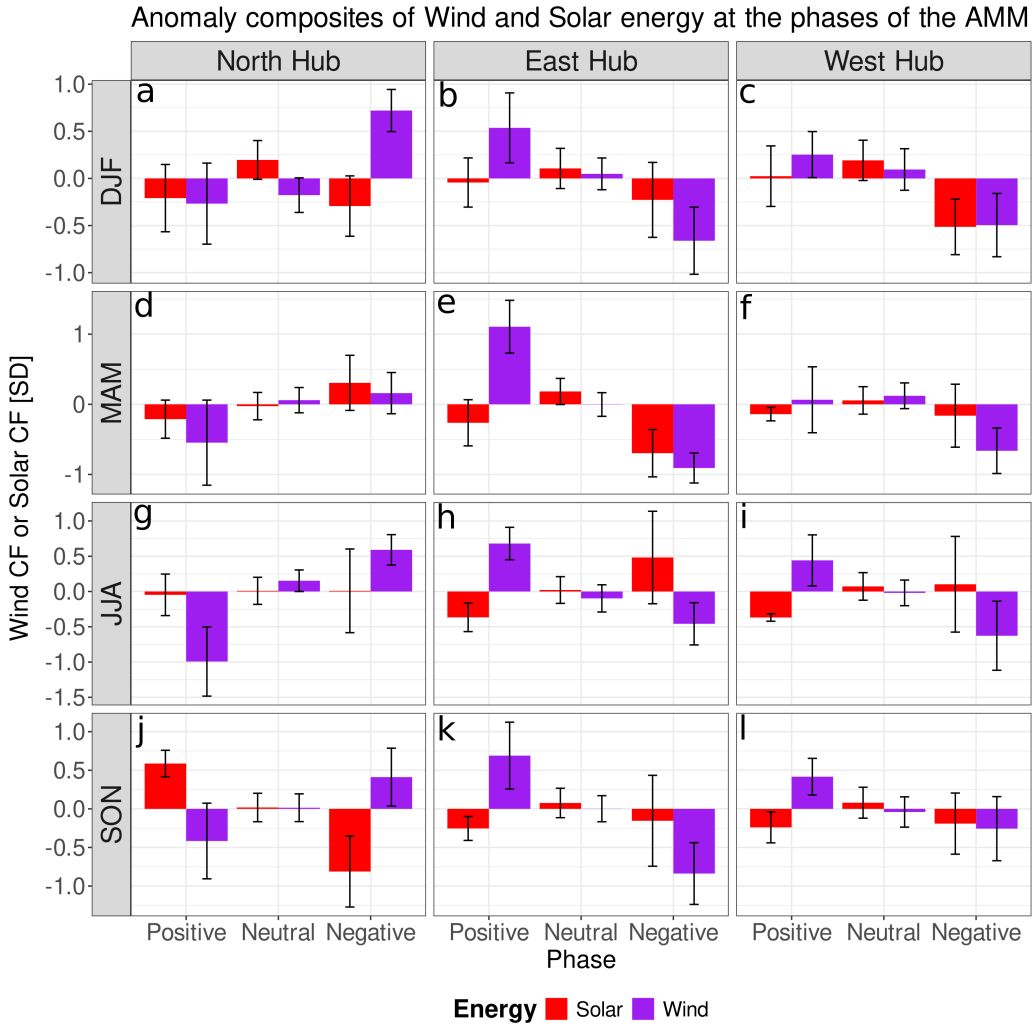

FIGURE 3.9: As Figure 3.8 but for the phases of the AMM

hubs are weak and spatially limited (Figs. S6 and S9). As a result, the role of the Atl3 in complementarity is negligible.

Finally, Spearman correlation analysis confirms that interannual solar-wind complementarity is limited (a coefficient close to -1 implying high complementarity, Table S1). Most coefficients are positive or close to zero, indicating that co-variability is weak and often reinforcing rather than offsetting, consistent with the composite results in Figures 3.8 and 3.9.

3.5 Discussion

There is substantial co-variability between the Atl3, AMM and ENSO due to shared atmospheric circulation patterns (Cai et al., 2019); i.e. the modes are interlinked between them. In our analysis, specifically in boreal spring, the Atl3 and AMM phases behave like a seesaw (Fig. 3.5, 3.7, S1, S4 and S5). For instance, wind anomalies during the Atl3 negative phase resemble those of the AMM positive phase (Fig. 3.5a,b, and S4). The positive AMM is associated with cooling in the equatorial east Atlantic, a defining feature of the negative Atl3 (Vallès-Casanova et al., 2020). The southward cross-equatorial winds in the AMM negative phase have been proposed as a mechanism driving the development of the Atl3 positive phase in JJA (Foltz

& McPhaden, 2010), these winds strongly affect the eastern Brazil wind hub. Our results therefore suggest that impacts on wind and solar energy are more strongly linked to the AMM mechanisms than to east equatorial Atlantic variability (Atl3). The AMM is also influenced by ENSO (Casselman et al., 2022; García-Serrano et al., 2017), as seen in El Niño composites over the Caribbean SLP in MAM (Fig. S6); however, further research is needed to clarify this connection. Two of the three energy hubs – the northern and eastern hubs – are particularly affected by the ENSO-AMM co-variability.

The impacts of El Niño and the Atl3 negative phase in JJA are similar, although the connection between the two modes is relatively weak (Lübbecke et al., 2018). In JJA, stronger eastern Atlantic trade winds are associated with the development of El Niño; the stronger winds enhance the Ekman pumping in the eastern equatorial Atlantic, producing the colder SSTAs related to the Atl3 negative phase (Fig. S4 and S6). The same stronger winds extend over eastern Brazil during the Atl3 negative phase. The solar CF anomalies are similarly correlated with both modes (Figures S5 and 3.6g), but the mechanism is probably more related to the atmospheric subsidence and moisture divergence (Fig. 3.6c), rather than to equatorial Atlantic cooling. In the case of the wind CF, the composites of the Atl3 are not significant. Moreover, some studies suggest a weakening of the Atl3 variability with future global warming due to ocean warming (Yang et al., 2022).

The impacts associated with the modes vary geographically with seasons, probably because the annual cycle of the ITCZ generates migration in the position of convergence, cloudiness, and precipitation. In some cases, modes are seasonally locked (e.g. ENSO) (Timmermann et al., 2018).

Interannual complementarity between solar or wind energy within hubs is generally low, but opportunities may exist with hydropower (Gonzalez-Salazar & Poganietz, 2021). Periods with weaker winds, greater cloudiness, and reduced solar radiation may coincide with increased rainfall, enhancing water storage and hydropower generation (Fig. 3.6 and 3.7). Conversely, drier periods bring higher solar radiation and are associated with stronger wind and energy production; for example, during El Niño in the three solar hubs (Fig. 3.8a,b,c). The northern and western energy hubs are near the Andes where several hydropower dams already operate. Expansion of non-conventional renewable energy might stop the hydropower expansion in the Amazon, thereby reducing several environmental impacts, such as river ecology disruption and aquatic biodiversity loss (Chaudhari et al., 2021). Hydroclimate is not the only factor affecting hydropower variability; basin size, soils, and topography also play a role (Ritter et al., 2020). Our analysis is limited to within-hub solar-wind complementarity; we do not assess inter-hub transmission constraints or implications for grid system-level reliability.

Predictability and complementarity are important for energy storage planning, whether in hydro-storage, gravitational or chemical batteries. Seasonal cycles (Fig. 3.1)matter for long-term storage planning, whereas interannual anomalies are more important for monthly operations (Figs. 3.8 and 3.9). Sub-seasonal predictability is key for complementarity. The pressure gradients associated with the ocean-atmospheric modes – shown in our results – could improve statistical forecasts, as SLP and SST variability are coupled in these modes. Thus, grid operators and energy planners could anticipate reduced renewable output or limited complementarity, based on improved seasonal forecasts of dominant climate modes such as ENSO and Atlantic variability. This will ensure a more reliable supply from combined sources and stored energy, thereby improving management of the grid. Day and night complementarity between solar and wind is necessary for operational (daily)

management. The daily cloud cycle – morning vs. afternoon convection – might impact solar energy; its evaluation requires considering small-scale meteorological processes, beyond the scope of our research.

Other climate phenomena may also affect renewable energy generation. Multidecadal oscillations influence atmospheric circulation, but their effect might be expressed in the dynamics of interannual modes. For instance, the Atlantic Multidecadal Oscillation, linked to aerosol forcing, might have influenced the AMM phases frequency (He et al., 2023); the Interdecadal Pacific Oscillation has also been associated with aerosol forcing (Qin et al., 2020). Other phenomena – at other time scales – also have impacts on renewables. Madden-Julian Oscillation changes the cloud cover and precipitation across South America (Alvarez et al., 2016; L. G. Fernandes & Grimm, 2023), potentially influencing both solar and wind CF.

The impact of climate change on South American renewable energy remains uncertain. Some studies predict increases in wind and solar availability but reduced complementarity (de Souza Ferreira et al., 2024; Martinez & Iglesias, 2024). Changes in diurnal wind cycle are also possible. However, it is still debatable how climate change – either by GHG and/or aerosols emissions – will change the frequency, strength and teleconnections of the ocean-atmospheric modes (Wills et al., 2022),potentially reshaping how renewable energy variability is modulated. Our results are underpinned on the homogeneous and physically consistent atmospheric interpolations (reanalysis), which represent regional circulation patterns and associated thermodynamics. The study omits fluctuations in efficiency due to turbine elements and electrical connections in both energy sources. Limitations also include dataset biases but general atmospheric circulation is believed to be well represented (Hersbach et al., 2020). Nonetheless, the datasets are sufficiently robust to study interannual energy variability.

3.6 Conclusions

This research advances the understanding of the ocean-atmospheric physical mechanisms linked to anomalies in potential renewable energy production. It also shows the possible complementarity between some renewable energy sources (wind and solar) and discusses options for balancing out meteorologically driven energy shortages. Our research identifies three regions of high climatological capacity factor (CF) in South America and focuses on the possible modulators of their variability. These energy hubs are: the North Caribbean, the Eastern Brazil and the Western Perú/Bolivia hub.

The interannual ocean-atmospheric modes act through a chain of processes:

- ENSO impacts: El Niño increases the wind CF in the northern Caribbean hub associated with negative SLP anomalies in the eastern equatorial Pacific, strengthening easterly Caribbean winds. It also boosts wind CF over northeast Brazil influenced by subsidence over the equatorial Atlantic, higher SLP, and stronger trade winds. The descending motion also modulates the three solar hubs through associated anomalous moisture divergence and reduced cloud cover, which increase solar radiation. La Niña enhances convection and cloudiness, reducing the solar CF over tropical South America (particularly in the eastern hub). Moreover, in La Niña, the higher eastern Pacific SLP weakens the Caribbean trade winds, which reduces the northern hub wind CF.

- Atlantic modes of variability: both renewable sources are modulated by mechanisms of the AMM rather than the changes in SLP and winds of the Atl3. The

AMM is associated with cross-equatorial SLP and wind anomalies, which produce opposite impacts on the Caribbean and northeast Brazil wind hubs. It also influences the solar CF in eastern Brazil and Orinoco hubs via meridional moisture advection, which modulates moisture convergence, clouds and solar radiation depending on the phase of the mode. Impacts are asymmetric; for example, the solar CF in the eastern hub only responds during the AMM negative phase. The AMM impacts seem to migrate westward seasonally, while Atl3 impacts on continental energy variability are minimal.

Interannual complementarity of solar and wind energy is limited. Exceptions occur in SON in the northern hub for ENSO and AMM events, and in JJA in the eastern and western hubs for AMM events. In most cases, both energy sources show anomalies of the same sign, but complementarity with hydropower is an alternative. Long-term planning of the eastern and western hubs must consider the low complementarity due to reduced availability between March and August for both energy sources.

Seasonal forecasts of energy production can be improved by considering the mechanisms studied in our research. Enhanced predictability of ENSO and Atlantic modes would help operators anticipate reduced renewable supply or weak complementarity and improve grid management. Considering short-scale phenomena is key for enhancing predictability and strengthening sub-seasonal to seasonal forecasts. Improved forecasts will enhance the resilience and sustainability of regional power systems.

Data Statement

Extended Reconstructed SST version 5 (Huang et al., 2017) is available at: https://www.ncei.noaa.gov/pub/data/cmb/ersst/v5/netcdf/. Mauna Loa CO2 concentrations are available at https://gml.noaa.gov/ccgg/trends/data.html. ECMWF ERA5 reanalysis (Hersbach et al., 2020) data are available from Copernicus Climate Data Store web portal https://cds.climate.copernicus.eu. MSWEP (Beck et al., 2019) is available at: http://www.gloh2o.org/mswep/. EUMETSAT CLARA-A3 (Karlsson et al., 2023) is available at: https://wui.cmsaf.eu/safira/action/viewProduktDetails?fid=40&eid=22277_22492.

Funding

N.D-G. was supported by the Federal Commission for Scholarships for Foreign Students through the Swiss Government Excellence Scholarship (ESKAS No. 2022.0563) for the academic year(s) 2024-2025. A.R.F. was funded by the European Union's Horizon 2020 research and innovation program under the Marie Skłodowska-Curie grant No. 894064 (AQUATIC).

Author contributions

Conceptualization: N.D-G and S.B.; Data Curation: N.D-G, A.R.F.; Formal Analysis: N.D-G; Funding Acquisition: N.D-G, S.B.; Investigation: N.D-G, S.B., E.D.T., A.R.F; Methodology: N.D-G, S.B., E.D.T., A.R.F., O.M.; Project Administration: N.D-G., S.B.; Resources: S.B.; Software: N.D-G; Supervision: S.B.; Validation: N.D-G, E.D.T., S.B.; Visualisation: N.D-G; Writing - original draft: N.D-G; Writing - review and editing: N.D-G, S.B, A.R.F., E.D.T., O.M.

Acknowledgements

We are grateful to the institutions that gather and freely disseminate the data used in this research. N.D-G thanks Helena Gardeazabal, Joaquin Duque and friends for their emotional support throughout this research.

Appendix

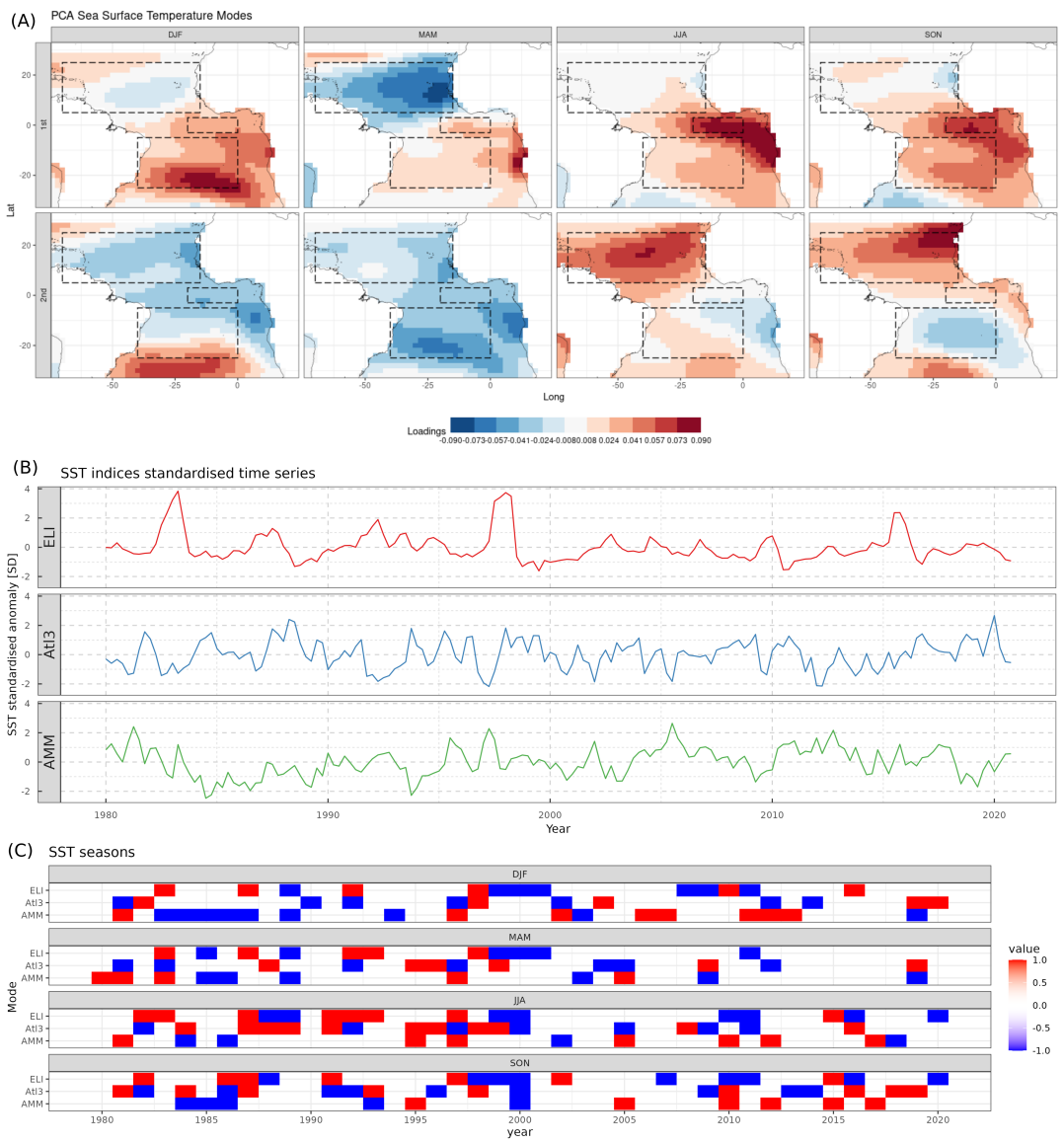

FIGURE 3.10: Figure S1. (A) Principal Components loadings, (B) continuous SST indices time series and (C) boolean seasonal time series of the SST indices. The Boolean classification is colour-coded with 1 meaning if the index is above 1 standard deviation (warm positive phase), -1 if the index is below -1 standard deviation (cold negative phase), and 0 if the index is between ±1 standard deviation.

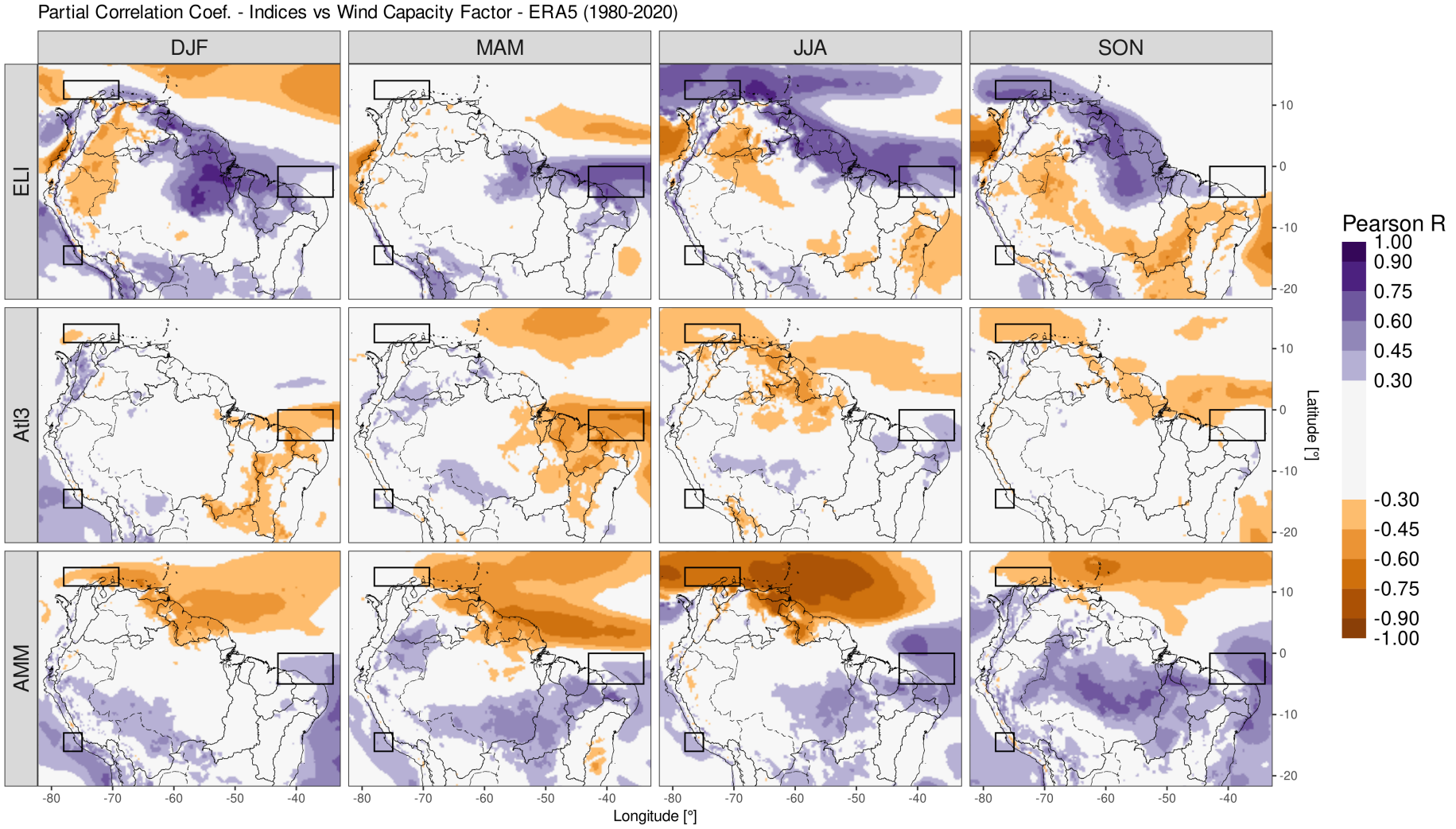

FIGURE 3.11: Figure S2. Partial correlation between Wind Capacity Factor at 100m and (a-d) El Niño Longitude Index (ELI), (e-h) Atlantic El Niño index (Atl3), (i-l) Atlantic Meridional Mode index (AMM), for each season individually: (a,e,i) in DJF and so on. Wind energy hubs are displayed with green dashed boxes in panel (a), same as in Figure 1a. Just statistically significant correlations at 95% are depicted in colours and white otherwise.

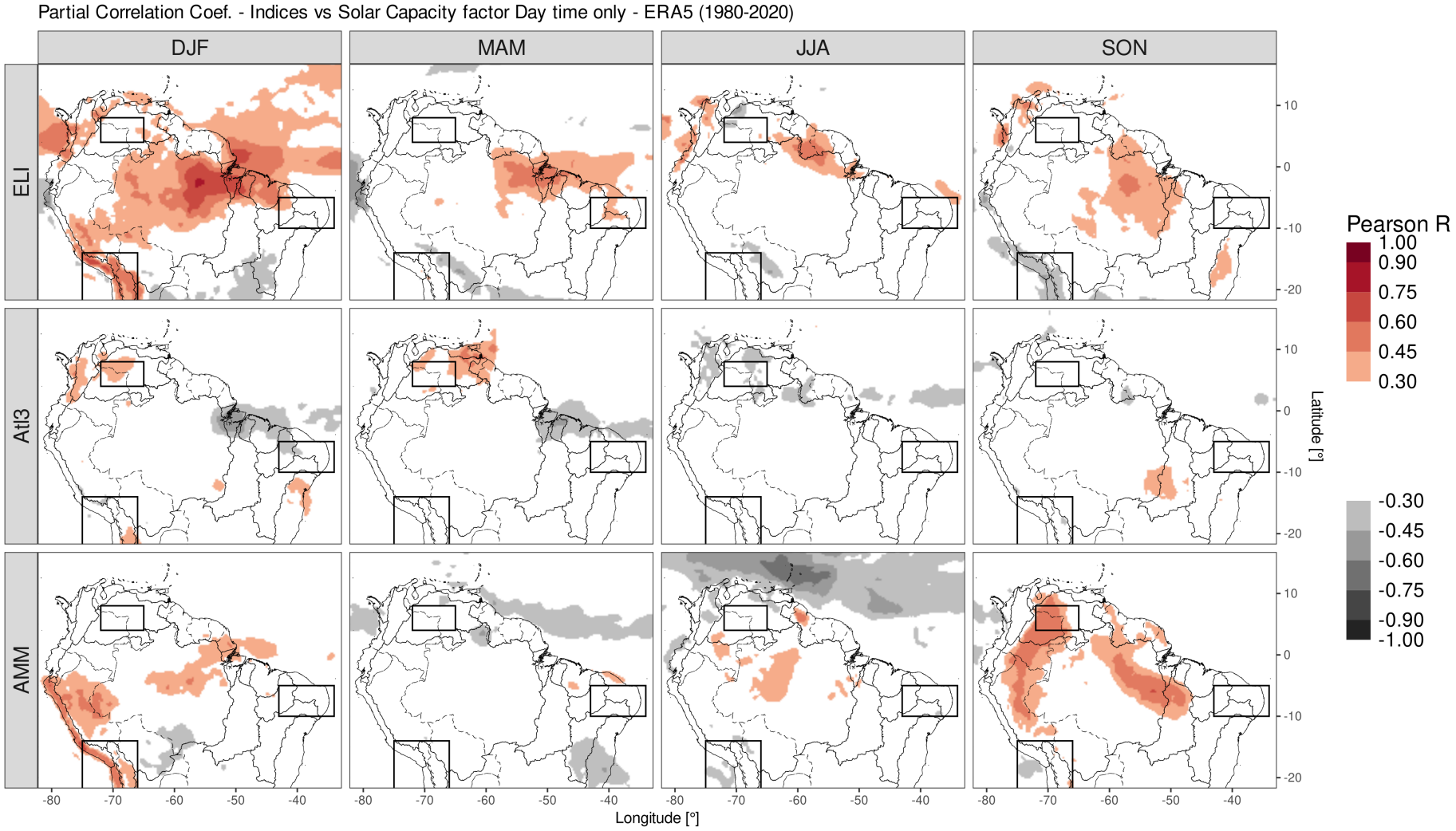

FIGURE 3.12: Figure S3. Partial correlation between Solar CF and (a-d) El Niño Longitude Index (ELI), (e-h) Atlantic El Niño index (Atl3), (i-l) Atlantic Meridional Mode index (AMM), for each season individually: (a,e,i) in DJF and so on. Solar energy hubs are displayed with green dashed boxes in panel (a), same as in Figure 1b and 1c. Just statistically significant correlations at 95% are depicted in colours and white otherwise.

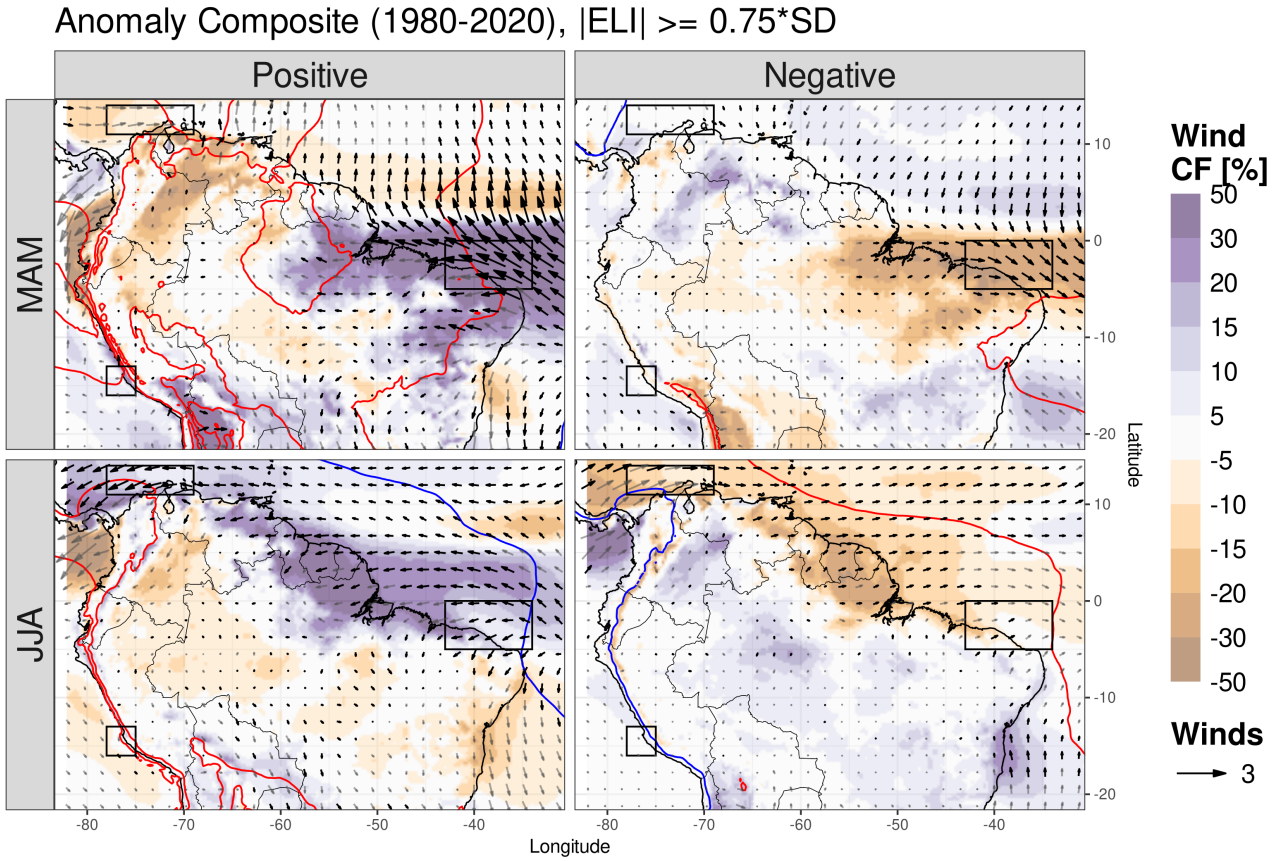

Figure S4. Anomaly composite – during both phases of ENSO – of Wind Capacity Factor (CF, shadings), Sea Level Pressure (SLP, contours every 100 Pa, negative in red, positive in blue), and 100 m wind components (arrows, depicted in black when the difference with the neutral phase is statistically significant at 95% confidence level and in grey otherwise). Panels on the left are for the positive phase and on the right for the negative phase, for the MAM and JJA seasons in the top and bottom row, respectively. Wind energy hubs are displayed with black boxes, the same as in Figure 1.

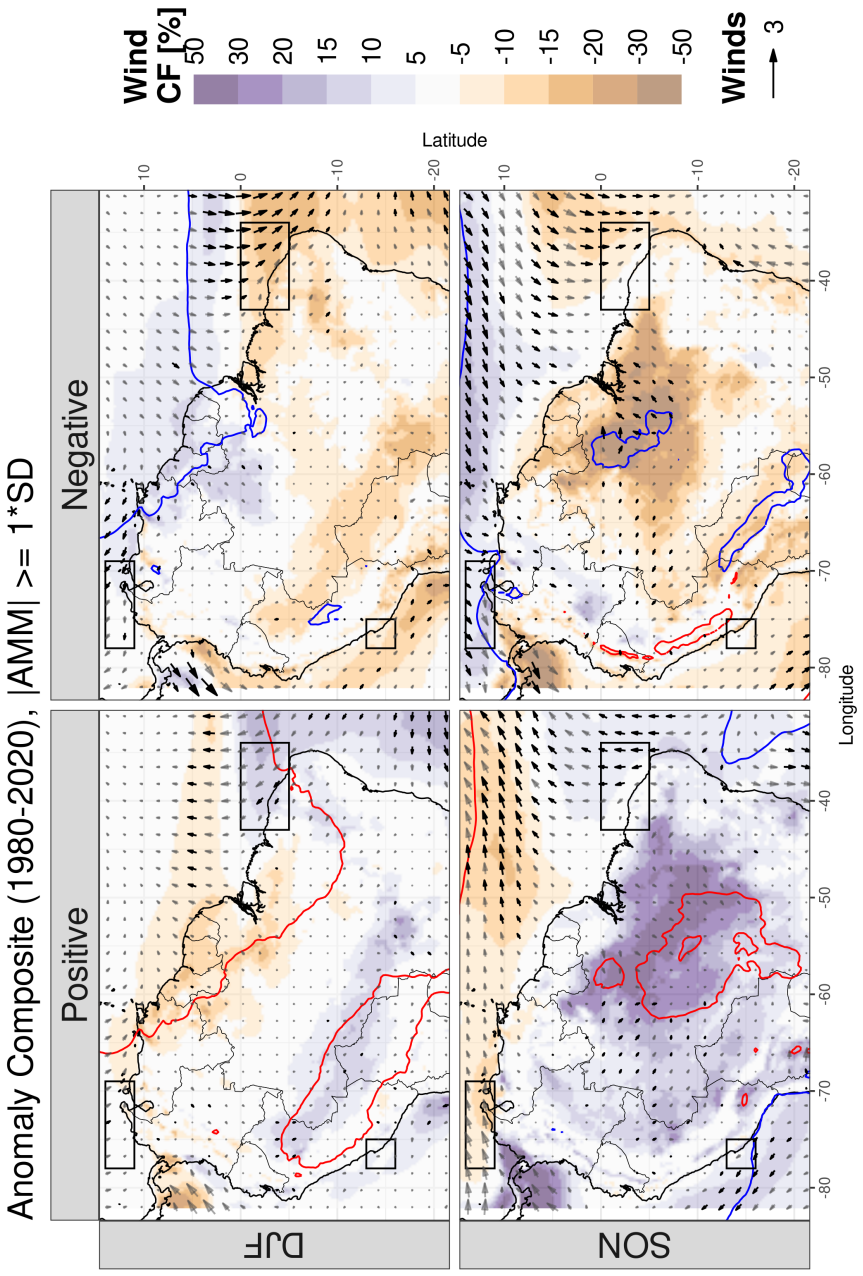

FIGURE 3.14: Figure S5. As in Figure S4 but for the DJF and SON seasons in the phases of AMM.

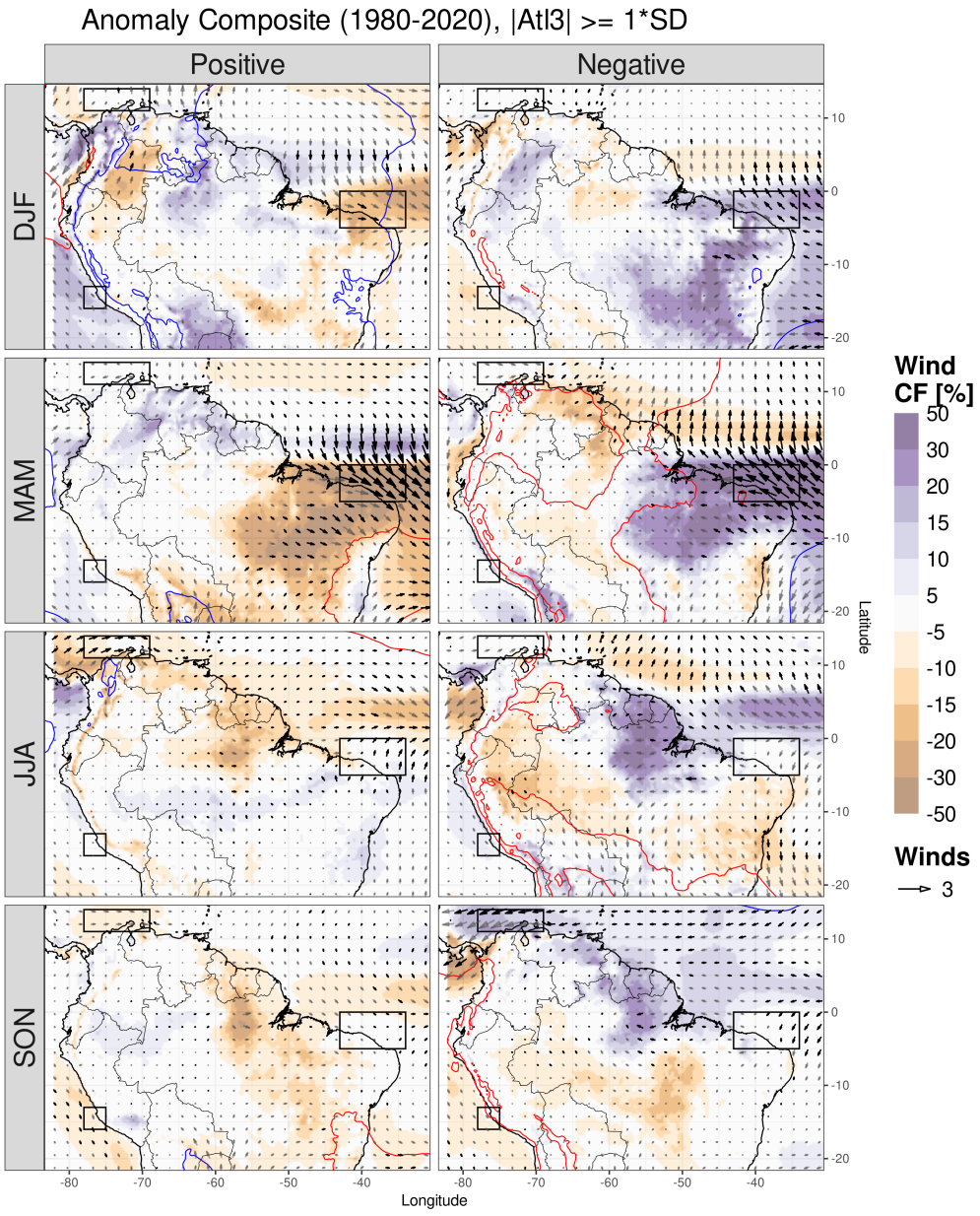

FIGURE 3.15: Figure S6. As in Figure S4 but during both phases of Atl3 and for each one of the seasons. Panels in the top row are for season DJF, and so on for the other seasons. Wind energy hubs are displayed with black boxes, the same as in Figure 1

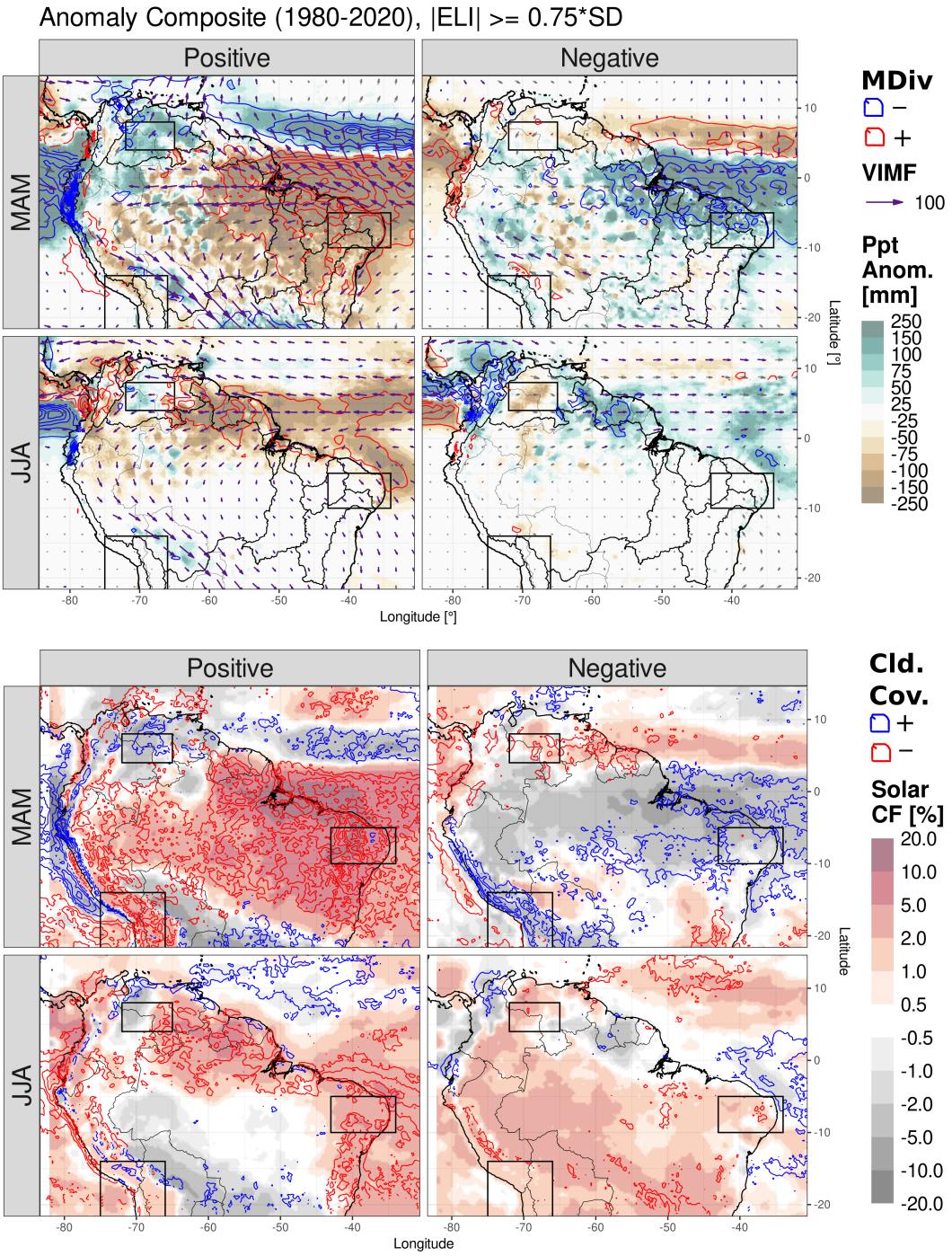

FIGURE 3.16: Figure S7. Anomaly composite – in the two phases of ENSO (ELI index) – of solar Capacity Factor (CF, shadings), Cloud Cover Fraction (contours every 4%, negative in red, positive in blue), and vertically integrated water vapour flux components (VIMF, arrows depicted in aquamarine when the difference with the neutral phase is statistically significant at 95% confidence level and in grey otherwise). Panels on the left are for the positive phase and on the right for thenegative phase. For each one of the seasons, panels in the top row are for season DJF and so on for the other seasons. Solar energy hubs are displayed with black dashed boxes, same as in Figure 1.

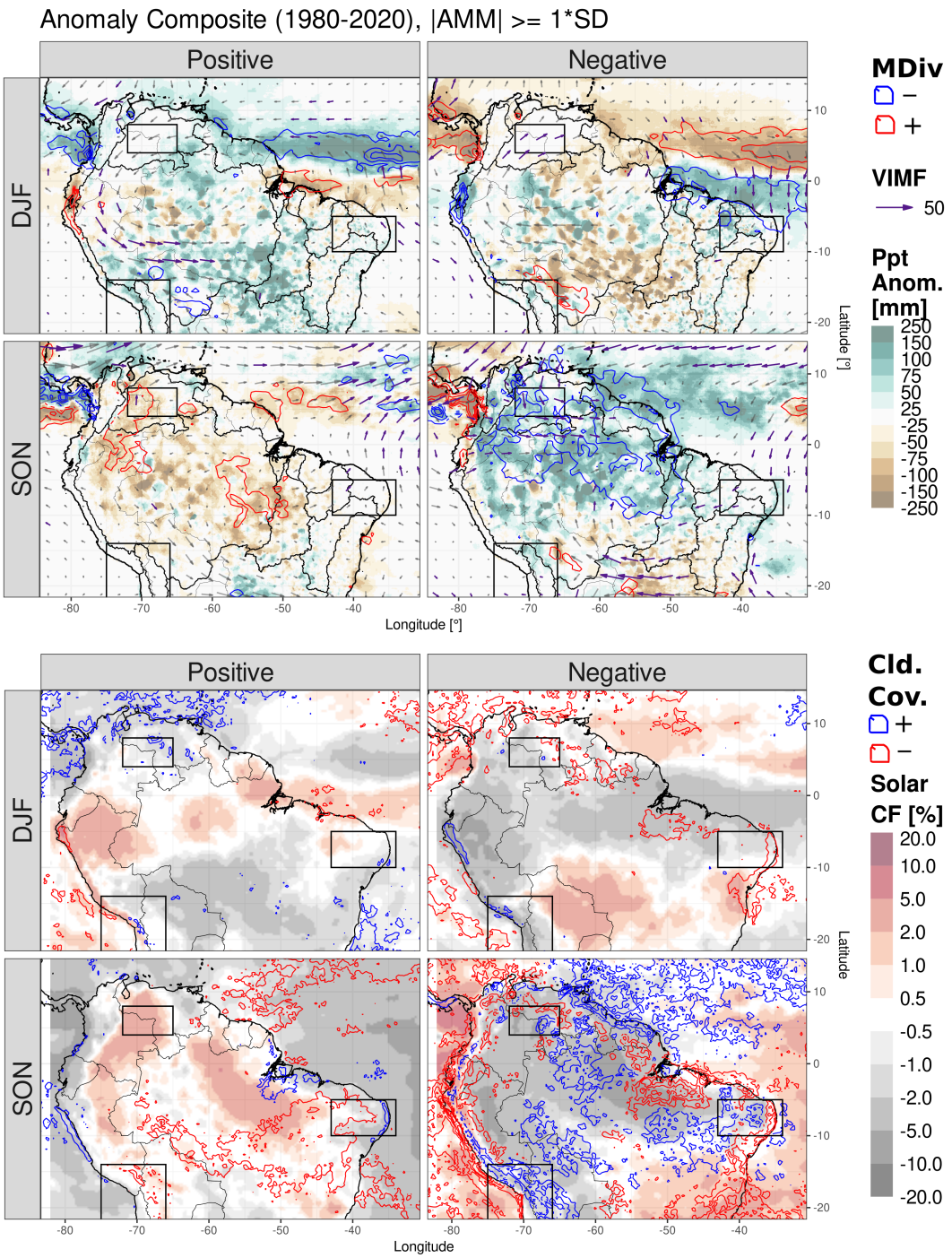

FIGURE 3.17: Figure S8. As in Figure S7 but for the DJF and SON seasons in the phases of AMM.

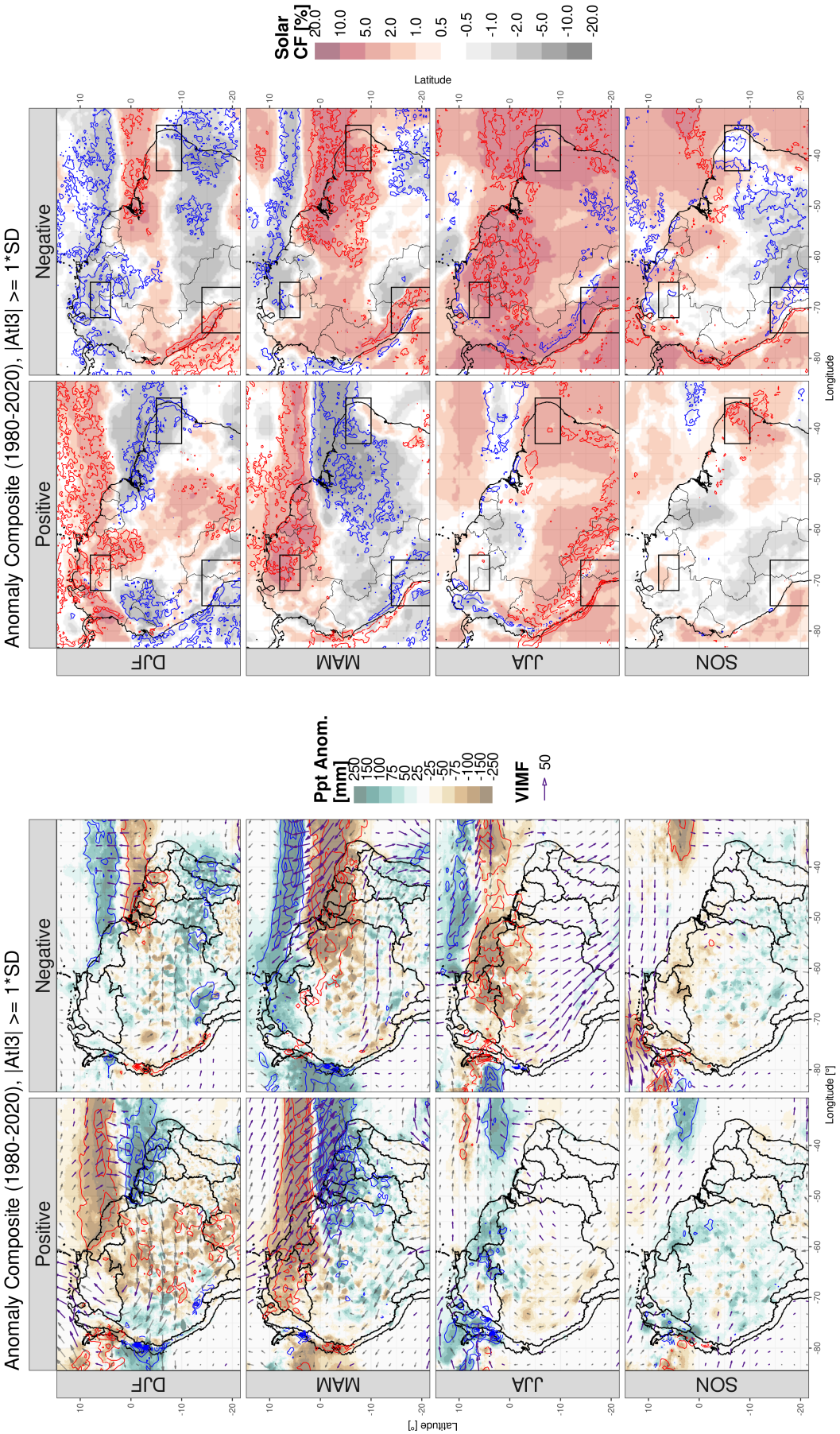

FIGURE 3.18: Figure S9. As in Figure S7, but for both phases of the Atl3 in all seasons.

TABLE 3.4: Table S1. Spearman correlation coefficient between the solar energy and the wind energy within each of the energy hubs, classified by season. A coefficient of -1 means high complementarity between the sources.

Source	Variable	Temporal resolution	Spatial resolution
DJF	0.02	0.43	0.26
MAM	0.30	0.53	0.09
JJA	-0.04	0.35	-0.07
SON	-0.12	0.13	-0.05

References

Alvarez, M. S., Vera, C. S., Kiladis, G. N., & Liebmann, B. (2016). Influence of the Madden Julian Oscillation on precipitation and surface air temperature in South America. *Climate Dynamics*, *46*(1-2), 245–262. https://doi.org/10.1007/s00382-015-2581-6

Andrian, L. G., Osman, M., & Vera, C. S. (2024). The role of the Indian Ocean Dipole in modulating the austral spring ENSO teleconnection to the Southern Hemisphere. *Weather and Climate Dynamics*, *5*(4), 1505–1522. https://doi.org/10.5194/wcd-5-1505-2024

Antonini, E. G., Virgüez, E., Ashfaq, S., Duan, L., Ruggles, T. H., & Caldeira, K. (2024). Identification of reliable locations for wind power generation through a global analysis of wind droughts. *Communications Earth and Environment*, *5*(1), 1–9. https://doi.org/10.1038/s43247-024-01260-7

Arango, S., & Larsen, E. R. (2010). The environmental paradox in generation: How South America is gradually becoming more dependent on thermal generation. *Renewable and Sustainable Energy Reviews*, *14*(9), 2956–2965. https://doi.org/10.1016/j.rser.2010.07.049

Arias, P. A., Martínez, J. A., Mejía, J. D., Pazos, M. J., Espinoza, J. C., & Wongchuig-Correa, S. (2020). Changes in Normalized Difference Vegetation Index in the Orinoco and Amazon River Basins: Links to Tropical Atlantic Surface Temperatures. *Journal of Climate*, *33*(19), 8537–8559. https://doi.org/10.1175/JCLI-D-19-0696.1

Beck, H. E., Wood, E. F., Pan, M., Fisher, C. K., Miralles, D. G., van Dijk, A. I. J. M., McVicar, T. R., & Adler, R. F. (2019). MSWEP V2 Global 3-Hourly 0.1° Precipitation: Methodology and Quantitative Assessment. *Bulletin of the American Meteorological Society*, *100*(3), 473–500. https://doi.org/10.1175/BAMS-D-17-0138.1

Bett, P. E., & Thornton, H. E. (2016). The climatological relationships between wind and solar energy supply in Britain. *Renewable Energy*, *87*, 96–110. https://doi.org/10.1016/j.renene.2015.10.006

Bianchi, E., Guozden, T., & Kozulj, R. (2022). Assessing low frequency variations in solar and wind power and their climatic teleconnections. *Renewable Energy*, *190*, 560–571. https://doi.org/10.1016/j.renene.2022.03.080

Bloomfield, H. C., Brayshaw, D. J., & Charlton-Perez, A. J. (2020). Characterizing the winter meteorological drivers of the European electricity system using targeted circulation types. *Meteorological Applications*, *27*(1), 1–18. https://doi.org/10.1002/met.1858

Bloomfield, H. C., Wainwright, C. M., & Mitchell, N. (2022). Characterizing the variability and meteorological drivers of wind power and solar power generation over Africa. *Meteorological Applications*, *29*(5), 1–19. https://doi.org/10.1002/met.2093

Boretti, A., & Castelletto, S. (2020). Cost of wind energy generation should include energy storage allowance. *Scientific Reports*, *10*(1), 2978. https://doi.org/10.1038/s41598-020-59936-x

Bustos, C., Watts, D., & Ayala, M. (2017). Financial risk reduction in photovoltaic projects through ocean-atmospheric oscillations modeling. *Renewable and Sustainable Energy Reviews*, *74*(March), 548–568. https://doi.org/10.1016/j.rser.2016.11.034

Cai, W., McPhaden, M. J., Grimm, A. M., Rodrigues, R. R., Taschetto, A. S., Garreaud, R. D., Dewitte, B., Poveda, G., Ham, Y. G., Santoso, A., Ng, B., Anderson, W., Wang, G., Geng, T., Jo, H. S., Marengo, J. A., Alves, L. M., Osman, M., Li, S., … Vera, C. (2020). Climate impacts of the El Niño–Southern Oscillation on South America. *Nature Reviews Earth and Environment*, *1*(4), 215–231. https://doi.org/10.1038/s43017-020-0040-3

Cai, W., Wu, L., Lengaigne, M., Li, T., McGregor, S., Kug, J. S., Yu, J. Y., Stuecker, M. F., Santoso, A., Li, X., Ham, Y. G., Chikamoto, Y., Ng, B., McPhaden, M. J., Du, Y., Dommenget, D., Jia, F., Kajtar, J. B., Keenlyside, N., … Chang, P. (2019). Pantropical climate interactions. *Science*, *363*(6430). https://doi.org/10.1126/science.aav4236

Cannon, D., Brayshaw, D., Methven, J., Coker, P., & Lenaghan, D. (2015). Using reanalysis data to quantify extreme wind power generation statistics: A 33 year case study in Great Britain. *Renewable Energy*, *75*, 767–778. https://doi.org/10.1016/j.renene.2014.10.024

Casselman, J. W., Jiménez-Esteve, B., & Domeisen, D. I. V. (2022). Modulation of the El Niño teleconnection to the North Atlantic by the tropical North Atlantic during boreal spring and summer. *Weather and Climate Dynamics*, *3*(3), 1077–1096. https://doi.org/10.5194/wcd-3-1077-2022

Chaudhari, S., Brown, E., Quispe-Abad, R., Moran, E., Müller, N., & Pokhrel, Y. (2021). In-stream turbines for rethinking hydropower development in the Amazon basin. *Nature Sustainability*, *4*(8), 680–687. https://doi.org/10.1038/s41893-021-00712-8

Chiang, J. C., & Sobel, A. H. (2002). Tropical tropospheric temperature variations caused by ENSO and their influence on the remote tropical climate. *Journal of Climate*, *15*(18), 2616–2631. https://doi.org/10.1175/1520-0442(2002)015<2616:TTTVCB>2.0.CO;2

Compo, G. P., & Sardeshmukh, P. D. (2010). Removing ENSO-related variations from the climate record. *Journal of Climate*, *23*(8), 1957–1978. https://doi.org/10.1175/2009JCLI2735.1

de Souza Ferreira, G. W., Reboita, M. S., Ribeiro, J. G. M., Carvalho, V. S. B., Santiago, M. E. V., Silva, P. L. L. S., Baldoni, T. C., & de Souza, C. A. (2024). Assessment of the wind power density over South America simulated by CMIP6 models

in the present and future climate. *Climate Dynamics*, *62*(3), 1729–1763. https://doi.org/10.1007/s00382-023-06993-3

Dolores-Tesillos, E., Otero, N., & Allen, S. (2025). Projections of standardised energy indices in future climate scenarios. *Environmental Research Letters*, *20*(1), 014026. https://doi.org/10.1088/1748-9326/ad9b3f

Drumond, A., Marengo, J., Ambrizzi, T., Nieto, R., Moreira, L., & Gimeno, L. (2014). The role of the Amazon Basin moisture in the atmospheric branch of the hydrological cycle: A Lagrangian analysis. *Hydrology and Earth System Sciences*, *18*(7), 2577–2598. https://doi.org/10.5194/hess-18-2577-2014

Duque-Gardeazabal, N., Friedman, A. R., & Brönnimann, S. (2025). An Atlantic influence on evapotranspiration in the Orinoco and Amazon basins. *Hydrology and Earth System Sciences*, *29*(14), 3277–3295. https://doi.org/10.5194/hess-29-3277-2025

Eelsalu, M., Montoya, R. D., Aramburo, D., Osorio, A. F., & Soomere, T. (2024). Spatial and temporal variability of wave energy resource in the eastern Pacific from Panama to the Drake passage. *Renewable Energy*, *224*, 120180. https://doi.org/10.1016/j.renene.2024.120180

Engeland, K., Borga, M., Creutin, J. D., François, B., Ramos, M. H., & Vidal, J. P. (2017). Space-time variability of climate variables and intermittent renewable electricity production – A review. *Renewable and Sustainable Energy Reviews*, *79*(May 2016), 600–617. https://doi.org/10.1016/j.rser.2017.05.046

Evans, D., & Florschuetz, L. (1977). Cost studies on terrestrial photovoltaic power systems with sunlight concentration. *Solar Energy*, *19*(3), 255–262. https://doi.org/10.1016/0038-092X(77)90068-8

Fernandes, K., Giannini, A., Verchot, L., Baethgen, W., & Pinedo-Vasquez, M. (2015). Decadal covariability of Atlantic SSTs and western Amazon dry-season hydroclimate in observations and CMIP5 simulations. *Geophysical Research Letters*, *42*(16), 6793–6801. https://doi.org/10.1002/2015GL063911

Fernandes, L. G., & Grimm, A. M. (2023). ENSO modulation of global MJO and its impacts on South America. *Journal of Climate*, 1–48. https://doi.org/10.1175/jcli-d-22-0781.1

Foltz, G. R., & McPhaden, M. J. (2010). Interaction between the Atlantic meridional and Niño modes. *Geophysical Research Letters*, *37*(18), n/a–n/a. https://doi.org/10.1029/2010GL044001

García-Serrano, J., Cassou, C., Douville, H., Giannini, A., & Doblas-Reyes, F. J. (2017). Revisiting the ENSO teleconnection to the tropical North Atlantic. *Journal of Climate*, *30*(17), 6945–6957. https://doi.org/10.1175/JCLI-D-16-0641.1

Gil Ruiz, S. A., Barriga, J. E. C., & Martínez, J. A. (2021). Wind power assessment in the Caribbean region of Colombia, using ten-minute wind observations and ERA5 data. *Renewable Energy*, *172*, 158–176. https://doi.org/10.1016/j.renene.2021.03.033

Gonzalez-Salazar, M., & Poganietz, W. R. (2021). Evaluating the complementarity of solar, wind and hydropower to mitigate the impact of El Niño Southern Oscillation in Latin America. *Renewable Energy*, *174*, 453–467. https://doi.org/10.1016/j.renene.2021.04.048

Gualtieri, G. (2022). Analysing the uncertainties of reanalysis data used for wind resource assessment: A critical review. *Renewable and Sustainable Energy Reviews*, *167*(June), 112741. https://doi.org/10.1016/j.rser.2022.112741

He, C., Clement, A. C., Kramer, S. M., Cane, M. A., Klavans, J. M., Fenske, T. M., & Murphy, L. N. (2023). Tropical Atlantic multidecadal variability is dominated

by external forcing. *Nature*, *622*(October). https://doi.org/10.1038/s41586-023-06489-4

Henley, B. J., Gergis, J., Karoly, D. J., Power, S., Kennedy, J., & Folland, C. K. (2015). A Tripole Index for the Interdecadal Pacific Oscillation. *Climate Dynamics*, *45*(11-12), 3077–3090. https://doi.org/10.1007/s00382-015-2525-1

Hersbach, H., Bell, B., Berrisford, P., Hirahara, S., Horányi, A., Muñoz-Sabater, J., Nicolas, J., Peubey, C., Radu, R., Schepers, D., Simmons, A., Soci, C., Abdalla, S., Abellan, X., Balsamo, G., Bechtold, P., Biavati, G., Bidlot, J., Bonavita, M., … Thépaut, J. N. (2020). The ERA5 global reanalysis. *Quarterly Journal of the Royal Meteorological Society*, *146*(730), 1999–2049. https://doi.org/10.1002/qj.3803

Huang, B., Thorne, P. W., Banzon, V. F., Boyer, T., Chepurin, G., Lawrimore, J. H., Menne, M. J., Smith, T. M., Vose, R. S., & Zhang, H. M. (2017). Extended reconstructed Sea surface temperature, Version 5 (ERSSTv5): Upgrades, validations, and intercomparisons. *Journal of Climate*, *30*(20), 8179–8205. https://doi.org/10.1175/JCLI-D-16-0836.1

Karlsson, K.-G., Riihelä, A., Trentmann, J., Stengel, M., Solodovnik, I., Meirink, J. F., Devasthale, A., Jääskeläinen, E., Kallio-Myers, V., Eliasson, S., Benas, N., Johansson, E., Stein, D., Finkensieper, S., Håkansson, N., Akkermans, T., Clerbaux, N., Selbach, N., Marc, S., & Hollmann, R. (2023). CLARA-A3: CM SAF cLoud, Albedo and surface RAdiation dataset from AVHRR data - Edition 3. https://doi.org/10.5676/EUM_SAF_CM/CLARA_AVHRR/V003

Kieffer, G., & López-Peña, Á. (2016). *Renewable energy market analysis: Latin America*. International Renewable Energy Agency.

Kies, A., Schyska, B. U., Bilousova, M., El Sayed, O., Jurasz, J., & Stoecker, H. (2021). Critical review of renewable generation datasets and their implications for European power system models. *Renewable and Sustainable Energy Reviews*, *152*, 111614. https://doi.org/10.1016/j.rser.2021.111614

Lopes, A. V., Chiang, J. C. H., Thompson, S. A., & Dracup, J. A. (2016). Trend and uncertainty in spatial-temporal patterns of hydrological droughts in the Amazon basin. *Geophysical Research Letters*, *43*(7), 3307–3316. https://doi.org/10.1002/2016GL067738

Lübbecke, J. F., Rodríguez-Fonseca, B., Richter, I., Martín-Rey, M., Losada, T., Polo, I., & Keenlyside, N. S. (2018). Equatorial Atlantic variability—Modes, mechanisms, and global teleconnections. *Wiley Interdisciplinary Reviews: Climate Change*, *9*(4), 1–18. https://doi.org/10.1002/wcc.527

Martinez, A., & Iglesias, G. (2024). Climate change and wind energy potential in South America. *Science of The Total Environment*, *957*, 177675. https://doi.org/10.1016/j.scitotenv.2024.177675

Martín-Rey, M., Rodríguez-Fonseca, B., Polo, I., & Kucharski, F. (2014). On the Atlantic–Pacific Niños connection: a multidecadal modulated mode. *Climate Dynamics*, *43*(11), 3163–3178. https://doi.org/10.1007/s00382-014-2305-3

Otero, N., Martius, O., Allen, S., Bloomfield, H., & Schaefli, B. (2022). A copula-based assessment of renewable energy droughts across Europe. *Renewable Energy*, *201*(P1), 667–677. https://doi.org/10.1016/j.renene.2022.10.091

Pabón, J., & Dorado, J. (2008). INTRASEASONAL VARIABILITY OF RAINFALL OVER NORTHERN SOUTH AMERICA AND CARIBBEAN REGION. *Earth Sciences Research Journal*, *12*(2), 194–212.

Perini de Souza, N. B., Cardoso dos Santos, J. V., Sperandio Nascimento, E. G., Bandeira Santos, A. A., & Moreira, D. M. (2022). Long-range correlations of the

wind speed in a northeast region of Brazil. *Energy*, *243*, 122742. https://doi.org/10.1016/j.energy.2021.122742

Qin, M., Dai, A., & Hua, W. (2020). Aerosol-forced multidecadal variations across all ocean basins in models and observations since 1920. *Science Advances*, *6*(29), 1–8. https://doi.org/10.1126/sciadv.abb0425

Ramirez Camargo, L., & Schmidt, J. (2020). Simulation of multi-annual time series of solar photovoltaic power: Is the ERA5-land reanalysis the next big step? *Sustainable Energy Technologies and Assessments*, *42*, 100829. https://doi.org/10.1016/j.seta.2020.100829

Ritter, J., Corzo, G., Solomatine, D. P., & Angarita, H. (2020). Multiobjective Direct Policy Search Using Physically Based Operating Rules in Multireservoir Systems. *Journal of Water Resources Planning and Management*, *146*(4). https://doi.org/10.1061/(ASCE)WR.1943-5452.0001159

Ruiz-Barradas, A., Carton, J. A., & Nigam, S. (2000). Structure of Interannual-to-Decadal climate variability in the tropical Atlantic sector. *Journal of Climate*, *13*(18), 3285–3297. https://doi.org/10.1175/1520-0442(2000)013<3285:SOITDC>2.0.CO;2

Sianturi, Y., Marjuki, & Sartika, K. (2020). Evaluation of ERA5 and MERRA2 reanalyses to estimate solar irradiance using ground observations over Indonesia region. *AIP conference procedings*, 020002. https://doi.org/10.1063/5.0000854

Thoning, K. W., Tans, P. P., & Komhyr, W. D. (1989). Atmospheric carbon dioxide at Mauna Loa Observatory: 2. Analysis of the NOAA GMCC data, 1974-1985. *Journal of Geophysical Research: Atmospheres*, *94*(D6), 8549–8565. https://doi.org/10.1029/JD094iD06p08549

Timmermann, A., An, S. I., Kug, J. S., Jin, F. F., Cai, W., Capotondi, A., Cobb, K., Lengaigne, M., McPhaden, M. J., Stuecker, M. F., Stein, K., Wittenberg, A. T., Yun, K. S., Bayr, T., Chen, H. C., Chikamoto, Y., Dewitte, B., Dommenget, D., Grothe, P., … Zhang, X. (2018). El Niño–Southern Oscillation complexity. *Nature*, *559*(7715), 535–545. https://doi.org/10.1038/s41586-018-0252-6

Towner, J., Ficchí, A., Cloke, H. L., Bazo, J., Coughlan de Perez, E., & Stephens, E. M. (2021). Influence of ENSO and tropical Atlantic climate variability on flood characteristics in the Amazon basin. *Hydrology and Earth System Sciences*, *25*(7), 3875–3895. https://doi.org/10.5194/hess-25-3875-2021

UN. (2015). *Transforming our world: the 2030 Agenda for Sustainable Development* (tech. rep.). https://documents.un.org/doc/undoc/gen/n15/291/89/pdf/n1529189.pdf

Vallès-Casanova, I., Lee, S.-K., Foltz, G. R., & Pelegrí, J. L. (2020). On the Spatiotemporal Diversity of Atlantic Niño and Associated Rainfall Variability Over West Africa and South America. *Geophysical Research Letters*, *47*(8), 1–10. https://doi.org/10.1029/2020GL087108

Vargas Gil, G. M., Bittencourt Aguiar Cunha, R., Giuseppe Di Santo, S., Machado Monaro, R., Fragoso Costa, F., & Sguarezi Filho, A. J. (2020). Photovoltaic energy in South America: Current state and grid regulation for large-scale and distributed photovoltaic systems. *Renewable Energy*, *162*, 1307–1320. https://doi.org/10.1016/j.renene.2020.08.022

Wilczak, J. M., Akish, E., Capotondi, A., & Compo, G. P. (2024). Evaluation and Bias Correction of the ERA5 Reanalysis over the United States for Wind and Solar Energy Applications. *Energies*, *17*(7), 1667. https://doi.org/10.3390/en17071667

Williams, I. N., & Patricola, C. M. (2018). Diversity of ENSO Events Unified by Convective Threshold Sea Surface Temperature: A Nonlinear ENSO Index.

Geophysical Research Letters, *45*(17), 9236–9244. https://doi.org/10.1029/2018GL079203

Wills, R. C. J., Dong, Y., Proistosecu, C., Armour, K. C., & Battisti, D. S. (2022). Systematic Climate Model Biases in the Large-Scale Patterns of Recent Sea-Surface Temperature and Sea-Level Pressure Change. *Geophysical Research Letters*, *49*(17). https://doi.org/10.1029/2022GL100011

Wind-turbine-models. (2025). Vestas V117-3.45. https://en.wind-turbine-models.com/turbines/1248-vestas-v117-3.45%7B%5C#%7Dpowercurve

Yang, Y., Wu, L., Cai, W., Jia, F., Ng, B., Wang, G., & Geng, T. (2022). Suppressed Atlantic Niño/Niña variability under greenhouse warming. *Nature Climate Change*, *12*(9), 814–821. https://doi.org/10.1038/s41558-022-01444-z

Chapter 4

Possible effects of anthropogenic and volcanic aerosols on the ITCZ and tropical rainfall, over South America

Nicolás Duque-Gardeazabal[1,2], Stefan Brönnimann[1,2], Andrew R.Friedman[1,2,3], Jörg Franke[1,2]

1. Oeschger Centre for Climate Change Research, University of Bern, Bern, Switzerland.
2. Institute of Geography, University of Bern, Bern, Switzerland.
3. now at Laboratoire de Météorologie Dynamique / Institute Pierre-Simon Laplace, Paris, France

Manuscript intended to be submitted to
***npj climate and atmospheric sciences*:**

Duque-Gardeazabal, N., Brönnimann, S., Friedman, A. R., and Franke, J. (manuscript). Possible effects of anthropogenic and volcanic aerosols on the ITCZ and tropical rainfall.

Abstract

Tropical rainfall variability strongly affects agriculture and food security across South America. It is influenced by mechanisms of ocean-atmospheric modes of variability, but the modes can be modulated by external forcing factors, and consequently, it is relevant to study and compare forced and unforced variability. Here, we compare the effects of anthropogenic and volcanic aerosols on tropical South American rainfall. We use three reanalyses of the 20th and 21st centuries and contrast them with rainfall and streamflow observations reaching back to the 1920s. We also utilise a paleo-reanalysis dataset family to analyse five large volcanic eruptions in the late 18th and early 19th century. Our results show concurrent changes in surface temperature, altered atmospheric mechanisms and precipitation, associated with negative radiative forcing from meridionally asymmetric and increasing tropospheric concentration, plus abrupt stratospheric injections. The analysis of meridional energy transport links aerosol forcing to changes in the interhemispheric temperature gradient (IHTG), atmospheric energy redistribution and changes in global atmospheric circulation. Tropospheric aerosols progressively modified the IHTG, regional circulation and the latitudinal position of rainfall, consistent with global changes in atmospheric circulation, specifically with the location of the strong ascent of moist air (ascending branch of the Hadley cell). Conversely, volcanic aerosols were related to overall reductions in rainfall. We discuss these dynamics against recent studies based on atmospheric simulations, while our study uses reanalysis.

4.1 Introduction

Approximately two billion people live around the Intertropical Convergence Zone (ITCZ), and their main source of freshwater is tropical rainfall (T. Schneider et al., 2014). In South America, people's food security and livelihoods are influenced by the ITCZ variability (e.g. droughts, floods, solar and hydropower, etc.; Duque-Gardeazabal et al., 2026; Merz et al., 2021). Coupled ocean-atmospheric variability modes – such as El Niño - Southern Oscillation (ENSO), the Atlantic Meridional Mode (AMM), among others – modulate South American hydroclimate through altered regional circulation (Cai et al., 2020; Duque-Gardeazabal et al., 2025; Gorenstein et al., 2023; Sengupta et al., 2025). However, the physical mechanisms of the modes can be modulated by external forcing (e.g. greenhouse gases, solar radiation, aerosols or volcanic gases and particles) (Li et al., 2022; Liu et al., 2022; Pausata et al., 2020).

Aerosols have impacts on the climate system and society, whether they come from anthropogenic or natural sources (organic and black carbon, dust, sea salt or volcanic) (Bayraktar, 2024; Zheng et al., 2020). The generalised atmospheric cooling of the anthropogenic aerosols is well documented, as well as the cooling exerted by volcanic forcing and their uncertainties (Hegerl et al., 2019; IPCC, 2021). Hence, aerosol injections have been proposed as a geoengineering solution for global warming (Sun et al., 2024). Two periods of modern history experienced high injections of aerosols: increasing after the 1950s in the troposphere with a decreasing trend after the 1990s (Diao et al., 2021), and the early 19th century is the most notable and recent example in the stratosphere (the transition between the Little Ice Age and the anthropogenic warming; IPCC, 2021). The former was related to anthropogenic burning of fossil fuels, and the latter to a cluster of large volcanic eruptions (Hegerl et al., 2019; Tuel et al., 2017).

Several atmospheric mechanisms influencing rainfall might be forced by aerosols. At the global scale, tropospheric aerosols scatter solar radiation (Li et al., 2022), cool surface and sea surface temperature (SST), which in turn alters the interhemispheric temperature gradient (IHTG) (Friedman et al., 2020). Because atmospheric circulation redistributes energy from the tropics to the poles (Hartmann, 2016), aerosol-forced SST and IHTG anomalies might modulate shifts in the latitudinal position of the ITCZ and the tropical belt (Brönnimann et al., 2015). Regional cooling might modulate the ocean-atmospheric modes and, subsequently, the regional circulation and hydroclimate. The Atlantic Multidecadal Oscillation (AMO) – an ocean-atmospheric mode – could be linked to the aerosol-induced cooling, but this is still debated (He et al., 2023). The AMO might also have induced the regional ITCZ shift through its relationship with the AMM and its effects over South America (Fernandes et al., 2015; Rodrigues & McPhaden, 2014). Conversely, a local mechanism is the modification of cloud condensation nuclei and smaller cloud droplets that take longer to fall (Li et al., 2022; Lin et al., 2018). Volcanic aerosols might force the atmospheric mechanisms influencing rainfall through increased stratospheric temperature, changes in surface temperature, which impact both the emitted long-wave radiation and the evaporation, and the reduction of tropospheric humidity (McGraw & Polvani, 2024).

Few studies have compared the mechanisms controlling rainfall under the influence of tropospheric and stratospheric aerosols, mainly due to the clear difference between the location of both types of injection. Tropospheric aerosols are chemically diverse, originate from the aforementioned natural sources and from fossil fuels (car, aircraft and ship traffic, coal-fired power, etc.), but they are quickly removed by atmospheric processes, thus remaining locally confined (Li et al., 2022). Conversely,

large volcanic eruptions inject aerosols at high altitude, often in the stratosphere, which influence their residence time and disperse particles poleward (Toohey et al., 2025). Herman et al. (2020) analysed the possible changes in Sahel rainfall due to both sources of aerosols. The volcanic-induced droughts have been extensively studied, but mainly with climate models; few studies use reanalysis due to the availability of observed data at the time of 19th century volcanic eruptions (Tejedor et al., 2021). Brönnimann et al. (2019) also focused on the early 19th century and analysed – with a paleo-reanalysis – the African, Indian, and Australian monsoon, finding weak monsoons after the five large volcanic eruptions.

However, the aerosol impacts on rainfall over South America have not been corroborated. Fernandes et al. (2015) identified some changes in rainfall and streamflow for the Amazon's dry season – boreal summer – in the late 20th century, the period affected by anthropogenic aerosols. The atmospheric moisture transport (VIMF) associated with these changes has not been studied, nor has it been for the volcanic-related droughts of the early 19th century eruptions. Water and drought risk management depend on understanding these dynamics, and therefore, it is relevant to report the differences between the effects of both types of aerosols.

To compare the forced mechanisms, we take advantage of the natural and anthropogenically forced events in modern history. We analyse time series, trends and composites of the ensemble means of three reanalyses, two uncoupled and one coupled: ERA5 (Hersbach et al., 2020) and 20CRv3 (Slivinski et al., 2021), and CERA-20C (Laloyaux et al., 2018), respectively. We also use an uncoupled SST-bounded ensemble paleo-reanalyses family (ModE-Sim, ModE-RA and ModE-RAclim; Hand et al., 2023; Valler et al., 2024; all analyses were performed per ensemble member except where noted), and a coupled climate model ensemble (CESM-LME; Otto-Bliesner et al., 2016). To use a multievidence approach, we contrast the dynamics in reanalysis with streamflow (GRDC, 2023), and rainfall observations when available (U. Schneider et al., 2022). Details are described in section 4.4 Methods. We focus on the periods with high aerosol concentrations – i.e. the early 19th century and post-1950s – identifying them with a ground-based machine learning visibility product (Hao et al., 2024), and two paleoclimate forcings (PMIP4 and ensemble built with EVA, see Sect. 4.4; Hand et al., 2023; Jungclaus et al., 2017). Although the 1815 Tambora eruption and the unidentified 1808/9 eruption have been studied, the early 19th-century cluster of eruptions is less explored (Brönnimann et al., 2019); e.g. the 1831 eruption was previously misattributed (Hutchison et al., 2025). Because tropospheric aerosols were concentrated in the Northern Hemisphere and volcanic aerosols exerted strong cooling effects there (Brönnimann et al., 2019), our analysis focuses on boreal summer (June to August, JJA). During JJA, the rainy season (convergence) unfolds over northern South America and the dry season (divergence) is mainly south of the equator (Fig. 4.1a, b and c).

4.2 Results and discussion

4.2.1 Impacts on the hydroclimate of tropical South America

During the period between 1950 and 2020, two out of three different reanalyses show increased wind divergence over northern South America and reduced over the Amazon (Fig. 4.1b and c; see boxes in Figure 4.1a). The Orinoco basin experienced several years with negative precipitation anomalies (Fig. S1a); there were 7 years with anomalies lower than 50 mm between 1980 and 2000, whereas just 3 of these events occurred in the periods 1940-1960 and 1960-1980. Streamflow records in northern

Orinoco registered an increased frequency of dry events per decade (values below and above one standard deviation for dry and wet events, respectively; Sect. 4.3 Methods), with peaks around 1960 and 1990 and concurrent reduction of wet events (Fig. 4.1b). Simultaneously, convergence increased south of the equator between 1970 and the late 1980s which shows several positive precipitation anomalies (Fig. 4.1c), coinciding with several cold AMM events after the 1960s and with the increase in hydrological dry periods in the north (Fig. 4.1d). This suggests stronger northeasterly winds over the tropical North Atlantic, enhanced Ekman pumping and oceanic cooling (similar to the Pacific trade winds strengthening; Takahashi and Watanabe, 2016), which displace the convergence and rainfall southward. Similar southward shifts in rainfall – e.g. in the Sahel – have been attributed to anthropogenic aerosol forcing in the northern hemisphere (He et al., 2023; Hua et al., 2019). After the 1991 Pinatubo eruption, GPCC shows a break in the increasing Amazonian rainfall trend of the late 1980s, but divergence was still low (Fig. 4.1c). While the Orinoco experienced strong negative anomalies below -50 and -75 mm in 1992 and 1993, respectively, and even greater deficits in boreal winter (DJF, Fig. S1a,b,c). The 1963 Agung and 1982 El Chichon eruptions might have induced negative rainfall anomalies, although less pronounced.

In the late 18th and early 19th century, the paleo-reanalysis also reveals some dry years in the northern box and, in some cases, concurrent wet years in the southern box (Fig. 4.1e and f). This is most noticeable in 1783, 1799, 1836 (Cosigüina eruption), and in 1842 in the uncoupled paleo-reanalysis ModE-RA, but not clearly shown by the CESM-LME. Because internal variability is smoothed in the CESM-LME ensemble mean, the anomalies in 1783 and 1836 are likely originating from volcanic eruptions, whereas those north-south anomalies of ModE-RA in 1799 and 1842 might reflect internal variability. The north-south rainfall seesaw could be interpreted as a possible southward shift of the moisture convergence and rainfall. Moreover, negative precipitation anomalies in the northern box were predominantly in those years after volcanic eruptions and lasted for one or two years, with almost all ModE-RA ensemble members showing a consistent forced response rather than internal variability. The frequent volcanic activity could be associated with historical documentary evidence that reported frequent droughts in the Bogotá altiplano during 1780-1828, with 1809, 1816 and 1828 considered very dry by several sources and 1816 also reported as very cold (Mora Pacheco, 2016). In DJF (Fig. S1), dry years also coincide with volcanic activity but are clearer in the southern box, where DJF corresponds to the rainy season (in both ModE-RA and CESM-LME). ModE-RAclim – the reanalysis without the prior model estimates and forcings – does not show a strong signal, probably because of scarce observations for assimilation (Sect. 4.3 Methods).

The two periods had high concentrations of aerosols, but their impacts differ in magnitude. The reduction associated with the anthropogenic aerosols in the 20th century was between 50 and 100 mm, while the volcanic rainfall reduction was on the order of hundreds of millimetres in the analysed season. What could have influenced or caused the aforementioned impacts?

4.2.2 Aerosol concentrations

Visibility observations after 1959 show that Aerosol Optical Depth (AOD) north of the equator is higher than south of it, more clearly after the 1970s (Fig. 4.2a). It generally registered a positive trend between 1959 and 1989, slowly decreasing after the 1990s, with mixed trends south of the equator (Fig. 4.2b). The subtropical north

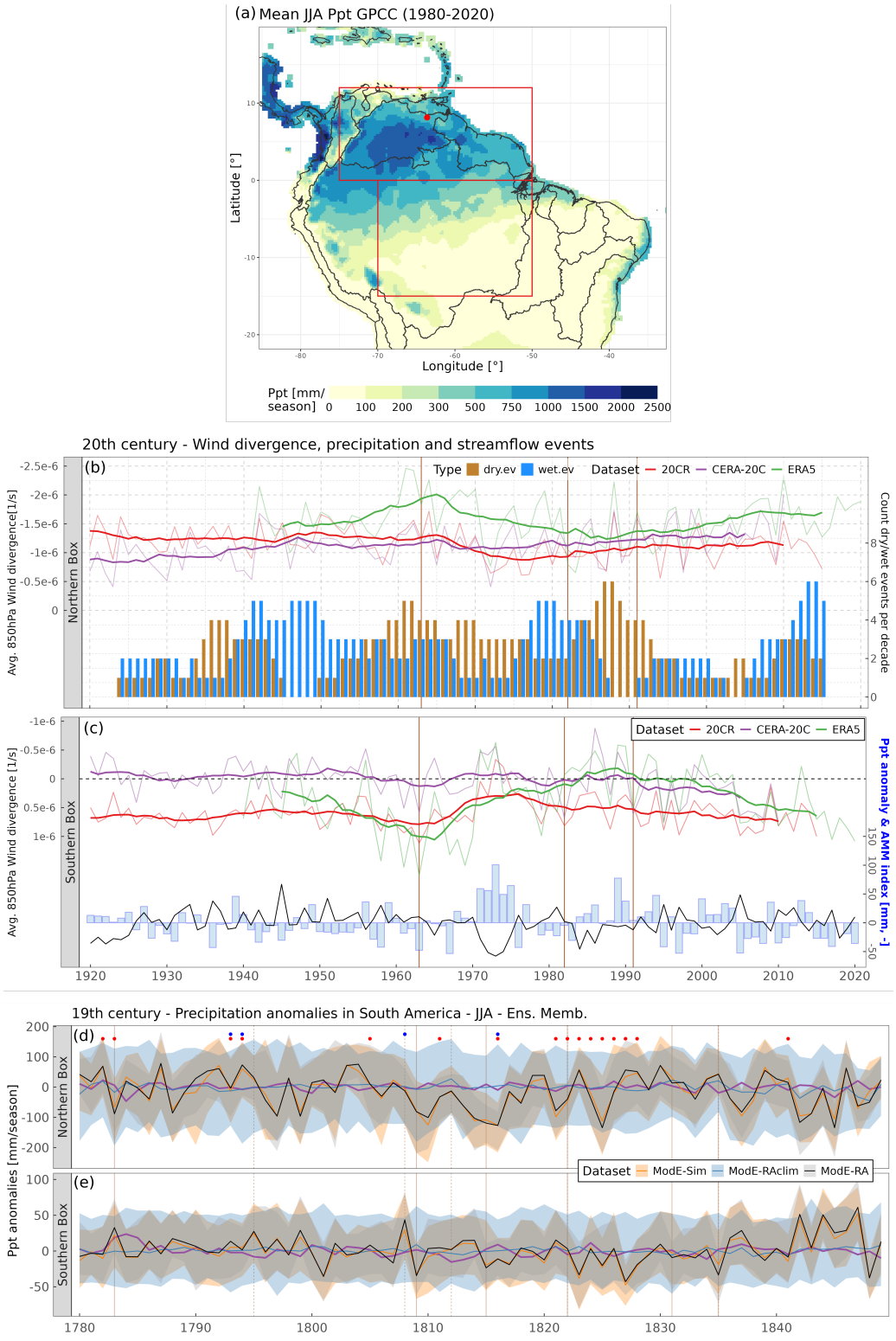

FIGURE 4.1: **Boreal summer changes in the hydroclimate of tropical South America** (a) 1980-2020 JJA multiannual mean precipitation from GPCC. Red boxes depict the regions for the area-average time series in panels (b) to (e), called hereafter as the northern and southern boxes. The red dot shows the position of the Pte Angostura streamflow gauge. Grey polygons depict the watersheds' boundaries.
(continuous on the next page).

(continued.) (b) 20th century time series of 850 hPa wind divergence in the northern box, inverted left y-axis, and 11-year moving count of dry and wet events per decade in the Pte Angostura gauge (bars, right y-axis). Different reanalyses are depicted with colours (faded lines - annual time series, tick lines - 11-year moving average). Vertical brown lines indicate the year of the Augung, El Chichon and Pinatubo volcanic eruptions. (c) Same as in (b) but with the GPCC precipitation anomalies in the southern box and the AMM index in black (right y-axis in mm/season and dimensionless, respectively). (e and f) early 19th-century time series of precipitation anomalies in the northern and southern boxes, using the ModE-RA reanalysis family. Lower and upper ribbons represent the 5 and 95 percentiles of the ensemble members' spread, and the tick colour line represents the ensemble mean. The purple line depicts the CESM-LME ensemble mean. Dots in panel (d) display the historical documentary data from table 2-2 of Mora Pacheco (2016); dry years in red and cold years in blue. Vertical orange lines denote years with volcanic eruptions highlighted in Hand et al. (2023).

also had the highest trends before the 1990s, probably associated with fossil fuel-related aerosol emissions in the western hemisphere (Smith et al., 2004). However, western aerosol emissions declined after the 1990s. The zonal mean AOD might have remained relatively stable after the 1990s due to a shift in emissions towards the eastern hemisphere, suggesting a general hemispheric effect (Diao et al., 2021). After the 1963, 1982 and 1991 volcanic eruptions, the AOD modestly increased in the tropics, almost symmetrically across the equator.

For the early 19th century, the ice core-based PMIP4 AOD reconstruction shows a clear increment after the volcanic eruptions compared to the climatology of the period 1740-1780 (Fig. 4.2c). The ModE-Sim Subset_2 individual members were forced with reconstructed AOD (thin lines, see 4.4 Methods), varying the strength and time of the eruptions (Hand et al., 2023). PMIP4 and ModE-Sim Subset_2 ensemble mean AOD – tick lines – show a latitudinal asymmetric distribution leaning toward the northern hemisphere, except for the 1815 and 1822 eruptions; the 1816 ModE-Sim estimate appears to lean southward but is highest in the tropics. For all eruptions, both datasets also display a high AOD in the tropics, and some ModE-Sim Subset_2 members have values higher than 0.5, even one year after the eruption. Sigl et al. (2022) classified aerosols from Holocene eruptions as tropical or northern hemisphere eruptions, probably because most large volcanic eruptions have unfolded either in the tropics or in that hemisphere.

Previous research on climatic effects of aerosol has focused on changes to radiative forcing and its effect on global and regional climate dynamics (Li et al., 2022). Aerosols have a generalised cooling effect, even if those from anthropogenic sources were confined to the troposphere and those from volcanic sources injected particles in the stratosphere (Kobashi et al., 2017; Li et al., 2022). Black carbon might have caused warming aloft clouds and cooling below them, but its concentration is lower (Menon et al., 2002). How much did the IHTG, the balancing atmospheric energy transport and the atmospheric circulation change due to altered radiative forcing?

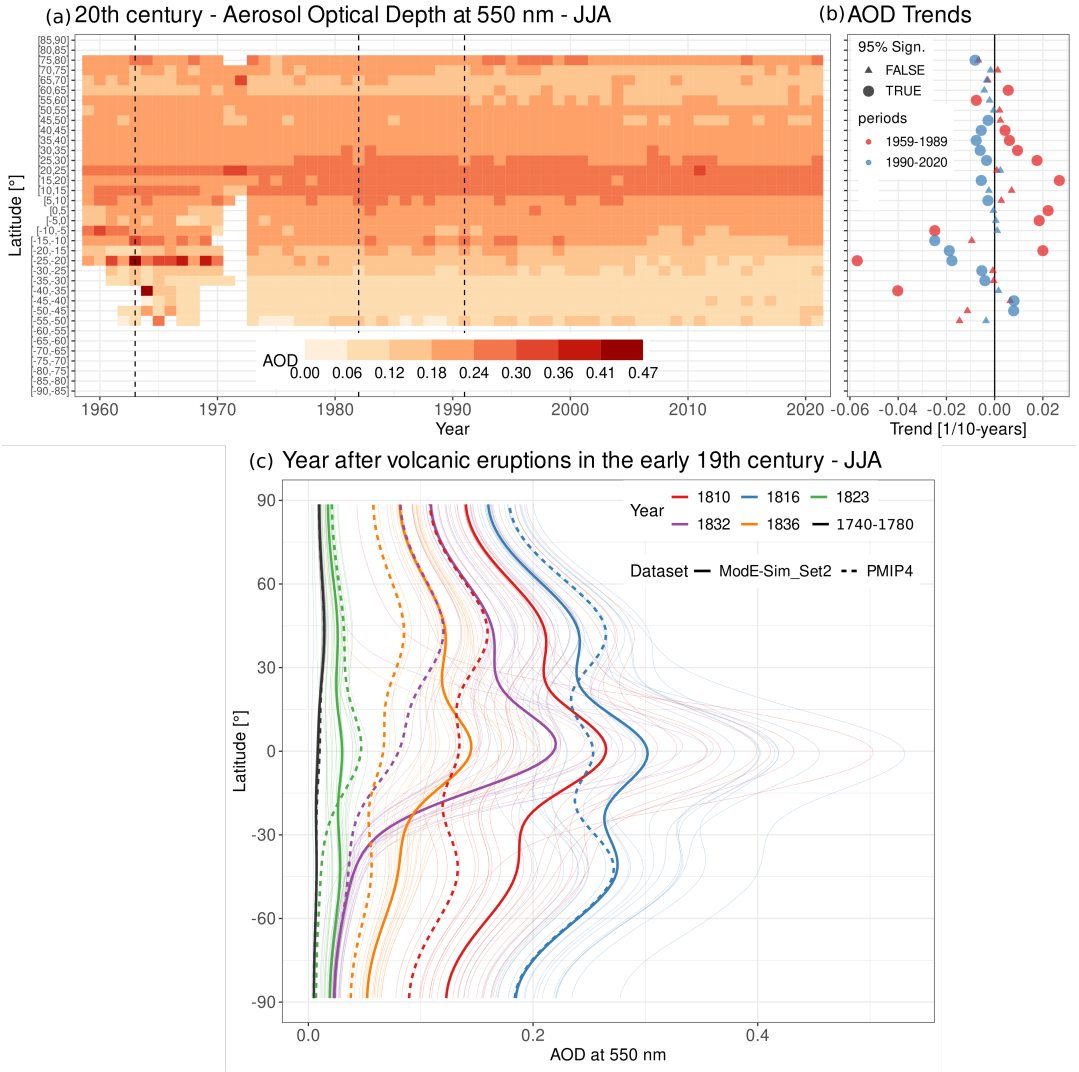

FIGURE 4.2: **Zonal mean latitudinal distribution of aerosols in the boreal summer - JJA** (a) Time series of zonal mean aerosol optical depth (AOD) at 550 nm classified in 5° latitudinal bands (colour bar) estimated by Hao et al. (2024). The vertical dashed line indicates the 1963, 1982 and 1991 Augung, El Chichon and Pinatubo volcanic eruptions. (b) trends for every latitudinal band as in (a) for the two periods in the 20th century (colours), trends at 95% significant level depicted in circles and otherwise in triangles. (c) Distribution of aerosols in the year after individual volcanic eruptions (colours) in PMIP4 (dashed line) and members of ModE-Sim set 2 (solid line). Individual members are plotted in thin lines and the composite of subset_2 members with tick line. The black line depicts the average for the period between 1740 and 1780.

4.2.3 Interhemispheric temperature gradient (IHTG) and shifts in regional atmospheric circulation

During 1950-2020, reanalyses indicate a negative trend of the IHTG in JJA (Fig. 4.3a). The difference between the 1940s and the 1980s is around 1°C in ERA5, even larger in 20CR. The northern hemisphere cooling has been attributed to tropospheric aerosols scattering solar radiation in that hemisphere (Fig. 4.2a); the cooling was noticeable not just in the SST (Qin et al., 2020), but also in the 2 m air temperature in the three

reanalyses, thereby reducing the IHTG (Fig. 4.3a). The AMM also exhibits a similar behaviour (Fig. 4.1c). Changes in the interhemispheric energy imbalance might affect the atmospheric general circulation and specifically the position of the Hadley cell (Brönnimann et al., 2015; T. Schneider et al., 2014). The reduced IHTG required slightly weaker southward Vertically Integrated Total Energy Flux (VITEF) between 1975-1995 than between 1950-1970 in ERA5 (Fig. S2a, southward VITEF at the equator), with the latitude of poleward energy division shifting from 17°N in the 1960s to close to 14°N in the 1980s. Consequently, the ascending branch of the Hadley cell – and with it the location of the ITCZ strong ascent – migrated southward regionally and globally as shown by ERA5 and CERA-20C (Atlantic-South American sector, Fig. 4.3b; 20CR shows the southward trend globally, Fig. S3a). The latter is associated with the displacement of tropical rainfall. The strong ascent location did not change after the 1991 Pinatubo eruption. Assimilation of aerosol effects in the three reanalyses is indirect (see 4.4 Methods). After the 1990s, the IHTG shows a recovering trend until 2020 (Fig. 4.3a), but the strong ascent does not display a full restitution of its position (Fig. 4.3b).

The volcanic activity of the late 18th and early 19th century is considered the most important forcing of the last phase of the Little Ice Age (Brönnimann et al., 2019). Boreal summer temperatures dropped substantially (e.g. 1816, the year without summer), but the IHTG did not radically change after every volcanic eruption (Fig. 4.3c). After the 1815 Tambora eruption, the IHTG decreased around 0.5°C in all ModE-RA family; after the 1783 Laki eruption, the reduction reached 1°C in the three ModE-Sim subsets, but only 0.5°C in ModE-RA. The IHTG differs across ModE-Sim subsets because there is a lower reconstructed sea ice extent in subsets _1 and _2 than in subset _3, which uses a recent sea ice climatology (Hand et al., 2023); sea ice extent influences the model's boundary conditions and consequently surface temperature. The energy transport only registered noticeable changes after the 1815 Tambora and 1822 Galaggung eruptions (Fig. S2b); only estimated with ModE-Sim (see 4.4 Methods). The position of the regional strong ascent exhibited interannual variability, but no trend and no uniform volcanic signal (Fig. 4.3d). Only after the 1808 and 1835 eruptions, the regional strong ascent migrated southward and northward after the 1822 eruption; this migration is even more modest in the global zonal mean (Fig. S3b). The ensemble spread is wide even after assimilation of covariates. Precipitable water and thus rainfall might also be influenced by tropical humidity, which is reduced after the volcanic eruptions in ModE-Sim (Fig. 4.3e), consistent with global cooling. ModE-Sim subset_2 humidity slightly differs from the other two subsets (_1 and _3), and originates from the distinct forcings (PMIP4 and EVA).

4.2.4 Effects on regional moisture transport (VIMF)

In the 20th century, the changes in the Hadley cell were also reflected in the regional circulation around South America (Fig. 4.4a,b). The ERA5 sea level pressure reports an increasing trend over the tropical north Atlantic and a decreasing trend over equatorial South America between 1960 and 1989, in conjunction with strengthened northeasterly winds (Fig. S4a). The strengthened winds before the 1990s coincide with the more frequent cooling of the tropical North Atlantic (more frequent negative AMM; Fig. 4.1c). Moreover, over the northern Amazon, there was a southward trend in the meridional winds. The winds in turn brought more moisture from the Atlantic towards the continent between 1960 and 1989 (estimated with ERA5; Fig. 4.4a), associated with an increasing trend in ERA5 convergence and GPCC rainfall south of the equator – northern Amazon basin – and divergence over northern

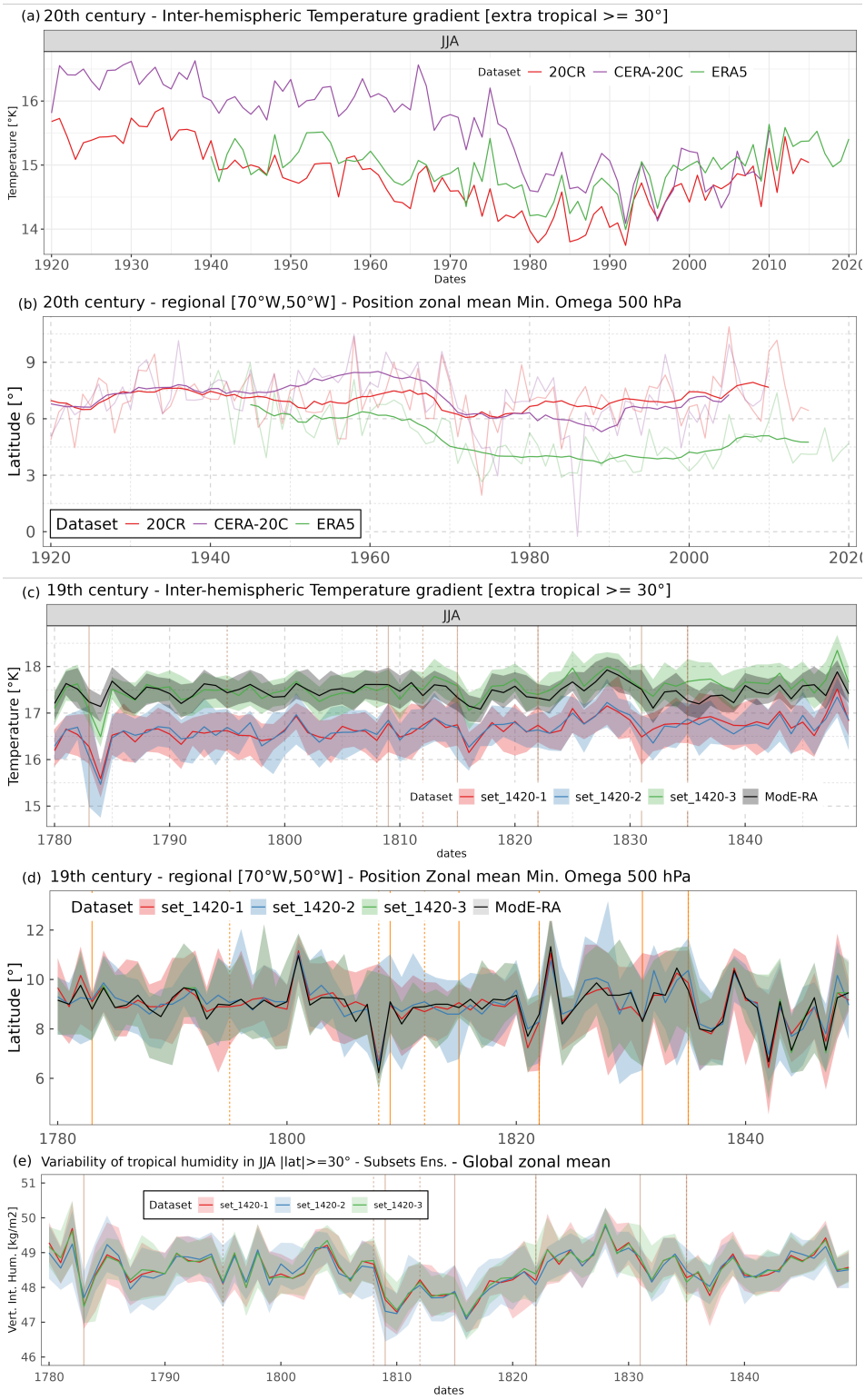

FIGURE 4.3: **Interhemispheric temperature gradient and shifts in regional strong ascent for the boreal summer - JJA** (a) Time series of the latitude-weighted mean interhemispheric 2 m air temperature gradient excluding the tropics (excluding the band between 30°S and 30°N), for three reanalyses in the 20th century (colours). (continues on next page)

(continued.)(b) Latitudinal position of the regional strong ascent of moist air (minimum zonal mean between [70°W,50°W] vertical velocity at 500 hPa), for the three reanalyses in the 20th century (colours). Tick lines represent the 11-year moving average, and the faded lines the annual time series. (c) same as (a) but for ModE-RA and subsets 1 to 3 of ModE-Sim. (d) Same as (b) but for ModE-RA and subsets 1 to 3 of ModE-Sim. (e) Latitude-weighted vertically integrated tropical humidity for subsets 1 to 3 of ModE-Sim. Ribbons display the 5 and 95 percentiles of the members of each subset, and the tick line depicts the ensemble mean time series. Vertical orange lines in (c-e) denote years with volcanic eruptions highlighted in Hand et al. (2023).

South America. Duque-Gardeazabal et al. (2025) found similar mechanisms associated with more frequent negative AMM, more clouds and increased rainfall south of the equator. This is consistent with what was shown in Figure 4.1b,c. After 1990 (Fig. 4.4b), the trends in ERA5 VIMF are less significant, and there is less consistency between the location of decreasing convergence and negative rainfall trends, compared to the first period (1960-1989)(limitations in GPCC data sources, see 4.4 Methods). In 1992, after Pinatubo's volcanic eruption, a strong weakening of the easterly moisture reduced the convergence and precipitation in DJF, yet in 1992 JJA, the VIMF recovered, but El Niño-related dry conditions persisted (Fig. S1b,c).

Volcanic eruptions with sulphur injections impact the strength of the monsoon systems (Brönnimann et al., 2019; Wegmann et al., 2014). In the early 19th century, ModE-Sim VIMF anomalies over the Atlantic and South America display a weakening of the rainfall season the year after the eruptions (weakening of trade winds, westerly VIMF anomalies, increase in divergence and decrease in ModE-RA rainfall; Fig. 4.4c-h and Fig. S4c-h). However, the VIMF after some eruptions exhibits anomalies in the meridional component, for instance, after the 1822 Galanggung eruption. The 1835 Cosigüina eruption shows a small increase in precipitation south of the equator, yet the moisture transport suggests that it is an effect of the weakening of the trade winds rather than a meridional (southward) component. A meridional ITCZ shift has been replicated by other experimental studies focusing on the influence of the ITCZ shift over the development of warm El Niño-Southern Oscillation events (Pausata et al., 2020). However, the experiments assumed that the aerosols are confined to one hemisphere, an assumption that does not hold for tropical eruptions (Toohey et al., 2011); plumes of extratropical eruptions might also have equatorward dispersion but in low concentrations (Wu et al., 2017).

Pausata et al. (2020) also shows a warming and a localised increase in rainfall in the east equatorial Atlantic. Interestingly, our results show positive rainfall anomalies in the five eruptions over the east equatorial Atlantic with different intensities (Fig. 4.4c-g), which can also be seen in the composite (Fig. 4.4h). This might be related to a quicker cooling in 2 m temperature over land compared to the change over the ocean (Fig. S5). The described rainfall impacts might just originate from the model simulations as tropical precipitation is weakly constrained in the paleoreanalysis, although SLP is assimilated assuming that observational errors are uncorrelated (Sect. 4.4 Methods). Nevertheless, some documentary data is consistent with these rainfall impacts (Mora Pacheco, 2016).

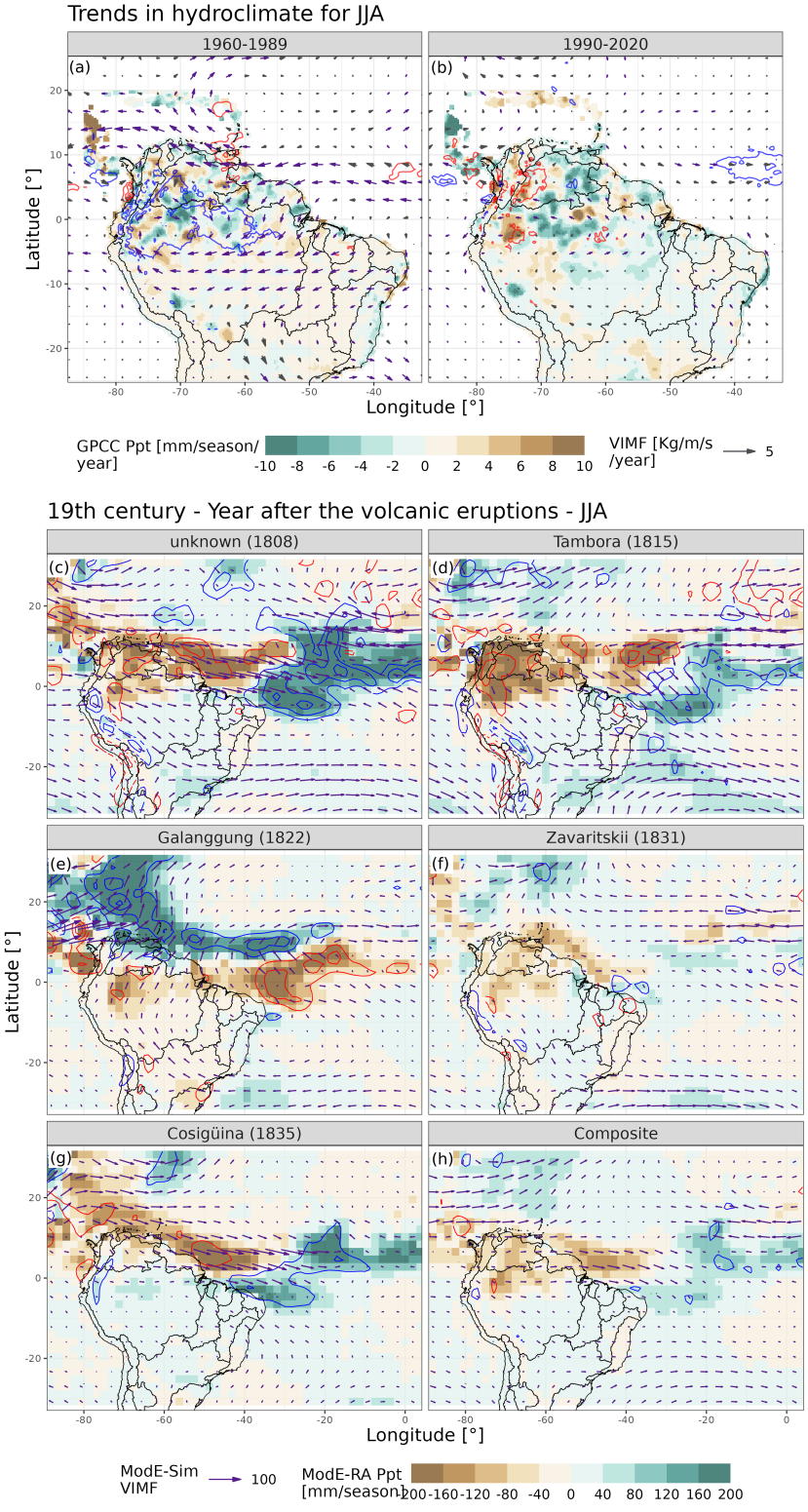

FIGURE 4.4: **Changes in regional moisture transport, convergence and rainfall.** (a) Linear slope coefficients of ERA5 vertically integrated moisture flux (VIMF) (arrows), convergence (contours) and GPCC rainfall (shading) against Gregorian year for the boreal summer -JJA- in the 1960-1989 period. (continues on the next page)

(continued.)Significant trends at 95% confidence interval are depicted in purple and otherwise in grey. (b) same as (a) but for the period 1990-2020. Contours are drawn every 0.1 $kg/m^2/year$ with increasing convergence in blue and decreasing in red. (c to g) Boreal summer anomalies in the year after the volcanic eruption with ModE-Sim ensemble mean VIMF (arrows), convergence (contours) and ModE-RA rainfall (shading). Contours are drawn every 2 kg/m^2 with positive convergence in blue and negative in red. (h) Same as (c), but the composite of the five eruptions.

4.3 Conclusions

Our research shows the influence aerosols have on the atmospheric mechanisms controlling rainfall in South America. It shows the influence of prolonged tropospheric aerosol-forced cooling on the reduction of the IHTG and, conversely, shows the weak effect early 19th century volcanic aerosols had on the IHTG, although their role in worldwide cooling is widely known. Then, variations in the IHTG and regionally in SSTs modulated the Hadley circulation, the poleward energy redistribution, regional winds and VIMF, thereby shifting the position of tropical rainfall over South America. Generalised volcanic cooling was associated with weakened trade winds, reduced moisture transport, and diminished tropical South American rainfall. Comparing the effects of tropospheric and stratospheric aerosols helps to understand the mechanisms influencing regional climate impacts, and here specifically, South America's tropical rainfall variability.

Our analysis indicates that increased Northern Hemisphere tropospheric aerosol concentrations were linked to weak southeasterly winds and strengthened northeasterly VIMF, transporting more moisture southward, increasing convergence and rainfall. Conversely, volcanic aerosols affected the atmospheric circulation via reduction of temperature, leading to weaker rainy seasons. Other studies using models have found similar effects (Paik et al., 2020; Undorf et al., 2018) and are consistent with reduced tropical humidity following generalised cooling (McGraw & Polvani, 2024), which reacts to the reduction in temperature. For example, the 1991 Pinatubo eruption reversed the increasing rainfall trend south of the equator, producing negative anomalies. We also found an increment of rainfall over the east equatorial Atlantic after the volcanic eruptions, probably linked to the reduced temperature contrast between the land and ocean after the volcanic eruptions (this differs from estimations with previous reanalysis; Brönnimann et al., 2019). However, paleoreanalyses suggest that some eruptions can trigger modest meridional shifts in convergence and rainfall.

The impacts of the two types of aerosol forcing differ in location and duration. The asymmetric increment of tropospheric aerosols was associated with anomalous meridional moisture transport, while the volcanic aerosols mainly weakened the westward moisture transport and consequently the whole rainy season. Changes in late 20th century rainfall were slow and manifested as more dry years and fewer wet years over the Orinoco; the northern Amazon experienced an inverse behaviour. Conversely, the changes due to the volcanic aerosols were short but intense (although the latter might be an effect of the background model simulations). These differences arise partly from aerosols distinct characteristics: tropospheric aerosols are lower in concentration than volcanic but were continuously emitted in the Northern Hemisphere (around 70 TgS/year in 1975-1990; Li et al., 2022; Smith et al., 2004), whereas volcanic aerosols are very short-period injections that are suspended where

no rain deposits them (Tambora between 37 and 58 TgS; Sigl et al., 2022). Consequently, anthropogenic aerosols primarily reduced the southward energy transport, while volcanic aerosols sharply reduced global energy availability for one to two years, with some hemispheric asymmetries. Evidence from the Galunggung and Cosigüina eruptions shows northward and southward moisture transport anomalies, with rainfall increasing over the Caribbean and Amazon, respectively (hemispheric asymmetry). Overall, our results reflect a regional expression of broader changes in global atmospheric circulation, particularly in the position of the strong ascent.

The seasonal timing of the aerosol injection influences the ocean-atmospheric modes and, down the chain, rainfall. While natural aerosols exhibit seasonal variability, fossil-fuel emissions occur year-round with sector-dependent patterns with the aforementioned trends (Smith et al., 2004). However, their radiative impact is strongest during boreal summer, when incoming solar radiation peaks in the northern hemisphere, where most aerosols were concentrated and fossil fuel emissions were injected in the 20th century (Diao et al., 2021). For volcanic injections, the season of the eruption determines the stratospheric Brewer-Dobson circulation and thus the suspension and transport of aerosols, shaping the hemispheric asymmetries. However, the latitude of the eruption exerts greater control, as aerosols and the radiation scattering generally remain confined to the hemisphere of origin (Pausata et al., 2020). Our results suggest that tropical eruptions weaken the rainy season. For the early 19th century, most eruptions were classified by Sigl et al. (2022) as equatorial or northern hemispheric eruptions, yet the latitudinal shifts in the ITCZ strong ascent and rainfall were relatively modest.

Other research has claimed a southward shift in the ITCZ in the Little Ice Age (LIA; Roldán-Gómez et al., 2022; Sacks et al., 2009). However, the paleo-reanalysis does not indicate a strong shift in either the IHTG, nor in the position of the strong ascent of moist air after the 15th century (intermediate results not shown).

In the future, our findings may inform the agricultural and energy sectors in South America with estimates of potential outcomes of aerosol injections. This is relevant in case humanity decides to (a)symmetrically inject aerosols to artificially cool the planet (geoengineering; Sun et al., 2024), or if another large volcanic eruption unfolds. This has implications for climate adaptation and mitigation, and risk management.

4.4 Methods

4.4.1 Data

Our study uses several data sources to analyse the atmospheric dynamics. It includes atmospheric model simulations, reanalysis and observed hydrometeorological data. We focus on the boreal summer season because it is the one receiving the highest solar radiation in the northern hemisphere, and thus, when the radiation scattering could have been the highest for the second half of the 20th century (considering that the anthropogenic aerosols were mainly expelled in the northern hemisphere; Smith et al., 2004). For the early 19th-century volcanic eruptions, Sigl et al. (2022) classified the five chosen volcanic eruptions as equatorial or northern hemisphere volcanic eruptions, based on the relation of sulphur deposition between Greenland and Antarctica. Therefore, the highest scattering for the volcanic eruptions might have also occurred during the boreal summer.

20th century data

Observed precipitation comes from the Global Precipitation Climatology Centre (GPCC; U. Schneider et al., 2014, 2022) and the Puente Angostura [3206720] streamflow records come from the Global Runoff Data Centre (GRDC, 2023). Dry and wet events in the streamflow gauge are defined when values are below or above 1 standard deviation of the JJA time series, and they are afterwards counted in an 11-year moving window. The GPCC has limitations in the amount of rain gauges used for its creation, which is low inside the Amazon and Colombia's Orinoco basin before the 1980s, but there were many stations in northern Venezuela in the 1960s (Kayano et al., 2020; U. Schneider et al., 2014). GPCC is one of the few precipitation datasets with records before the 1980s, yet in recent decades, the number of rain gauges has also decreased. The Atlantic Meridional Mode index is calculated using the Extended Reconstructed Sea Surface Temperature (SST) version 5 dataset (ERSSTv5; Huang et al., 2017, with the spatial boxes definition used by Fernandes et al. (2015). SST indices in the tropics reflect the coupling between the atmosphere and the ocean and are indicative of atmospheric dynamics. Aerosol optical depth at 550 nm is analysed with a ground-based visibility machine learning-derived dataset (Hao et al., 2024).

We use three reanalyses with estimates of the 20th century and a paleo-reanalysis family of the Modern era. We utilise zonal and meridional wind components at 850 hPa, 850 hPa wind divergence, vertical velocity at 500 hPa (omega500), sea level pressure (SLP) and 2 m temperature from ERA5 (Hersbach et al., 2020), 20CRv3 (Slivinski et al., 2021), and CERA-20 (Laloyaux et al., 2018) to analyse the changes in atmospheric circulation in the global zonal mean and the regional atmospheric circulation. CERA-20C is a coupled reanalysis that assimilates marine winds and pressure, whereas 20CR is uncoupled and assimilates only surface pressure; ERA5 assimilates several variables. We also use the vertically integrated water vapour flux (VIMF), the vertically integrated moisture divergence (MDiv, inverted for analysing convergence) and the meridional vertically integrated total energy flux (VITEF) from ERA5.

Paleo-reanalysis

The period between 1780 and 1850 is studied with the ModE-RA family of reanalyses (Valler et al., 2024). This dataset provides three monthly global fields back to 1421:

1. An atmospheric model simulation (ModE-Sim, subdivided into 3 subset ensembles of 20 members – set-1420_1, _2 and _3; Hand et al., 2023), which is used as a prior estimate for the retrospective analysis. Subsets _1 and _3 use Paleoclimate Modelling Intercomparison Project - Phase 4 forcing (PMIP4; Jungclaus et al., 2017), whereas subset _2 individual members were built with the Easy Volcanic Aerosol model (EVA; Toohey et al., 2016) and the volcanic stratospheric sulfur injection (VSSI) reconstruction of Sigl et al. (2022), varying the strength and time of the eruptions (Hand et al., 2023). PMIP4 forcing includes anthropogenic sources of aerosols.

2. The ModE-RA reanalysis, which uses a three-cycle monthly off-line data assimilation system to ingest thousands of data records in the 18th and 19th centuries (Valler et al., 2024).

3. ModE-RAclim, an assimilation of the observations into a random sample of the prior dataset (Valler et al., 2024); it does not see the time-varying forcing and reflects more directly the observations.

For the construction of the reanalysis, it was assumed that observational errors are uncorrelated. All results are separately obtained in all members of the ensemble, unless otherwise noted. We used the same variables from the other reanalyses, plus geopotential, humidity and precipitation for certain analyses or calculations of derived fluxes (e.g. the total energy flux). Precipitation from the CESM-LME (Otto-Bliesner et al., 2016) is also used for comparison. CESM-LME uses CMIP5 climate forcing reconstructions (Schmidt et al., 2012), and other forcings, but we used the all forcing ensemble mean. We analysed the AOD meridional distribution in the early 19th century with the AOD at 550 nm.

The oceanic boundary conditions in ModE-Sim and ModE-RA are constrained by proxies in the tropics (Samakinwa et al., 2021). This helps the model to represent the occurrence of ocean-atmospheric variability modes such as El Niño-Southern Oscillation in the specific period analysed. However, precipitation is poorly constrained in tropical South America in the period analysed (one assimilated station in the analysed boxes and thus ModE-RAclim has an almost constant spread and ensemble mean); therefore, the precipitation dynamics in the early 19th century come mainly from the response of ModE-Sim and possible updates from correlations with SLP.

4.4.2 Atmospheric moisture and energy fluxes

We calculated the VIMF, MDiv and the meridional VITEF from ModE-Sim (ModE-RA does not have certain variables necessary for the calculation of these fluxes). They are defined as follows:

$$H = L_v \cdot q + c_p \cdot T + g \cdot z \tag{4.1}$$

$$VITEF = \oint \int_0^{P_s} v \cdot E \frac{dp}{g} dx = \oint \int_0^{P_s} v(H + \frac{1}{2}V^2) \frac{dp}{g} dx \tag{4.2}$$

$$VIMF_x = \int_0^{P_s} q \cdot u \frac{dp}{g} \tag{4.3}$$

$$VIMF_y = \int_0^{P_s} q \cdot v \frac{dp}{g} \tag{4.4}$$

$$MDiv = \nabla \cdot VIMF = (\frac{\partial}{\partial x} VIMF_x) + (\frac{\partial}{\partial y} VIMF_y) \tag{4.5}$$

Where L_v is the latent heat of vaporisation, q is the specific humidity, c_p is the air specific heat at constant pressure, T is the air temperature, g is the gravity, z is the geopotential height, H is moist static energy and E is the total specific energy, u and v are the zonal and meridional wind components, p is the pressure level, and P_s is the pressure level at surface.

The calculations with ModE-Sim of the aforementioned fluxes have some limitations. The variables were just available at 7 levels, impacting the vertical integration. The effects can be seen in the global zonal mean (Fig. S2b), ModE-Sim reports a northward energy flux between 65°S and 30°S when a complete southward energy flux is expected in the southern hemisphere (as reproduced by ERA5 in Fig. S2a).

However, it still shows, at around 15°N, the southward energy transport expected from the upper branch of the Hadley cell, which in JJA should bring the energy towards the coldest hemisphere (the southern).

4.4.3 Anomalies and composites for volcanic eruptions

To analyse the interannual to decadal changes leading to impacts in the hydroclimate, we deseasonalise rainfall, streamflow, VIMF and its divergence. The anomalies are calculated with the mean from 1980 to 2020 for the analysis of the 20th century. For the early 19th-century analysis, we chose the period from 1740 to 1780 to exclude possible effects from the 1783 Laki eruption. The occurrence of a streamflow wet and dry event is defined as the event exceeding ±1 standard deviation, respectively; we consider the period 1980-2020 for the calculation of the mean and variance.

The composite of the volcanic eruptions is built with the average of the boreal summer of the year after the five large volcanic eruptions between 1800 and 1850. The five volcanic eruptions were selected based on those that had more than 1 Tg S injection in the aforementioned period, according to Sigl et al. (2022). We also analysed the AOD at 550 nm for the boreal summer of the year after the volcanic eruptions.

4.4.4 Atmospheric indices

To study the global changes in atmospheric circulation, we estimate the strong ascent of moist air and its latitude. The strong ascent is defined as the minimum global zonal mean vertical velocity at 500 hPa between 30°N and 30°S. The minimum vertical velocity was interpolated between grid points by fitting a spline curve to the 5 points closer to the minimum value coming from the dataset. If the zonal mean reported double minima, we chose the one corresponding to the highest absolute value. We prefer the identification of the ITCZ based on a minimum rather than zero-crossing positions because the latter are more affected by biases (Brönnimann et al., 2015). In the case of the reanalysis covering the 20th century, we display the 11-year moving average to ease the visualisation of the progressive change.

The interhemispheric temperature gradient (IHTG) and the tropical humidity might influence the atmospheric dynamics, leading to the hydroclimate changes. We calculate the IHTG by generating the 2 m temperature global zonal mean, and subsequently calculate the difference between the latitude-weighted average of the extratropical north and south (extratropical defined as north or south of 30°N or 30°S, respectively). Conversely, the tropical humidity is calculated as the vertically integrated zonal mean of the specific humidity.

The meridional VITEF indicates how the atmosphere is redistributing the energy between the equator and the poles. We analyse the Hovmöller diagram to see the interannual changes in the division of the ascending branch of the Hadley cell. We also extract the meridional VITEF at the equator to see the changes in the strength of the energy redistribution, expecting interannual to decadal changes in the southward energy transport for the boreal summer.

4.4.5 Trends in the tropospheric aerosols

Since anthropogenic aerosols were emitted in trends after the 1950s, increasing the concentration of troposheric aerosols, we analyse the regional atmospheric circulation with trends. We include the two decades of the 21st century and divide the

analysis into two periods, periods based on the amount of sulfuric aerosols released to the atmosphere (IPCC, 2021; Smith et al., 2004). The period from 1955 to 1990 experienced an increase in sulphur dioxide emissions, whereas the emissions slightly decreased from the 1990s. Hence, we define the periods 1960-1989 and 1990-2020 for analysing the SLP, winds at 850 hPa, the VIMF, the MDiv and the precipitation.

A limitation of the analysis in the 20th century is that neither of the three reanalyses assimilates directly aerosol concentration or optical depth. This limits the radiation dynamics and, thus, its influence over the surface temperature. Then, the effects of aerosols are only included through the prescribed observed SSTs. However, the reanalyses assimilate directly variables of the atmospheric circulation (such as pressure, geopotential height, wind speed and direction), and hence they are believed to properly represent the regional atmospheric circulation, moisture transport and convergence at seasonal time scales.

Data Statement

GPCC precipitation data is available at: https://opendata.dwd.de/climate_environment/GPCC/html/fulldata-monthly_v2022_doi_download.html. GRDC streamflow data is at: https://portal.grdc.bafg.de/applications/public.html?publicuser=PublicUser#dataDownload/Stations. Extended Reconstructed SST version 5 is available at: https://www.ncei.noaa.gov/pub/data/cmb/ersst/v5/netcdf/. 20CRv3 is available at: https://psl.noaa.gov/data/gridded/data.20thC_ReanV3.html. CERA-20C is available at: http://apps.ecmwf.int/datasets/data/cera20c. ERA5 is available at: https://cds.climate.copernicus.eu/. ModE-RA dataset family and its forcing is available at: https://www.wdc-climate.de/ui/entry?acronym=ModE-RA_s14203-18501. CESM-LME precipitation ensemble mean is available at: https://gdex.ucar.edu/datasets/d651058/. The Visibility-derived aerosol optical depth is available at: https://doi.org/10.11888/Atmos.tpdc.300822.

Funding

N.D-G. was supported by the Federal Commission for Scholarships for Foreign Students through the Swiss Government Excellence Scholarship (ESKAS No. 2022.0563) for the academic year(s) 2024-2025. A.R.F. was funded by the European Union's Horizon 2020 research and innovation program under the Marie Skłodowska-Curie grant No. 894064 (AQUATIC). Stefan Brönnimann was funded by the Swiss National Science Foundation (grant no. 10001375).

Author contributions

Conceptualization: N.D-G, A.R.F. and S.B.; Data Curation: N.D-G, A.R.F.; Formal Analysis: N.D-G; Funding Acquisition: N.D-G, S.B.; Investigation: N.D-G, A.R.F, S.B.; Methodology: N.D-G, A.R.F., S.B., J.F; Project Administration: N.D-G., S.B.; Resources: S.B.; Software: N.D-G; Supervision: S.B.; Validation: N.D-G, A.R.F., S.B.; Visualisation: N.D-G; Writing - original draft: N.D-G; Writing - review and editing: N.D-G, A.R.F., S.B, J.F.

Acknowledgements

We are grateful to the institutions that gather and freely disseminate the data used in this research. N.D-G thanks Helena Gardeazabal, Joaquin Duque and friends for their emotional support throughout this research.

Appendix

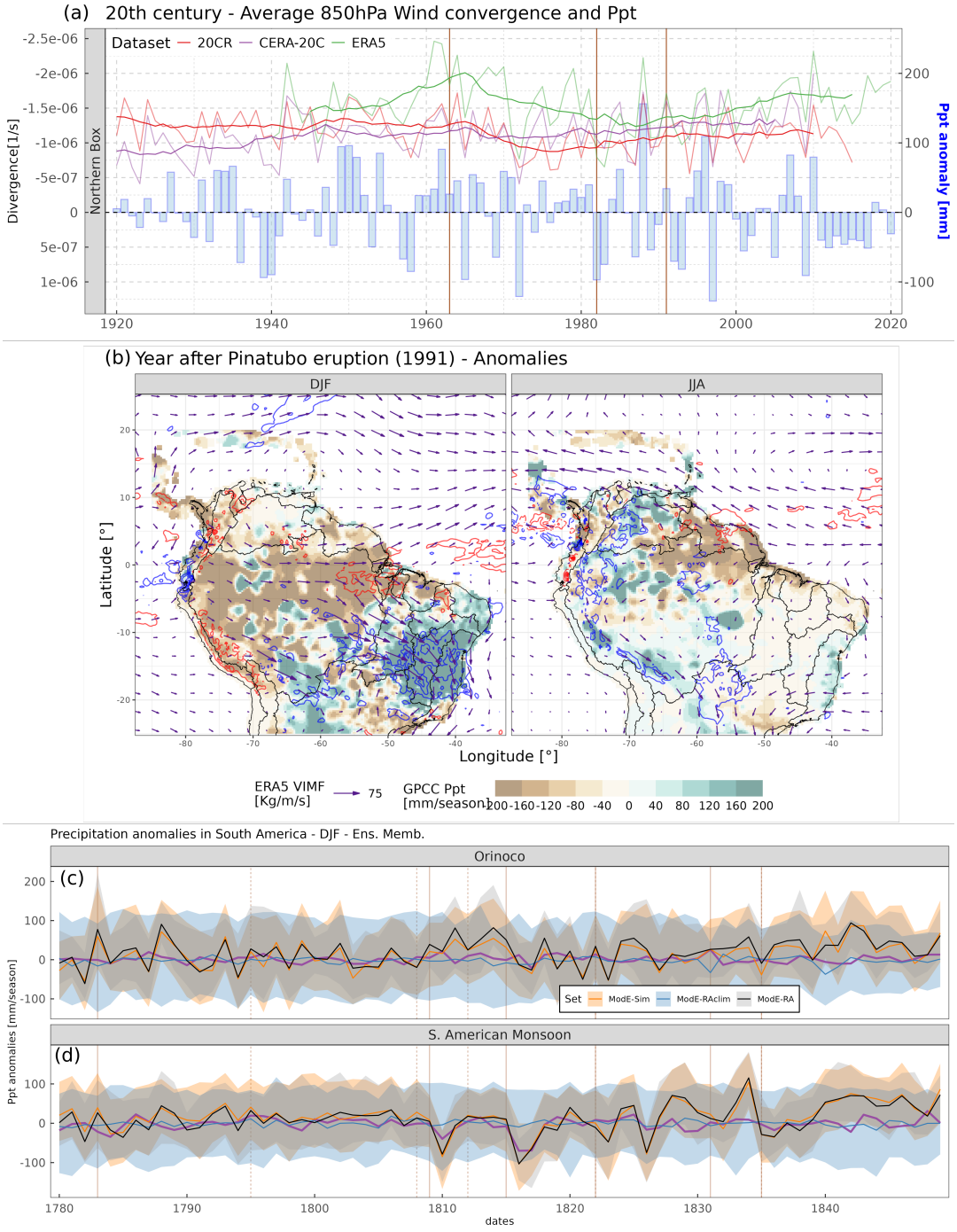

FIGURE 4.5: **Figure S1. Other hydroclimate anomalies in tropical South America** (a) Time series of JJA 850 hPa wind convergence and GPCC precipitation anomalies (right-side y-axis) in the northern box (Fig. 1a). (b) Anomalies of ERA5 VIMF (arrows), moisture divergence (contours) and GPCC precipitation (shading), in the year 1992 (year after mount Pinatubo's eruption). (c) and (d)Time series of precipitation anomalies in December to February for the northern and southern box (Fig. 1a) for the 19th century, using the ModE-RA reanalysis family. Lower and upper ribbon represent the 5 and 95 percentile ensemble members spread and tick color line the ensemble mean. Purple line depicts the CESM-LME ensemble mean. Vertical orange lines denote years with volcanic eruptions highlighted in Hand et al. (2023).

FIGURE 4.6: **Figure S2. ERA5 meridional vertically integrated total energy flux in June to August** for (top) the late 20th and early 21st centuries and (bottom) the early 19th century using ModE-Sim. Green shadings indicate northward flux while purple indicates southward flux. The orange line depicts the energy flux at the equator (right axis, negative values indicate southward flux). Vertical lines in the bottom panel denote years with volcanic eruptions highlighted in Hand et al. (2023).

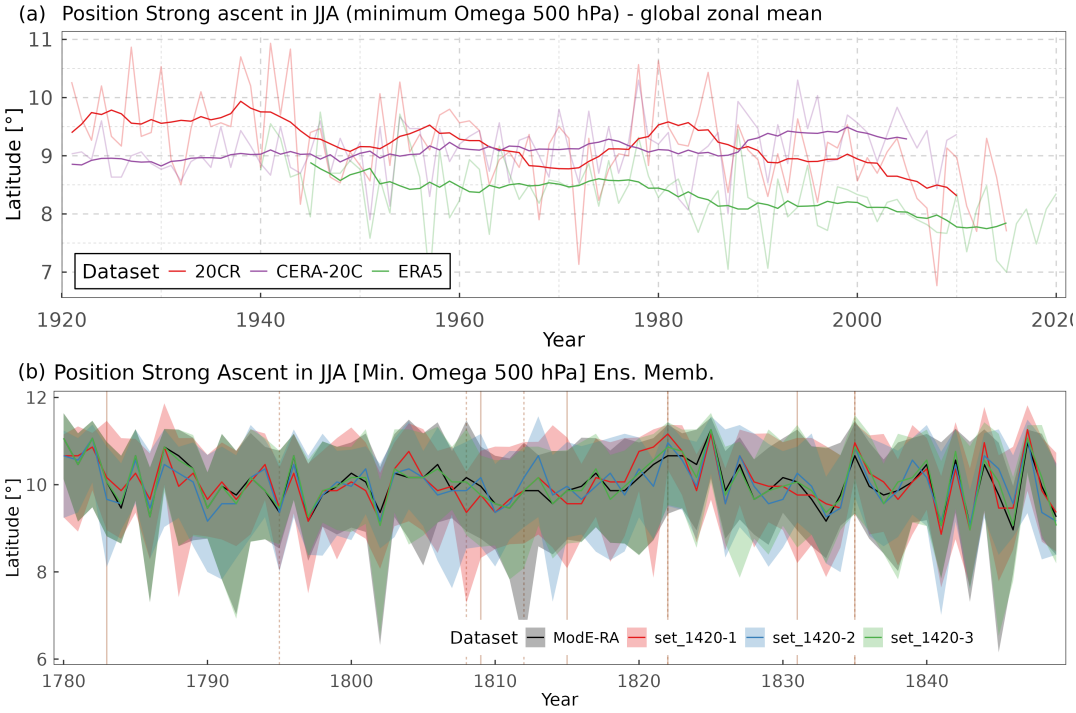

FIGURE 4.7: **Figure S3. Global position of the strong ascent of moist air** (Global zonal mean minimum vertical velocity at 500 hPa), for (a) the 20th century and (b) the early 19th century bottom. Colors depict three different reanalyses in the 20th century and the three subsets in the ModE-RA family of reanalyses. In the top panel, tick lines represent the 11-year moving average and the faded lines the annual time series. In the bottom panel, lower and upper ribbon represent the 5 and 95 percentiles ensemble members' spread and tick color line represents the ensemble mean. Vertical lines in the bottom panel denote years with volcanic eruptions highlighted in Hand et al. (2023).

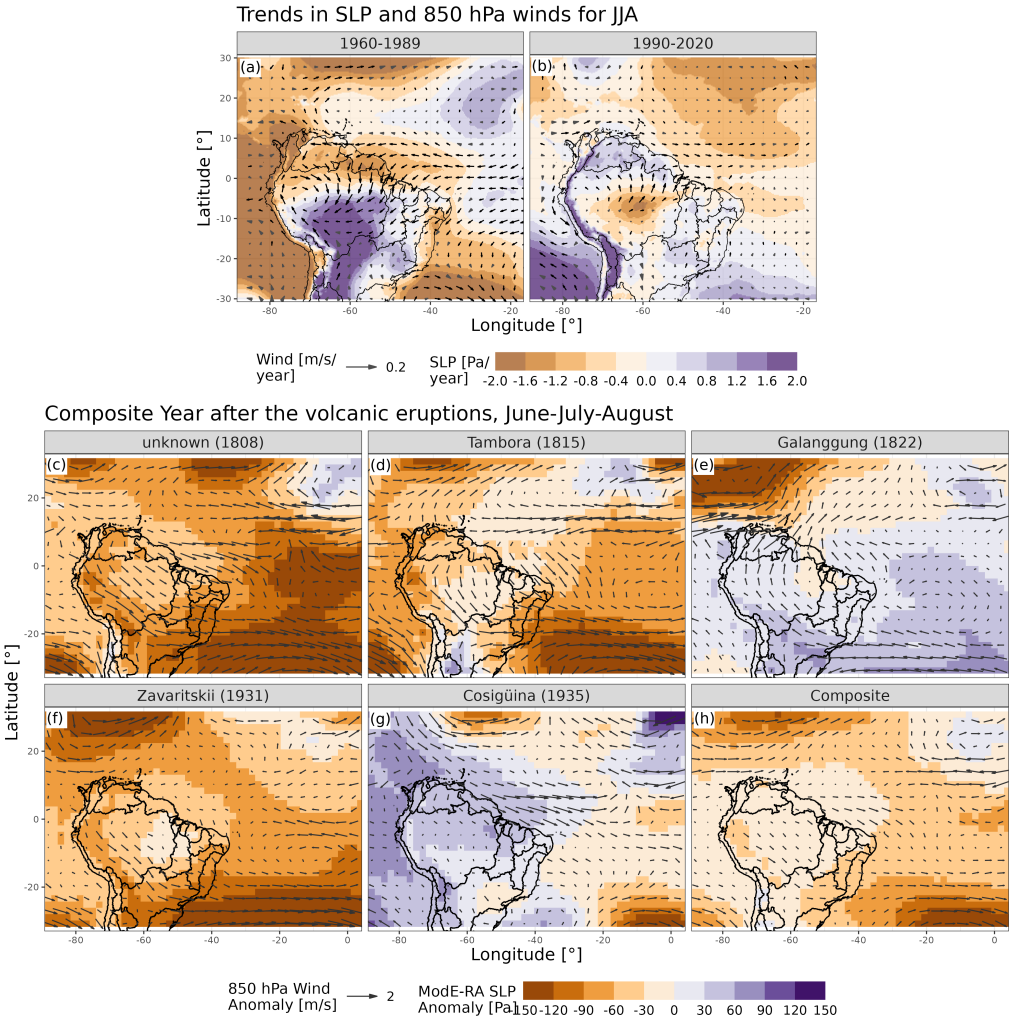

FIGURE 4.8: **Figure S4. Changes in sea level pressure and 850 hPa wind** (a) Linear slope coefficients of ERA5 850 hPa wind components (arrows), and Sea Level Pressure (shading) against Gregorian year for the boreal summer -JJA- in the 1960-1989 period. (b) same as (a) but for the period 1990-2020. (c to g) Boreal summer anomalies in the year after the volcanic eruption with ModE-RA wind components (arrows), and ModE-RA Sea Level Pressure (shading). (h) Same as (c) but the composite of the five eruptions.

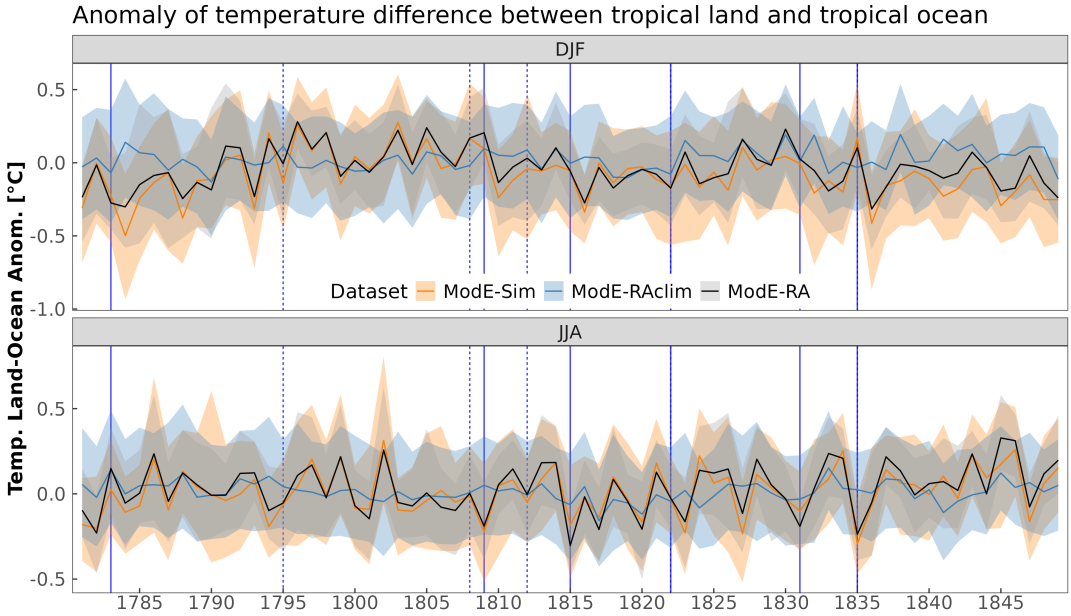

FIGURE 4.9: **Figure S5. Early 19th century anomalies of the temperature contrast between the land and the ocean in the tropics** for (a) DJF and (b) JJA. Vertical lines display years with volcanic eruptions highlighted in Hand et al. (2023).

References

Bayraktar, M. (2024). Volcanic Eruptions & Socioeconomic Results: A Systematic Review. https://doi.org/10.2139/ssrn.4947436

Brönnimann, S., Fischer, A. M., Rozanov, E., Poli, P., Compo, G. P., & Sardeshmukh, P. D. (2015). Southward shift of the northern tropical belt from 1945 to 1980. *Nature Geoscience*, *8*(12), 969–974. https://doi.org/10.1038/ngeo2568

Brönnimann, S., Franke, J., Nussbaumer, S. U., Zumbühl, H. J., Steiner, D., Trachsel, M., Hegerl, G. C., Schurer, A., Worni, M., Malik, A., Flückiger, J., & Raible, C. C. (2019). Last phase of the Little Ice Age forced by volcanic eruptions. *Nature Geoscience*, *12*(8), 650–656. https://doi.org/10.1038/s41561-019-0402-y

Cai, W., McPhaden, M. J., Grimm, A. M., Rodrigues, R. R., Taschetto, A. S., Garreaud, R. D., Dewitte, B., Poveda, G., Ham, Y. G., Santoso, A., Ng, B., Anderson, W., Wang, G., Geng, T., Jo, H. S., Marengo, J. A., Alves, L. M., Osman, M., Li, S., … Vera, C. (2020). Climate impacts of the El Niño–Southern Oscillation on South America. *Nature Reviews Earth and Environment*, *1*(4), 215–231. https://doi.org/10.1038/s43017-020-0040-3

Diao, C., Xu, Y., & Xie, S. P. (2021). Anthropogenic aerosol effects on tropospheric circulation and sea surface temperature (1980-2020): Separating the role of zonally asymmetric forcings. *Atmospheric Chemistry and Physics*, *21*(24), 18499–18518. https://doi.org/10.5194/acp-21-18499-2021

Duque-Gardeazabal, N., Brönnimann, S., Friedman, A. R., Dolores-Tesillos, E., & Martius, O. (2026). Wind and solar energy variability in tropical South America: Ocean-atmospheric modulators. *Meteorological Applications*.

Duque-Gardeazabal, N., Friedman, A. R., & Brönnimann, S. (2025). An Atlantic influence on evapotranspiration in the Orinoco and Amazon basins. *Hydrology*

and Earth System Sciences, *29*(14), 3277–3295. https://doi.org/10.5194/hess-29-3277-2025

Fernandes, K., Giannini, A., Verchot, L., Baethgen, W., & Pinedo-Vasquez, M. (2015). Decadal covariability of Atlantic SSTs and western Amazon dry-season hydroclimate in observations and CMIP5 simulations. *Geophysical Research Letters*, *42*(16), 6793–6801. https://doi.org/10.1002/2015GL063911

Friedman, A. R., Hegerl, G. C., Schurer, A. P., Lee, S. Y., Kong, W., Cheng, W., & Chiang, J. C. (2020). Forced and unforced decadal behavior of the interhemispheric SST contrast during the instrumental period (1881–2012): Contextualizing the late 1960s–early 1970s shift. *Journal of Climate*, *33*(9), 3487–3509. https://doi.org/10.1175/JCLI-D-19-0102.1

Gorenstein, I., Wainer, I., Pausata, F. S. R., Prado, L. F., Khodri, M., & Dias, P. L. S. (2023). A 50-year cycle of sea surface temperature regulates decadal precipitation in the tropical and South Atlantic region. *Communications Earth & Environment*, *4*(1), 427. https://doi.org/10.1038/s43247-023-01073-0

GRDC. (2023). Global Runoff Data Centre. https://www.bafg.de/GRDC/EN/Home/homepage%7B%5C_%7Dnode.html

Hand, R., Samakinwa, E., Lipfert, L., & Brönnimann, S. (2023). ModE-Sim - a medium-sized atmospheric general circulation model (AGCM) ensemble to study climate variability during the modern era (1420 to 2009). *Geoscientific Model Development*, *16*(16), 4853–4866. https://doi.org/10.5194/gmd-16-4853-2023

Hao, H., Wang, K., Zhao, C., Wu, G., & Li, J. (2024). Visibility-derived aerosol optical depth over global land from 1959 to 2021. *Earth System Science Data*, *16*(7), 3233–3260. https://doi.org/10.5194/essd-16-3233-2024

Hartmann, D. (2016). *Global Physical climatology* (2nd editio). Elsevier Inc.

He, C., Clement, A. C., Kramer, S. M., Cane, M. A., Klavans, J. M., Fenske, T. M., & Murphy, L. N. (2023). Tropical Atlantic multidecadal variability is dominated by external forcing. *Nature*, *622*(October). https://doi.org/10.1038/s41586-023-06489-4

Hegerl, G. C., Brönnimann, S., Cowan, T., Friedman, A. R., Hawkins, E., Iles, C., Müller, W., Schurer, A., & Undorf, S. (2019). Causes of climate change over the historical record. *Environmental Research Letters*, *14*(12). https://doi.org/10.1088/1748-9326/ab4557

Herman, R. J., Giannini, A., Biasutti, M., & Kushnir, Y. (2020). The effects of anthropogenic and volcanic aerosols and greenhouse gases on twentieth century Sahel precipitation. *Scientific Reports*, *10*(1), 12203. https://doi.org/10.1038/s41598-020-68356-w

Hersbach, H., Bell, B., Berrisford, P., Hirahara, S., Horányi, A., Muñoz-Sabater, J., Nicolas, J., Peubey, C., Radu, R., Schepers, D., Simmons, A., Soci, C., Abdalla, S., Abellan, X., Balsamo, G., Bechtold, P., Biavati, G., Bidlot, J., Bonavita, M., … Thépaut, J. N. (2020). The ERA5 global reanalysis. *Quarterly Journal of the Royal Meteorological Society*, *146*(730), 1999–2049. https://doi.org/10.1002/qj.3803

Hua, W., Dai, A., Zhou, L., Qin, M., & Chen, H. (2019). An Externally Forced Decadal Rainfall Seesaw Pattern Over the Sahel and Southeast Amazon. *Geophysical Research Letters*, *46*(2), 923–932. https://doi.org/10.1029/2018GL081406

Huang, B., Thorne, P. W., Banzon, V. F., Boyer, T., Chepurin, G., Lawrimore, J. H., Menne, M. J., Smith, T. M., Vose, R. S., & Zhang, H. M. (2017). Extended reconstructed Sea surface temperature, Version 5 (ERSSTv5): Upgrades, validations, and intercomparisons. *Journal of Climate*, *30*(20), 8179–8205. https://doi.org/10.1175/JCLI-D-16-0836.1

Hutchison, W., Sugden, P., Burke, A., Abbott, P., Ponomareva, V. V., Dirksen, O., Portnyagin, M. V., MacInnes, B., Bourgeois, J., Fitzhugh, B., Verkerk, M., Aubry, T. J., Engwell, S. L., Svensson, A., Chellman, N. J., McConnell, J. R., Davies, S., Sigl, M., & Plunkett, G. (2025). The 1831 CE mystery eruption identified as Zavaritskii caldera, Simushir Island (Kurils). *Proceedings of the National Academy of Sciences*, *122*(1). https://doi.org/10.1073/pnas.2416699122

IPCC. (2021, July). *Climate Change 2021: The Physical Science Basis*. Cambridge University Press. https://doi.org/10.1017/9781009157896

Jungclaus, J. H., Bard, E., Baroni, M., Braconnot, P., Cao, J., Chini, L. P., Egorova, T., Evans, M., González-Rouco, J. F., Goosse, H., Hurtt, G. C., Joos, F., Kaplan, J. O., Khodri, M., Klein Goldewijk, K., Krivova, N., LeGrande, A. N., Lorenz, S. J., Luterbacher, J., … Zorita, E. (2017). The PMIP4 contribution to CMIP6 – Part 3: The last millennium, scientific objective, and experimental design for the PMIP4 past1000 simulations. *Geoscientific Model Development*, *10*(11), 4005–4033. https://doi.org/10.5194/gmd-10-4005-2017

Kayano, M. T., Andreoli, R. V., & de Souza, R. A. (2020). Pacific and Atlantic multidecadal variability relations to the El Niño events and their effects on the South American rainfall. *International Journal of Climatology*, *40*(4), 2183–2200. https://doi.org/10.1002/joc.6326

Kobashi, T., Menviel, L., Jeltsch-Thömmes, A., Vinther, B. M., Box, J. E., Muscheler, R., Nakaegawa, T., Pfister, P. L., Döring, M., Leuenberger, M., Wanner, H., & Ohmura, A. (2017). Volcanic influence on centennial to millennial Holocene Greenland temperature change. *Scientific Reports*, *7*(1), 1441. https://doi.org/10.1038/s41598-017-01451-7

Laloyaux, P., de Boisseson, E., Balmaseda, M., Bidlot, J.-R., Broennimann, S., Buizza, R., Dalhgren, P., Dee, D., Haimberger, L., Hersbach, H., Kosaka, Y., Martin, M., Poli, P., Rayner, N., Rustemeier, E., & Schepers, D. (2018). CERA-20C: A Coupled Reanalysis of the Twentieth Century. *Journal of Advances in Modeling Earth Systems*, *10*(5), 1172–1195. https://doi.org/10.1029/2018MS001273

Li, J., Carlson, B. E., Yung, Y. L., Lv, D., Hansen, J., Penner, J. E., Liao, H., Ramaswamy, V., Kahn, R. A., Zhang, P., Dubovik, O., Ding, A., Lacis, A. A., Zhang, L., & Dong, Y. (2022). Scattering and absorbing aerosols in the climate system. *Nature Reviews Earth & Environment*, *3*(6), 363–379. https://doi.org/10.1038/s43017-022-00296-7

Lin, L., Xu, Y., Wang, Z., Diao, C., Dong, W., & Xie, S.-P. (2018). Changes in Extreme Rainfall Over India and China Attributed to Regional Aerosol-Cloud Interaction During the Late 20th Century Rapid Industrialization. *Geophysical Research Letters*, *45*(15), 7857–7865. https://doi.org/10.1029/2018GL078308

Liu, Y., Cai, W., Lin, X., & Li, Z. (2022). Increased extreme swings of Atlantic intertropical convergence zone in a warming climate. *Nature Climate Change*, *12*(9), 828–833. https://doi.org/10.1038/s41558-022-01445-y

McGraw, Z., & Polvani, L. M. (2024). How Volcanic Aerosols Globally Inhibit Precipitation. *Geophysical Research Letters*, *51*(13), 1–10. https://doi.org/10.1029/2023GL107930

Menon, S., Hansen, J., Nazarenko, L., & Luo, Y. (2002). Climate Effects of Black Carbon Aerosols in China and India. *Science*, *297*(5590), 2250–2253. https://doi.org/10.1126/science.1075159

Merz, B., Blöschl, G., Vorogushyn, S., Dottori, F., Aerts, J. C., Bates, P., Bertola, M., Kemter, M., Kreibich, H., Lall, U., & Macdonald, E. (2021). Causes, impacts and patterns of disastrous river floods. *Nature Reviews Earth and Environment*, *2*(9), 592–609. https://doi.org/10.1038/s43017-021-00195-3

Mora Pacheco, K. G. (2016). *Adaptación de sociedades agrarias a la variabilidad climática. Sabana de Bogotá, Andes Orientales colombianos, 1690-1870* [Doctoral dissertation, Universidad Nacional de Colombia]. https://repositorio.unal.edu.co/handle/unal/57731

Otto-Bliesner, B. L., Brady, E. C., Fasullo, J., Jahn, A., Landrum, L., Stevenson, S., Rosenbloom, N., Mai, A., & Strand, G. (2016). Climate variability and change since 850 ce an ensemble approach with the community earth system model. *Bulletin of the American Meteorological Society*, *97*(5), 787–801. https://doi.org/10.1175/BAMS-D-14-00233.1

Paik, S., Min, S. K., Iles, C. E., Fischer, E. M., & Schurer, A. P. (2020). Volcanic-induced global monsoon drying modulated by diverse El Ninõ responses. *Science Advances*, *6*(21), 1–8. https://doi.org/10.1126/sciadv.aba1212

Pausata, F. S., Zanchettin, D., Karamperidou, C., Caballero, R., Battisti, D. S., & Battisti, D. S. (2020). ITCZ shift and extratropical teleconnections drive ENSO response to volcanic eruptions. *Science Advances*, *6*(23), 1–11. https://doi.org/10.1126/sciadv.aaz5006

Qin, M., Dai, A., & Hua, W. (2020). Aerosol-forced multidecadal variations across all ocean basins in models and observations since 1920. *Science Advances*, *6*(29), 1–8. https://doi.org/10.1126/sciadv.abb0425

Rodrigues, R. R., & McPhaden, M. J. (2014). Why did the 2011-2012 La Niña cause a severe drought in the Brazilian Northeast? *Geophysical Research Letters*, *41*(3), 1012–1018. https://doi.org/10.1002/2013GL058703

Roldán-Gómez, P. J., González-Rouco, J. F., Melo-Aguilar, C., & Smerdon, J. E. (2022). The Role of Internal Variability in ITCZ Changes Over the Last Millennium. *Geophysical Research Letters*, *49*(4), 1–10. https://doi.org/10.1029/2021GL096487

Sacks, W. J., Cook, B. I., Buenning, N., Levis, S., & Helkowski, J. H. (2009). Effects of global irrigation on the near-surface climate. *Climate Dynamics*, *33*(2-3), 159–175. https://doi.org/10.1007/s00382-008-0445-z

Samakinwa, E., Valler, V., Hand, R., Neukom, R., Gómez-Navarro, J. J., Kennedy, J., Rayner, N. A., & Brönnimann, S. (2021). An ensemble reconstruction of global monthly sea surface temperature and sea ice concentration 1000–1849. *Scientific Data*, *8*(1), 261. https://doi.org/10.1038/s41597-021-01043-1

Schmidt, G. A., Jungclaus, J. H., Ammann, C. M., Bard, E., Braconnot, P., Crowley, T. J., Delaygue, G., Joos, F., Krivova, N. A., Muscheler, R., Otto-Bliesner, B. L., Pongratz, J., Shindell, D. T., Solanki, S. K., Steinhilber, F., & Vieira, L. E. A. (2012). Climate forcing reconstructions for use in PMIP simulations of the Last Millennium (v1.1). *Geoscientific Model Development*, *5*(1), 185–191. https://doi.org/10.5194/gmd-5-185-2012

Schneider, T., Bischoff, T., & Haug, G. H. (2014). Migrations and dynamics of the intertropical convergence zone. *Nature*, *513*(7516), 45–53. https://doi.org/10.1038/nature13636

Schneider, U., Becker, A., Finger, P., Meyer-Christoffer, A., & Ziese, M. (2022). GPCC full data monthly product version 2022 at 0.25: Monthly land-surface precipitation from rain-gauges built on GTS-based and historical data. https://doi.org/10.5676/DWD_GPCC/FD_M_V2022_025

Schneider, U., Becker, A., Finger, P., Meyer-Christoffer, A., Ziese, M., & Rudolf, B. (2014). GPCC's new land surface precipitation climatology based on quality-controlled in situ data and its role in quantifying the global water cycle. *Theoretical and Applied Climatology*, *115*(1-2), 15–40. https://doi.org/10.1007/s00704-013-0860-x

Sengupta, A., Waliser, D. E., DeFlorio, M. J., Guan, B., Delle Monache, L., & Ralph, F. M. (2025). Role of evolving sea surface temperature modes of variability in improving seasonal precipitation forecasts. *Communications Earth & Environment*, *6*(1), 256. https://doi.org/10.1038/s43247-025-02235-y

Sigl, M., Toohey, M., McConnell, J. R., Cole-Dai, J., & Severi, M. (2022). Volcanic stratospheric sulfur injections and aerosol optical depth during the Holocene (past 11 500 years) from a bipolar ice-core array. *Earth System Science Data*, *14*(7), 3167–3196. https://doi.org/10.5194/essd-14-3167-2022

Slivinski, L. C., Compo, G. P., Sardeshmukh, P. D., Whitaker, J. S., McColl, C., Allan, R. J., Brohan, P., Yin, X., Smith, C. A., Spencer, L. J., Vose, R. S., Rohrer, M., Conroy, R. P., Schuster, D. C., Kennedy, J. J., Ashcroft, L., Brönnimann, S., Brunet, M., Camuffo, D., … Wyszyński, P. (2021). An Evaluation of the Performance of the Twentieth Century Reanalysis Version 3. *Journal of Climate*, *34*(4), 1417–1438. https://doi.org/10.1175/JCLI-D-20-0505.1

Smith, S. J., Concepcion, R. A., & Lurz, J. (2004). *Historical Sulfur Dioxide Emissions 1850-2000 : Methods and Results* (tech. rep. No. January). Joint Global Change Research Institute, College Park, MD. http://www.osti.gov/energycitations/product.biblio.jsp?osti%7B%5C_%7Did=15020102

Sun, H., Bourguet, S., Luan, L., & Keith, D. (2024). Stratospheric transport and tropospheric sink of solar geoengineering aerosol: a Lagrangian analysis. *npj Climate and Atmospheric Science*, *7*(1), 115. https://doi.org/10.1038/s41612-024-00664-8

Takahashi, C., & Watanabe, M. (2016). Pacific trade winds accelerated by aerosol forcing over the past two decades. *Nature Climate Change*, *6*(8), 768–772. https://doi.org/10.1038/nclimate2996

Tejedor, E., Steiger, N. J., Smerdon, J. E., Serrano-Notivoli, R., & Vuille, M. (2021). Global hydroclimatic response to tropical volcanic eruptions over the last millennium. *Proceedings of the National Academy of Sciences*, *118*(12). https://doi.org/10.1073/pnas.2019145118

Toohey, M., Krüger, K., Niemeier, U., & Timmreck, C. (2011). The influence of eruption season on the global aerosol evolution and radiative impact of tropical volcanic eruptions. *Atmospheric Chemistry and Physics*, *11*(23), 12351–12367. https://doi.org/10.5194/acp-11-12351-2011

Toohey, M., Jia, Y., Khanal, S., & Tegtmeier, S. (2025). Stratospheric residence time and the lifetime of volcanic stratospheric aerosols. *Atmospheric Chemistry and Physics*, *25*(6), 3821–3839. https://doi.org/10.5194/acp-25-3821-2025

Toohey, M., Stevens, B., Schmidt, H., & Timmreck, C. (2016). Easy Volcanic Aerosol (EVA v1.0): an idealized forcing generator for climate simulations. *Geoscientific Model Development*, *9*(11), 4049–4070. https://doi.org/10.5194/gmd-9-4049-2016

Tuel, A., Naveau, P., & Ammann, C. M. (2017). Skillful prediction of multidecadal variations in volcanic forcing. *Geophysical Research Letters*, *44*(6), 2868–2874. https://doi.org/10.1002/2016GL072234

Undorf, S., Polson, D., Bollasina, M. A., Ming, Y., Schurer, A., & Hegerl, G. C. (2018). Detectable Impact of Local and Remote Anthropogenic Aerosols on the 20th Century Changes of West African and South Asian Monsoon Precipitation. *Journal of Geophysical Research: Atmospheres*, *123*(10), 4871–4889. https://doi.org/10.1029/2017JD027711

Valler, V., Franke, J., Brugnara, Y., Samakinwa, E., Hand, R., Lundstad, E., Burgdorf, A. M., Lipfert, L., Friedman, A. R., & Brönnimann, S. (2024). ModE-RA: a

global monthly paleo-reanalysis of the modern era 1421 to 2008. *Scientific Data*, *11*(1), 1–19. https://doi.org/10.1038/s41597-023-02733-8

Wegmann, M., Brönnimann, S., Bhend, J., Franke, J., Folini, D., Wild, M., & Luterbacher, J. (2014). Volcanic influence on European summer precipitation through monsoons: Possible Cause for "years without summer". *Journal of Climate*, *27*(10), 3683–3691. https://doi.org/10.1175/JCLI-D-13-00524.1

Wu, X., Griessbach, S., & Hoffmann, L. (2017). Equatorward dispersion of a high-latitude volcanic plume and its relation to the Asian summer monsoon: a case study of the Sarychev eruption in 2009. *Atmospheric Chemistry and Physics*, *17*(21), 13439–13455. https://doi.org/10.5194/acp-17-13439-2017

Zheng, Y., Davis, S. J., Persad, G. G., & Caldeira, K. (2020). Climate effects of aerosols reduce economic inequality. *Nature Climate Change*, *10*(3), 220–224. https://doi.org/10.1038/s41558-020-0699-y

Conclusions and Outlook

Humans and fauna depend on the variability of environmental conditions to survive and thrive. Understanding how Earth system drivers influence environmental variability is relevant for avoiding disasters. In the following, we summarise the conclusions of our thesis and propose possible future studies.

5.1 Conclusions

Our research advances the understanding of the teleconnections between ocean-atmospheric modes of variability and hydroclimatic processes in tropical South America. Moreover, it also shows how the modes influence the potential solar and wind energy production.

The physical mechanisms are graphically summarised in chapter 1 through a sketch of the chain of processes (Fig. 1.1). The chain consists of coupled sea surface temperature and sea level pressure (SLP) anomalies, which are associated with altered regional atmospheric circulation. The resulting anomalous winds modify the atmospheric moisture flux and, consequently, the variability of moisture flux divergence. The latter influences local weather, impacting ecological and socio-economic dynamics. In the following, we detail the subsequent impacts on other variables (e.g. precipitation, evapotranspiration, among others), studied in previous chapters.

We investigated the variability of evapotranspiration, using reanalysis and satellite data in a multi-evidence approach (chapter 2). While previous studies focused mainly on precipitation variability, we focus on the variability of evapotranspiration because it was less explored before and is relevant for agriculture, and carbon and energy cycles (Boamah et al., 2024; Humphrey et al., 2021). The main findings of this study are:

- The local controllers of evapotranspiration – soil moisture and net radiation – are influenced by the tropical rainfall annual cycle. Hence, the energy-limited regime unfolds in the rainy season, while the water-limited regime unfolds mainly in the dry season and the transition from dry to wet periods.
- The AMM modulates the meridional moisture flux and consequently evapotranspiration variability. The location of its impacts varies depending on the season analysed due to the ITCZ annual cycle. The local weather is modulated over eastern South America in MAM, while in JJA the impacts migrate to central Amazon and southern Orinoco, and migrate to the western regions close to the Andes during SON.
- The warm Atl3 weakens the trade winds in JJA, producing convergence over the Guianas and eastern Orinoco. However, its effect on soil moisture, radiation, and evapotranspiration is not strong.

- Evapotranspiration anomalies depend on both the evapotranspiration regime and the phase of the ocean-atmospheric mode. The latter alter the local weather and the land surface conditions.
- ENSO impacts similar regions to those influenced by the AMM and the Atl3 (e.g. northeastern Brazil and the Guianas) but only on MAM and JJA, respectively. In the other seasons, all modes affect different regions.

Similarly, potential solar and wind energy are mainly influenced by ENSO and the AMM (chapter 3). Understanding their mechanisms can help improve seasonal to subseasonal forecasts of renewable energy production and is critical to achieve a reliable and decarbonised energy supply. The key insights of this study are:

- Tropical South America has three potential co-located regions with high multi-annual solar and wind capacity factors. These energy hubs are: the North Caribbean, the Eastern Brazil and the Western Perú/Bolivia hub.
- ENSO impacts the three energy hubs through changes in the SLP over the Eastern equatorial Pacific and the equatorial Atlantic, which change the wind speed and the wind capacity factor in South America. El Niño inhibits convection and clouds, which in turn increases solar radiation and the solar capacity factor. Conversely, La Niña enhances convection and cloudiness, leading to reduced solar capacity factor but only over the Eastern Brazil hub.
- The mechanisms associated with the AMM exert a stronger influence than those linked to the Atl3. The AMM inversely modulates the wind capacity factor on the North Caribbean and Eastern Brazil hubs through cross-equatorial SLP and wind anomalies, which also modify moisture transport. The resulting anomalous moisture divergence also alters clouds and radiation, thereby affecting the solar capacity factor in the same hubs.
- The hubs exhibit limited complementarity at interannual time scale under the influence of the modes in almost all seasons. However, the complementarity with hydropower is an option since periods with low radiation and winds also have high precipitation and increased hydropower potential.

Other research has also examined the projected behaviour of the ocean-atmospheric modes under future climate scenarios, which could then alter the chain of processes. For instance, the AMM variability is expected to increase in the 21st century with a faster warming north of the Equator (Liu et al., 2022), whereas the east equatorial Atlantic (Atl3) might reduce its variability with future global warming due to the warming of the oceans (Yang et al., 2022). This could imply more frequent southerly wind anomalies over northeastern Brazil and the Amazon, resulting in increased divergence and droughts over the northern Amazon. Wind speed and capacity factor might thus increase in the Eastern Brazil wind energy hub in JJA, but weaken winds in the North Caribbean hub.

Moreover, our thesis also explores the influence of aerosol forcing on the studied mechanisms and the subsequent impacts on the ITCZ and rainfall over tropical South America (chapter 4). The conclusions from this study are:

- Tropospheric aerosols were linked to the cooling of the northern hemisphere after the 1950s. This was evidenced both over land and in ocean-atmospheric modes such as the Atlantic Multidecadal Oscillation and AMM. The cooling influenced the interhemispheric temperature gradient, which modulates the meridional energy transport, and subsequently altered the position of the Hadley cell and the ITCZ.

- Changes in the regional ITCZ were linked to stronger winds from the anomalously cold northern hemisphere. Stronger northerlies were associated with displaced convergence towards the anomalously warm southern hemisphere (He et al., 2023; Hua et al., 2019). The stronger northerlies around South America influenced more frequent negative AMM events. The latter is associated with an alteration of the chain of processes, which in turn influenced the migration of precipitation southward.
- Conversely, the global cooling – associated with the early 19th-century stratospheric volcanic aerosols – led to reduced tropical atmospheric humidity. The latter influenced global tropical precipitation, decreasing it. However, our results did not reveal significant changes in the position of the tropical strong ascent of moist air after all eruptions.
- The global cooling also affected the temperature contrast between the land and the oceans (the contrast is associated with the first step in the chain), thereby reducing the easterly moisture flux from the Atlantic. This attenuation of moisture transport led to weaker monsoon systems and reduced precipitation. Other studies have found a similar mechanism (Paik & Min, 2017; Pausata et al., 2020).

5.2 Outlook

Several applications and questions originated from the results of our analysis. In the following, we propose some topics for further research and application.

Our results can support the development of predictive tools (seasonal forecasts or early-warning systems), aimed to advise: farmers, energy producers and managers, among others (K. Fernandes et al., 2020; Lledó et al., 2019; White et al., 2017). Such forecasts can also aid in the prevention of socio-ecological disasters such as flooding (through streamflow prediction, Petry et al., 2025), or forest fires. Studying forest fires is increasingly relevant since South America has registered more heat extremes and has become more flammable (Feron et al., 2024). The ocean-atmospheric indices could directly serve as predictors in statistical and machine learning-based forecasting systems for weather, hydroclimate and renewable energy variability (K. Fernandes et al., 2020; Galván Fraile et al., 2025); machine and deep learning could also account for non-linearities in the chain of processes. Causal inference approaches could help overcome prediction barriers and unravel the reasons for the migration of impacted regions (Reichstein et al., 2019; Runge et al., 2019).

Extreme hydrometeorological events are influenced by the ocean-atmospheric variability. Further research is needed to determine whether the anomalous moisture associated with Atlantic modes primarily influences the frequency of wet days or the intensity of rainfall, or both. Understanding this distinction would improve agricultural planning and flood risk management (K. Fernandes et al., 2020; Towner et al., 2021).

Evapotranspiration estimates remain uncertain due to measurement and modelling limitations (Wang & Dickinson, 2012). However, monitoring evapotranspiration-related ecological variables could help corroborate the evapotranspiration dynamics studied here. Vegetation indices, such as the normalised difference vegetation index, are related to the availability of water and radiation (Nemani et al., 2003). We explored lagged correlations between the modes and the aforementioned vegetation index, and found similar affected locations compared to those found in chapter 2 (not shown). Future studies should further explore these links using high-resolution

datasets. Moreover, evapotranspiration is the source of moisture recycling, which might also influence convergence and cloud formation (Makarieva et al., 2023). The extent to which moisture recycling modulates radiation and evapotranspiration remains an open question.

Other sources of climate variability – at shorter than seasonal scale – are worth exploring because they could improve subseasonal predictions and anticipate extreme events such as heavy rainfall, flash droughts, flammable conditions, low energy production, etc. (White et al., 2022). The possible influencing phenomena include: Madden-Julian Oscillations, Caribbean or African easterly waves, among others (Mariotti et al., 2018; Vitart et al., 2025). The Madden-Julian Oscillations are associated with the variability of radiation and precipitation in the tropics and extratropics (L. G. Fernandes & Grimm, 2023) and could therefore influence evapotranspiration or weekly solar energy production. The Caribbean easterly waves can also influence hydrometeorological extremes, yet they influence Central America more than South America (Giraldo-Cardenas et al., 2022). Future research should also consider the relationship between the subseasonal phenomena and the large-scale ocean-atmospheric modes and their teleconnections. This is how westerly wind events and Madden-Julian Oscillations in the tropical Pacific influence ENSO diversity and how the latter generates different teleconnections with the other ocean basins (García-Serrano et al., 2017; Thual & Dewitte, 2023).

Regarding aerosol forcing, comparing forced and unforced coupled atmospheric models could expand the understanding of aerosol-driven impacts. It could help discern whether the increased dryness and evapotranspiration in the Amazon is due to the current positive Atlantic Multidecadal Oscillation and AMM dynamics (linked to reduced aerosols), or if it is mainly caused by greenhouse gas-induced warming and increased evaporative demand (He et al., 2023; Vicente-Serrano et al., 2020). This is important because it also affects flammable conditions. Distinguishing between aerosol and greenhouse gas effects is also essential to evaluate the potential consequences of deliberate aerosol injection for geoengineering (Kravitz et al., 2015; Sun et al., 2024). Additionally, after some volcanic eruptions, we found an upwind shift of rainfall towards the Atlantic Ocean; it might be worth exploring the effects of other volcanic eruptions in other periods to corroborate the ocean-land temperature contrast mechanism and to expand the assessment to other tropical regions. Moreover, using other model ensembles (e.g. CMIP6 as opposed to previous studies with CMIP5, Paik et al., 2020, or CMIP7 in the near future) would enable a more robust evaluation of the uncertainty by considering different model structures and parametrisations.

References

Boamah, P. O., Onumah, J., Apam, B., Salifu, T., Abunkudugu, A. A., & Alabil, S. A. (2024). Climate variability impact on crop evapotranspiration in the upper East region of Ghana. *Environmental Challenges*, *14*, 100828. https://doi.org/10.1016/j.envc.2023.100828

Fernandes, K., Muñoz, A. G., Ramirez-Villegas, J., Agudelo, D., Llanos-Herrera, L., Esquivel, A., Rodriguez-Espinoza, J., & Prager, S. D. (2020). Improving seasonal precipitation forecasts for agriculture in the orinoquía Region of Colombia. *Weather and Forecasting*, *35*(2), 437–449. https://doi.org/10.1175/WAF-D-19-0122.1

Fernandes, L. G., & Grimm, A. M. (2023). ENSO modulation of global MJO and its impacts on South America. *Journal of Climate*, 1–48. https://doi.org/10.1175/jcli-d-22-0781.1

Feron, S., Cordero, R. R., Damiani, A., MacDonell, S., Pizarro, J., Goubanova, K., Valenzuela, R., Wang, C., Rester, L., & Beaulieu, A. (2024). South America is becoming warmer, drier, and more flammable. *Communications Earth and Environment*, *5*(1), 1–10. https://doi.org/10.1038/s43247-024-01654-7

Galván Fraile, V., Rodríguez-Fonseca, M. B., Polo, I., Martín-Rey, M., & Moreno-García, M. N. (2025, July). Assessing seasonal climate predictability using a deep learning application: NN4CAST. https://doi.org/10.5194/egusphere-2025-3162

García-Serrano, J., Cassou, C., Douville, H., Giannini, A., & Doblas-Reyes, F. J. (2017). Revisiting the ENSO teleconnection to the tropical North Atlantic. *Journal of Climate*, *30*(17), 6945–6957. https://doi.org/10.1175/JCLI-D-16-0641.1

Giraldo-Cardenas, S., Arias, P. A., Vieira, S. C., & Zuluaga, M. D. (2022). Easterly waves and precipitation over northern South America and the Caribbean. *International Journal of Climatology*, *42*(3), 1483–1499. https://doi.org/10.1002/joc.7315

He, C., Clement, A. C., Kramer, S. M., Cane, M. A., Klavans, J. M., Fenske, T. M., & Murphy, L. N. (2023). Tropical Atlantic multidecadal variability is dominated by external forcing. *Nature*, *622*(October). https://doi.org/10.1038/s41586-023-06489-4

Hua, W., Dai, A., Zhou, L., Qin, M., & Chen, H. (2019). An Externally Forced Decadal Rainfall Seesaw Pattern Over the Sahel and Southeast Amazon. *Geophysical Research Letters*, *46*(2), 923–932. https://doi.org/10.1029/2018GL081406

Humphrey, V., Berg, A., Ciais, P., Gentine, P., Jung, M., Reichstein, M., Seneviratne, S. I., & Frankenberg, C. (2021). Soil moisture–atmosphere feedback dominates land carbon uptake variability. *Nature*, *592*(7852), 65–69. https://doi.org/10.1038/s41586-021-03325-5

Kravitz, B., Robock, A., Tilmes, S., Boucher, O., English, J. M., Irvine, P. J., Jones, A., Lawrence, M. G., MacCracken, M., Muri, H., Moore, J. C., Niemeier, U., Phipps, S. J., Sillmann, J., Storelvmo, T., Wang, H., & Watanabe, S. (2015). The Geoengineering Model Intercomparison Project Phase 6 (GeoMIP6): simulation design and preliminary results. *Geoscientific Model Development*, *8*(10), 3379–3392. https://doi.org/10.5194/gmd-8-3379-2015

Liu, Y., Cai, W., Lin, X., & Li, Z. (2022). Increased extreme swings of Atlantic intertropical convergence zone in a warming climate. *Nature Climate Change*, *12*(9), 828–833. https://doi.org/10.1038/s41558-022-01445-y

Lledó, L., Torralba, V., Soret, A., Ramon, J., & Doblas-Reyes, F. J. (2019). Seasonal forecasts of wind power generation. *Renewable Energy*, *143*, 91–100. https://doi.org/10.1016/j.renene.2019.04.135

Makarieva, A. M., Nefiodov, A. V., Nobre, A. D., Baudena, M., Bardi, U., Sheil, D., Saleska, S. R., Molina, R. D., & Rammig, A. (2023). The role of ecosystem transpiration in creating alternate moisture regimes by influencing atmospheric moisture convergence. *Global Change Biology*, *29*(9), 2536–2556. https://doi.org/10.1111/gcb.16644

Mariotti, A., Ruti, P. M., & Rixen, M. (2018). Progress in subseasonal to seasonal prediction through a joint weather and climate community effort. *npj Climate and Atmospheric Science*, *1*(1), 2–5. https://doi.org/10.1038/s41612-018-0014-z

Nemani, R. R., Keeling, C. D., Hashimoto, H., Jolly, W. M., Piper, S. C., Tucker, C. J., Myneni, R. B., & Running, S. W. (2003). Climate-Driven Increases in Global Terrestrial Net Primary Production from 1982 to 1999. *Science*, *300*(5625), 1560–1563. https://doi.org/10.1126/science.1082750

Paik, S., & Min, S. K. (2017). Climate responses to volcanic eruptions assessed from observations and CMIP5 multi-models. *Climate Dynamics*, *48*(3-4), 1017–1030. https://doi.org/10.1007/s00382-016-3125-4

Paik, S., Min, S. K., Iles, C. E., Fischer, E. M., & Schurer, A. P. (2020). Volcanic-induced global monsoon drying modulated by diverse El Ninõ responses. *Science Advances*, *6*(21), 1–8. https://doi.org/10.1126/sciadv.aba1212

Pausata, F. S., Zanchettin, D., Karamperidou, C., Caballero, R., Battisti, D. S., & Battisti, D. S. (2020). ITCZ shift and extratropical teleconnections drive ENSO response to volcanic eruptions. *Science Advances*, *6*(23), 1–11. https://doi.org/10.1126/sciadv.aaz5006

Petry, I., Fan, F. M., & Wood, A. W. (2025). Observed streamflow data shows El Niño–Southern Oscillation increases likelihood of extreme events in South America. *Communications Earth & Environment*, *6*(1), 699. https://doi.org/10.1038/s43247-025-02714-2

Reichstein, M., Camps-Valls, G., Stevens, B., Jung, M., Denzler, J., Carvalhais, N., & Prabhat. (2019). Deep learning and process understanding for data-driven Earth system science. *Nature*, *566*(7743), 195–204. https://doi.org/10.1038/s41586-019-0912-1

Runge, J., Bathiany, S., Bollt, E., Camps-Valls, G., Coumou, D., Deyle, E., Glymour, C., Kretschmer, M., Mahecha, M. D., Muñoz-Marí, J., van Nes, E. H., Peters, J., Quax, R., Reichstein, M., Scheffer, M., Schölkopf, B., Spirtes, P., Sugihara, G., Sun, J., … Zscheischler, J. (2019). Inferring causation from time series in Earth system sciences. *Nature Communications*, *10*(1), 1–13. https://doi.org/10.1038/s41467-019-10105-3

Sun, H., Bourguet, S., Luan, L., & Keith, D. (2024). Stratospheric transport and tropospheric sink of solar geoengineering aerosol: a Lagrangian analysis. *npj Climate and Atmospheric Science*, *7*(1), 115. https://doi.org/10.1038/s41612-024-00664-8

Thual, S., & Dewitte, B. (2023). ENSO complexity controlled by zonal shifts in the Walker circulation. *Nature Geoscience*, *16*(April). https://doi.org/10.1038/s41561-023-01154-x

Towner, J., Ficchí, A., Cloke, H. L., Bazo, J., Coughlan de Perez, E., & Stephens, E. M. (2021). Influence of ENSO and tropical Atlantic climate variability on flood characteristics in the Amazon basin. *Hydrology and Earth System Sciences*, *25*(7), 3875–3895. https://doi.org/10.5194/hess-25-3875-2021

Vicente-Serrano, S. M., McVicar, T. R., Miralles, D. G., Yang, Y., & Tomas-Burguera, M. (2020). Unraveling the influence of atmospheric evaporative demand on drought and its response to climate change. *Wiley Interdisciplinary Reviews: Climate Change*, *11*(2), 1–31. https://doi.org/10.1002/wcc.632

Vitart, F., Robertson, A. W., Brookshaw, A., Caltabiano, N., Coelho, C. A., de Coning, E., Dirmeyer, P. A., Domeisen, D. I., Hirons, L., Kim, H. J., Lin, H., Kumar, A., Molod, A., Robbins, J., Segele, Z., Spillman, C. M., Stan, C., Takaya, Y., Woolnough, S., … Wu, T. (2025). The WWRP/WCRP S2S Project and Its Achievements. *Bulletin of the American Meteorological Society*, *106*(5), E791–E808. https://doi.org/10.1175/BAMS-D-24-0047.1

Wang, K., & Dickinson, R. E. (2012). A review of global terrestrial evapotranspiration: Observation, modeling, climatology, and climatic variability. *Reviews of Geophysics*, *50*(2), 1–54. https://doi.org/10.1029/2011RG000373

White, C. J., Carlsen, H., Robertson, A. W., Klein, R. J., Lazo, J. K., Kumar, A., Vitart, F., Coughlan de Perez, E., Ray, A. J., Murray, V., Bharwani, S., MacLeod, D., James, R., Fleming, L., Morse, A. P., Eggen, B., Graham, R., Kjellström, E., Becker, E., … Zebiak, S. E. (2017). Potential applications of subseasonal-to-seasonal (S2S) predictions. *Meteorological Applications*, *24*(3), 315–325. https://doi.org/10.1002/met.1654

White, C. J., Domeisen, D. I., Acharya, N., Adefisan, E. A., Anderson, M. L., Aura, S., Balogun, A. A., Bertram, D., Bluhm, S., Brayshaw, D. J., Browell, J., Büeler, D., Charlton-Perez, A., Chourio, X., Christel, I., Coelho, C. A., DeFlorio, M. J., Monache, L. D., Giuseppe, F. D., … Wilson, R. G. (2022). Advances in the Application and Utility of Subseasonal-to-Seasonal Predictions. *Bulletin of the American Meteorological Society*, *103*(6), E1448–E1472. https://doi.org/10.1175/BAMS-D-20-0224.1

Yang, Y., Wu, L., Cai, W., Jia, F., Ng, B., Wang, G., & Geng, T. (2022). Suppressed Atlantic Niño/Niña variability under greenhouse warming. *Nature Climate Change*, *12*(9), 814–821. https://doi.org/10.1038/s41558-022-01444-z

Acknowledgements

First and foremost, I want to thank my parents, who willingly used their time and looked for alternatives to always give me the best they could afford. Without their continuous emotional support, this research and journey would also not be possible. Thanks to their teachings, I decided to help this world, discuss how to improve it. But thanks to them, I am also able to joke about expanding our surface area or joke about white powder.

I want to thank Prof. Stefan Brönnimann, who supported me with the application to ESKAS, but also with guidance and feedback. His enthusiasm for South America and the stories about Latin American countries was also a source of motivation for doing this work. Thanks to Andrew, Jörg, Prof. Olivia, Aurea and other members of the OCCR for their support of this work. Thank you, Prof. Francina Dominguez, for being very willing to be the external examiner of this thesis.

I am also grateful to the ESKAS commission and the international centre (Jasmin and others) for providing the funding opportunity to many students and taking care of them. We wish that the future brings even more commitment to support those looking to create a better world. I also want to thank the faculty of science for providing resources for going to the PAGES conference in Shanghai.

I am especially grateful to the UniBe's Latinoamerican community (Adrian, Edgar, Gaby, Leo, Marce, Paul, Daniel, y el Latin Gang), who know my internal and external forcings, helped me to fight hard moments and cheered me up with many laughs. I thank you for also letting me take care of you. I want to thank my friends in Colombia, Japan, and other countries (Paula, Laura, Pedro, los cilantrines, Yoshinao, Mio, Philipa, Rafa, David), who also looked after my life during the good and bad times. Thanks to the colleagues of the GIUB's physical geography and from OCCR groups, for the breaks, hikes, lunch, beers and ice-cream we shared; my surface area has happily expanded and contracted thanks to that. I want to also thank the partners with whom I decided not to share my life any more; this world requires sacrifice (In this hour of victory, we taste only defeat). Und an alle, deren Gehirn Launen schreit.

This work is for all people at risk from natural hazards (Don Rufino, Ismael and many more), and for those who dedicate their lives to build a better world.

Declaration of consent

on the basis of Article 18 of the PromR Phil.-nat. 19

Name/First Name: Duque Gardeazabal, Nicolás

Registration Number: 22-127-427

Study program: PhD in Climate Sciences

Bachelor ☐ Master ☐ Dissertation ☑

Title of the thesis: Some sources of hydroclimate and renewable energy variability in tropical South America

Supervisor: Prof. Dr. Stefan Brönnimann

I declare herewith that this thesis is my own work and that I have not used any sources other than those stated. I have indicated the adoption of quotations as well as thoughts taken from other authors as such in the thesis. I am aware that the Senate pursuant to Article 36 paragraph 1 litera r of the University Act of September 5th, 1996 and Article 69 of the University Statute of June 7th, 2011 is authorized to revoke the doctoral degree awarded on the basis of this thesis.
For the purposes of evaluation and verification of compliance with the declaration of originality and the regulations governing plagiarism, I hereby grant the University of Bern the right to process my personal data and to perform the acts of use this requires, in particular, to reproduce the written thesis and to store it permanently in a database, and to use said database, or to make said database available, to enable comparison with theses submitted by others.

Bern, Switzerland, 2025.10.09

Place/Date

Signature